第 49 回
フラーレン・ナノチューブ・グラフェン
総合シンポジウム

The 49th Fullerenes-Nanotubes-Graphene General Symposium

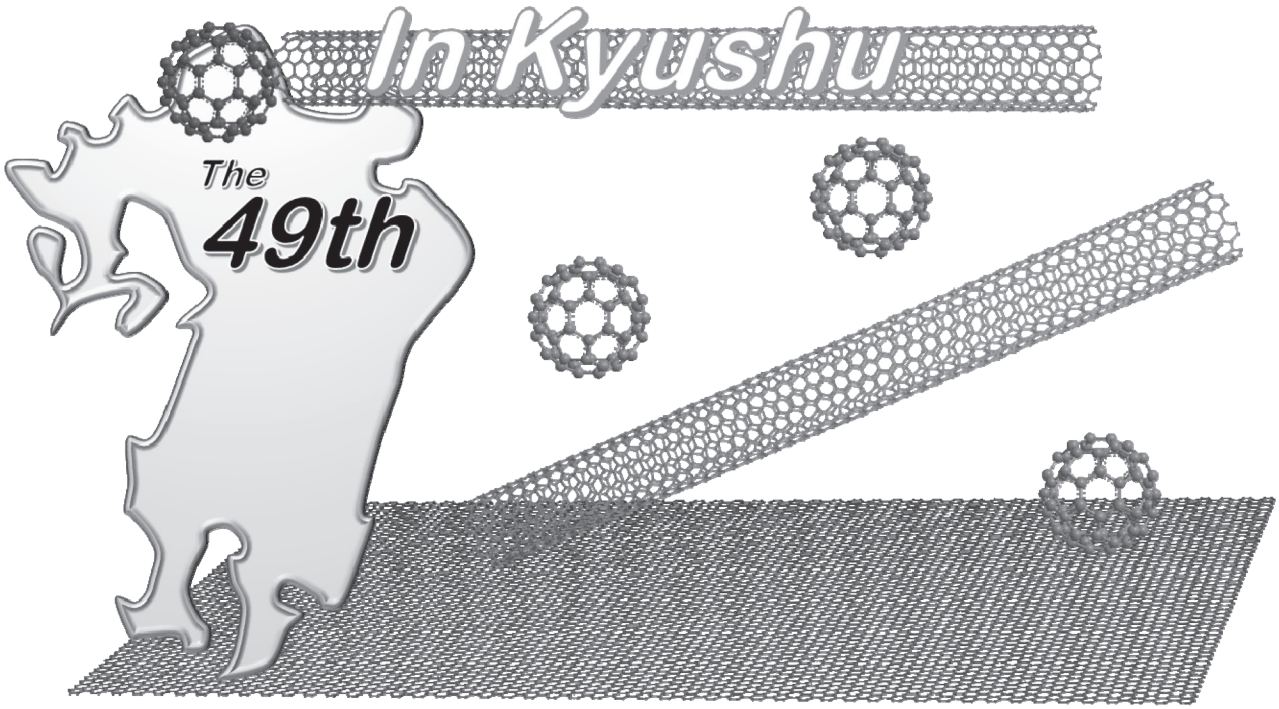

講演要旨集
Abstracts

2015 年 9 月 7 日（月）～　9 日（水）
北九州国際会議場
Kitakyushu International Conference Center

主催　フラーレン・ナノチューブ・グラフェン学会
The Fullerenes, Nanotubes and Graphene Research Society

共催
日本化学会　The Chemical Society of Japan

FNTG Research Society

協賛
日本物理学会　The Physical Society of Japan
応用物理学会　The Japan Society of Applied Physics
高分子学会　The Society of Polymer Science, Japan
電気化学会　The Electrochemical Society of Japan
北九州市　City of Kitakyushu
文部科学省 新学術領域研究 π造形科学　π-System Figuration (MEXT)
九州大学 分子・物資合成プラットフォーム　Kyushu Univ. Nanotechnology Platform
文部科学省 新学術領域研究 原子層科学　Science of Atomic Layers (MEXT)

WITec
focus innovations

共焦点ラマン顕微鏡
クラス最高性能/全自動

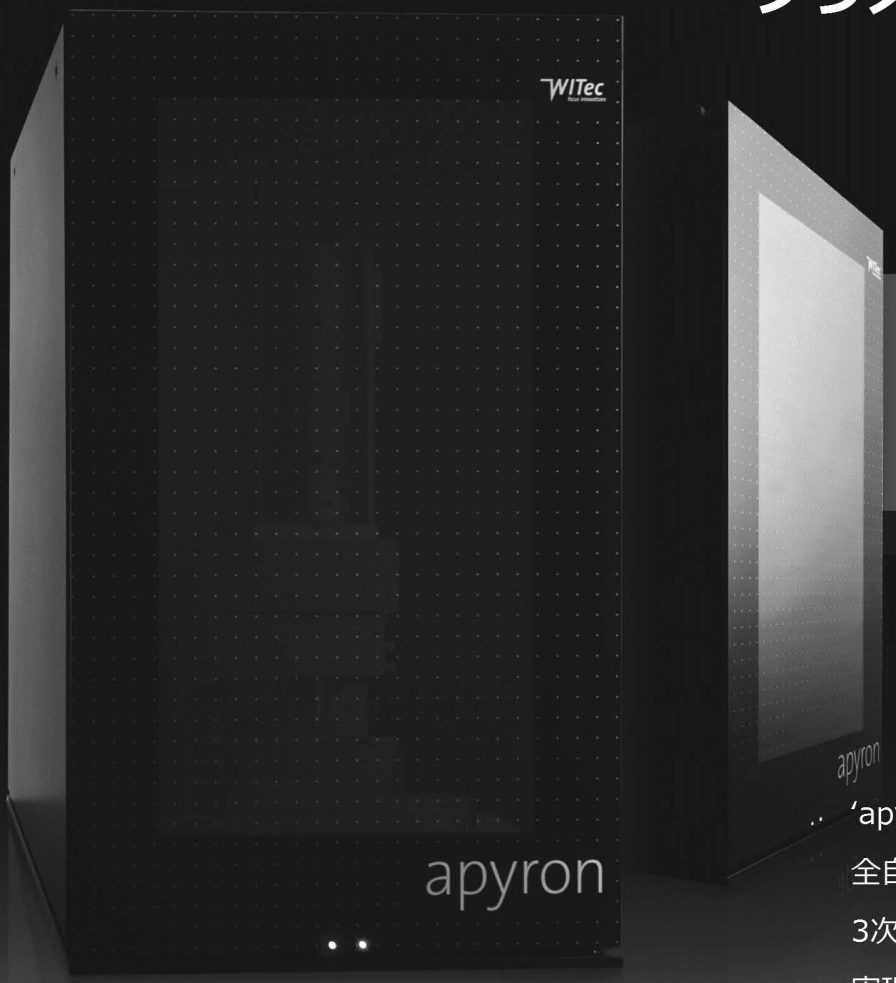

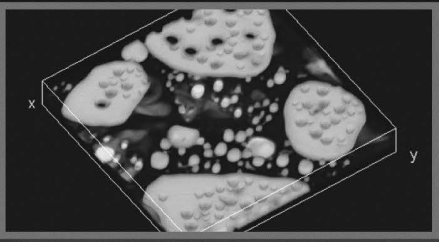

エマルジョンの3次元ラマンイメージ

'apyron'は、クラス最高性能を有しながら、
全自動で使いやすい共焦点ラマン顕微鏡です。
3次元イメージングにおいて、最高の分解能を
実現し、高精度レーザーパワー設定等、
今までにない機能を提供いたします。

PITTCON® Editors' GOLD AWARD
R&D 100 2011
Microscopy TODAY INNOVATION AWARD
PRISM AWARDS

WITec Headquarters
WITec GmbH
Lise-Meitner-Strase 6. D-89081 Ulm Germany

WITec株式会社
〒213-0012 神奈川県川崎市高津区坂戸3-2-1 KSP西713B
TEL 044-819-7773 info@witec-instruments.biz

www.witec.de

Abstract of
The 49th Fullerenes-Nanotubes-Graphene General Symposium

Sponsored by : The Fullerenes, Nanotubes and Graphene Research Society

Co-Sponsored by : The Chemical Society of Japan

Supported by : The Physical Society of Japan
The Japan Society of Applied Physics
The Society of Polymer Science, Japan
The Electrochemical Society of Japan
City of Kitakyushu
π-System Figuration (Grant-in-Aid for Scientific Research on Innovative Areas, MEXT)
Kyushu University Nanotechnology Platform
Science of Atomic Layers (Grant-in-Aid for Scientific Research on Innovative Areas, MEXT)

Date : September 7th (Mon.) – 9th (Wed.), 2015

Place : Kitakyushu International Conference Center
3-9-30 Asano, Kokurakita-ku, Kitakyushu-shi, Fukuoka 802-0001

Presentation Time : Plenary Lecture (40 min presentation + 5 min discussion)
Special Lecture (25 min presentation + 5 min discussion)
General Lecture (10 min presentation + 5 min discussion)
Poster Preview (1 min presentation without discussion)

第 49 回フラーレン･ナノチューブ･グラフェン総合シンポジウム
講演要旨集

主催 ： フラーレン･ナノチューブ･グラフェン学会

共催 ： 日本化学会

協賛 ： 日本物理学会、応用物理学会、高分子学会、電気化学会、北九州市、文部科学省 新学術領域研究 π造形科学、九州大学 分子・物資合成プラットフォーム、文部科学省 新学術領域研究 原子層科学

日時 ： 平成 27 年 9 月 7 日(月)～9 日(水)

場所 ： 北九州国際会議場
〒802-0001 福岡県北九州市小倉北区浅野 3 丁目 9-30

発表時間 ： 基調講演　（発表　40 分 ＋ 質疑応答　5 分）
特別講演　（発表　25 分 ＋ 質疑応答　5 分）
一般講演　（発表　10 分 ＋ 質疑応答　5 分）
ポスタープレビュー　（発表　1 分・質疑応答　なし）

展示団体御芳名 （五十音順、 敬称略）

IOP英国物理学会出版局
九州大学　分子・物質合成プラットフォーム
（株）島津製作所
（株）シンキー
（株）セントラル科学貿易
ナカライテスク（株）
ナノフォトン（株）
日本電子（株）
（株）ニューメタルスエンドケミカルスコーポレーション
（株）名城ナノカーボン
レニショー(株)
ワケンビーテック(株)

広告掲載団体御芳名 （五十音順、 敬称略）

WITec(株)
関東化学(株)
サンケイ化学薬品（株）
シグマアルドリッチジャパン（同）
シュレーディンガー（株）
（株）新興精機
正晃（株）
（株）セントラル科学貿易
ナカライテスク（株）
（株）ニコンインステック九州支店
日本カンタム・デザイン（株）
日本電子（株）
日本分光（株）
日立工機（株）
フロンティアカーボン（株）
（株）名城ナノカーボン

Contents

目次

プログラム早見表

9月7日 （月）

	受付開始 8:30～ 講演開始 9:30～
9:30	基調講演（Rodney S. Ruoff） 9:30–10:15
10:15	一般講演 3件 （グラフェンの生成） 10:15–11:00
11:00	休憩 11:00–11:15
11:15	特別講演（Esko I. Kauppinen） 11:15–11:45
11:45	一般講演 3件 11:45–12:30 （ナノチューブの生成と精製・ ナノチューブの応用）
12:30	昼食 （幹事会） 12:30–13:45
13:45	特別講演(齋藤 弥八) 13:45–14:15
14:15	一般講演 3件 14:15–15:00 （ナノチューブの物性 ・内包ナノチューブ）
15:00	一般講演 2件 15:00–15:30 （ナノチューブの応用・グラフェンの応用）
15:30	休憩 15:30–15:45
15:45	一般講演 3件 （フラーレン） 15:45–16:30
16:30	ポスタープレビュー （ 1P-1～1P-35 ） 16:30–17:10
17:10	ポスターセッション （イベントホール） 17:10–18:40
18:40	

9月8日 （火）

	受付開始 8:30～ 講演開始 9:00～
9:00	基調講演（Zhongfan Liu） 9:00–9:45
9:45	一般講演 4件 （グラフェンの物性・原子層） 9:45–10:45
10:45	休憩 10:45–11:00
11:00	一般講演3件 （飯島賞受賞対象者講演） 11:00–12:00
12:00	昼食 12:00–13:15
13:15	若手奨励賞表彰式13:15–13:30
13:30	総会 13:30–14:00
14:00	特別講演（冨永 昌人） 14:00–14:30
14:30	ポスタープレビュー （ 2P-1～2P-35 ） 14:30–15:10
15:10	ポスターセッション （イベントホール） 15:10–16:40
17:10	バス出発
17:30	見学 （門司港レトロ地区） 17:30–18:40
19:00	懇親会 （門司港ホテル） 19:00–21:00
21:00	

9月9日 （水）

	受付開始 8:30～ 講演開始 9:00～
9:00	特別講演（大澤 映二） 9:00–9:30
9:30	一般講演 3件 （フラーレンの化学） 9:30–10:15
10:15	一般講演 2件 10:15–10:45 （ナノチューブの応用）
10:45	休憩 10:45–11:00
11:00	特別講演(粟野 祐二) 11:00–11:30
11:30	一般講演 4件 （ナノチューブの応用・ グラフェンの応用） 11:30–12:30
12:30	昼食 12:30–13:45
13:45	特別講演(柳 和宏) 13:45–14:15
14:15	一般講演 3件 （ナノチューブの物性） 14:15–15:00
15:00	休憩 15:00–15:15
15:15	ポスタープレビュー （ 3P-1～3P-36 ） 15:15–15:55
15:55	ポスターセッション （イベントホール） 15:55–17:25
17:25	

基調講演　　発表40分・質疑5分
特別講演　　発表25分・質疑5分
一般講演　　発表10分・質疑5分
賞対象講演　発表10分・質疑10分
ﾎﾟｽﾀｰﾌﾟﾚﾋﾞｭｰ 発表1分・質疑なし

Time table

September 7 (Mon.)

	Registration begins at 8:30 Lectures begin at 9:30
9:30	Plenary Lecture （Rodney S. Ruoff) 9:30-10:15
10:15	General Lectures [3] （Graphene synthesis) 10:15-11：00
11:00	Coffee Break 11:00-11：15
11:15	Special Lecture （Esko I. Kauppinen) 11：15-11：45
11:45	General Lectures [3] (Formation and purification of nanotubes・Applications of nanotubes) 11：45-12：30
12:30	Lunch (Administrative Meeting) 12:30-13：45
13:45	Special Lecture (Yahachi Saito) 13:45-14：15
14:15	General Lectures [3] (Properties of nanotubes・Endohedral nanotubes) 14：15-15：00
15:00	General Lectures [2] (Applications of nanotubes・Applications of graphene) 15：00-15：30
15:30	Coffee Break 15:30-15:45
15:45	General Lectures [3] (Fullerenes） 15：45-16：30
16:30	Poster Preview (1P-1～1P-35) 16：30-17：10
17:10	Poster Session (Event Hall) 17：10-18：40
18:40	

September 8（Tue.）

	Registration begins at 8:30 Lectures begin at 9:00
9:00	Plenary Lecture （Zhongfan Liu）9:00-9:45
9:45	General Lectures [4] (Properties of graphene・Atomic Layers） 9：45-10：45
10:45	Coffee Break 10：45-11：00
11:00	General Lectures [3] (Lectures of Iijima Award Nominees) 11：00-12：00
12:00	Lunch 12:00-13:15
13:15	Award Ceremony 13：15-13：30
13:30	General Meeting 13：30-14：00
14:00	Special Lecture （Masato Tominaga）14：00-14：30
14:30	Poster Preview (2P-1～ 2P-35) 14：30-15：10
15:10	Poster Session (Event Hall) 15：10-16：40
17:10	Departure of the chartered bus
17:30	Site Visit (Mojiko Retro Area) 17：30-18：40
19:00	Banquet (Mojiko Hotel) 19:00-21:00
21:00	

September 9（Wed.）

	Registration begins at 8:30 Lectures begin at 9:00
9:00	Special Lecture (Eiji Osawa) 9:00-9:30
9:30	General Lectures [3] (Chemistry of fullerenes） 9:30-10：15
10:15	General Lectures [2] (Applications of nanotubes） 10：15-10：45
10:45	Coffee Break 10：45-11：00
11:00	Special Lecture (Yuji Awano) 11：00-11：30
11:30	General Lectures [4] (Applications of nanotubes・Applications of graphene） 11：30-12：30
12:30	Lunch 12：30-13：45
13:45	Special Lecture (Kazuhiro Yanagi) 13：45-14：15
14:15	General Lectures [3] (Properties of nanotubes） 14：15-15：00
15:00	Coffee Break 15:00-15:15
15:15	Poster Preview (3P-1 ～3P-36) 15：15-15：55
15:55	Poster Session (Event Hall) 15：55-17：25
17:25	

Plenary Lecture: 40 min (Presentation) + 5 min (Discussion)

Special Lecture: 25 min (Presentation) + 5 min (Discussion)

General Lecture: 10 min (Presentation) + 5 min (Discussion)

Award Nominee Lecture : 10 min (Presentation)
+ 10 min (Discussion)

Poster Preview: 1 min (Presentation)

座長一覧 (Chairpersons)

9月7日(月) （敬称略）

セッション	時　　間	座　　長
基調講演 (Rodney S. Ruoff)	9:30 ~10:15	中嶋　直敏
一般講演	10:15 ~11:00	吾郷　浩樹
特別講演 (Esko I. Kauppinen)	11:15 ~ 11:45	大野　雄高
一般講演	11:45 ~ 12:30	千足　昇平
特別講演 (齋藤 弥八)	13:45 ~ 14:15	野田　優
一般講演	14:15 ~ 15:00	佐野　正人
一般講演	15:00 ~ 15:30	秋田　成司
一般講演	15:45 ~ 16:30	宮田　耕充
ポスタープレビュー	16:30 ~ 17:10	根岸　良太

9月8日(火)

セッション	時　　間	座　　長
基調講演 (Zhongfan Liu)	9:00 ~ 9:45	丸山　茂夫
一般講演	9:45 ~10:45	斎藤　晋
一般講演 (受賞対象者)	11:00 ~ 12:00	岡田　晋
特別講演 (冨永 昌人)	14:00 ~ 14:30	宮内　雄平
ポスタープレビュー	14:30 ~ 15:10	白木　智丈

9月9日(水)

セッション	時　　間	座　　長
特別講演 (大澤 映二)	9:00 ~ 9:30	森山　広思
一般講演	9:30 ~ 10:15	八田　泰三
一般講演	10:15 ~ 10:45	加藤　俊顕
特別講演 (粟野 祐二)	11:00 ~ 11:30	松田　一成
一般講演	11:30 ~ 12:30	齋藤　理一郎
特別講演 (柳 和宏)	13:45 ~ 14:15	藤ヶ谷　剛彦
一般講演	14:15 ~ 15:00	北浦　良
ポスタープレビュー	15:15 ~ 15:55	中西　亮

９月７日（月）

基調講演　　発表 40分 ・ 質疑応答 5分
特別講演　　発表 25分 ・ 質疑応答 5分
一般講演　　発表 10分 ・ 質疑応答 5分
ポスタープレビュー　　発表 1分 ・ 質疑応答 なし

基調講演（9:30-10:15）

一般講演（10:15-11:00）
グラフェンの生成

＞＞＞＞＞＞＞ 休憩（11:00-11:15）＜＜＜＜＜＜＜

特別講演（11:15-11:45）

一般講演（11:45-12:30）
ナノチューブの生成と精製・ナノチューブの応用

＞＞＞＞＞＞＞ 昼食（12:30-13:45）＜＜＜＜＜＜＜

特別講演（13:45-14:15）

９月７日（月）

一般講演（ 14:15-15:00 ）
ナノチューブの物性・内包ナノチューブ

一般講演（ 15:00-15:30 ）
ナノチューブの応用・グラフェンの応用

>>>>>>> 休憩（ 15:30-15:45 ）<<<<<<<

一般講演（ 15:45-16:30 ）
フラーレン

ポスタープレビュー（ 16:30-17:10 ）
ポスターセッション（ 17:10-18:40 ）　　（☆） 若手奨励賞候補
フラーレンの化学

フラーレンの応用

金属内包フラーレン

ナノチューブの物性

ナノチューブの応用

ナノチューブの生成と精製

その他

９月８日（火）

基調講演　　発表 40分 ・ 質疑応答 5分
特別講演　　発表 25分 ・ 質疑応答 5分
一般講演　　発表 10分 ・ 質疑応答 5分
飯島賞受賞対象者講演　　発表 10分 ・ 質疑応答 10分
ポスタープレビュー　　発表 1分 ・ 質疑応答 なし

基調講演（9:00-9:45）

一般講演（9:45-10:45）
グラフェンの物性・原子層

＞＞＞＞＞＞＞ 休憩（ 10:45-11:00 ）＜＜＜＜＜＜＜

飯島賞受賞対象者講演（11:00-12:00）

＞＞＞＞＞＞＞ 昼食（12:00-13:15）＜＜＜＜＜＜＜

若手奨励賞の授賞式（13:15-13:30）

総会（13:30-14:00）

９月８日（火）

特別講演（14:00-14:30）

ポスタープレビュー（14:30-15:10）
ポスターセッション（15:10-16:40）　（☆） 若手奨励賞候補
フラーレンの応用

ナノチューブの物性

ナノチューブの応用

ナノチューブの生成と精製

原子層

その他

９月９日（水）

特別講演　　発表 25分 ・ 質疑応答 5分
一般講演　　発表 10分 ・ 質疑応答 5分
ポスタープレビュー　　発表 1分 ・ 質疑応答 なし

＞＞＞＞＞＞＞ 休憩（10:45−11:00）＜＜＜＜＜＜＜

＞＞＞＞＞＞＞ 昼食 (12:30-13:45) ＜＜＜＜＜＜＜

特別講演 (13:45-14:15)

一般講演 (14:15-15:00)

ナノチューブの物性

＞＞＞＞＞＞＞ 休憩 (15:00-15:15) ＜＜＜＜＜＜＜

ポスタープレビュー (15:15-15:55)

ポスターセッション (15:55-17:25)　　(☆) 若手奨励賞候補

フラーレンの化学

フラーレン

ナノチューブの物性

ナノチューブの応用

ナノチューブの生成と精製

内包ナノチューブ

グラフェン生成

グラフェンの応用

グラフェンの物性

原子層

September 7th, Mon.

Plenary Lecture: 40min (Presentation) + 5min (Discussion)
Special Lecture: 25min (Presentation) + 5min (Discussion)
General Lecture: 10min (Presentation) + 5min (Discussion)
Poster Preview: 1min (Presentation)

General Lecture (14:15-15:00)
Properties of nanotubes ・ Endohedral nanotubes

General Lecture (15:00-15:30)
Applications of nanotubes ・ Applications of graphene

>>>>>>> Coffee Break (15:30-15:45) <<<<<<<

General Lecture (15:45-16:30)
Fullerenes

Poster Preview (16:30-17:10)
Poster Session (17:10-18:40 (☆)Candidates for the Young Scientist Poster Award
Chemistry of fullerenes

Applications of fullerenes

Atomic Layers

Other topics

September 8th, Tue.

Plenary Lecture: 40min (Presentation) + 5min (Discussion)
Special Lecture: 25min (Presentation) + 5min (Discussion)
General Lecture: 10min (Presentation) + 5min (Discussion)
Award Nominee Lectures: 10min (Presentation) + 10min (Discussion)
Poster Preview: 1min (Presentation)

Plenary Lecture (9:00–9:45)

General Lecture (9:45–10:45)

Properties of graphene・Atomic Layers

>>>>>>> Coffee Break (10:45–11:00) <<<<<<<

Iijima Award Nominee Lectures (11:00–12:00)

>>>>>>> Lunch Time (12:00–13:15) <<<<<<<

Awards Ceremony (13:15–13:30)

General Meeting (13:30–14:00)

Special Lecture (14:00-14:30)

Poster Preview (14:30-15:10)
Poster Session (15:10-16:40) (☆)Candidates for the Young Scientist Poster Award
Applications of fullerenes

Properties of nanotubes

Applications of nanotubes

Formation and purification of nanotubes

Special Lecture: 25min (Presentation) + 5min (Discussion)
General Lecture: 10min (Presentation) + 5min (Discussion)
Poster Preview: 1min (Presentation)

>>>>>>> Coffee Break (10:45–11:00) <<<<<<<

>>>>>>> Lunch Time (12:30-13:45) <<<<<<<

Special Lecture (13:45-14:15)

General Lecture (14:15-15:00)
Properties of nanotubes

>>>>>>> Coffee Break (15:00-15:15) <<<<<<<

Poster Preview (15:15-15:55)
Poster Session (15:55-17:25) (☆)Candidates for the Young Scientist Poster Award
Chemistry of fullerenes

Chemistry of fullerenes

Fullerenes

Applications of nanotubes

Formation and purification of nanotubes

基調講演
Plenary Lecture
&
特別講演
Special Lecture

1S – 1 ～ 1S – 3
2S – 4 ～ 2S – 5
3S – 6 ～ 3S – 8

Introduction to the CMCM, Carbon Materials for the Future, and Some New Results on Graphene

Rodney S. Ruoff[1, 2]

[1]*Center for Multidimensional Carbon Materials (CMCM), Institute for Basic Science (IBS), Center on the UNIST Campus, Ulsan 689-798, Republic of Korea*
[2]*Department of Chemistry and School of Materials Science, Ulsan National Institute of Science & Technology (UNIST), Ulsan 689-798, Republic of Korea*

I appreciate the opportunity to introduce the Center for Multidimensional Carbon Materials (CMCM), an Institute of Basic Science (IBS) Center located at the Ulsan National Institute of Science and Technology (UNIST) campus. I then offer a personal perspective of what new carbon and related materials might be achieved in the future. These include 'negative curvature carbons', 'diamane' and related ultrathin sp^3-bonded carbon films/foils, sp^2/sp^3-hybrid materials, and others. I also plan to discuss some of our recent results achieved through the preparation of 'special types' of metal foils as substrates for graphene and multilayer graphene growth, as well as some results on functionalizing graphene in new ways.

Of possible interest for this talk are these articles:

[1] (a) X. K. Lu, M. F. Yu, H. Huang, and R. S. Ruoff. Nanotechnology, **10**, 269-272 (1999). (b) X. K. Lu, H. Huang, N. Nemchuk, and R. S. Ruoff. Applied Physics Letters, **75**, 193-195 (1999).

[2] Y. W. Zhu, S. Murali, M. D. Stoller, K. J. Ganesh, W. W. Cai, P. J. Ferreira, A. Pirkle, R. M. Wallace, K. A. Cychosz, M. Thommes, D. Su, E. A. Stach, and R. S. Ruoff. Science **332**, 1537-1541 (2011).

[3] D. Odkhuu, D. Shin, R. S. Ruoff, and N. Park. Scientific Reports **3**, 3276 (2013).

[4] R. S. Ruoff. MRS Bulletin, **37**, 1314-1318 (2012).

[5] Y. F. Hao, M. S. Bharathi, L. Wang, Y. Liu, H. Chen, S. Nie, X. Wang, H. Chou, C. Tan, B. Fallahazad, H. Ramanarayan, C. W. Magnuson, E. Tutuc, B. I. Yakobson, K. F. McCarty, Y. W. Zhang, P. Kim, J. Hone, L. Colombo, and R. S. Ruoff. Science, **342**, 720-723 (2013).

Corresponding Author: R. S. Ruoff
Tel: +82 52 217 5505
E-mail: ruofflab@gmail.com
http://cmcm.ibs.re.kr/html/cmcm_en/

Floating catalyst CVD synthesis of non-bundled SWNTs with narrow chiral angle distribution

Esko I. Kauppinen
Department of Applied Physics, Aalto University School of Science
Puumiehenkuja 2, P.O. Box 16100, FI-00076 Aalto, FINLAND

esko.kauppinen@aalto.fi

We report recent studies on the synthesis of high quality, narrow helical distribution single walled carbon nanotubes from CO with a ferrocene-based floating catalyst chemical vapor deposition (FC-CVD) reactor and show that SWNT networks consisting of long, clean and highly individualized SWNTs exhibit substantially improved transparent conducting film (TCF) performance [1]. Patterned SWNT films show record high conductivity of 67 Ω/□ at 97 % transmittance. In addition, we present recent studies on novel floating catalyst synthesis route for individual, i.e. non-bundled, small diameter single-walled carbon nanotubes (SWCNTs) with narrow chiral angle distribution close to armchair [2]. An *ex situ* spark discharge generator was used to form iron particles with geometric number mean diameters of 3-4 nm and fed into a laminar flow chemical vapor deposition reactor for the continuous synthesis of long and high-quality SWCNTs from ambient pressure carbon monoxide. The Raman G/D intensity ratios up to 48 and mean tube lengths up to 4 μm were observed. The chiral, i.e. (n,m) distributions, as directly determined by electron diffraction in the transmission electron microscope clustered around (7,6), (8,6), (8,7) and (9,6) tube species with up to 70% of tubes having chiral angles of 20° or greater. The tube mean diameter was reduced from 1.10 to 1.04 nm by reducing the growth temperature from 880 to 750 °C, simultaneously increasing the fraction of semiconducting tubes from 67 to 80%. Limiting the nanotube gas phase number concentration to ~10^5 cm^{-3} successfully prevented nanotube bundle formation due to collisions induced by Brownian diffusion. Up to 60-80 % of the total of 500 as-deposited tubes observed by atomic force and transmission electron microscopy were individual. Tube growth mechanisms are discussed based on detailed HR-TEM analyses of active and non-active catalyst particles. Transparent conducting films directly deposited from individual tubes exhibited a record low sheet resistance of 63 Ω/□ at 90 % transparency with 550 nm wavelength.

[1] A. Kaskela et al. (2015). Submitted.

[2] K. Mustonen et al. (2015) Appl. Phys. Lett. **107**, 013106.

Unique properties of nanocarbon materials revealed by *in situ* TEM and FEM

Yuji Shinomiya, Noboru Yokoyama, Koji Asaka, Hitoshi Nakahara, ○Yahachi Saito

Department of Quantum Engineering, Nagoya University, Nagoya 464-8603, Japan

Nanocarbon materials such as carbon nanotube (CNT) and graphene are potential candidates for various active and passive elements for future nanoscale electronic devices. In order to realize the applications of nanocarbon to such devices, it is required to clarify physical properties of individual nanomaterial. We have studied electrical properties of CNT and graphene by in situ transmission electron microscopy (TEM), and electron emission properties by field emission microscopy (FEM). Here, electrical properties of multiwall carbon nanotube (MWCNT) and field emission properties of graphene revealed by in situ TEM and by FEM are reported.

For the measurement of electrical resistance of a MWCNT bridged between Au and Mo electrodes, inner shells were successively retracted into the Mo electrode during electric current application, and the change in the electrical resistance of MWCNT corresponding to the retraction was observed, indicating that the inner shells contribute to the electrical conduction. From the dependence of resistance on the area of contact region between the inner-shell being retracted and the adjacent outer-shell, the inter-shell conductance was estimated to $[0.3\text{- }0.5\ \mathrm{k\Omega}]^{-1}/\mu\mathrm{m}^2$.

In the study of field emission from nanocarbon materials, intriguing FEM images, indicating sub-nanometer sized structures of emitting sites, have been observed. Graphene emitters with free edges (i.e., open edges) show a striped pattern (we dubbed a “lip pattern”); the direction of striations is perpendicular to the graphene sheet, and each stripe are divided into two wings due to a dark band which runs perpendicular to the striation in the center of pattern, as shown in Fig. 1. The pattern indicates coherent interference of electrons from electron orbitals at the graphene edges. When aluminum was deposited on the graphene emitter, FEM images of atomic clusters of aluminum were observed as shown in Fig. 2(a). The image, showing atomic resolution, indicates that the structure of the cluster has a shape of truncated octahedron as illustrated in Fig. 2(b). Similar images of polyhedral Al clusters have also been observed for Al-deposited CNT emitters [1].

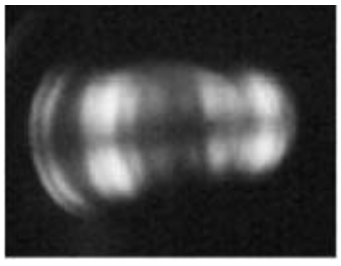

Fig. 1 FEM image of graphene

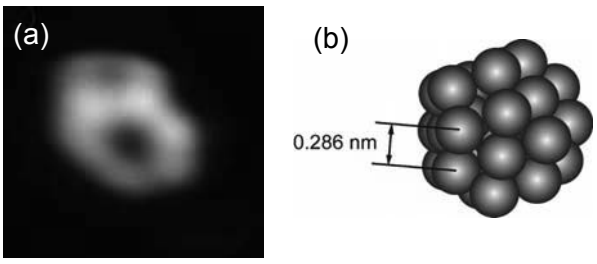

Fig. 2 (a) FEM image and (b) structure model of an Al cluster

[1] K. Nakakubo, K. Asaka, H. Nakahara and Y. Saito, Appl. Phys. Exp. **5**, 055101 (2012)

Corresponding Author: Y. Saito
Tel: +81-52-789-4459, Fax: +81-52-789-3703, E-mail: ysaito@nagoya-u.jp

Graphene and beyond: Attraction, Reality and Future

Zhongfan Liu

Center for Nanochemistry, Beijing Science and Engineering Center for Nanocarbons, College of Chemistry and Molecular Engineering, Peking University, Beijing 10087, China

The gold rush of graphene research has passed over ten years history since its first isolation in 2004, which ignited one's enthusiasm on 2D materials such as *h*-BN, transition metal dichacogenides, graphynes, silicene, germanene, phosphorene, etc. We have been focusing our research interests on the growth issue of these kinds of 2D atomic crystals together with 2D chemistry. Our research activities up to now involve CVD growth of graphene and its hybrid structures, MoS_2, *h*-BN, Bi_2Se_3, Bi_2Te_3, GaSe, etc. By rationally designing the growth catalysts and the elementary steps in the growth process, we have been able to make a precise control of graphene layer number, stacking structures, doping, wrinkle structures and even bandgaps by hybridization with different 2D materials. This talk will present our recent progresses along this direction. A particular focus will be laid on growing graphene on wide-gap semiconducting substrates such as *h*-BN and high *k* strontium titanate, and on groups IVB-VIB early transition metal foils together with the designed growth of mosaic graphene, an in-plane graphene superlattice with other 2D atomic crystals. The talk will also include our recent efforts beyond graphene, focusing on the synthesis of novel 2D atomic crystals using van der Waals epitaxial technique.

1. JY Sun, ZF Liu et al., Direct Growth of High-Quality Graphene on High-κ Dielectric $SrTiO_3$ Substrates，***J. Am. Chem. Soc.*** 136, 6574(2014).
2. Y Kai, ZF Liu et al., Modulation-doped growth of mosaic graphene with single-crystalline p-n junctions for efficient photocurrent generation, ***Nature Commun.*** 3, 1280(2012).
3. CH Zhang, HL Peng, ZF Liu et al., Direct growth of large-area graphene and boron nitride heterostructures by a co-segregation method, ***Nature Commun.,*** 6, 6519(2015).
4. T Gao, XJ Song, HW Du, YF Nie, YB Chen, QQ Ji, JY Sun, YL Yang, YF Zhang, ZF Liu, Temperature-triggered chemical switching growth of in-plane and vertically stacked graphene-boron nitride heterostructures, ***Nature Commun.,*** 6,6835(2015).
5. K Yan, L Fu, HL Peng, ZF Liu, Designed CVD Growth of Graphene via Process Engineering, ***Acc. Chem. Res.***, 10, 2263 (2013).

Spectroscopic analysis on electrochemical oxidation reaction of single-walled carbon nanotubes

Masato Tominaga*[1,2]

[1] *Graduate School of Science and Technology, Kumamoto University, Kumamoto 860-8555, Japan*
[2] *Kumamoto Institute for Photo-Electro Organics (Phoenics), Kumamoto 862-0901, Japan*

The oxidative corrosion of carbon is an urgent problem because carbon is widely used as a platform electrode to immobilize catalysts. One of the factors in the gradual decrease of output power in fuel cells such as a polymer electrolyte fuel cell is the oxidative corrosion of the carbon supports. The oxidative corrosion of carbon is a complicated process that includes parallel oxidation pathways. Furthermore, the electrochemical oxidation reaction of carbon by water molecules occurs at a much more negative potential than that thermodynamically expected, although the rate of this reaction is very slow:

$$C + 2H_2O = CO_2 + 4H^+ + 4e^- \quad 0.207 \text{ V vs. NHE.}$$

Understanding the mechanism of nucleation and growth in oxidative corrosion at the surface of sp^2-carbon is important for advancing its application. A considerable amount of electrochemical research has been directed towards elucidating the mechanism of the oxidation of the hexagonal plane sp^2 carbon family, such as highly oriented pyrolytic graphite (HOPG), carbon nanotubes and graphene as model reaction systems. Recently, a number of studies using *ab* initio molecular orbital calculations have focused on the oxidation steps of hexagonal plane sp^2 carbons. However, the detailed oxidation mechanism of such sp^2 carbons is still unclear. We recently reported the oxidative corrosion potential vs. pH diagram for single-walled carbon nanotubes (SWCNTs) [1]. The current Raman spectroscopic studies based on the encapsulation of β-carotene into SWCNTs revealed that there are three types of oxidative corrosion of SWCNTs: non-oxidized, end-cap oxidized, and side-wall oxidized SWCNTs (Fig. 1). Adsorbed molecular oxygen affects nucleation and growth in the electrochemical oxidative corrosion of SWCNTs in an aqueous electrolyte [2]. We have been investigating diameter-dependent onset potential for the oxidation reaction of SWCNTs in various aqueous solutions [3]. Knowledge of the onset oxidation potential of SWCNTs gives insight into the oxidative corrosion reactions of sp^2 carbons.

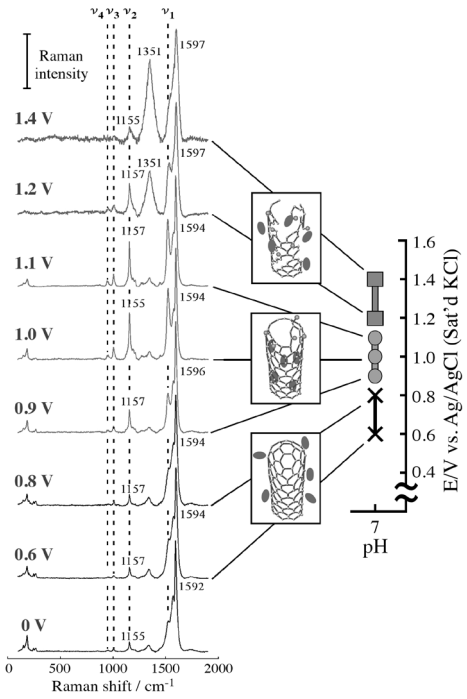

Fig. 1 Raman spectra of SWCNTs after controlled-potential electrolysis followed by β-carotene encapsulation treatment.

[1] M. Tominaga *et al*. RSC Adv., **4**, 27224 (2014).
[2] M. Tominaga *et al*. RSC Adv., **4**, 53833 (2014).
[3] M. Tominaga *et al*. Chem. – Asian J., **8**, 2680 (2013) .

* M. Tominaga
Tel: +81-96-342-3655, F+81-96-342-3655,
E-mail: masato@gpo.kumamoto-u.ac.jp

Thirty Years after C_{60} Discovery and Fifteen Years after Detonation Nanodiamond Rediscovery

Eiji Ōsawa

NanoCarbon Research Institute, AREC, Faculty of Fiber Science and Engineering, Shinshu University, 3-15-1 Tokida, Ueda, Nagano, Japan

Two topics will be briefly introduced to commemorate the 30 years' anniversary of C_{60} discovery, which literally changed the research interests in many of us in a day. Naturally we are greatly concerned on the reason why fullerene fever declined. My personal opinion is that we rushed too fast for their applications before we understood the formation mechanism, which is still incomplete [1]. For this reason, recent discovery of 10^{20} tons (estimated) of C_{60}+C_{70} in Planetary Nebula Tc1 by NASA Spitzer Space Telescope equipped with IR spectrometer attracted our attention with regard to their formation mechanism in outer space [2,3]. The conditions of fullerenes formation in outer space are comparable to those set up by Irle for QM(NCC-DFTB)/MD simulation of C_{60} formation from C_2 [4]. Irle is the first to have proposed that the formation of fullerenes should follow Prigogine's chaos physics under irreversible and non-equilibrium conditions. This is highly likely proposal in view of a large number of chemical mechanisms that failed. We will mention possible participation of giant fullenes up to C_{350} in the final stage of C_{60} formation by the chaotic mechanism, taking into accounts of Daedelus' daydream [5] and the Maruyama-Smalley experiments carried out in the early period after the C_{60} discovery [6].

In contrast to fullerenes, mechanism of diamond crystallization is such a well-known matter that 3nm diamond, the primary particle of detonation nanodiamond (PPDND) and our present major target [7], may appear an easy material. However, the truth is that it was so difficult that for about half a century after its early discovery in 1963 it was left unexplored. It is only recent that fundamental structure and properties finally disclosed and intensive world-wide research activities began [8]. In the lecture we will disclose surprising structural and electronic features of PPDND and mention peculiar behaviors of the first archetypal nanocarbon particle, including important of modelling, extremely high number density effects of single-nano particles, invalidation of purity supremacy, quantization limits, and the most enigmatic phenomenon that occur in its colloidal solution that we named 'dispersion upon concentration, aggregation upon dilution' [9]. The last mentioned phenomenon is due to abnormally strong hydration [10] and provides a good manifestation of colloidal crystals [11]. A few examples of grand-scale applications of PPDND under intensive developments will also be mentioned.

[1] Ōsawa, E. *Fullerenes, Carbon Nanotubes and Related Nanocarbons*, **2012**, *20*, 299. [2] Cami, J. et al. *Science*, **2010**, *329*, 1182. [3] See also: Garcia-Hernandez, D. A. et al., *Astrophys. J. Lett.* **2012**, *760*, 107. [4] Irle, S.; Zheng, G.; Wang, Z.; Morokuma, K. *J. Phys. Chem. B*, **2006**, *110*, 14531. [5] D. E. H. Jones, 'The Invention of Daedalus', W. H. Freeman, Oxford, 1982, p. 118. [6] Maruyama, S.; Anderson, L. R.; Smalley, R. E. *Rev. Sci. Instrum.* **1990**, *61*, 3686. [7] Ōsawa, E. *New Diamond,* **2013**, April Issue, p. 10. [8] Krueger, A. *J. Mater. Chem.* **2012**, *21*, 12571. [9] Ōsawa, E. *Ukr. J. Phys.* submitted for publication. [10] Petit, T. *et al*. *J. Phys. Chem. Lett.* **2015**, *6*, 2909. [11] Mchedlov-Petrossyan, N. *et al*., *Phys. Chem. Chem. Phys*. **2015**, *17*, 16186.
Corresponding Author: E. Ōsawa, Tel: +81-268-75-8381, Fax: +81-268-75-8551, E-mail: osawa@nano-carbon.jp

Nano-Carbon Interconnect Technologies for LSIs: Important Considerations of Edge Control

○Yuji Awano[1]

[1] *Department of Electronics and Electrical Engineering, Keio University, Yokohama 231-0862, Japan*

Nano-carbon materials, such as carbon nanotubes (CNTs) and graphene, have attracted attention as promising emerging research materials (ERMs) for future electron devices, in particular, ones to replace Cu in the next generation of Si LSI interconnects because of their high electron mobility and high electro-migration tolerance [1–4]. In Japan, technologies for CNT vertical interconnects were developed in the MIRAI project (2006–2010) [1], while technologies for graphene interconnects were developed or are being developed in some projects: the green nano-electronics center (GNC) project (2010–2014) [5,6] and the Ultra-Low Voltage Device Project (2010-2016) [7-9]. In this talk, we report on these advances and on future prospects of CNT and graphene interconnect technologie. In the sessions on interconnect technology and ERM of the International Technology Roadmap of Semiconductors (ITRS), the strong needs and difficult challenges of these materials were mentioned [10]. One of the most important challenges is edge control of nano-carbon materials. With the minimum feature size of LSI interconnects getting smaller, manufacturing variants, such as edge roughness, cannot be avoided as long as lithography and dry etching processes are used. Theoretical calculations have predicted that electrical properties of graphene nanoribbons (GNRs) are strongly affected by edge roughness [11, 12]. In order to obtain a higher current reliability in CNT vertical interconnects (vias), it has become increasingly important to increase the number of current paths, not only by increasing the CNT density but also by further improving the CNT contacts with the metal electrodes or the horizontal metal lines [13]. Regarding ohmic contact formation between nano-carbon and metal materials, the edge-contact configuration, in which a metal electrode comes into contact with the edges of the graphene layers, can significantly reduce the contact resistivity because of a higher cohesive energy at the interface between the metal and carbon atoms, comparing with a conventional side-contact configuration [14].

Acknowledgement

This work was partly performed as “Ultra-Low Voltage Device Project" funded and supported by the Ministry of Economy, Trade and Industry (METI) and the New Energy and Industrial Technology Development Organization (NEDO).

References

[1] Y. Awano et al., Proc. of the IEEE, 98-12, p. 2015 (2010), [2] N. Srivastava et al., IEDM2005, p.257 (2005), [3] X. Chen et al., IEEE ED-57, 11, p. 3137 (2010), [4] A. Naeemi et al., IEEE EDL28, p. 428 (2007), [5] S. Sato, IEEE IITC 2015, p. 313 (2015), [6] D. Kondo et al., IEEE IITC 2014, p. 189 (2014), [7] T. Sakai et al., ADMETA 2013 (2013), [8] A. Isobayashi et al., ADMETA 2014, (2014), [9] T. Ishikura et al., IEEE IITC 2015, p. 321 (2015), [10] http://www.ITRS.net/, [11] K. Takashima et al., Appl. Phys. Lett. 104, 093105 (2014), [12] K. Yabusaki et al., IEEE IITC 2015 (2015), [13] M. Sato et al., JJAP 49, 105102 (2010), [14] K. Ito et al., Applied Physics Express 8, 025101 (2015)

Tel: +81-45-566-1506, Fax: +81-45-566-1506, E-mail: awano@elec.keio.ac.jp

Control of Physical Properties of Single Wall Carbon Nanotubes by Electric double layer carrier injections

○Kazuhiro Yanagi

Department of Physics, Tokyo Metropolitan University, Hachioji 192-0397, Japan

Single wall carbon nanotubes (SWCNTs) have sharp van-Hove singularities in their density of states reflecting their one-dimensional nature. Progress of purification techniques has enabled us to clarify the physical properties of high-purity metallicity or chirality selected SWCNTs, and the physical properties strongly depend on the shape of density of states and the location of Fermi level. We have revealed that the physical properties can be tuned by electro-chemical doping (electric double layer carrier injections) techniques. Electrochemical doping techniques have been widely used for carrier injections on SWCNTs since 2001,[1] and we have revealed that the techniques are very suitable for control of various physical properties of high-purity metallicity or chirality selected SWCNTs because its precise tunability of Fermi level.[2-6] For example, SWCNTs show various colors depending on their chiralities, and the colors were controlled by carrier injections through electric double layers using ionic liquids.[2] The capacitance line-shape as a function of applied voltages indicate clear peak structures due to the van-hove singularities, thus we confirmed that the Fermi level can be shifted to approximately ± 1 eV by this techniques.[6] In addition, when the carriers are accumulated in high-density in SWCNTs, a new optical absorption band was formed around the 1 μm wavelength region. As the increase of the density of injected carriers, the peak of the new band blue shifted and its intensity increased.[6] We recently identified that the new band was caused by the formation of the transverse surface plasmon mode, which was normal to the nanotube axis.[6] Not only optical properties but also thermoelectric properties can be controlled by precise tuning of Fermi level.[5] Thermoelectric properties are a very important technology to efficiently convert waste heat into electric power. Hicks and Dresselhaus have proposed an important approach to innovate the performance of devices.[7] They indicated the importance to use one-dimensional materials, and to tune their Fermi level properly because Seebeck coefficients are strongly influenced by the line-shape of density of states and location of Fermi level. We found that the Seebeck coefficients of SWCNTs were also precisely controlled by the carrier injections through electric double layers. We observed clear peak structures of Seebeck coefficient in the p-type and n-type regions in the semiconducting SWCNTs with diameter of 1.4 nm,[5] and the absolute values of the Seebeck coefficient of both the p-type and the n-type can be enhanced to more than 100 $\mu V\ K^{-1}$, indicating the importance of precise tuning of the Fermi level.

[1] S. Kazaui et al., *Appl. Phys. Lett.* **78** 3433 (2001), Kavan et al., *J. Phys. Chem. B* **105**, 10764 (2001) [2] K. Yanagi et al., *Adv. Mater.* **23**, 2811 (2011), [3] M. Kawai, K. Yanagi et al., *J. Am. Chem. Soc.* **134**, 9545 (2012), [4] K. Yanagi et al., *Phys. Rev. Lett.* **110**, 86801 (2013) [5] K. Yanagi et al., *Nano Lett.* **14**, 6437 (2014) [6] T. Igarashi, K. Yanagi et al. *Phys. Rev. Lett.* **114**, 176807 (2015) [7] Hicks & Dresselhaus, *Phys. Rev.* B 47, 16631 (1993)

Corresponding Author: K. Yanagi,
Tel: +81-42-677-2494, E-mail: yanagi-kazuhiro@tmu.ac.jp

一般講演
General Lecture

1 – 1 ～ 1 – 14
2 – 1 ～ 2 – 7
3 – 1 ～ 3 – 12

Electrical properties of graphene synthesized by low temperature plasma techniques

○T. Yamada, Y.Okigawa, M. Ishihara, H. Kato and M. Hasegawa

National Institute of Advanced Industrial Science and Technology, Ibaraki 305-8565, Japan

Low temperature synthesis of graphene is one of the most important technologies for practical applications using graphene. Plasma CVD techniques are expected to reduce temperature [1], however high sheet resistances and small flake sizes are still remaining issues [2]. We reported relatively low sheet resistances of graphene synthesized by plasma treatments of PMMA [3]. In order to improve the electrical properties of graphene obtained by low temperature plasma techniques, the relationship between the electrical properties and the Raman spectrum are examined.

Tow kinds of graphene films obtained by plasma CVD (sample#1) using CH_4 as a carbon source and plasma treatments of PMMA (sample#2) were examined by Hall effect measurements and Raman signal mappings. Both graphene were transferred onto SiO_2/Si substrate. Squares (30x30 μm^2) were patterned by photolithography and oxygen plasma, and then Ti/Au electrodes were deposited on four corners by EB deposition The Hall effect measurements were carried out in the temperature range between 80 to 450K in He atmosphere. Raman spectroscopy was used to characterize the film qualities of the areas of Hall effect measurements. Raman signal mappings were measured at 1x1μm grid points in the x-y plane. A laser of 532nm wavelength was used to excite and the spot size was 1μm in diameter.

Both graphene showed p-type conduction in the measured temperature ranges. Week temperature dependence of the hole mobility of sample#2 are confirmed, while hole mobility of sample#1 is increased with increasing temperatures. The highest hole mobility of sample #1 was 18 cm^2/Vs at 450K and the highest hole mobility was 710 cm^2/Vs at 300K for sampe#2. The obtained results indicated that carrier transport mechanisms were different for two samples. For the results of Raman characterizations, I_G/I_D ratios of sample#1 were between 1 and 8, while those of sample #2 were less than 1. Peak positions of 2D bands for sample #1 are between from 2658 to 2670cm^{-1}, while those of sample#2 are in the range 2650 and 2665cm^{-1}. It is considered that sample#2 is consisted of large size domain with small strain. It is found that there are strong relationships between Hall effect results and Raman characterizations. It is considered that the obtained results are attributed to the difference in decomposition of CH_4 and PMMA by the low temperature plasma.

This work was partially supported by a JSPS Grant-in-Aid for Scientific Research on Innovative Areas “Science of Atomic Layers.

[1] T. Yamada *et al*. J. Phys. D **46**, 063001 (2013).
[2] Y. Okigawa et al., Appl. Phys. Lett. **103**, 153106 (2013)
[3] T. Yamada et al., Appl. Phys. Exp. **6**, 115102 (2013)
Corresponding Author: T.Yamada
Tel: +81-29-861-3851, Fax: +81-29-861-4522,
E-mail: takatoshi-yamada@aist.go.jp

Formation mechanism of anisotropic cracks in graphene grown on copper foil

○Miho Fujihara[1], Ryosuke Inoue[2], Rei Kurita[2], Toshiyuki Taniuchi[3], Yoshihito Motoyui[3], Shik Shin[3], Fumio Komori[3], Yutaka Maniwa[2], Hisanori Shinohara[1], Yasumitsu Miyata[2,4]

[1] Department of Chemistry, Nagoya University, Nagoya 464-8602, Japan
[2] Department of Physics, Tokyo Metropolitan University, Hachioji 192-0397, Japan
[3] Institute for Solid State Physics, The University of Tokyo, Kashiwa 277-8581, Japan
[4] JST, PRESTO, Kawaguchi, 332-0012, Japan

Graphene edges have attracted much attention due to its unique electrical and magnetic properties depending on their edge structures. To understand their properties, it is highly desired to prepare clean, smooth, and structure-controlled edges. Recently, our group reported the preferential formation of zigzag edges in graphene cracks.[1] These cracks can be observed for as-prepared graphene films grown on Cu foil by chemical vapor deposition. However, the formation mechanism of such cracks is still unclear because graphene was just cooled after the growth and no tension was artificially imparted during the cooling process. Furthermore, Raman analysis indicates the presence of compressive strain in graphene at room temperature due to the thermal shrinkage of Cu substrate.

Here, we demonstrate that the transient lattice expansion could be generated in specific Cu grains during cooling process.[2] From optical microscope observations, we find that the cracks are preferentially formed in graphene grains on narrow Cu (100) face surrounded by Cu (111) faces (Fig.1a). Statistical analysis of visual observations indicates that the crack formation results from the stress concentration of uniaxial tension at notches in the polycrystalline graphene films. Based on simulation results using a simplified thermal shrinkage model, we propose that the cooling-induced tension is derived from the transient lattice expansion of narrow Cu grains imparted by the thermal shrinkage of adjacent Cu grains (Fig. 1b). The simulation also predicts that Cu could shrink uniformly after the adequate time, which is consistent with the observed upshift of G- and 2-D band Raman modes. The present results provide an insight into fabricating long, smooth zigzag edges in graphene and other two-dimensional materials.

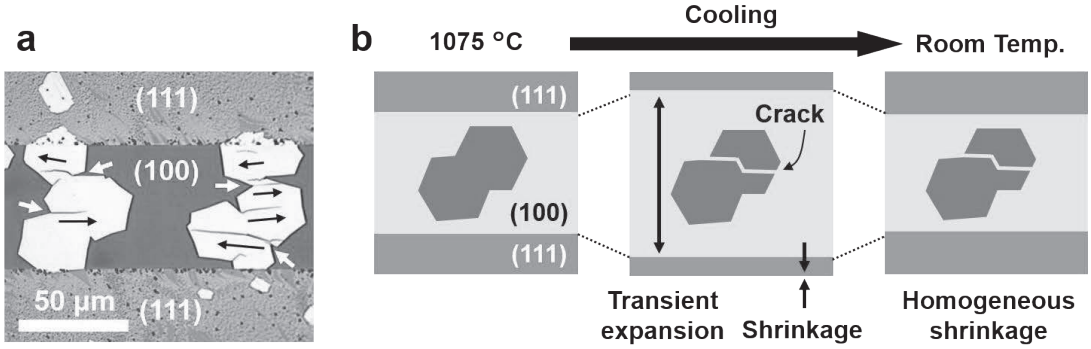

Fig.1: (a) Optical image of anisotropic cracks in graphene on copper foil. (b) Schematic illustration of the proposed mechanism of crack growth by transient lattice expansion of Cu (100) face.

[1] M. Fujihara *et al.* The 48th FNTG Symposium (2015). [2] M. Fujihara *et al.* submitted.

Corresponding Authors: Y. Miyata, H. Shinohara

Tel: +81-42-677-2508, +81-52-789-2482, E-mail: ymiyata@tmu.ac.jp, noris@nagoya-u.jp

Large scale synthesis of densely-aligned suspended graphene nanoribbons array by plasma CVD

○Hiroo Suzuki, Toshiaki Kato, and Toshiro Kaneko

Department of Electronic Engineering, Tohoku University, Sendai 980-8579, Japan

Graphene nanoribbons (GNRs) combine the unique electronic and spin properties of graphene with a transport gap that arises from quantum confinement and edge effects. This makes them an attractive candidate material for the channels of next-generation transistors. Although GNRs can be made in a variety of ways, the reliable site and alignment control of GNRs with high on/off current ratios remains a challenge.

Up to now, we developed a novel method based on the advanced plasma CVD method [1] with nano scale Ni catalyst (Ni nanobar) for directly fabricating suspended GNRs devices [2]. However, the growth yield of suspended GNRs is low and understanding the growth mechanism is required to solve this problem. In this study, we found that the stability of Ni nanobar can be drastically improved during plasma CVD. Since GNR nucleates during the cooling process, the Ni nanobar structure has to be maintained even under the high temperature condition (just before cooling) for the growth of suspended GNR. Our experimental results show that the high rate supply of carbon species into Ni during plasma CVD can improve the thermal stability of Ni nanobar under the high temperature condition. Furthermore, phase separation between graphene and Ni happens during the cooling process, which accelerates the destabilization of Ni nanobar, resulting in the formation of suspended GNR (Fig. 1(a)). By following this growth model, precise adjustment of plasma CVD conditions was carried out. As a result, the yield of suspended GNR growth can be improved (～90%) and the high density GNRs array has been successfully fabricated in large scale (Figs. 1(b), 1(c)).

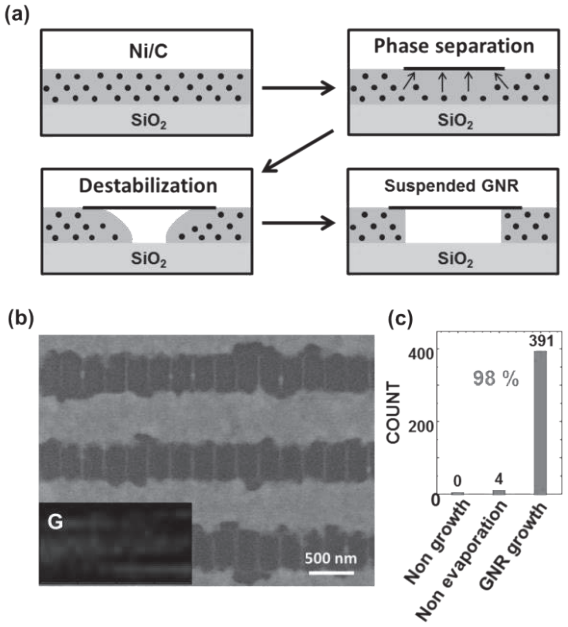

Fig.1: (a) Schematic images of formation mechanism of suspended GNR during cooling. (b) Typical scanning electron microscope image (inset shows the G band intensity mapping of Raman spectra) and (c) histogram of GNR growth yield.

[1] H. Suzuki, T. Kato and T. Kaneko, Plasma and Fusion Res. **9,** 1206079 (2014).
[2] T. Kato and R. Hatakeyama, Nat. Nanotechnol. **7**, 651 (2012).

Corresponding Author: H. Suzuki
Tel: +81-22-795-7046
E-mail: suzuki12@ecei.tohoku.ac.jp

Relationship between growth rate and catalyst lifetime on carbon nanotube forest synthesis

○Naoyuki Matsumoto[1,2], Guohai Chen[1], Robert C. Davis[3], Hiroe Kimura[1], Shunsuke Sakurai[1,2], Motoo Yumura[1,2], Don N. Futaba[1,2], Kenji Hata[1,2]

[1] *Technology Research Association for Single Wall Carbon Nanotubes (TASC), Central 5, 1-1-1 Higashi, Tsukuba, Ibaraki 305-8565, Japan*
[2] *National Institute of Advanced Industrial Science and Technology (AIST), Central 5, 1-1-1 Higashi, Tsukuba, Ibaraki 305-8565, Japan*
[3] *Department of Physics and Astronomy, Brigham Young University, Provo, UT 84602, USA.*

Generally, there are two dominant competing processes during carbon nanotube (CNT) synthesis: CNT growth and catalyst deactivation. The carbon feedstock will affect both processes, because a fraction will contribute to the synthesis, reflecting in the growth rate, and the remaining unused fraction will contribute to the deactivation of the catalyst through carbon coating, i.e. the catalyst lifetime. Therefore, from this standpoint, the growth rate and lifetime are expected to be fundamentally inversely related. This point is empirically known as observed by the results mentioned above [1-3]. However, the inverse relationship itself has yet to be studied.

In this work, we report an inverse relationship between the CNT growth rate and catalyst lifetime by investigating the dependence of growth kinetics for ~330 CNT forests and the dependence on carbon feedstock, carbon concentration, and growth temperature. We found that increased growth temperature led increased CNT growth rate and shortened catalyst lifetime for all carbon feedstocks, following an inverse relationship of fairly constant maximum height. For increased carbon concentration, the carbon feedstocks fell into two groups where ethylene / butane showed increased/decreased growth rate and decreased / increased in lifetime indicating different rate-limiting growth processes. In addition, this inverse relationship held true for different types of CNTs synthesized by varied chemical vapor deposition techniques and continuously spanned 1000-times range in both growth rate and catalyst lifetime, indicating the generality and the fundamental nature of this behavior originating from the growth mechanism of CNTs itself. These results suggest it would be fundamentally difficult to achieve a fast growth with long lifetime.

This study is based on results obtained from a project commissioned by the New Energy and Industrial Technology Development Organization (NEDO).

[1] G. F. Zhong *et al.* J. Phys. Chem. B **111**, 1907 (2007).
[2] S. P. Patole *et al.* Appl. Phys. Lett. **93**, 114101 (2008).
[3] G. H. Chen *et al.* Nanoscale. **7**, 8873, (2015).

Corresponding Author: Don N. Futaba
Tel: +81-29-861-4654, Fax: +81-29-861-4851
E-mail: d-futaba@aist.go.jp

Control of bioreactions in living organisms by carbon nanotube supramolecular nanohybrids

○Eijiro Miyako[1], Svetlana A. Chechetka[1], Motomichi Doi[2], Eiji Yuba[3], Kenji Kono[3]

[1] *Department of Materials and Chemistry, Nanomaterial Research Institute (NMRI), National Institute of Advanced Industrial Science and Technology (AIST), Central 5, 1-1-1 Higashi, Tsukuba 305-8565 (Japan)*
[2] *Department of Life Science and Biotechnology, Biomedical Research Institute (BRI) & DAILAB, AIST, Central 6, 1-1-1 Higashi, Tsukuba 305-8566 (Japan)*
[3] *Department of Applied Chemistry, Graduate School of Engineering, Osaka Prefecture University, 1-1 Gakuen-cho, Naka-ku, Sakai, Osaka 599-8531 (Japan)*

There is currently great interest in understanding and achieving remote operation of functional nanorobots[1–4] in physiological environments. We developed a carbon nanotube–liposome-based supramolecular nanohybrid[1] capable of permeation through cells with high biocompatibility. The nanohybrid can be loaded with a variety of functional molecules and is structurally controlled by near-infrared laser irradiation for the release of molecules from the nanohybrids in a targeted manner via microscopy. We implemented the controlled release of molecules from nanohybrids and demonstrated their efficacy in remote regulation of photo-induced nanohybrid functions. As a proof of principle, nanohybrids loaded with drugs were successfully used in spatiotemporal blocking of targeted channel proteins in living *Caenorhabditis elegans* (*C. elegans*). Our prototype could inspire new designs with biomimetic parasitism and symbiosis and biologically active nanorobots for higher-level manipulation of organisms.

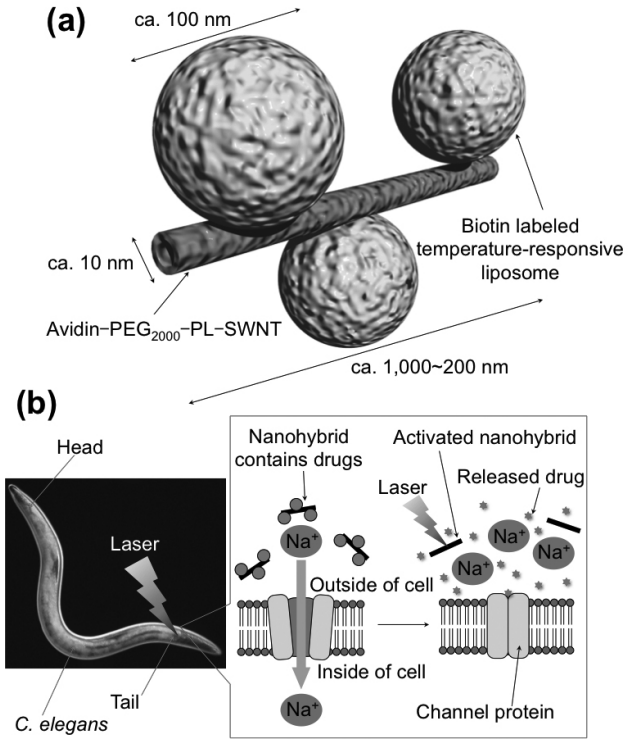

Fig.1: (a) Schematic illustration of carbon nanotube supramolecular nanohybrid. (b) Remote control of bioreactions in living *C. elegans* by laser-induced nanohybrids.

[1] E. Miyako *et al*. **Angew. Chem. Int. Ed.** in press (2015).
[2] E. Miyako *et al.* **Angew. Chem. Int. Ed.** 53, 13121 (2014).
[3] E. Miyako *et al.* **Nature Commun.** 3, 1226 (2012).
[4] E. Miyako *et al.* **Proc. Natl. Acad. Sci. USA** 109, 7523 (2012).

Corresponding Author: E. Miyako
Tel: +81-87-869-3574, Fax: +81-29-861-4413,
E-mail: e-miyako@aist.go.jp

Dispersion of carbon nanotubes in organic solvents using inorganic salts

○Kazuya Matsumoto, Takuro Takahashi, Mitsutoshi Jikei

Department of Applied Chemistry, Akita University, Akita 010-8502, Japan

Dispersion techniques of carbon nanotubes (CNTs) are quite important to utilize CNTs for nano-applications. Although the physical modification is a useful CNT dispersion technique, organic dispersants often remain as electrical insulating impurities. Recently, we have found that inorganic salts act as dispersants of CNTs and give CNT dispersions in common organic solvents. In this study, we examined the favorable combination of inorganic salts and organic solvents as well as the dispersion mechanism.

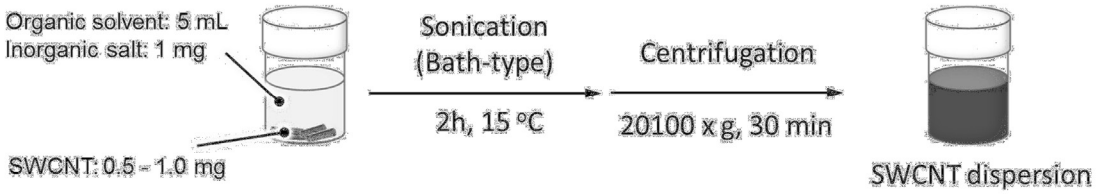

Fig. 1: Dispersion of SWCNT using inorganic salts

Single-walled carbon nanotubes (SWCNTs) were dispersed in organic solvents using inorganic salts by sonication (Fig. 1). As a result, weak acid salts such as potassium carbonate and tripotassium phosphate (K_3PO_4) dispersed SWCNTs effectively. On the other hand, strong acid salts such as potassium chloride and potassium nitrate did not work as dispersants (Fig. 2). Among organic solvents, relatively low polar solvents such as tetrahydrofuran (THF) were suitable for SWCNT dispersion. We evaluated the amount of K_3PO_4 attached on the SWCNT wall by ion chromatography. The attached K_3PO_4 was determined as 0.17 wt% with respect to the SWCNT weight. This result clearly indicates that inorganic salts work as dispersants in only a small amount compared to conventional organic dispersants.

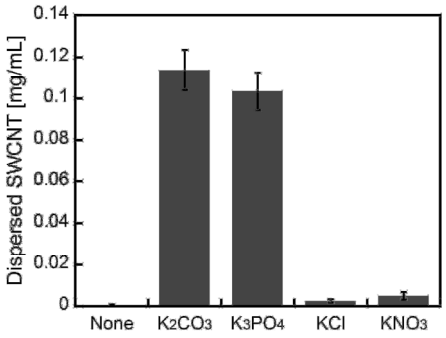

Fig. 2: The amount of dispersed SWCNT

Table 1: Zeta potentials of SWCNT dispersions in THF

Inorganic salt	Zeta potential (mV)
K_2CO_3	-51.5
K_3PO_4	-50.8

In order to examine dispersion mechanism, we measured zeta potential of the SWCNT dispersion in THF using inorganic salts. The zeta potential results are summarized in Table 1. The SWCNT dispersions exhibited zeta potential values of about -50 mV, which indicates that the CNT surface is negatively charged and the anion parts of the inorganic salts are attached on the CNT surface. The electrostatic repulsion between negatively charged CNTs would play a key role in the CNT dispersion using inorganic salts.

Corresponding Author: K. Matsumoto,
Tel&Fax: +81-18-889-2745, Email: kmatsu@gipc.akita-u.ac.jp

Lattice vibration in isotopic superlattice of carbon nanotubes

○Susumu Saito[1-3], Yuki Bando[1]

[1]*Department of Physics, Tokyo Institute of Technology, Tokyo 152-8551, Japan*
[2]*International Research Center for Nanoscience and Quantum Physics, Tokyo Institute of Technology, Tokyo 152-8551, Japan*
[3]*Materials Research Center for Element Strategy, Tokyo Institute of Technology, Yokohama, Kanagawa 226-8503, Japan*

Isotopic superlattice of diamond consisting of ^{12}C and ^{13}C diamond layers has been produced and its interesting electronic properties including the carrier confinement to the ^{12}C layers have been reported [1]. Because of the strong electron-phonon interaction in carbon-based materials, the fundamental-gap value of diamond is found to depend sensitively on the isotopic composition of ^{12}C and ^{13}C atoms [2], and it should result in the carrier confinement in the isotopic diamond superlattice. Therefore, it is of high interest to study the isotopic superlattice of carbon nanotubes which may possess unique vibrational and electronic properties being different from those of carbon nanotubes of natural isotopic abundance. In this study, we report the vibrational properties of isotopic superlattice of carbon nanotubes studied by using the density-functional perturbation theory.

We consider the (6,6) armchair nanotube, which consists of alternatively stacked n layers of ^{12}C and ^{13}C, and is now named as $\{n, n\}$ nanotube superlattice. Its unit cell is shown in the figure below. The lattice vibration of this carbon nanotube suprelattice is then analyzed by utilizing the Fourier transformation and inverse Fourier transformation procedure for the dynamical matrix of the isotopically controlled superlattice [3]. We analyze the details of the n-dependence of the so-called radial breathing mode (RBM). It is found that the spatial distribution of the mode amplitude is not uniform anymore but sensitively depends on the position from the ^{12}C/^{13}C boundary as well as on the isotope mass of the site considered.

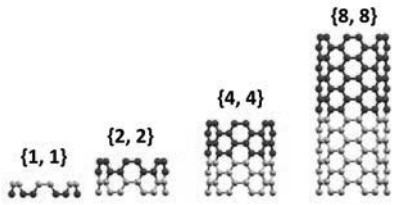

[1] H. Watanabe, C. E. Nebel, and S. Shikata, Science **324**, 1425 (2009).
[2] H. Watanabe, T. Koretsune, S. Nakashima, S. Saito, and S. Shikata, Phys. Rev. B **88**, 205420 (2013)
[3] Y. Bando and S. Saito, to be published.

Corresponding Author: S. Saito
E-mail: saito@stat.phys.ttiech.ac.jp
Fax: +81-3-5734-2739

Analytical transmission electron microscopy of water encapsulated in single-wall carbon nanotubes at 97 K

○Keita Kobayashi[1], Ryosuke Kuroiwa[2], Yasuda Hidehiro[1,2]

[1] *Research Center for Ultra-High Voltage Electron Microscopy, Osaka University, 7-1, Mihogaoka, Ibaraki, Osaka 567-0047, Japan*
[2] *Division of Materials and Manufacturing Science, Graduate School of Engineering, Osaka University, 2-1, Yamadaoka, Suita, Osaka 565-0871, Japan*

Water exhibits polymorphic structures depending on temperature and pressure, and so novel phases in various environments have been investigated to discover new structures and clarify the properties of water. It has recently been reported that water encapsulated within single-wall carbon nanotubes (SWCNTs) exhibits a unique tubular crystalline structure, based on results of molecular dynamics simulation, X-ray diffractometry, and nuclear magnetic resonance spectroscopy [1,2]. Moreover, the studies have shown that the structure of crystalline water depends on SWCNT diameter [2], suggesting that the size and dimensions of confining spaces in nanomaterials affect the phase transitions of encapsulated materials. However, these findings were obtained through simulation and interpretation of macroscopic structural analysis, not direct microscopic observation of structures. To accurately determine the structure of water encapsulated in SWCNTs and elucidate its phase transitions, direct structural analysis of the water by analytical transmission electron microscopy (TEM) is needed.

Accordingly, in this study we performed structural analysis of water encapsulated in SWCNTs by TEM, transmission electron diffractometry (TED), and electron energy loss spectroscopy (EELS) at a low temperature (97 K).

Figure 1 shows EELS spectra of a crystalline water (ice) nanoparticle, water encapsulated in SWCNTs with diameter of 1.2 nm, and a liquid–vapor mixture of water [3] in the oxygen *K*-shell region. Although a distinct crystal structure of water was not found by TEM or TED of the SWCNTs, the EELS spectrum contained an unequivocal oxygen signal. The spectral structure of the water in the SWCNTs was different from that of the ice nanoparticle but analogous to that of the vapor–liquid mixture of water. These results might indicate that water encapsulated in the SWCNTs has an amorphous-like disordered structure.

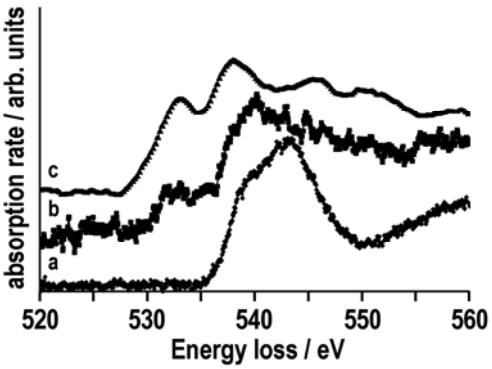

Fig. 1: EELS spectra of (a) a crystalline ice nanoparticle, (b) water encapsulated in SWCNTs, and (c) a liquid-vapor mixture of water

[1] Y. Maniwa *et al*. J. Phys. Soc. Jpn. **71**, 2863 (2002).
[2] Y. Maniwa *et al*. Chem. Phys. Lett. **401**, 534 (2005).
[3] G. Algara-Siller *et al.* Nature **519**, 443 (2015).

Corresponding Author: K. Kobayashi
Tel: +81-6-6879-7941, Fax: +81-6-6879-7942,
E-mail: kobayashi-z@uhvem.osaka-u.ac.jp

Magnetic properties of nano metals

○Hidetsugu Shiozawa

[1] *Faculty of Physics, University of Vienna, Boltzmanngasse 5, 1090 Vienna, Austria*

Unique physical properties emerge when matters are organized in small dimensions. Our research is focused on studies of electronic and magnetic properties of atoms and molecules that are naturally arranged in low dimensions within the interior of carbon nanostructures [1-3]. For instance, molecular arrays and nanomagnets can be created within carbon nanotubes or carbon fibers that can outperform their bulky counterparts. Iron and nickel clusters inside carbon nanotubes behave as single-domain magnets exhibiting large coercive fields as the cluster size becomes as small as the exchange length. Encapsulated inside carbon nanotubes otherwise chemically reactive nanomaterials become stable to be examined by means of different experimental techniques. Octahedrally coordinated transition metal ions arranged in one dimension are ideal systems in which anisotropic magnetic coupling can be studied. Our experiments using X-ray diffraction, Raman, photoemission, SQUID, X-ray magnetic circular dichroism spectroscopy, electron microscopy and magnetotransport measurements seek to probe their intrinsic properties with no environmental factors and reveal electronic and magnetic interactions at molecular interfaces that are responsible for their unique magnetic properties.

[1] M. Kharlamova *et al*. Nanoscale **7**, 1383 (2015).
[2] A. Briones-Leon *et al*. Phys. Rev. B **87**, 195435 (2013).
[3] H. Shiozawa *et al*. Sci. Rep. **3**, 1840 (2013).

Corresponding Author: H. Shiozawa
Tel: +43-1-4277-72628, Fax: +43-1-4277-9726,
E-mail: hidetsugu.shiozawa@univie.ac.at

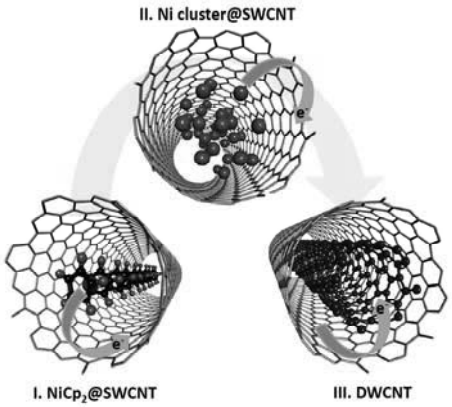

Fig.1: Schematic of one-dimensional structures inside carbon nanotubes [1].

High-efficiency biological imaging using single-chiral (9,4) SWCNTs

○Yohei Yomogida[1], Minfang Zhang[2], Masako Yudasaka[1], Xiaojun Wei[1], Takeshi Tanaka[1], and Hiromichi Kataura[1]

[1]*Nanomaterials Research Institute, AIST, Ibaraki 305-8562, Japan*

[2]*CNT Application Research Center, AIST, Ibaraki 305-8562, Japan*

Recently, single-wall carbon nanotubes (SWCNTs) have attracted much attention as a fluorescence probe for biological imaging owing to their strong absorption and bright emission within near infrared (NIR) biological transparency window (700-1400 nm), where light penetrates body deeply [G. Hong et al, Nature Medicine 18 (2012) 1841]. However, currently-used HiPco SWCNTs contain various chiral species with different excitation (S_{22}) wavelength and thus degrade their excitation efficiency for a single excitation source. Therefore, the chirality enriched SWCNTs were desired for high-efficiency imaging. In previous, we developed a novel gel chromatography method for chirality separation of SWCNTs and successfully separated high-purity single-chiral (9,4) SWCNTs in large scale with low cost. Owing to both the S_{11} emission and S_{22} excitation of (9,4) SWCNTs in the lower absorption regions of water and various biological tissues, they should be more suitable candidates. In this work, we demonstrated high-efficiency biological imaging of mouse vasculature using biocompatible single-chiral (9,4) SWCNTs.

To make the (9,4) SWCNTs biocompatible, surfactants on SWCNTs were replaced with biocompatible surfactants (DSPE-PEG*). Fig. 1 shows the optical absorption spectra of the (9,4) and raw HiPco sample which was prepared as a reference. Their mass concentrations were estimated to be 0.17 for (9,4) and 0.64 mg/mL for raw HiPco. After each sample was injected intravenously through a tail of mice, each NIR image of the mouse was recorded using an InGaAs 2D array camera under illumination with a LED (~730 nm) light. Fig. 2 shows the images of each mouse under the same shooting conditions. In spite of lower mass concentration, (9,4) exhibited brighter image than raw HiPco sample. It is calculated that (9,4) sample is more than an order of magnitude brighter than raw HiPco sample at the same mass concentration. Interestingly, we can perform imaging using even two orders of magnitude lower dose of 0.3 μg per mouse than reported values. The use of biocompatible and low-dose (9,4) SWCNTs will reduce any possible risk to the subject.

This work was supported by KAKENHI No. 25220602.

*1,2-distearoyl-sn-glycero-3-phosphoethanolamine-N-[amino(poly(ethylene glycol))-5000]

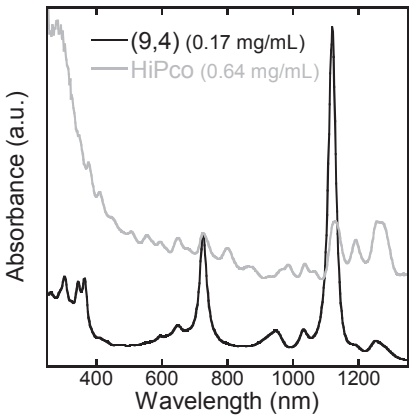

Fig. 1 Absorption spectra of (9,4) and HiPco SWCNTs

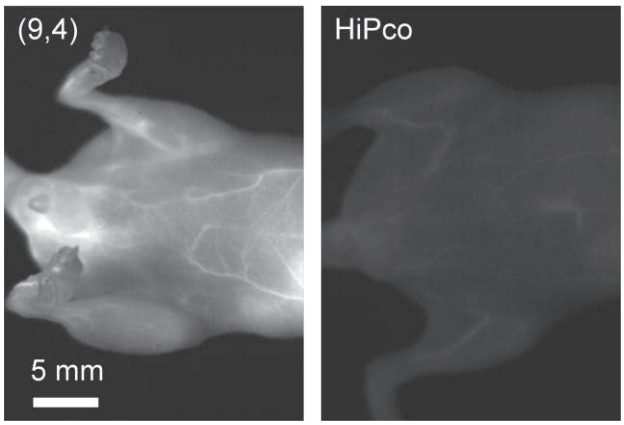

Fig. 2 NIR fluorescence images of mice injected with the (9,4) SWCNTs (left) and HiPco SWCNTs (right)

Graphene Oxide as a Multifunctional Platform for Cell Imaging

○Zhenyu Zhang, Qinghai Liu, Juan Yang, and Yan Li*

Beijing National Laboratory for Molecular Sciences, College of Chemistry and Molecular Engineering, Peking University, Beijing, 100871, China

Graphene oxide (GO) possesses a single-layered, two-dimensional sp^2 hybrid structure with sufficient hydrophilic surface groups [1], which are important for biocompatibility. GO can serve as a unique double-sided, easily accessible platform for multifarious functionalization and efficient loading of various substances for bioapplications. In this study, we demonstrate strategies of using GO as a multifunctional platform in fluorescence and Raman bimodal imaging based on GO/gold nanoparticles (AuNPs) /2-aminoethanethiol (AET)/fluorescein isothiocyanate (FITC, a fluorescent dye) hybrids and in multi-frequency Raman imaging based on GO/ AuNPs /p-aminothiophenol (p-ATP, a Raman probe) hybrids (Figure 1 &2) [2]. GO acts as not only a Raman probe, but also a substrate for Raman and fluorescent probes to load on. Our study demonstrates that GO has great potential in biomedical applications, acting as a multifunctional platform to facilitate various cell imaging processes and substance delivery into cells.

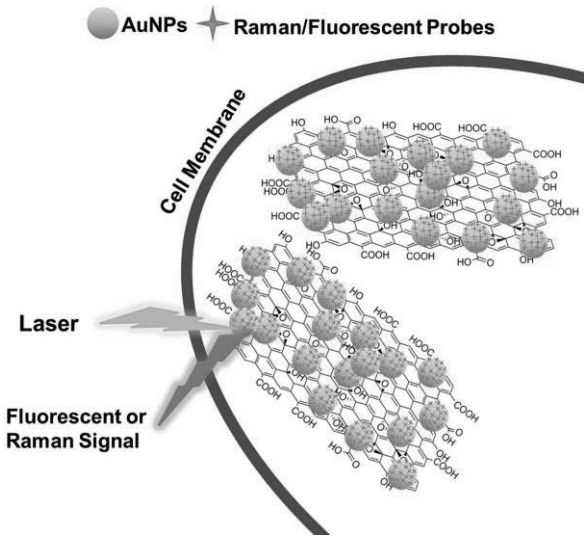

Fig.1: Scheme showing the structure of GO decorated with AuNPs and Raman/fluorescent probes, and the strategies for fluorescence and Raman imaging of cells.

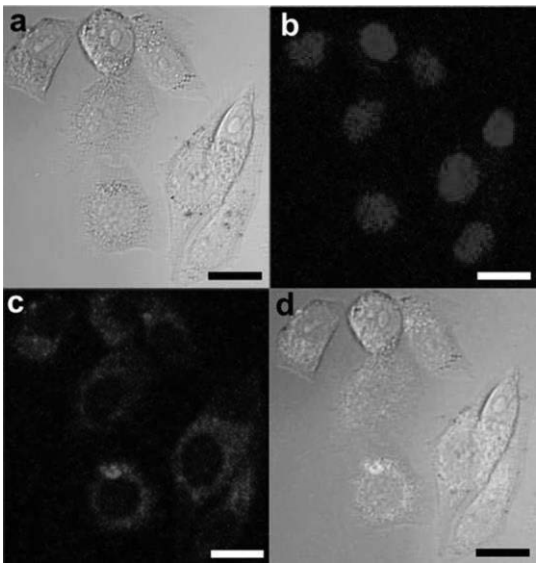

Fig.2: Confocal fluorescence microscopy images of Hela 229 cells incubated with GO/AuNPs/AET/FITC. Images from (a) to (d) show bright field (a), cell nuclei stained by DAPI (b), FITC fluorescence in cells (c), and overlays of three images (d). Scale bar is 10 μm. Objective is 60x.

[1] Q. Liu *et al*. Nanoscale **4**, 7084 (2012).
[2] Z. Zhang *et al*. Small **11**, 3000 (2015).

Corresponding Author: Y. Li
Tel & Fax: +86-10-6275-6773
E-mail: yanli@pku.edu.cn

Alkali-metal-doped fullerene for application to superconducting wires

○Hiroyuki Takeya, Toshio Konno, Chika Hirata, Takatsugu Wakahara, Kunich Miyazawa, Masashi Tanaka, Takahide Yamaguchi, Yoshihiko Takano

National Institute for Materials Science, Tsukuba 305-0047, Japan

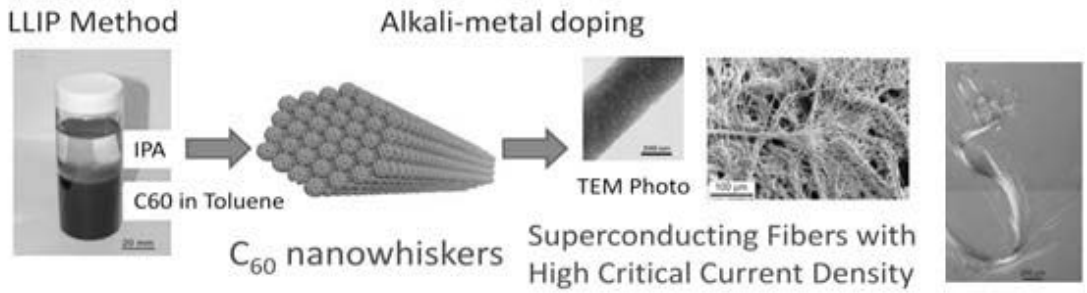

Fig.1: Schematic Process of C60 Superconducting Fibers.

Superconductivity of alkali-metal(A)-doped fullerenes was found in 1991. A-doped fullerides A_xC_{60} [0<x<6] are particularly interesting since their structures and electronic properties are strongly related to the doping carrier concentration. The compound, A_3C_{60}, shows superconducting transition at 19K (A=K), 29K (A=Rb) or 33K (A=Cs_2Rb). Fullerene-based nanowhiskers (C_{60}NWs) have been developed by Miyazawa et al.[1] using a liquid-liquid-interfacial-precipitation (LLIP) technique. If such a form of C_{60}NWs turns out to be a superconductor, it will be a promising material for superconductive fibers or wires.

As we have reported [2,3], we tried to dope alkali metals (K, Rb, Cs_2Rb) into the C_{60}NWs for future application to superconducting light fibers. First, superconductivity was observed at 17 K in the K-doped C_{60}NWs heated at 200ºC and their superconducting volume fraction reached 80 % in 24 hours. In contrast, low superconducting volume fractions around 1 % in K_3C_{60} superconductors has been reported in previous papers by many researchers. We concluded this difference was caused from nanopores in C_{60}NWs by the LLIP, which assist K-migration in the materials. We reported the critical current density (J_c) of A_xC_{60}NW was estimated over 10^5A/cm^2 up to 5 T using the Bean model in *M-H* curves.

In such a result, there was a problem for application that the superconductivity of alkali-metal-doped fullerenes was disappeared in air. Recently, we found a good sheath pipe for it. Figure 2 shows the currency dependence of superconducting transition in K_3C_{60} materials. This is the first measurement result of bulk superconductivity in the sheath. We will report the result above and a process making short superconducting wires of K_3C_{60} in my presentaion.

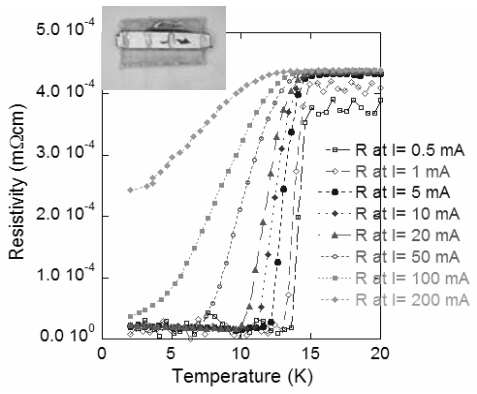

Fig.2: Superconducting transitions of K_3C_{60} in a sheath. Superconducting

[1] K. Miyazawa. J. Mater. Res., 2002, 17, 83-88. DOI: 10.1557/JMR.2002.0014

[2] H. Takeya *et al.* Molecules, 2012, 4851-4859. DOI:10.3390/molecules17054851.

[3] H. Takeya *et al.* Mater. Res. Bull., 2013, 48, 343-345. DOI: 10.1016/j.materresbull.2012.10.033.

Corresponding Author: H. Takeya, Tel: +81-29-859-2318, E-mail: takeya.hiroyuki@nims.go.jp

Singlet oxygen generation from $Li^+@C_{60}$ nano-aggregates dispersed by laser irradiation in aqueous solution

○Kei Ohkubo[1], Naoki Kohno[1], Shunichi Fukuzumi[1,2]

[1] Department of Material and Life Science, Graduate School of Engineering, Osaka University, ALCA and SENTAN, Japan Science and Technology Agency, Suita, Osaka 565-0871, Japan

[2] Faculty of Science and Technology, Meijo University and ALCA and SENTAN, Japan Science and Technology Agency (JST), Nagoya, Aichi 468-8502, Japan

Fullerenes, especially [60]fullerene (C_{60}), are known as efficient photosensitisers to generate the triplet excited state and ROS with high quantum yields. Additionally, fullerenes are remarkably photostable and non-toxic reagents. However, pristine C_{60} is hardly soluble in water and biological media to prevent expression of the photoactivity and PDT efficiency. Recently, a lithium ion-encapsulated fullerene hexafluorophosphate salt ($Li^+@C_{60}$ PF_6^-) has been reported as an efficient photosensitiser to form the long-lived triplet excited state, which is comparable to that of C_{60}.[1] However, neither solubilisation of $Li^+@C_{60}$, C_{60} or C_{70} to water nor the photoinduced singlet oxygen generation efficiency has been studied. We report herein highly water-dispersed heterogeneous fullerene nano-aggregates composed of $Li^+@C_{60}$, C_{60}, and C_{70}, which have absorption bands in the visible region as well as an efficient singlet oxygen generation properties.

Laser pulse irradiation (λ = 532 nm; 500 mW; 10 Hz, 60 min, i.d. = 8 mm) of a deaerated aqueous solution (2.5 mL) containing the dispersed $Li^+@C_{60}PF_6^-$ salt (1.0 mg) resulted in formation of $Li^+@C_{60}$ nano-aggregates [$(Li^+@C_{60})_n$]. A brown colour supernatant solution containing nano-aggregates was obtained after the centrifugation and the decantation procedures. The size of the nano-aggregates was significantly decreased to 30 nm by the laser pulse excitations determined by the dynamic light scattering (DLS) measurements. Photoirradiation of an oxygen-saturated deuterated water (D_2O) solution of $(Li^+@C_{60})_n$ results in formation of singlet oxygen, which was detected by the $^1O_2$ phosphorescence at 1270 nm. The quantum yield (Φ) of $^1O_2$ generation was 0.55 for $(Li^+@C_{60})_n$. The values of nano-aggregates are smaller than those of the corresponding fullerenes in C_6D_6/C_6H_5CN (1:1 v/v) probably because of the excited state annihilation, which was confirmed by time-resolved femtosecond transient absorption spectral measurements [2].

[1] K. Ohkubo, Y. Kawashima, S. Fukuzumi, Chem. Commun., **48**, 4314 (2012).
[2] K. Ohkubo, N. Kohno, Y. Yamada, S. Fukuzumi, Chem. Commun., **51**, 8082 (2015).

Corresponding Author: K. Ohkubo
Tel: +81-6-6879-7369, Fax: +81-6-6879-7370,
E-mail: ookubo@chem.eng.osaka-u.ac.jp

Chemical and physical control of superconductivity and magnetism

○Yasuhiro. Takabayashi,[1] Ruth H. Zadik,[2] Kosmas Prassides[1,3]

[1]WPI-Advanced Institute for Materials Research (WPI-AIMR), Tohoku University, Sendai 980-8577, Japan
[2]Department of Chemistry, Durham University, Durham DH1 3LE, UK
[3]Japan Science and Technology Agency, ERATO Isobe Degenerate π-Integration Project, Tohoku University, Sendai 980-8577, Japan

Face-centered-cubic (fcc) alkali fullerides (A_3C_{60}) were long considered as archetypal conventional BCS superconductors. Metallic fcc A_3C_{60} transforms to superconductor below transition temperature, T_c. Early work showed that T_c of A_3C_{60} increases monotonically with inter-C_{60} separation, which is controlled by the A^+ cation size. Inter-C_{60} separation can be also controlled by applying hydrostatic pressure. We succeeded to synthesize the most expanded alkali-doped fcc Cs_3C_{60} which is an antiferromagnetic insulator at ambient pressure with an ordering temperature of 2.2 K [1]. Application of hydrostatic pressure can then induce superconductivity. The T_c-V plot shows a dome-like relationship. The T_c-V curve after peaking at 35 K merges into the T_c-V linear line of the less expanded fcc A_3C_{60}.

It is possible to approach to the superconductor – insulator boundary across the maximum of superconductivity dome chemically, by increasing the Rb content in the family of superconductors, $Rb_xCs_{3-x}C_{60}$ [2]. We show that applying chemical pressure transforms the hyperexpanded Cs_3C_{60} Mott-Jahn-Teller (MJT) insulator first into an unconventional correlated Jahn-Teller metallic (JTM) state (an inhomogeneous state where localized electrons coexist with metallicity and the on-molecule distortion persists). It then crosses over to a conventional Fermi liquid state where the molecular electronic signature fades away. This normal state crossover is mirrored in the evolution of the superconducting state, with the highest T_c found at the boundary between unconventional correlated and conventional weak-coupling BCS superconductivity, where the interplay between extended and molecular aspects of the electronic structure is optimized to create the dome.

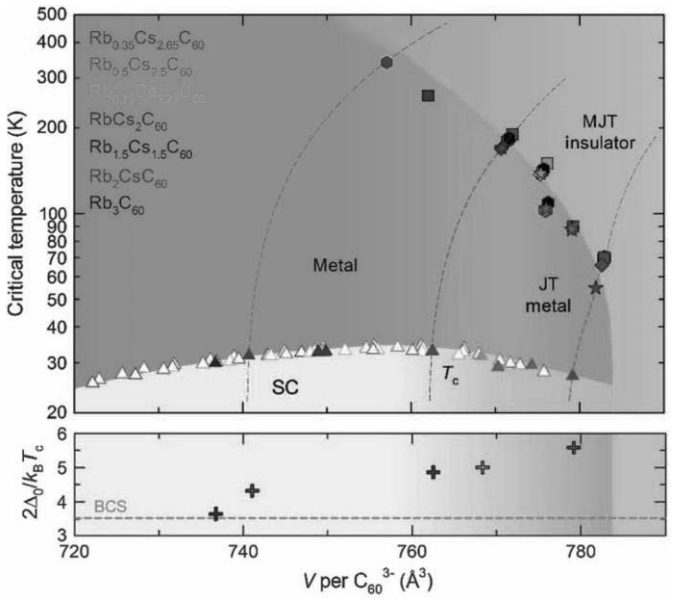

Fig. 1: Global electronic phase diagram of fcc A_3C_{60} fullerides.

[1] A. Y. Ganin, Y. Takabayashi *et al*., Nature **466**, 221 (2010).
[2] R. H. Zadik, Y. Takabayashi, G. Klupp, R. H. Colman, A. Y. Ganin, A. Potočnik, P. Jeglič, D. Arčon, P. Matus, K. Kamarás, Y. Kasahara, Y. Iwasa, A. N. Fitch, Y. Ohishi, G. Garbarino, K. Kato, M. J. Rosseinsky, K. Prassides, Science Advances, **1**, e1500059 (2015).

Corresponding Author: Y. Takabayashi
Tel/Fax: +81-22-217-5953
E-mail:
takabayashi.yasuhiro.87e@st.kyoto-u.ac.jp

Tunable absorption of electromagnetic wave in graphene for a total reflection geometry of dielectric materials

○R. Saito, C. Reynolds, and M. S. Ukhtary

Department of Physics, Tohoku University, Sendai 980-8578, Japan

Here we discussed a possible switching device of electromagnetic wave (EM) in THz region which is controlled by gate electrode. What is special in the present result are that (1) we can change the absorption probability of EM from 0% to 100% by changing the Fermi energy from 0 to 1eV, and that (2) we adopted so-called total reflection geometry of two dielectric materials at which interface we put a single layer of graphene. Because of the high Drude conductivity, we expect surface plasmon excitation in graphene which is essential for obtaining 100% absorption of EM even for mono layer graphene [1]. Now we consider a possible modification to improve the performance in which two single graphene layers are taken into account, in which two graphene layers are separated by the third dielectric materials. We will propose to experimental people a possible EM switching device.

Reference

[1] M. Shoufie Ukhtary, Eddwi H. Hasdeo, Ahmad R. T. Nugraha and Riichiro Saito, *Appl. Phys. Express* **8** 055102 (2015).

Energetics and electronic structure of h-BN nanoribbons

○Ayaka Yamanaka, Susumu Okada

Graduate School of Pure and Applied Sciences, University of Tsukuba, Tennodai, Tsukuba 305-8577, Japan

Hexagonal boron nitride (h-BN) is attracting much attention due to its unique physical properties such as mechanically strong structure, high thermal conductivity, and wide band gap those make them as the insulating version of graphene. Indeed, h-BN possesses honeycomb networks of BN bond with the length of 0.144 nm. Because of these properties, h-BN is applicable for the wide areas in the present and future nanotechnologies. For practical applications of h-BN, it is very important to control their shapes and sizes those seriously affect their fundamental properties. In this work, we study the energetics and electronic structure of h-BN with various edge structures. All calculations are performed by using the density functional theory (DFT) with the generalized gradient approximation. We use an ultrasoft pseudopotential to describe the interaction between valence electrons and ions. The effective screening medium (ESM) method is applied to avoid the unintentional dipole interactions with the periodic images arising from their polar edges in the framework of the conventional DFT calculations.

In this study, we consider h-BN nanoribbons with various edge shape of which edge angles are θ = 0° (armchair), 8°, 16°, 23°, and 30° (zigzag) shown in Fig. 1(a)-1(e). As shown in Fig. 1(f), the edge formation energy of hydrogenated nanoribbons keeps constant value of 0.25 eV throughout all θ. Therefore, the h-BN flakes with hydrogenated edges may exhibit rich variation in their morphology and edge structures, in sharp contrast to the graphene nanoribbons. Small and constant edge formation energy is ascribed to the semiconducting electronic properties of h-BN nanoribbons with hydrogenated edges. On the other hand, edge formation energy monotonically increases with increasing the edge angle in the case of h-BN nanoribbons with clean edges. In the case, increase of density of state at E_F arising from dangling bond states leads to the monotonical increase of edge formation energy.

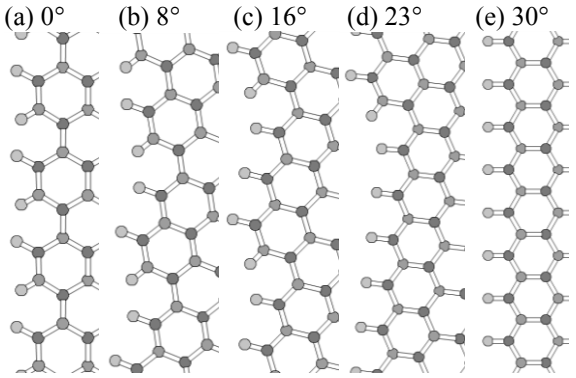

(f) Edge Formation Energy

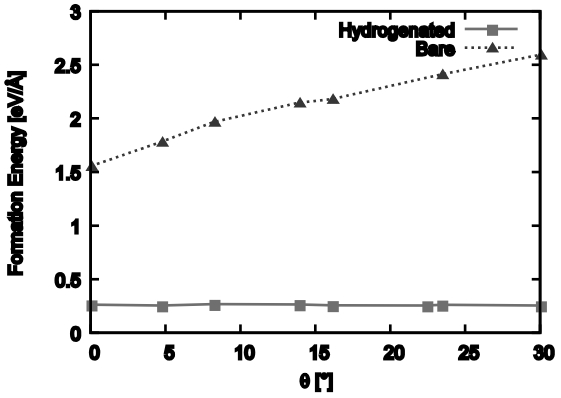

Fig.1: (a)-(e) Geometric structures and (f) edge formation energy of h-BN nanoribbons.

Corresponding Author: A. Yamanaka
Tel: +81-29-853-5600 (ext. 8233), Fax: +81-29-853-5924,
E-mail: ayamanaka@comas.frsc.tsukuba.ac.jp

Carrier-density- and Electric-field-dependent Electroluminescence of Monolayer WSe_2

○Jiang Pu[1], Leiqiang Chu[2], Lain-Jong Li[3], Tomo Sakanoue[1], Goki Eda[2], Taishi Takenobu[1,4]

[1] *Department of Advanced Science and Engineering, Waseda Univ., Tokyo 169-8555, Japan*
[2] *Physics Department, National University of Singapore, Singapore 117542, Singapore*
[3] *Physical Sciences and Engineering Division, KAUST, Thuwal 23955-6900, Saudi Arabia*
[4] *Kagami Memorial Laboratory, Waseda University, Tokyo 169-0051, Japan*

The strong confined system of monolayer transition metal dichalcogenides is raising much attention to realize remarkable optical properties, such as the formation of charged exciton (trion) and the quantum-confined Stark effect [1]. For example, the electrical control of exciton and trion photoluminescence has already realized. In addition, the large Stark effect have been suggested, however, it has been only discussed qualitatively [2,3]. One possible barrier for investigation Stark effect might be due to the insufficiency of electric field because current researches have been performed by SiO_2 back-gate structure. The interfacial traps of SiO_2 would also affect the excitonic properties, which could hamper the intrinsic effect of electric field. Therefore, for revealing Stark effect of excitons and trions, the clean interface which can contribute to both high carrier-density- and high electric-field-modulation are required. Recently, we proposed electric double layer light-emitting diodes (EDLEDs), which can increase carrier density up to ~ 10^{14} /cm^2 and electric field up to ~ 10^6 V/cm simultaneously to generate electroluminescence (EL). Here, we fabricated EDLEDs with monolayer WSe_2 and evaluate its carrier-density- and electric-field-dependent EL properties.

The EDLEDs were constructed from exfoliated monolayer WSe_2 and ion gels, gelation of ionic liquids. Importantly, EDLEDs are two-terminal devices, which *p-i-n* junction can be self-organized to obtain EL when the lateral potential gradient that is larger than bandgap of WSe_2 is applied (Fig. 1(a)). As shown in *I-V* curve of Fig. 1(a), we measured EL spectrum as varying applied voltage. Figure 1(b) exhibits the voltage-dependent EL of WSe_2 EDLEDs. The clear spectrum broadening and non-linear red shift were observed. By understanding operation mechanism of EDLEDs and analyzing obtained spectrum, we discuss these unique EL properties from the both aspect of carrier-density- and electric-field-modulation, resulting in generation (and control) of trion EL and Stark effect of excitons and trions.

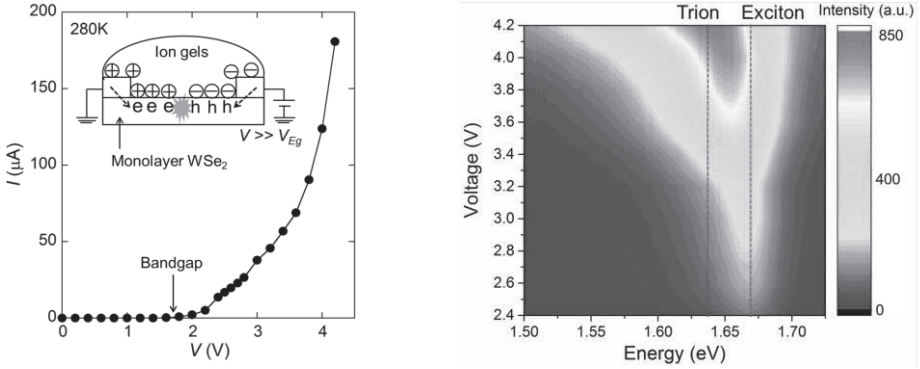

Fig. 1 Left: (a) Schematic of a WSe_2 EDLED and its *I-V* curve. Right: (b) Voltage-dependent EL spectrum.

[1] X. Xu, *et al*. Nat. Phys. **10**, 343 (2014)
[2] A. Ramasubramaniam, *et al*. Phys. Rev. B. **84**, 205325 (2011)
[3] A. M. Jones, *et al*. Nat. Nanotechnol. **8**, 634 (2013)

Corresponding Author: J. Pu, T. Takenobu
Tel/Fax: +81-3-5286-2981
E-mail: hokoh.apple@fuji.waseda.jp, takenobu@waseda.jp

Memristive phase switching in two-dimensional crystals

○Masaro Yoshida[1], Ryuji Suzuki[1], Yijin Zhang[1], Masaki Nakano[1], Yoshihiro Iwasa[1,2],

[1] *Quantum-Phase Electronics Center (QPEC) and Department of Applied Physics, The University of Tokyo, Tokyo, 113-8656, Japan*
[2] *RIKEN Center for Emergent Matter Science (CEMS), Wako, 351-0198, Japan*

Two-dimensional (2D) crystals, extending from graphene, transition metal dichalcogenides to black phosphorene, provide an ideal platform for exotic electronic band structures in mono- or multi-layer forms. The thinning-induced modification of their band structures results in novel semiconductor functionalities, which is exemplified by the emergent valleytronics in molybdenum disulfide (MoS_2) and tungsten diselenide (WSe_2).

The thinning to nanoscale may also affect collective phenomena in interacting electron systems, leading to unconventional electronic states and related functionalities. Among 2D crystals with correlated electrons, 1T-type tantalum disulfide (1T-TaS_2) is attracting growing interests, because its first-order phase transition in nano-thick crystals is found to be highly controllable [1-4]. For example, we employed electric double-layer (EDL) technique to a 61-nm-thick crystal, and succeeded in the complete suppression of the phase transition by electrostatic carrier doping as displayed in Fig. 1 [2].

Here, we show memristive phase switching in nano-thick crystals of 1T-TaS_2 [5]. The ordering kinetics of the phase transition was revealed to become slow as the thickness is reduced, resulting in an emergence of metastable states. Furthermore, we realized the unprecedented memristive switching to multi-step non-volatile states by applying in-plane electric field. Moreover, we discovered current-induced metastable states which have never been realized in bulk single crystals. The reduction of thickness is essential to achieve such non-volatile electrical switching behavior. The thinning-induced slow kinetics probably makes the various metastable states robust and consequently realizes the non-volatile memory operation. The present result indicates that 2D crystal with correlated electrons is a novel nano-system to explore and functionalize multiple metastable states, which are inaccessible in its bulk form.

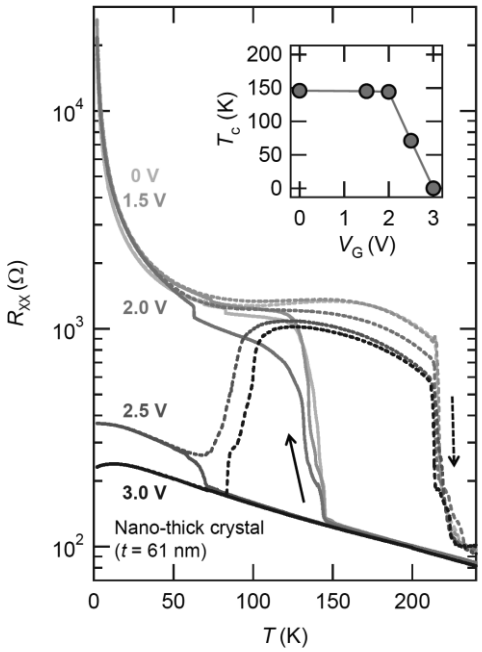

Fig.1: Temperature (T) versus four-terminal resistance (R_{xx}) curves of a 61-nm-thick 1T-TaS_2 crystal measured at various gate voltages (V_G). Inset: the on-set temperature of the first-order phase transition (Tc) as a function of V_G.

[1] L. Stojcheska *et al.* Science **344**, 177 (2014).
[2] M. Yoshida *et al.* Sci. Rep. **4**, 7302 (2014).
[3] M. J. Hollander *et al.* Nano Lett. **15**, 1861 (2015)
[4] Y. Yu *et al.* Nat. Nanotech. **10**, 250 (2015).
[5] M. Yoshida *et al.* accepted.

Corresponding Author: M. Yoshida
Tel: +81-3-5841-6822, Fax: +81-3-5841-6822,
E-mail: masaro-yoshida@mp.t.u-tokyo.ac.jp

Direct Analysis of Exciton Band Structure of SWCNTs using Their Circular Dichroism Spectra

○Xiaojun Wei, Mayumi Tsuzuki, Takuya Hirakawa, Yohei Yomogida, Atsushi Hirano, Shunjiro Fujii, Takeshi Tanaka and Hiromichi Kataura

Nanomaterials Research Institute, National Institute of Advanced Industrial Science and Technology (AIST), Tsukuba, Ibaraki 305-8562, Japan

Band structure of single-wall carbon nanotubes (SWCNTs) was well calculated by density functional theory (DFT) to date. However, there has been very limited the number of experimental analysis reports because we didn't have good way to analyze them. In this work, we report experimentally obtained excitonic band structures of SWCNTs for the first time. This analysis was based on the circular dichroism (CD) spectra. It is well known that $E_{i,i}$ transitions are allowed for parallel polarization of electric field to nanotube axis and $E_{i,j}$ transitions for cross polarization. Usually, we can observe only $E_{i,i}$ transitions due to a strong local field effect. However, all these allowed optical transitions can be observed in CD spectra [1]. If we have single-chirality enantiomers, we can analyze all allowed optical transitions using CD spectra.

For this purpose, we developed an effective gel chromatography method by combining the overloading selective adsorption and stepwise elution using a mixed surfactant. Using this technique, 9 kinds of high-purity single-chirality enantiomers have been separated. Extremely high CD peak intensity indicates the highest purity of enantiomers compared with previous reports [2]. The high intensity CD signals enabled us detail analysis of CD spectra. Using a simple assumption, we could analyze detailed excitonic band structure of SWCNTs for the first time without any theoretical support. We compared our results with the DFT calculations. Interestingly, our results could highly reproduce asymmetric structure of valence and conduction bands of SWCNTs that were predicted by DFT calculations. Typical result for (6, 5) enantiomers was indicted in Fig. 1. We will discuss the other chiralities and a family pattern of them.

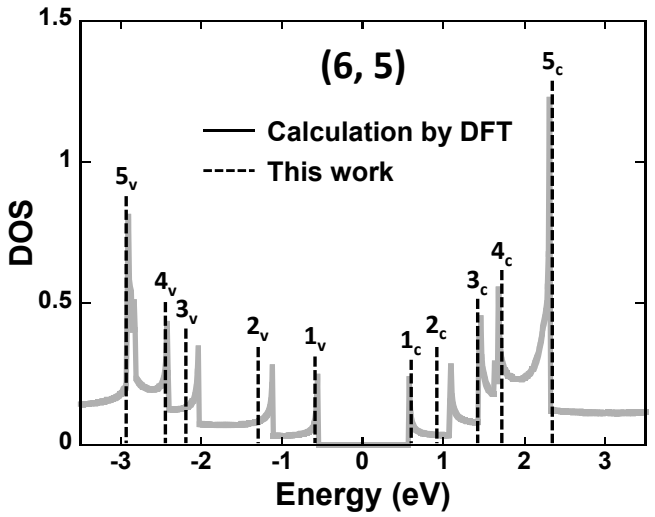

Figure 1. Asymmetric band structure comparison between experimental analysis based on CD spectra (broken line) and theoretical calculation by DFT (solid line) for (6, 5) SWCNTs.

This work was supported by KAKENHI No. 25220602.

[1] A. Sánchez-Castillo and C. Noguez, J. Phys. Chem. C **114,** 9640-9644 (2010).

[2] S. Ghosh et al. Nat. Nanotechnol. **5**, 443-450 (2010).

Corresponding Author: H. Kataura

Tel: +81-29-861-2551, Fax: +81-29-861-2786, E-mail: h-kataura@aist.go.jp

On-chip monolithic integration of microsupercapacitors with tunable performance.

○Karolina Laszczyk[1], Kobashi Kazufumi[2], Shunsuke Sakurai[2], Atsuko Sekiguchi[2], Don N. Futaba[2], Takeo Yamada[2], Kenji Hata[2]

[1] *Technology Research Association for Single Wall Carbon Nanotubes (TASC), Tsukuba 305-8565, Japan*
[2] *National Institute of Advanced Industrial Science and Technology (AIST), Tsukuba 305-8565, Japan*

The progress in thin light-weight electronics has been advanced about new class of tiny energy devices [1-2]. This approach takes benefit of use of novel nano-carbon materials and Si-based technology to form planar, micro-scale supercapacitor electrodes with the power densities of commercial bulky energy devices. Recently, we developed the microsupercapacitor possessing the same performance (operational voltage, capacitance, speed) as a commercial target Al capacitor despite being $1/1000^{th}$ in size [3]. To achieve it, we proposed the technology to isolate electrochemically micro-scale EDLCs with 100 μm cell-to-cell distance and used basic physical rules to achieve high voltage and capacitance by addition of capacitors in series or in parallel, respectively. It means a single electrochemically isolated micro-EDLC with defined performance can be used as a building block to form arbitrary arrangements. In this way we approach the new class of energy devices where the capacitance and the operational voltage are not limited by chemical and physical properties of used materials, whereas the speed is unchanged. As a result our IEDC could achieved ~173 higher volumetric capacitance, the power density of 2271 Wcm^{-3}, energy density of ~7 $mWhcm^{-3}$, and as high as 100 operational voltage.

Towards the practical application of our device, there is a need to support it with an additional characterization of the arbitrary arrangements of cells. Here, the use of the complex capacitance calculated from the impedance spectroscopy data could provide the evaluation of performance related to porous electrodes uniformity among the cells. By set of 1-10 cells in series and in parallel we investigated the complex plot of capacitance versus frequency (Fig.1).The results of real capacitance transition and imaginary capacitance peaks provide the useful information towards further improvements and future directions for industrialization of our tiny energy circuit. This presentation is based on results obtained from a project commissioned by the NEW Energy and Industrial Technology Development Organization (NEDO).

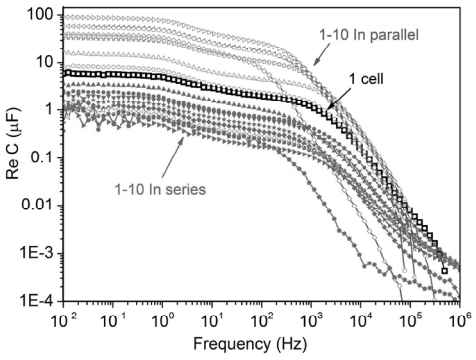

Fig.1. Graph of complex capacitance: frequency vs real capacitance for 1-10 cells in parallel and in series.

[1] M.F. El-Kady et al., *Nat. Comm. 2013,* pp. 1-9.
[2] Z.-S. Wu et al., *Nat. Comm. 2013,* pp. 1-8.
[3] K. Laszczyk et al., *Adv. En. Mat,* published online on 7th july 2015, DOI: 10.1002/aenm.201500741
Corresponding Author: A. Sekiguchi ,
Tel: +81-29-861-4611, Fax: +81-29-861-4851, E-mail: atsuko-sekiguchi@aist.go.jp

In-plane TEM investigation on mono- and bi- metallic catalyst for growth of single walled carbon nanotubes

○Rong Xiang[1], Akihito Kumamoto[2], Kehang Cui[1], Hua An[1], Yang Qian[1], Taiki Inoue[1], Shohei Chiashi[1], Yuichi Ikuhara[2], Shigeo Maruyama[1, 3]

[1] *Department of Mechanical Engineering, The University of Tokyo, Tokyo 113-8656, Japan*
[2] *Institute of Engineering Innovation, The University of Tokyo, Yayoi 2-11-16, Tokyo 113-8656, Japan*
[3] *Energy NanoEngineering Laboratory, National Institute of Advanced Industrial Science and Technology (AIST), 1-2-1 Namiki, Tsukuba 205-8564, Japan*

We propose a technique to obtain the in-plane view of catalyst particles using a Si/SiO_2 TEM grid, which contains a thin SiO_2 film window made by micro-fabrication. This high temperature resistible grid allows the direct imaging of nano-sized particles on the SiO_2 film and minimizes information change/loss from growth chamber to TEM column. Crystal structure, elemental distribution, as well as statistical information of hundred thousands of particles can be obtained. By this technique, we achieve a series of improved/new understanding on the catalyst for SWNT growth.

1) For monometallic particles, morphology and structure of catalyst before and after chemical vapor deposition are directly observed, which clearly suggests Co forms much smaller particles on SiO_2 than Fe or Ni, and explains the difference in efficiency for SWNT growth.

2) In CoCu bimetallic catalyst, Z-contrast Scanning TEM images shows that Cu prohibits Co from aggregating into larger growth sites by anchoring smaller Co on Cu (Fig. 1). SWNTs with all sub-nm diameter are produced on flat substrate from this combination.

3) In CoW system, strong interaction and alloying between Co and W occurs at temperatures higher than 700 °C, as evidence by EDS and electron diffraction. This is in good agreement with experimental observations that high temperature reduced CoW catalyst selectively produces (12, 6) SWNTs while low temperature reduced one has no selectivity. At optimized condition, simple sputtered CoW produce (12, 6) SWNTs with an enrichment of 60-70%.

We expect this technique provide a unique chance towards fundamental understanding of SWNT growth, as well as novel strategies for better control over SWNT structure, such as diameter, and chirality.

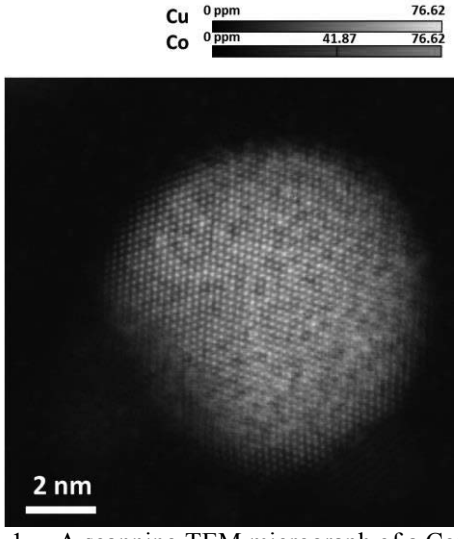

Fig. 1. A scanning TEM micrograph of a CoCu particle on SiO_2 film overlapped EDS mapping.

Corresponding Author:
R. Xiang, Tel: +81-3-5841-6408; E-mail: xiangrong@photon.t.u-tokyo.ac.jp
S. Maruyama, Tel: +81-3-5841-6421; E-mail: maruyama@photon.t.u-tokyo.ac.jp

Selective Synthesis of Cobalt-sulfur Nano Cluster Using a Templating Fullerene Ligand

○Yutaka Matsuo[1]

[1] *Department of Chemistry, School of Science, The University of Tokyo, 7-3-1 Hongo, Bunkyo-ku, Tokyo 113-0033, Japan*

Metal chalcogenide clusters are known as highly potential structural motifs of enzymatic active sites, catalysts, optical/optoelectronic materials, and so on. Among such cluster complexes, those containing of cobalt and sulfur are particularly attractive because their photoelectric and optomagnetic properties. Moreover, some intriguing properties are known for cobalt sulfide nanoparticles, giving rise to interests on cobalt–sulfur cluster complexes.

In this presentation, we discuss the selective synthesis of the well-defined Co_8S_{15} cluster complex (Figure 1) starting from a cobalt trisulfide complex.[1–3] The precursor cobalt trisulfide complex served as a cobalt–sulfur source as well as a powerful sterically templating terminal ligand. Crystallographic, electrochemical, and magnetic measurements elucidated a mixed-valence nature of the cluster with two high-spin cobalt(II) centers. The present study will provide new opportunities for development of artificial functional metal–sulfur cluster complexes for various applications.

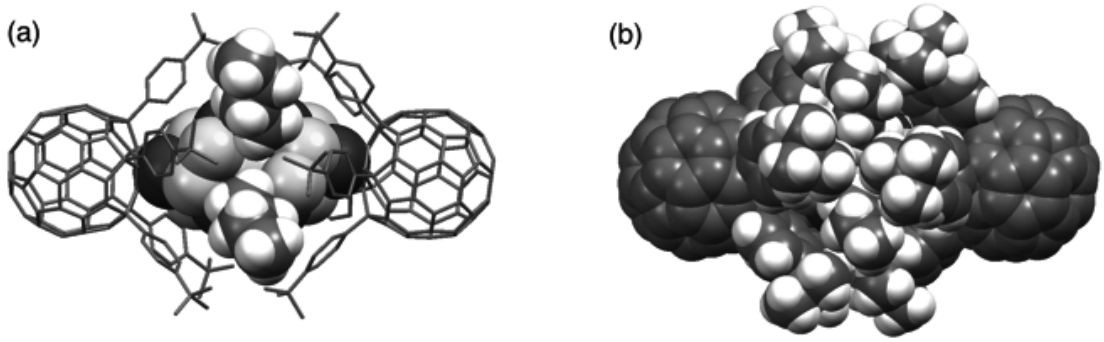

Figure 1. Crystal structure of the Co_8S_{15} cluster complex (solvent molecules and disordered moieties are omitted). (a) Space-filling model for the central $Co_8S_{13}(SR)_2$ moiety. (b) Space-filling model for the whole molecule.

[1] M. Maruyama, J.-D. Guo, S. Nagase, E. Nakamura, Y. Matsuo, *J. Am. Chem. Soc.* **2011**, *133*, 6890.
[2] Y. Matsuo, M. Maruyama, *Chem. Commun.* **2012**, *48*, 9334. (Feature Article)
[3] M. Maruyama, M. König, D. M. Guldi, E. Nakamura, Y. Matsuo, *Angew. Chem. Int. Ed.* **2013**, *52*, 2613.
[4] M. Maruyama, K. Imoto, M. König, D. M. Guldi, S. Ohkoshi, E. Nakamura, Y. Matsuo, *J. Am. Chem. Soc.* **2013**, *135*, 10914.

Corresponding Author: Y. Matsuo
Tel: +81-3-5841-1476, Fax: +81-3-5841-1476
E-mail: matsuo@chem.s.u-tokyo.ac.jp

Regioselectively controlled synthesis of multifunctionalized C_{60} and C_{70} fullerenes

○Hiroshi Moriyama[1], Kouya Uchiyama[1], Miki Igarashi[1], Keita Watanabe[1], Haruka Takahashi[1], Kenji Yoza[2]

[1]*Department of Chemistry, Toho University, Miyama 2-2-1, Funabashi 274-8510, Japan*
[2]*Bruker AXS, Moriyacho 3-9, Yokohama, 221-0022, Japan*

Regioselectively controlled synthesis of fullerene derivatives with multiaddends has attracted much attention because multifunctionalized fullerenes have unique properties derived from their contracted π system as well as addends attached to the fullerene frameworks. However, it is difficult to synthesize them regioselectively because there are many reaction sites on the carbon skeleton of the fullerenes for successive substitution reactions. We have noted that the halogenofullerenes, $C_{60}Br_6$ and $C_{60}Br_8$ [1] have unique well-characterized structures suitable for a starting material, although they have never been used for that purpose, particularly $C_{60}Br_8$, because of their extremely low solubility in organic solvents. We report here regioselective synthesis of novel octaalkoxyfullerenes, $C_{60}(OR)_8$ (R = CH_3, C_2H_5, CH_2CF_3) by a substitution reaction of the halogenofullerenes, $C_{60}Br_8$, as well as alkoxyfullerenes and their derivatives, $C_{60}(OH)_5X$ and $C_{60}(OSiMe_3)_5X$ (X = Cl, Br), from the corresponding starting fullerenes, $C_{60}X_6$. These fullerene compounds, isostructural with the starting material, were fully characterized using ^1H, ^{13}C, and ^{19}F NMR spectroscopy as well as X-ray single-crystal structural analysis.

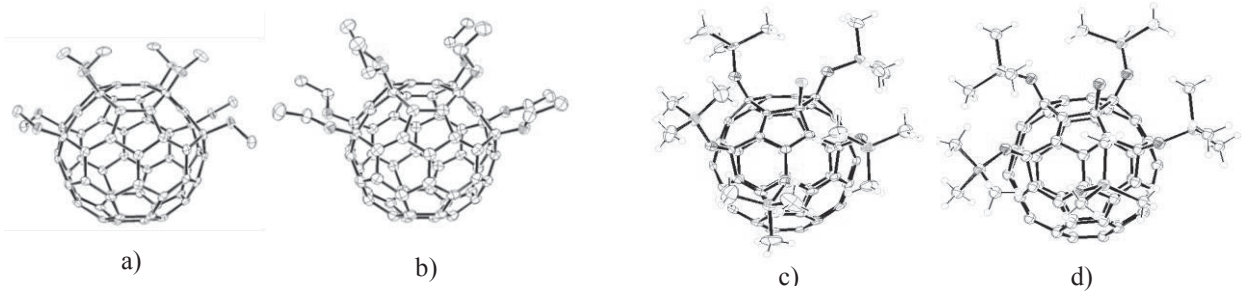

Fig. 1. Crystal structures of a) $C_{60}(OMe)_8$, b) $C_{60}(OEt)_8$, c) $C_{60}(OSiMe_3)_5Cl$, and d) $C_{60}(OSiMe_3)_5Br$.

In addition, we have also succeeded in the regioselective synthesis of $C_{70}(OR)_{10}$ (R = CH_3, C_2H_5, C_3H_7, $CH(CH_3)_2$) from $C_{70}Br_{10}$ [2], as shown in the following scheme.

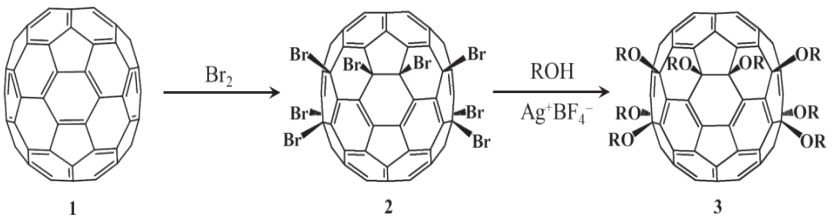

Scheme 1.

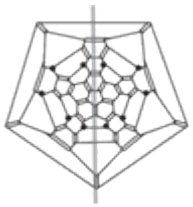

Fig. 2. Schlegel diagram of $C_{70}Br_{10}$ and $C_{70}(OR)_{10}$

[1] P. R. Birkett, P. B. Hitchcock, H.W. Kroto, R. Taylor, D. R. M. Walton, *Nature* **1992**, *357*, 479–481.
[2] M. M. Wienk, J. M. Kroon, W. J. H. Verhees, J. Knol, J. C. Hummelen, P. A. van Hal, R. A. J. Janssen, *Angew. Chem. Int. Ed.* **2003**, *42*, 3371–3375.

Corresponding Author : Hiroshi Moriyama TEL: +81-47-472-1211, FAX: +81-47-472-1188, E-mail: moriyama@chem.sci.toho-u.ac.jp

Electronic structure of $Y_2@C_{82}$-C_{3v} and $Lu_2@C_{82}$-C_{3v}

○Takafumi Miyazaki[1, 3], Gaku Takasumi[1], Hajime Yagi[1], Hisanori Shinohara[2] and Shojun Hino[1]

[1]*Graduate School of Science and Engineering, Ehime University, Matsuyama 790-8577, Japan*

[2]*Graduate School of Science, Nagoya University, Nagoya 464-8602, Japan*

[3]*Faculty of Science, Okayama University, Okayama 700-8530*

We have been measuring ultraviolet photoelectron spectra (UPS) of endohedral fullerenes to clarify their electronic structure [1, 2]. Here, we present UPS of $Y_2@C_{82}$-C_{3v} and $Lu_2@C_{82}$-C_{3v} and discuss their electronic structures with an aid of DFT calculation.

The UPS onset energy of $Y_{2@}C_{82}$ and $Lu_2@C_{82}$ is slightly smaller than empty C_{82}. The deeper valence band UPS (BE > 5 eV) of $Y_2@C_{82}$-C_{3v} and $Lu_2@C_{82}$-C_{3v} are analogous to those of other endohedral fullerenes, while the upper valence band UPS (BE < 5 eV) are significantly different from those of endohedral C_{82} fullerenes of other cage symmetry.

The UPS of $Y_2@C_{82}$-C_{3v} was well reproduced by a simulated spectrum obtained from DFT geometry optimized structure. However, the UPS of $Lu_2@C_{82}$-C_{3v} could not be reproduced well by simulated spectra obtained from DFT calculation. Actually DFT calculation yields two optimized structure for $Lu_2@C_{82}$-C_{3v}. The formulation energy difference between these two optimized structures is very small. A simulated spectrum obtained by adding these two simulated spectra reproduced the UPS of $Lu_2@C_{82}$-C_{3v} very well. From the calculated energy diagrams of $Lu_2@C_{82}$, empty C_{82} of the same C_{3v} cage symmetry, a formal oxidation state of the fullerene can be described as C_{82}^{4-}. However, the XPS Lu3d of $Lu@C_{82}$-C_{3v} and $Lu_2@C_{82}$-C_{3v} suggested Lu^{3+} oxidation state [3]. The DFT calculation results present new binding orbital formation between two entrapped Lu atoms. Thus, the electronic configuration of $Lu_2@C_{82}$ is $(Lu\text{-}Lu)^{4+}@C_{82}^{4-}$. Similarly, it could be clarified the binding orbital formation between entrapped Y atoms in $Y_2@C_{82}$-C_{3v}. Present results could be to support an empirical rule that the electronic structure of endohedral fullerenes was principally governed by the number of transferred electrons and cage structure.

[1] T. Miyazaki, S. Hino et al, Chem. Phys., 447 (2015) 71, [2] T. Miyazaki, S. Hino et al, Chem. Phys., 431-432 (2014) 47, [3] The 38st Fullerene-Nanotube-Graphene General Symposium p25 (2010).

Corresponding Authors: T. Miyazaki, E-mail: tmiyazaki@okayama-u.ac.jp, phone: 086-251-7901; S. Hino, E-mail: hino@gakushikai.jp.

Effect of layered-structure carbon-nanotube sheets on electric properties of brain wave electrodes

○Shunzo Suematsu[1], Akira Kawamoto[2], Kousuke Awara[3], Ryuhei Kitai [3]

[1] *Basic Research Center, R&D Headquarters, Nippon Chemi-Con Corporation, Kanagawa 213-0012, Japan*

[2] *Electrical and Electronic Engineering, Fukui National College of Technology, Geshi-cho, Sabae-city, Fukui 916-8507, Japan.*

[3] *Department of Neurosurgery, University of Fukui, 23 Shimoaizuki Eiheijimatsuoka, Yoshida-gun, Fukui 910-1193, Japan.*

Carbon nanotube (CNT) sheets have been developed for fabricating brain wave electrodes. In our previous study, we found that a multi-wall CNT/polymethyl-methacrylate (MWCNT/PMMA) composite electrode allowed the measurement of brain waves as accurately as conventional Ag disk electrodes, without distorting X-ray, computed tomography (CT), and magnetic resonance imaging (MRI) [1]. In order to measure brain waves more accurately, we next focused on binder-free sheets made of long CNTs which were originally prepared for electric double layer capacitor electrodes. In this study, electric properties of these sheets with layered or non-layered structure were investigated.

Layered and non-layered CNT sheets were prepared using the paper-making method. The obtained four types of sheets, i.e., layered single-wall CNT (SWCNT), non-layered SWCNT, layered MWCNT, and non-layered MWCNT were analyzed by sheet conductivity measurement and impedance spectroscopy. Table 1 shows the sheet resistance of the prepared CNT sheets and a carbon fiber (CF) sheet. The layered SWCNT and MWCNT sheets exhibited lower resistance than the non-layered SWCNT and MWCNT sheets, respectively. This would be caused by a lower contact resistance of the highly densified CNT layers and/or a high interfacial contact area between the layers. For impedance spectroscopy, all of the CNT sheets exhibited absolute impedance values lower by one to three orders of magnitude compared with the CF sheet and Ag disk electrode in the frequency range from 1 to 10 Hz, where most of the brain waves exist (Fig.1). This suggests that the CNT sheets, especially the layered sheets, could measure brain waves more accurately compared with the CF sheet and Ag disk electrodes.

Table 1. Sheet resistance and density of CNT sheets.

	Sheet resistance (Ω)	Sheet density (g/cc)
Layered SWCNT	14	0.36
Non-layered SWCNT	17	0.26
Layered MWCNT	43	0.33
Non-layered MWCNT	60	0.19
cf. Carbon fiber	5000	0.04

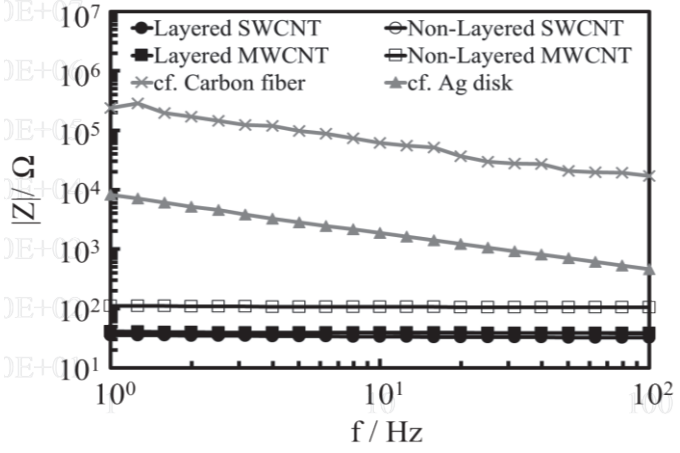

Fig.1. Absolute impedance values (|z|) *vs.* frequency (f) for four different CNT sheets and a carbon fiber sheet and Ag disk electrode (non-layered SWCNT is highly overlapped with layered MWCNT).

[1] Awara *et al.* BioMedical Engineering OnLine, **13**:166 (2015).

Corresponding Author: A. Kawamoto
Tel: +81-778-62-8267, Fax: +81-778-62-3413,
E-mail: kawamoto@fukui-nct.ac.jp

Robust and Soft Elastomeric Field Effect Transistors Tolerant to Diverse Variety of Applied Loads

○Atsuko Sekiguchi[1], Fumiaki Tanaka[2], Shunsuke Sakurai[2], Don N. Futaba[2], Takeo Yamada[2], Kenji Hata[2]

[1] *National Institute of Advanced Industrial Science and Technology, Tsukuba 305-8565, Japan*

[2] *Technology Research Association for Single Wall Carbon Nanotubes (TASC), Tsukuba 305-8565, Japan*

Realization of electronics that can withstand the mechanical loads in our daily actions and provide softness for human body to feel comfort with freedom of movement would enable new applications, such as wearable system for personal health monitoring and therapeutics. While recent progress in material engineering has afforded flexibility and stretchability to electronics either designing new structure architectures [1] of conventional materials or developing new materials [2], it is still a great challenge to realize the devices tolerant to diverse variety of applied loads, such as bending, twisting, stretching, compression and impact.

Here, we have fabricated elastomeric field effect transistors (FET) where the substrate, electrodes and gate dielectric were all made from elastomeric materials with two types of single walled carbon nanotubes (SWNTs) [2, 3] that introduce electrical functionality. The mechanical softness and robustness of both the channel and electrodes benefit from the SWCNT network structure resulting from the use of such high aspect ratio and pure SWCNTs. Our elastomeric FET could tolerate every punishment our clothes experience, such as being stretched (elasticity: ~110%), bent, compressed (>4.0 MPa), and impacted (>6.26 kgm/s). In addition to this, we have demonstrated that it could still be operated after exposure to the harshest environment in our daily life, such as being run over by a car, stepped on by high heeled shoes, hammer strikes, and laundering.

Our electronic device provides a novel design principle for electronics and wide range applications representing one step forward towards electronics that are fully compatible with clothes or our daily actions.

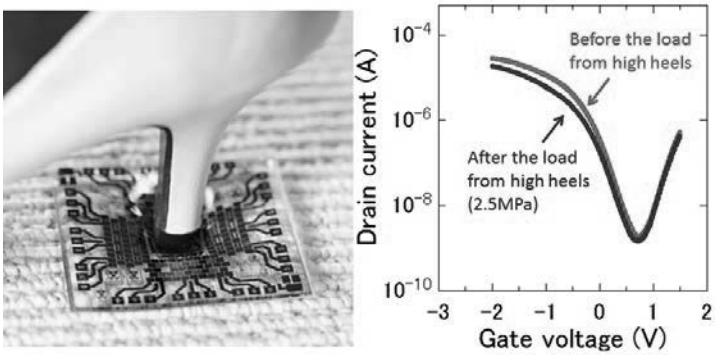

Transfer characteristics of the FET before (red) and after (blue) the load from high heels

[1] D.-H. Kim et al. *Science*, ***320***, 507 (2008).

[2] T. Sekitani et al. *Science* ***321***, 1468 (2008).

[3] K. Ihara et al. *Phys. Chem. C*, ***115***, 22827(2011).

Corresponding Author: A. Sekiguchi

Tel: +81-29-861-4654, Fax: +81-29-861-4851,

E-mail: atsuko-sekiguchi@aist.go.jp

Indium-Free Flexible Planar Heterojunction Perovskite Solar Cells using Single-walled Carbon Nanotube film as Electrode, and Investigation of Hole-transporting Layers and Dopants thereof

○ Il Jeon[1], Takaaki Chiba[2], Clement Delacou[2], Esko I. Kauppinen[3], Shigeo Maruyama[2], Yutaka Matsuo[1]

1 Department of Chemistry, School of Science, The University of Tokyo, 7-3-1 Hongo, Bunkyo-ku, Tokyo 113-0033, Japan
2 Department of Mechanical Engineering, School of Engineering, The University of Tokyo, 7-3-1 Hongo, Bunkyo-ku, Tokyo 113-8656, Japan
3 Department of Applied Physics, Aalto University School of Science, 15100, FI-00076 Aalto, Finland

Recent emergence of perovskite solar cells have drawn much attention owing to excellent power conversion efficiency arising from a long exciton diffusion length, high absorption and carrier mobility. Since ITO is indispensible in perovskite solar cells much like in other photovoltaic devices, there are numerous problems such as rising cost and inflexibility. Many organic solar cells researchers have been vigorously working on replacement of ITO by carbon nanotube. Yet, the same application in perovskite solar cells has not been reported to date. Therefore, in this work, we investigated diverse methodologies that can achieve carbon nanotube electrode in indium-free perovskite solar cells. We found that modified PEDOT:PSS function as both electron- blocking layer and dopant analogue to the organic photovoltaics while MoO_3 is not compatible which is unique to the perovskite system. We discovered that diluted nitric acid doping with a concentration of 35% serves as the most effective method to enhance optical conductivity of carbon nanotube in a safe manner. A PCE of 6.32% in an ITO-free planar heterojunction perovskite solar cell was recorded when its indium tin oxide based reference gave 9.05%. Further flexible application showed 5.38% on a PET substrate.

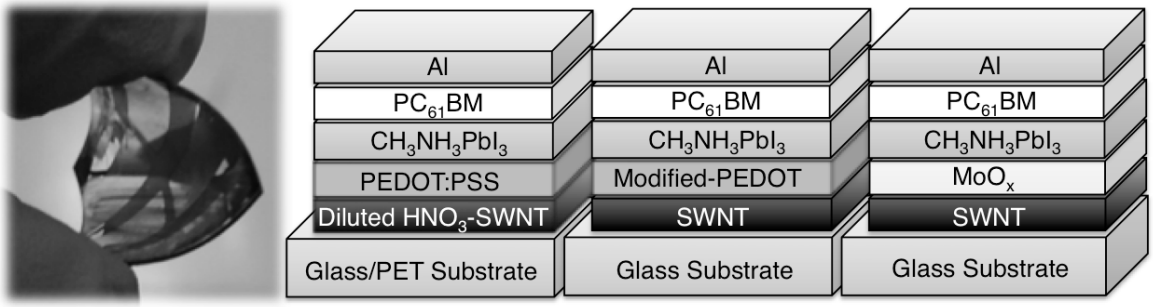

Fig.1: Illustration of various single-walled carbon nanotube based inverted perovskite solar cells

Corresponding Author: Y. Matsuo, Tel: +81-3-5841-1476, E-mail: matsuo@chem.s.u-tokyo.ac.jp

Contact resistivity evaluation of parallel adjacent CNTs from in-plane conductivity of dense CNT forest on silicon carbide

○Masafumi Inaba[1], Wataru Norimatsu[2], Michiko Kusunoki[2], Hiroshi Kawarada[1]
[1] *Graduate School of Advanced Science and Engineering, Waseda University, Tokyo 169-8555, Japan*
[2] *Eco Topia Science Institute, Nagoya University, Aichi 464-8603, Japan*

It is important to understand the electrical contact of parallel adjacent CNTs for CNT thin film transistors with dispersed CNT channels and CNT yarns. We have reported the in-plane conductivity of dense carbon nanotube forest on silicon carbide substrate (CNT forest on SiC).[1] Here we additionally discuss the contact conductivity estimation of parallel adjacent CNTs evaluated from the in-plane conductivity.

The in-plane conductivity of dense CNT forest on SiC was evaluated to be ~50 S/cm. In CNT bulk region, CNT should be parallel adjacent to each other. We assumed three approximations to evaluate the contact resistivity. First, CNTs have the same diameter and are densely packed with the hexagonal pattern. Second, CNT/CNT contact conductivity is the same for CNTs with the same diameter. Third, CNT conductivity is much higher than the CNT/CNT contact conductivity. With these approximations, CNT forest is described as the net-like circuit in Fig.1. In CNT bundle or forest, CNTs are parallel adjacent to each other, and should have deformative cross-section like hexagon, where CNTs contact to each other with the larger area than the case of having perfectly circle cross-section. Fig. 2 shows the schematic image of microscopic deformative CNT contact. For large diameter CNTs, the maximum contact width is estimated to be D/2-0.1 nm, where D is the diameter of CNT. Considering the CNT diameter is 5–10 nm, the contact resistivity was in the range of 0.8–1.7×10^{-8} Ωcm^2.

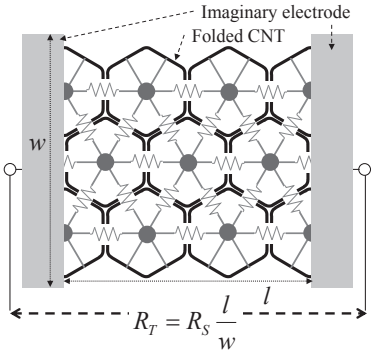

Fig. 1 Approximated resistance network of parallel adjacent CNT forest.

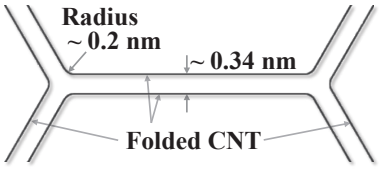

Fig. 2 The schematic image of microscopic folded CNT contact.

To verify the CNT/CNT contact resistivity, we calculated the tunneling resistance of graphene/graphene interlayer. The tunneling contact resistivity R_{TC} is written as

$$R_{TC} = \frac{V}{J_T} = \left[\left(\frac{q^2}{h^2 d} \right) \sqrt{2m_e \phi} \exp\left(-\left(\frac{4\pi d}{h} \right) \sqrt{2m_e \phi} \right) \right]^{-1}$$

where q is elementary charge, h is Plank's constant, d is the tunneling distance, m_e is the electron (effective) mass, and ϕ is the barrier height. Fig. 3 shows the calculated contact resistivity as a function of the tunneling distance d, where m_e=m_0 (electron mass), and ϕ=5.0 eV are assumed.[2] In CNT/CNT contact, d corresponds to be the distance between sp^2 electron clouds on contact area of graphene sheets. Thus d should be lower than the graphite interlayer distance (~0.34 nm). From fig. 3, the corresponding to 0.24 -0.28 nm, which is lower than graphite interlayer distance and is in good agreement with the assumption.

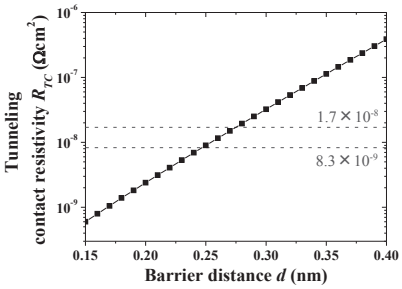

Fig. 3 Relationship between tunneling contact resistivity R_{TC} and barrier distance d.

[1] Inaba et al., The 47th FNTG General Symposium, 2P-7
[2] P. Sutter et al., Nature Materials **7**, 406 - 411 (2008).

Corresponding Author: M. Inaba Tel&Fax: +81-3-5286-3391 E-mail: inaba-ma@ruri.waseda.jp

Photovoltaic performance of perovskite solar cells using carbon nanotubes/graphene oxide hole transport layer

Feijiu Wang[1], Masaru Endo[2], Shinichiro Mouri[1], Yuhei Miyauchi[1], Yutaka Ohno[3], Atsushi Wakamiya[2], Yasujiro Murata[2], and Kazunari Matsuda[1]

[1]Institute of Advanced Energy, Kyoto University, Uji, Kyoto 611-0011, Japan

[2]Institute for Chemical Research, Kyoto University, Uji, Kyoto 611-0011, Japan

[3]EcoTopia Science Institute, Nagoya University, Nagoya 464-8603, Japan

Photovoltaic applications using nano-carbon materials (carbon nanotube, graphene, and graphene oxide) have been intensively studied because of their excellent optical and electronic properties.[1-3] Recent researches on the organo-lead perovskite solar cell have been drastically progressed, and high photovoltaic efficiency in the perovskite solar cell has been reported. However, the photovoltaic performance of perovskite solar cell only using carbon nanotube is not high enough at the current stage. Here, we report photovoltaic properties of perovskite solar cells using single-walled carbon nanotube (SWNT) and graphene oxide (GO) as the hole transporting layer. Figure 1 shows the current density-voltage (*J-V*) curves of organo-lead perovskite solar cell ($CH_3NH_3PbI_3$) using only SWNT and SWNT/GO layer as a hole-transport layer under AM 1.5 conditions. The *J-V* curve of perovskite solar cell using only SWNT layer (perovskite/SWNT) shows a short-circuit current density (J_{sc}) of 10.5 mA/cm^2, an open-circuit voltage (V_{oc}) of 0.73 V, a fill factor (FF) of 64%, resulting in an efficiency of 4.9%. In contrast, the *J-V* curve of perovskite solar cell using SWNT/GO layer (perovskite/SWNT/GO) exhibits high J_{sc} of 20.1 mA/cm^2 associated with V_{oc} of 0.95 V, and a FF of 61%, which results the high efficiency of 11.7%. The GO in the SWNT network contributes to reduction of recombination loss as an electron blocking layer and enhance the build-in-voltage giving a higher short circuit current density and open circuit voltage.

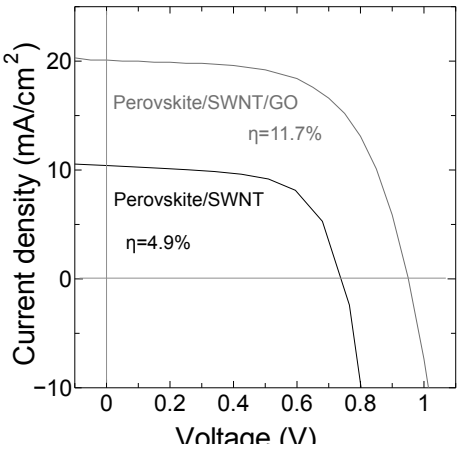

Fig. 1 *J-V* curve of perovskite solar cell using only SWNT layer (perovskite/SWNT) and SWNT/GO layer (perovskite/SWNT/GO)

References

[1] Appenzeller, J. *et al*., Phys. Rev. Lett. **89,** 126801 (2002).

[2] Miyauchi, Y. *et al*., Nat. Photonics **7,** 715 (2013).

[3] Wang, F., Nat. Commun. **6,** 6305 (2015).

Corresponding Author: Feijiu Wang

Tel: +81-774-38-3460, Fax: +81-774-38-3460

E-mail: wang.feijiu.75w@st.kyoto-u.ac.jp

Preparation of metal oxide nanofilms using graphene templates

○Sakae Takenaka[1,2], Shuhei Miyake[1], Hideki Matsune[1], Masahiro Kishida[1]

[1] *Department of Chemical Engineering, Kyushu University, Fukuoka 819-0395, Japan*
[2] *JST, PRESTO, 4-1-8 Honcho, Kawaguchi, Saitama, 332-0012*

Nanosheet and nanofilm of metal oxides have lately attracted significant attention due to their specific chemical and physical properties based on their molecular thickness. The nanosheets which are composed of single crystallites of metal oxides have generally been prepared by exfoliation of layered metal oxides and hydroxides. The types of metal oxide nanosheets obtained by this method are inevitably limited because the method requires the layered compounds as host materials. In the present study, we prepared metal oxide nanofilms using graphene oxide (GO) as a template [1]. The nanofilms are composed of polycrystallites of metal oxides.

Dried GO powders were dispersed in cyclohexane containing $Ti(OC_4H_9)_4$, followed by treated in the autoclave at 453 K for 8 h. The sample thus obtained was denoted as TiO_x/rGO. The TiO_x/rGO was calcined at 723 K in air for 5 h to remove graphene by combustion. The samples thus obtained was denoted as TiO_2 nanofilms.

Figure 1 shows TEM images for TiO_x/rGO and TiO_2 nanofilm. The TEM image for TiO_x/rGO was very transparent, although the samples contained TiO_2 of 20 wt%. Any particulate compounds were not seen in the TEM image for the TiO_x/rGO. On the other hand, elemental mappings for TiO_x/rGO indicated the uniform distribution of Ti atoms on the graphene sheets. FT-IR spectrum for TiO_x/rGO suggested the reduction of GO into reduced GO (rGO) during the treatment of the sample in the autoclave at 453 K. Thus, very thin Ti oxide species were uniformly stabilized on the rGO in the TiO_x/rGO. The TiO_x/rGO was calcined in air at 723 K for removal of rGO. The TEM image of the sample obtained by calcination (Figure 1b) was very similar to that of TiO_x/rGO before calcination (Figure 1a). The two dimensional structure of the sample maintained unchanged after the calcination of TiO_x/rGO in air, although the rGO was removed by combustion. The thickness of the TiO_2 nanofilms was evaluated with AFM image to be ca. 1 nm. The selected area electro diffraction patterns implied that the TiO_2 nanofilms are composed of polycrystallites of anatase TiO_2. These results indicated that TiO_x nanofilms were stabilized on the rGO during the treatment of GO in cyclohexane containing $Ti(OC_4H_9)_4$ in the autoclave at 453 K. In addition, free-standing nanofilms composed of polycrystallites of anatase TiO_2 can be obtained by the calcination of TiO_x/rGO in air. Various metal oxide nanofilms such as ZrO_2, Nb_2O_5, Ta_2O_5 and SnO_2 can be prepared by the present method.

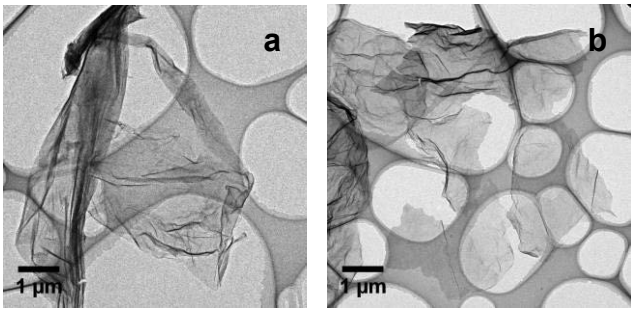

Fig. 1 TEM images for TiO_x/rGO (a) and TiO_2 nanofilms (b).

[1] S. Takenaka *et al*. J. Phys. Chem. C **119**, 12445 (2015).

Corresponding Author: S. Takenaka
Tel: +81-92-802-2752, Fax: +81-92-802-2752,
E-mail: takenaka@chem-eng.kyushu-u.ac.jp

Electrical activation of dark excitonic states in carbon nanotubes

○T. Uda, M. Yoshida, A. Ishii, Y. K. Kato*

Institute of Engineering Innovation, The University of Tokyo, Tokyo 113-8656, Japan

Electric-field effects on exciton states in single-walled carbon nanotubes are investigated by simultaneous photocurrent and photoluminescence excitation spectroscopy. We utilize field-effect transistors with suspended carbon nanotubes in order to apply longitudinal fields [1]. Photoluminescence imaging and excitation spectroscopy are performed to locate individual nanotubes and to identify their chirality. When a bias voltage is applied, we observe an emergence of a new absorption peak near the first excited state in both photoluminescence and photocurrent spectra [2]. With excitation at the new peak, photocurrent begins to flow above a threshold bias, while the luminescence intensity starts to decrease. Furthermore, we have found another bias-induced peak at a higher energy in the photocurrent spectra which has a threshold at a lower bias. Measurements of several nanotubes with different chirality reveal that the energy separation between these bias-induced peaks and the ground state of E_{11} excitons is inversely proportional to the tube diameter. The results suggest that the new peaks are the dark excited states of the E_{11} excitons which became optically active due to the applied fields.

Work supported by KAKENHI (24340066, 26610080), the Canon Foundation, Asahi Glass Foundation, as well as the Photon Frontier Network Program of MEXT, Japan. The devices were fabricated at the Center for Nano Lithography & Analysis at The University of Tokyo. M.Y. is supported by ALPS, and A.I. is supported by MERIT and JSPS Research Fellowship.

[1] Y. Kumamoto, M. Yoshida, A. Ishii, A. Yokoyama, T. Shimada, and Y. K. Kato, Phys. Rev. Lett. **112**, 117401 (2014)..

[2] T. Uda, M. Yoshida, A. Ishii, Y. K. Kato, 6th Workshop on Nanotube Optics and Nanospectroscopy (WONTON2015) P67, Kloster Banz, Germany, June 3, 2015; The Sixteenth International Conference on the Science and Application of Nanotubes (NT15) P193, Nagoya, Japan, June 30, 2015; manuscript in preparation.

Corresponding Author: Y. K. Kato
Tel: +81-3-5841-7702, Fax: +81-3-5841-7772,
E-mail: ykato@sogo.t.u-tokyo.ac.jp

Optical transitions in oxygen-doped (5,4) and (6,4) carbon nanotubes

○Mari Ohfuchi[1], Yoshiyuki Miyamoto[2]

[1] *Fujitsu Laboratories Ltd., Atsugi 243-0197, Japan*
[2] *National Institute of Advanced Industrial Science and Technology (AIST), Tsukuba 305-8568, Japan*

Oxygen (O) doping of single-wall carbon nanotubes (SWCNTs) has attracted attention because of their greater luminescence quantum yield than that of pristine CNTs [1]. Low temperature photoluminescence (PL) experiments have revealed multiple peaks associated with different adsorption structures of an O atom [2]. In this study, to advance the fundamental understanding in PL spectra of O-doped SWCNTs, we theoretically investigate the optical transitions in different type semiconducting CNTs, (5,4) and (6,4).

We employed a finite length model (8 nm) for a SWCNT with the edges terminated by hydrogen atoms. The optimized geometries and the adsorption energies (Fig.1) were obtained [3] using the density functional theory (DFT) code, OpenMX [4]. The optical transition energies (Fig.2) and densities (Fig.3) were determined using time-dependent DFT approach based on STO-3G basis set and B3LYP functional as implemented in Gaussian program. The "epoxy-b" and "epoxy-c" structures were obtained in addition to the most stable "ether-a" structure for both CNTs. In (5,4), the energy level of E_{11}^* peak originating from the oxidation sharply drops below the level of the dark states with "epoxy-b" structure; meanwhile this sharp drop is the case with "epoxy-c" structure for (6,4). This is attributed to the different electronic structures between type I and II of SWCNTs, which also cause the behavior in the adsorption energies (Fig.1). Our results may explain the split of E_{11} and E_{11}^* into three in low temperature PL experiments [2].

Although the setting in the present study is considered to be sufficient to describe a qualitative picture [2], results with longer CNTs and larger basis sets will also be presented at the symposium.

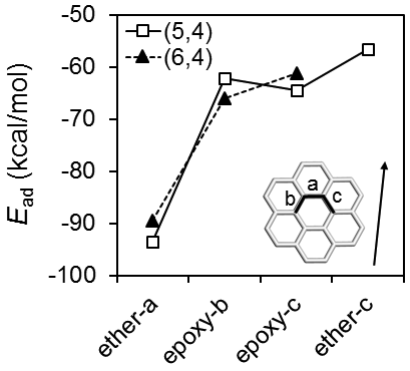

Fig.1: Adsorption energies, E_{ad} = E(CNT + O) − E(CNT) − E(O), of different adsorption structures. The definition of bonds "a", "b", and "c" is inserted. The nanotube axis is indicated by an arrow.

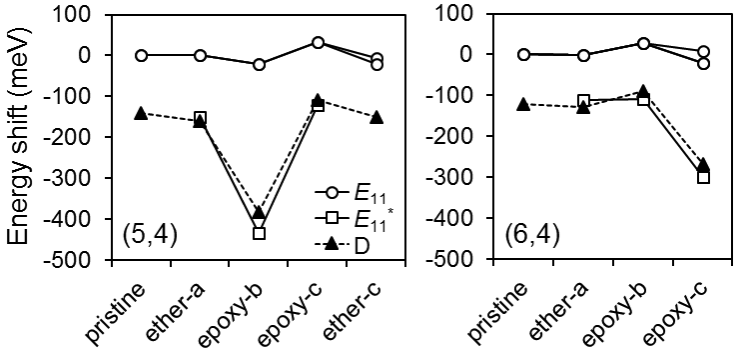

Fig.2: Energy shifts of the optical transitions from E_{11} of pristine nanotubes. The E_{11}^* is red-shifted states originating from the oxidation. The D stands for the optically forbidden dark states.

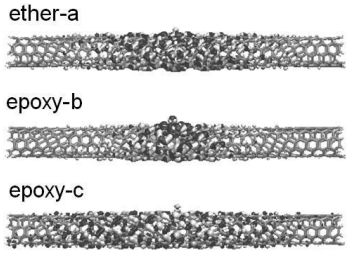

Fig.3: Spatial distributions of the transition densities for E_{11}^* of (5,4) nanotubes. Gray sticks represent carbon−carbon bonds. The electron and holes are represented in black and light gray, respectively.

[1] S. Ghosh *et al*., Science **330**, 1656 (2010). [2] X. Ma *et al.*, ACS Nano **8**, 10782 (2014).
[3] M. Ohfuchi, J. Phys. Chem. C **119**, 13200 (2015). [4] http://www.openmx-square.org/.

Corresponding Author: M. Ohfuchi
Tel: +81-46-250-8194, Fax: +81-46-250-8274, E-mail: mari.ohfuti@jp.fujitsu.com

Effect of sp^3 defect on the electronic states of single-walled carbon nanotubes determined by in situ PL spectroelectrochemistry

Tomonari Shiraishi[1], Tomohiro Shiraki[1], Naotoshi Nakashima[1,2]

[1]*Department of Applied Chemistry, Kyushu University, Fukuoka 819-0395, Japan*
[2] *WPI-I2CNER, Kyushu University, 744 Motooka, Fukuoka 819-0395, Japan*

Single-walled carbon nanotubes modified with introduction of a very limited amount of sp^3 defect (sp^3-doped SWNTs) are interesting novel materials due to their unique photoluminescence (PL) with enhanced quantum yields compared to those of pristine SWNTs [1]. The sp^3-doping has been achieved by modification with aryl functional groups (Fig. 1), providing the optical property-enhanced SWNTs with unique dependence on the substituent groups. However, the detailed mechanisms on the new optical properties induced by the chemical modification and the effect of sp^3 defect on the electronic properties of SWNTs have been still unclear. One can consider that the appearance of new optical properties is essentially due to changes in the electronic states induced by sp^3 defect on the SWNTs. Thus characterization of the resulting electronic states is crucial to understand fundamental properties of the sp^3-doped SWNTs.

In this study, we report the electronic states of the sp^3-doped SWNTs and the substituent effect of aryl functionalization through the *in-situ* PL spectroelectrochemical method that we developed previously[2]. Fig. 2 shows the evaluated energy levels of the pristine and the sp^3-doped SWNTs modified with three different substituents (-OCH_3, -Br, and –NO_2), in which the highest occupied molecular orbital (HOMO) and lowest unoccupied molecular orbital (LUMO) of the sp^3-doped SWNTs were found to shift to negative and positive values, respectively, compared to those of the pristine SWNTs. Interestingly, we clarified that the HOMO of the sp^3-doped SWNTs showed dependence of the chemical structure of the aryl substituent groups. We will discuss about a possible mechanism for the energy level shifting on the sp^3-doped at the meeting.

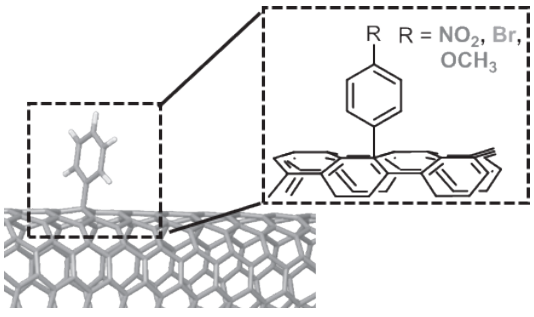

Fig. 1. Chemical structures of sp^3-doped SWNT.

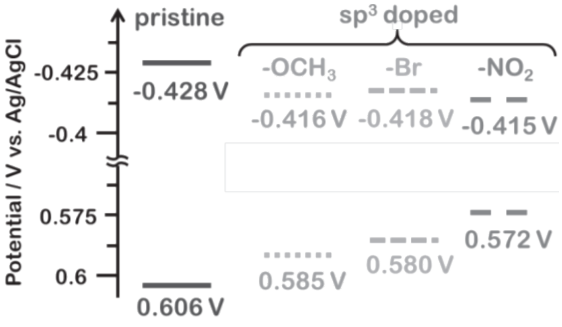

Fig. 2. Evaluated energy levels of the pristine and the sp^3-doped SWNTs.

[1] Y. Wang *et al*., *Nat. Chem*. **5**, 840 (2013). [2] N. Nakashima *et al*., *Angew. Chem. Int. Ed.* **48**, 7655 (2009).
Corresponding Author: Naotoshi Nakashima
E-mail: nakashima-tcm@mail.cstm.kyushu-u.ac.jp

ポスター発表
Poster Preview

1P – 1 ～ 1P – 35
2P – 1 ～ 2P – 35
3P – 1 ～ 3P – 36

Regioselectively Arylated Fullerenes by Acid-catalyzed Reaction of Azafulleroids as an Ambident Base

○Naohiko Ikuma, Koichi Fujioka, Yuta Doi, Ken Kokubo,
Hidehiro Sakurai, Takumi Oshima

Division of Applied Chemistry, Graduate School of Engineering,
*Osaka University, Suita 565−0871, Japa*n

Azafulleroid, derived from 1,3-dipolar cycloaddition of azide with C_{60} followed by nitrogen evolution, behaves as an ambident nucleophile containing one basic nitrogen and two reactive bridgehead double bonds. DFT calculations indicated the larger proton affinity at the bridged nitrogen for alkyl-substituted azafulleroid and at the bridgehead Cα-position for aryl substituted one (Fig. 1). Thus, azafulleroid can be useful synthetic precursor for various fullerene derivatives, depending on its substituents. Here, we report the acid-promoted arylation of variously substituted azafulleroids to give regioselectively arylated fullerene derivatives.

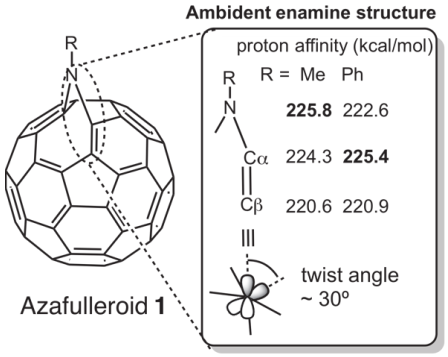

Fig. 1. Proton affinities of azafulleroids (B3LYP/6-31G(d,p))

The arylation of alkyl-substituted azafulleroids with CF_3SO_3H and aryl nucleophiles provided 1,4-arylaminofullerenes **2** (Scheme 1). On the other hand, arylation of aryl-substituted azafulleroids gave tetra- or penta-adducts **3a**/**b**. XRD analysis showed **3b** had cyclopentenyl center [1], in contrast to the previously obtained pentaarylated fullerene having cyclopentadienyl center [2].

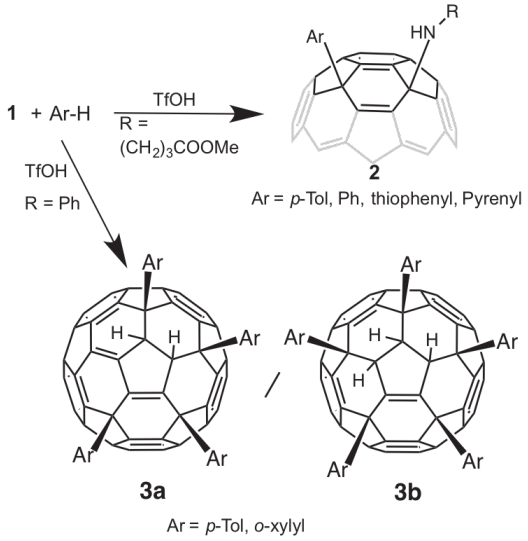

Scheme 1

[1] N. Ikuma *et al.*, Chem. Asian J. **9,** 3084 (2014).
[2] E. Nakamura *et al*., J. Am. Chem. Soc. **118**, 12850 (1996).

Corresponding Author: N. Ikuma
Tel: +81-6-6879-4592, Fax: +81-6-6879-4593
E-mail: ikuma@chem.eng.osaka-u.ac.jp

Solid-State NMR Studies on the Aggregated Structures of Organic Bulk Heterojunction Solar Cells with Solvent Additives (III)

◦Saki Kawano[1] and Hironori ogata[1,2]

[1] Grad. School of Sci. and Engin. , Hosei Univ. , [2]Res.Center for Micro-Nano Technol., Hosei Univ.

E-mail: hogata@hosei.ac.jp

Bulk heterojunction (BHJ) organic solar cells are an emerging technology that has the potential to provide a low cost photovoltaic devices. It is well known that the nanomorphology of the polymer:fullerene BHJ is a critical factor which affects the solar cell performance. The addition of processing additives such as 1,8-diiodooctane (DIO) is widely used approach to increase power conversion efficiencies for many organic solar cells[1-2]. Solid-state solar NMR spectroscopy offers several techniques for the investigation of the morphological, structural, and dynamics properties of BHJ organic solar cells.

We have explored the effects of DIO addition of P3HT/PCBM BHJ films on the local crystallinity and morphology by using solid-state NMR spectroscopy. In this study, we investigated the change in the crystallinity, morphology, and the properties of molecular motions of P3HT/PCBM BHJ film by adding another solvent additives(1,8-Octanedithiol(ODT) and 1-Chloronaphthalene(CN)) and also effects of annealing by using ^{13}C and ^{1}H solid-state NMR spectroscopy.

Mixed solution of P3HT/PCBM of 1:1(w/w) was prepared by mixing P3HT and PCBM into chlorobenzene at a concentration of 1 wt% for 50 hrs in a glove box under argon atmosphere. A 3% by volume of additive ODT or CN was then dropped into the solution and then stirred for 1 hr. The solution was filtered using 0.45μm filter before making films to remove undissolved materials. P3HT/PCBM BHJ films were prepared by dropping the solution in a glass plate and dried in a glove box under argon atmosphere for 40 hrs and then put in the vacuum for 24hrs. Dried film were removed from the glassplate and sealed into 4 mm zirconia NMR rotor. Solid-state NMR spectra were collected on Bruker AVANCE300 spectrometer.

Figure 1 shows the ^{13}C-CP/MAS NMR spectra of (a)P3HT/PCBM BHJ film with CN additive and (b)P3HT/ PCBM BHJ film. The detailed results of the change of morphology and the properties of molecular conformations of P3HT/PCBM BHJ films by CN or ODT addition will be presented.

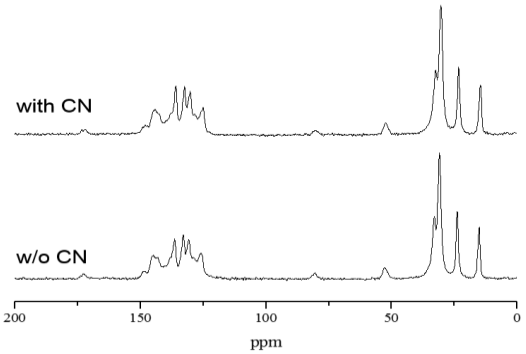

Figure 1. ^{13}C-CP/MAS NMR spectra of (a)P3HT /PCBM BHJ film with CN additive and (b)P3HT/PCBM BHJ film.

References:

1) J. K. Lee et al., *J.Am.Chem.Soc.*,**130**(2008)3619.

2) B.R.Aïch *et al, Organic Electronics*,**13** (2012)1736.

A new method for the isolation of the hidden metallofullerenes like $Y_2@C_{80}$

○Natsumi Nakatori[1], Aimi Togashi[1], Wataru Fujita[2], Koichi Kikuchi[1],
Yohji Achiba[1], Takeshi Kodama[1]

[1]*Department of Chemistry, Tokyo Metropolitan University, Hachioji, 192-0397, Japan*

[2]*Department of Information and Basic Science, Nagoya City University, Nagoya, 467-8501, Japan*

A "hidden" or sometimes called as "missing" fullerene means the fullerenes those which have never been isolated by a conventional separation technique, although their generations themselves have highly been expected. The metallofullerene, $Y_2@C_{80}$, encapsulated in I_h symmetry C_{80} cage is a typical example to be included in such a class of fullerene. Actually, in 2011, Kodama et al. succeeded in extracting $Y_2@C_{80}$ anion directly from the raw soot with a mixed solvent of triethylamine (TEA) and acetone and suggested that some $M_2@C_{80}$ such as $Y_2@C_{80}$ would be simply hidden in the raw soot due to their electronic properties, resulting in their isolations beyond the range of possibility [1]. In the previous study, however, the isolation of $Y_2@C_{80}$ was failed under the conventional HPLC condition, because of their instabilities in toluene. Therefore, no structural evidence on $Y_2@C_{80}$ has been deduced so far. In this study, we intended to develop an *ion-pair chromatography* for isolating $Y_2@C_{80}$ by leaving the anion form as it is. Moreover, we also intended to characterize the cage structure of $Y_2@C_{80}$ whether it is of I_h symmetry or not.

Soot containing Y-metallofullerenes was produced by direct-current (40 A) arc discharge of Y/C composite rods (Y:C=2:98) under a 500 Torr He atmosphere. The raw soot was extracted for 8 h with a mixed solvent of TEA and acetone. The isolation of $Y_2@C_{80}$ was accomplished by three-stage HPLC. Acetone with an ion-pair reagent, tetrabutylammonium bromide, was used as an eluent in all the stages. Firstly, the portion of metallofullerenes was roughly separated, and secondly, $Y_2@C_{80}$ with some impurities was separated. A Buckyprep column was used in the first and second stages. Finally, $Y_2@C_{80}$ was isolated with a Buckyprep-M column. As shown in Fig.1, the UV-vis-NIR absorption spectrum of the isolated $Y_2@C_{80}$ anion is very similar to that of $Ce_2@C_{80}(I_h)$ anion, which is generated electrochemically. Therefore, it is strongly suggested that the $Y_2@C_{80}$ isolated by the present method has $C_{80}(I_h)$ cage. The method combining the ion-pair chromatography with the mixed solvent extraction is a powerful tool to explore the world of hidden metallofullerenes.

[1] T. Kodama, et al. *The 41st Fullerenes-Nanotubes-Graphene General Symposium* 31 (2011).

Corresponding Author: Takeshi Kodama
E-mail: kodama-takeshi@tmu.ac.jp
Tel:+81-42-677-2530, Fax:+81-42-677-2525

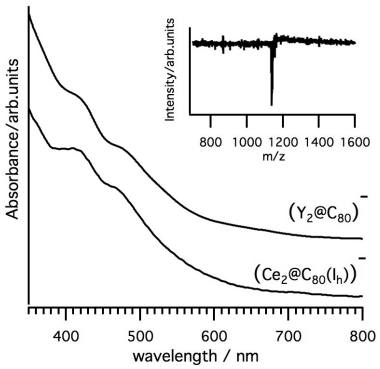

Fig.1 UV-vis-NIR absorption spectra of $Y_2@C_{80}$ anion and $Ce_2@C_{80}$ anion. The inset shows the negative LD-TOF-MS spectrum for $Y_2@C_{80}$ anion.

An atlas of thermoelectric power of semiconducting carbon nanotubes

○ N. T. Hung, A. R. T. Nugraha, R. Saito
Department of Physics, Tohoku University, Sendai 980-8578, Japan

Thermoelectric figure of merit (ZT) is significantly enhanced in one-dimensional (1D) semiconducting nanostructures [1], in particular for semiconducting single wall carbon nanotubes (s-SWNTs), which provide a unique opportunity for high-performance thermoelectricity with large thermoelectric power (TEP) [2]. However, the s-SWNTs can have a wide range of diameter and different geometrical structures, which are denoted by two integers (n, m) known as chirality [3]. Finding a suitable s-SWNT chirality that has a specific value of TEP is thus necessary to apply the s-SWNT in thermoelectric devices.

In this work, we develop an atlas of the TEP for many s-SWNTs within a diameter range of 0.5–1.5 nm by using the Boltzmann transport formalism combined with an extended tight-binding model (ETB) based on the density functional theory (DFT) [4]. We find that the TEP of the s-SWNTs increases with decreasing the tube diameter. For the small s-SWNT with diameter less than 0.6 nm, the TEP can reach a value of 2000 μVK^{-1}, which is about 3-4 times larger than commonly used semiconducting materials in thermoelectric applications. We derive a simple formula to reproduce the numerical calculation and we find that the TEP of the s-SWNTs has a band gap term, which explains the shape of the TEP plot as a function of diameter that looks similar to the so-called Kataura plot [4,5], showing the $2n + m$ family pattern (see Fig. 1). Our results highlight potential properties of s-SWNTs as thermoelectric materials.

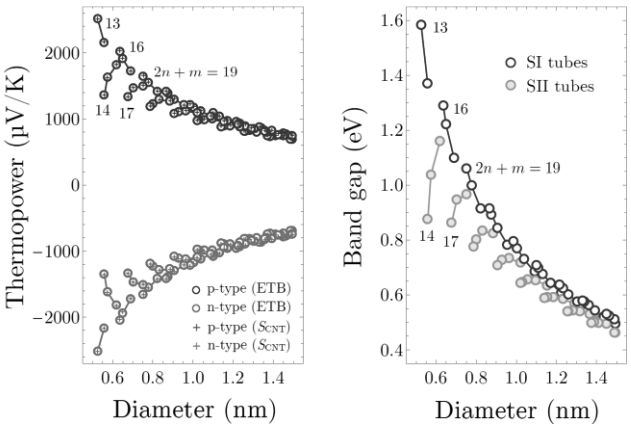

Fig. 1: Thermopower and band gap for s-SWNTs with diameter of 0.5–1.5 nm.

[1] L. D. Hicks et al., Phys. Rev. B **47**, 16631R (1993).
[2] K. Yanagi et al. Nano Lett. **14**, 6437 (2014).
[3] R. Saito, G. Dresselhaus, M. S. Dresselhaus, "Physical properties of carbon nanotubes", Imperial college press (1998).
[4] G. G. Samsonidze et al., Appl. Phys. Lett. **85**, 5703 (2004).
[5] R. Saito et al., Phys. Rev. B **61**, 2981 (2000).

Corresponding Author: Nguyen Tuan Hung
TEL: +81-22-795-6442, FAX: +81-22-795-6447, E-mail: nguyen@flex.phys.tohoku.ac.jp

Stability of chemisorbed oxygen on carbon nanotube surface

○Gergely Juhász[1], Naotoshi Nakashima[2]

[1] *Department of Chemistry, Graduate School of Science, Tokyo Institute of Technology, Tokyo 152-8550, Japan*
[1] *Department of Applied Chemistry, Kyushu University, Fukuoka 819-0395, Japan*

Carbon nanotubes have unique luminescent properties, including sharp, well defined emitting peaks in the NIR region. However, the weak luminescent intensity is a major disadvantage practical applications. Covalent functionalization of nanotubes often induces drastic changes in the optical properties. Gosh et al. have reported [1] an ozonization method that leads to oxygen doped CNTs with red-shifted, bright peaks in their luminescence spectrum [2]. This brighter luminescence can have a great practical importance for industry.

For better understanding the formation and properties oxygen doped sites, we studied the stability and migration of chemisobed oxygen on the surface of single walled carbon nanotubes (SWNTs) with different chirality. For the calculations we used models with periodic boundary condition and DFTB method, which has already been useful in our previous works. To estimate the activation energy of the migration on the surface, we used the Nudged Elastic Band (NEB) method as implemented in ASE (as illustrated in Figure 1).

The curvature of the nanotube surface has strong effect on the stability of different oxygen sites. Nanotubes with high θ angle, like (6,4) and (6,5) strongly stabilize an ether like O sites. On the other hand, tubes with low θ angle, like (9,2) or (9,1) this energy difference is much smaller. Interestingly, the curvature effect on the O migration is relatively small, and the required activation energy is high for all the tubes and O sites.

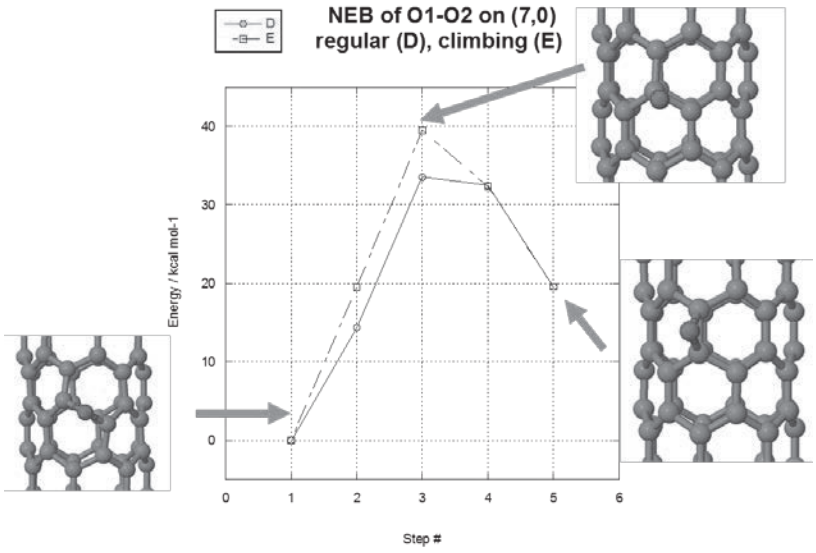

Fig.1: The activation energy of the oxygen migration between two stable chemisorption sites on (7,0) tube surface.

[1] S. Ghosh *et al.* Science **330**, 1656 (2010).
[2] Y. Miyauchi *et al.* Nature Photonics **7**, 715 (2013).

Corresponding Author: G. Juhász
Tel: +81-03-5734-2357, Fax: +81-03-5734-2357,
E-mail: juhasz@chem.titech.ac.jp

Anomalous potential properties between CNTs under a weak external electric field

○U Ishiyama and Susumu Okada

Graduate School of Pure and Applied Sciences, University of Tsukuba, Tennodai, Tsukuba 305-8577, Japan

Carbon nanotubes (CNTs) are attracting much attention because of it unique geometric and electronic structures those allow them being an emerging material for semiconductor electronic devices in the next generation. It has been shown experimentally that CNTs work as a conducting channel of field-effect transistors (FETs), in which the CNTs form a film structure with nano-scale interfaces among these CNTs. However, the fundamental properties of these CNT-CNT interfaces under an electric field are not fully understood. In this work, we aim to elucidate the electronic properties of the CNT thin films, which consist of the bilayer of CNTs, under the external electric field.

All calculations are performed by using the density functional theory with local density approximation. We use an ultrasoft pseudopotential to describe the interaction between valence electrons and ions. The effective screening medium (ESM) method is applied to investigate electronic properties of CNT under the parallel external electric field in the framework of the first-principles calculations. Here, we consider thin films of CNTs consisting of (11,0), (12,0), (13,0), (14,0), and (15,0) CNTs forming CNT bilayer structure mimicking CNT-FET device (Fig.1).

Figure 2 shows the electrostatic potential of a CNT bilayer consisting of (13,0) and (11,0) CNTs under the parallel electric field of 0.0154 V/Å. The potential exhibit unusual fearture at the space between CNTs: The potential possess opposite gradient at the spacing against the external electric field. The anomalous potential properties strongly depend on the external electric field: The opposite field against the external field vanishes by increasing the external electric field.

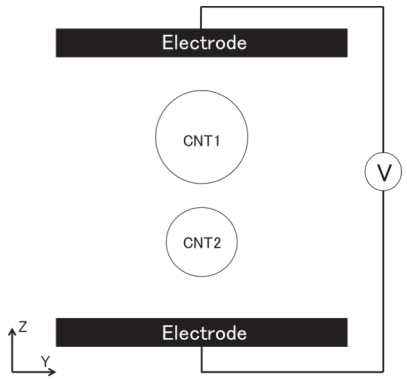

Fig.1 A structural model of CNT thin films

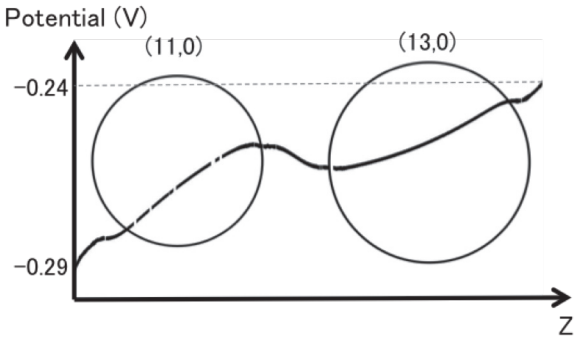

Fig.2 Electrostatic potential of a CNT thin film under an external field.

Corresponding Author: U Ishiyama
Tel: +81-29-853-5600 (ext. 8233), Fax: +81-29-853-5924,
E-mail: yishiyama@comas.frsc.tsukuba.ac.jp

Dependence of Thermoelectric Properties on Chiralities of Single Wall Carbon Nanotubes

○Yuki Oshima, Yoshimasa Kitamura, Hideki Kawai, Yutaka Maniwa, Kazuhiro Yanagi

Department of Physics, Tokyo Metropolitan University, Minami-Osawa 192-0397, Japan

Thermoelectrics are a very important technology for efficiently converting waste heat into electric power. As Hicks and Dresselhaus have proposed,[1] for realization of high-performance thermoelectric devices, it is important to use low-dimensional materials and to tune their Fermi level. In this context, we have reported across-bandgap p-type and n-type control over the Seebeck coefficients of semiconducting single wall carbon nanotube (SWCNT) network films by Fermi level tuning through electrolyte gating.[2] By freezing the motion of the electrolyte, we fabricated thermoelectric devices using the precisely p-type and n-type tuned semiconducting SWCNT films.[2] SWCNTs have various electronic structures depending on their chiralities. It has been expected that Seebeck coefficient will be significantly influenced by the band-gap width,[3] thus the thermoelectric properties will largely depend on their chirality. Therefore, clarification of relationships between chiralities and thermoelectric properties is of great importance for their applications as well as basic science. Recent progress of purification techniques enables us to prepare metallic, semiconducting and single-chiral states of SWCNTs.

In this study, we prepared (6,5) SWCNTs (diameter of 0.76 nm) through gel-purification techniques and investigated their thermoelectric properties and compared the results with those of semiconducting SWCNTs with diameter of 1.4 nm.

The results are shown in Figure 1. The peak gap between the P-peak and N-type peak in (6,5) SWCNTs was larger than that in Semi 1.4 nm SWCNTs. The gap width is almost consistent with the capacitance gap of (6,5) SWCNTs, which reflects the semiconducting gap of the sample. Those results indicate the chiralities of SWCNTs will significantly influence on Seebeck coefficient and thermoelectric performance of SWCNTs.

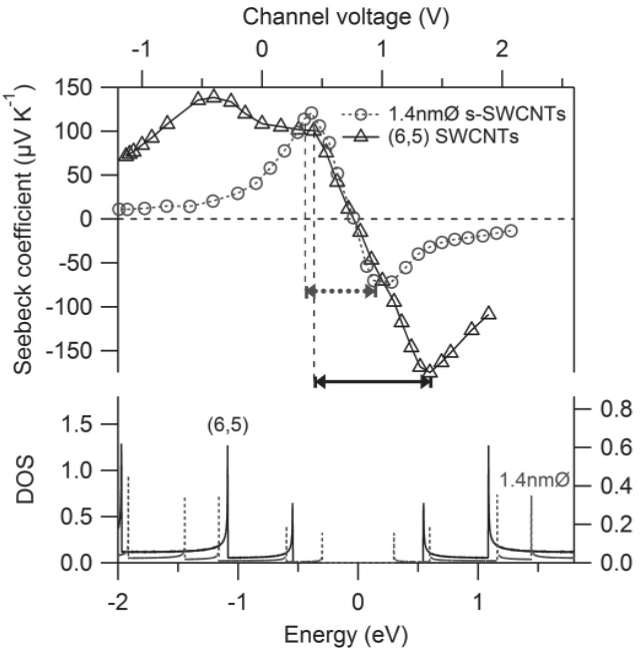

Fig.1: (Top) Comparison between Seebeck coefficient of Semi with 1.4 nm-SWCNTs and (6,5) SWCNTs. (Bottom) Density of states (DOS) of Semi with 1.4 nm-SWCNT and (6,5) SWCNT calculated using the tight-binding model.

[1] Hicks & Dresselhaus, Phys. Rev. B 47, 16631 (1993)
[2] Yanagi et al., Nano Lett. 14, 6437 (2014)
[3] X. Tan et al., Nanoscale Res. Lett. 7, 116 (2012)

Corresponding Author: K. Yanagi
Tel: +81-42-677-2494,
Fax: +81-42-677-2483,
E-mail: yanagi-kazuhiro@tmu.ac.jp

Metal-free Transparent Organic Solar Cell using Dopant Enhanced Carbon Nanotube Electrode and its Transfer Methodologies

○ Il Jeon[1], Clement Delacou[2], Esko I. Kauppinen[3], Shigeo Maruyama[2], Yutaka Matsuo[1]

1 Department of Chemistry, School of Science, The University of Tokyo, 7-3-1 Hongo, Bunkyo-ku, Tokyo 113-0033, Japan
2 Department of Mechanical Engineering, School of Engineering, The University of Tokyo, 7-3-1 Hongo, Bunkyo-ku, Tokyo 113-8656, Japan
3 Department of Applied Physics, Aalto University School of Science, 15100, FI-00076 Aalto, Finland

Future organic solar cells are greener technology that possesses multi-functionality such as wearable devices and surface conforming photovoltaic textiles, and window solar cells. Prerequisites of these include metal-free, mechanical resilience, and translucency while retaining high power conversion efficiency. For this to be realized, replacing metal electrode with flexible and transparent material is the first step towards this achievement. Previously, many attempts have been made in demonstrating visibly transparent and mechanically resilient solar cells. However, transparent conductors often result in low visible light transparency and device efficiency with no flexibility because no suitable material as a transparent conductor was deployed in device design and fabrication. Here we report a carbon nanotube based metal-free OSC and its doping that are most effectively structured to date. High-quality dry-deposited carbon nanotube film doped with nitric acid was used as an anode in a transparent organic photovoltaic device. Such concept is unprecedented in the field of organic solar cells and application of CNT doping in this structure is the first-time attempt in a transparent photovoltaic device. Our 90% and 65% transparent SWCNTs employed OSCs showed PCEs of 3.70% and 4.58%, while the leading ITO-based OSC showed a PCE of 7.21%.

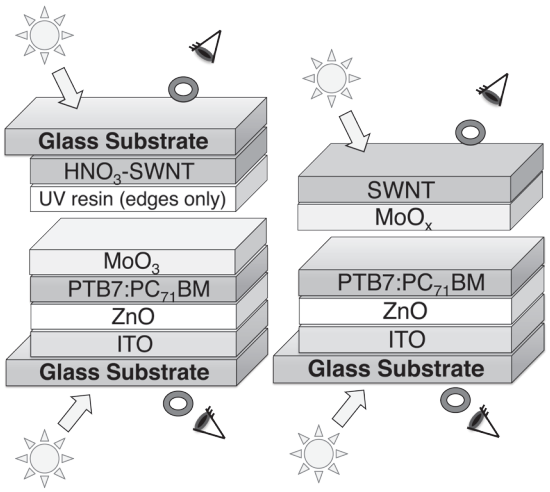

Fig.1: Schematics of transparent solar devices

Corresponding Author: Y. Matsuo
Tel: +81-3-5841-1476,
E-mail: matsuo@chem.s.u-tokyo.ac.jp

Carbon nanotube papers capturing Si nanoparticles for binder-free anodes of lithium ion batteries

○Takayuki Kowase, Kei Hasegawa, and Suguru Noda*

Department of Applied Chemistry, Waseda University, Tokyo 169-8555, Japan

Si is a candidate material for lithium ion battery anodes due to its high theoretical capacity (4200 mAh/g_{Si}), however it suffers from the rapid degradation due to its huge volume change (up to 400%) during charge/discharge cycles. Si anodes with various nanostructures have been developed and encouraging cycle performances have been demonstrated. However, most of them were fabricated with small loads of Si (about 1 μm or less) on thick and heavy Cu current collectors (15 μm or thicker) through complicated processes. For practical application, it is essential to enhance the Si loads through easy/simple processes.

In this work, we propose and develop Si-based anodes by capturing Si nanoparticles (Si-NPs) at a high load within carbon nanotube (CNT) papers through simple processes. Si-NPs were synthesized by rapid vapor deposition method [1], in which Si source was heated to > 2000 °C (well above the melting point) and evaporated in <1 min under low-pressure Ar. Sub-millimeter-long few wall CNTs by fluidized bed chemical vapor deposition (CVD) method [2] were used, which were shown effective in capturing activated carbon particles for electrochemical capacitor electrodes [3]. Si-NPs and CNTs were co-dispersed in isopropanol and filtrated to yield self-supporting Si/CNT films. Finally, carbon layer was deposited by CVD from C_2H_2 to enhance the connection between Si-NPs and CNTs.

Si-NPs were synthesized with a range of diameter, from a few tens nm at 5 Torr to a few hundreds nm at 50 Torr, at 20−60% yields (Fig. 1). Co-dispersion and filtration yielded self-supporting paper, in which CNTs hold Si-NPs uniformly (Fig. 2). Carbon coating realized high discharge capacities of ~1250 mAh/g_{Si} and ~0.7 mAh/cm^2 at the 100th cycle (Fig. 3).

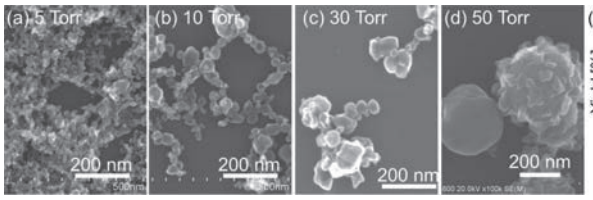

Fig. 1 SEM images (a,b,c,d) and yield (e) of Si-NPs.

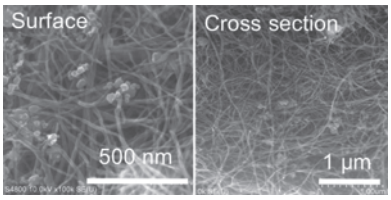

Fig. 2 SEM images of a Si/CNT film.

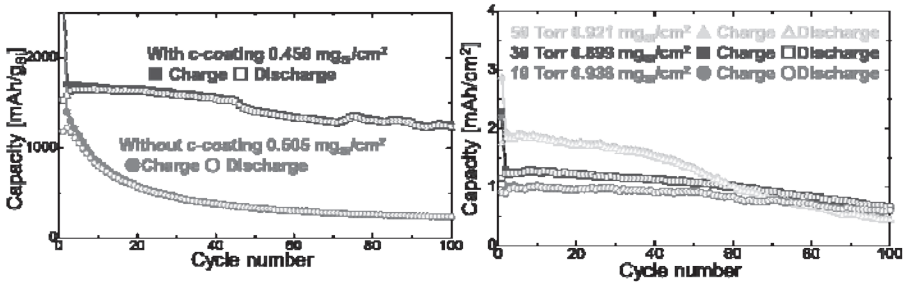

Fig. 3 Cycle performances of Si-NP(10 Torr)/CNT anodes with and without C-coating (a) and those using various Si-NPs (b). Conditions: EC/DEC (v/v=1/1) + 1 wt% VC, 0.005−1.2 V (Li/Li$^+$), 0.3C (1.26 A/g_{Si}).

Acknowledgements: The authors thank Prof. Osaka and Prof. Momma in their support in making coin cells. This work is supported in part by Grant-in-Aid for Scientific Research (A) #25249111 from MEXT, Japan.

[1] J. Lee and S. Noda, RSC Adv. 5 (4), 2938-2946 (2015).
[2] D.Y. Kim, et al., Carbon 49, 1972-1979(2011).
[3] R. Quintero, et al., RSC Adv. 4 (16), 8230-8237 (2014).

Corresponding Author: S. Noda, Tel&Fax: +81-3-5286-2769, E-mail: noda@waseda.jp

Computational analysis of inelastic electronic transport properties in single-walled carbon nanotubes

Keisuke Ishizeki[1], Kenji Sasaoka[2], Takahiro Yamamoto[1]

[1] *Department of Electrical Engineering, Tokyo University of Science*
[2] *Organization of Advanced Science and Technology, Kobe University*

Development of LSI technology based on downsizing CMOS transistors will reach a limit due to process limitation in the near future. For more development of the performance, single-walled carbon nanotubes (SWNTs) are potential candidates for channel materials of CMOS transistors and wiring materials in LSI circuits because of their high carrier mobility and their stability for the current density. As the electronic devices are usually operated at room temperature or more, it is expected that electronic transport properties of SWNTs are subjected to influence of phonon scattering. Moreover, it is expected that electronic transport in short-length SWNTs belong to a crossover regime between the ballistic and diffusive transport regimes. For the above reasons, it is needed that electronic transport properties of SWNTs are investigated at finite temperature from a quantum-mechanical point of view.

We have developed a new quantum-transport simulation method to investigate inelastic electron transport in nanoscale materials including electron-phonon interaction. In this work, we have calculated the inelastic current flowing through both semiconducting SWNTs (s-SWNTs) and metallic SWNTs (m-SWNTs) with various tube lengths at respective temperatures using the new simulation method. As is expected, we have confirmed that the electric resistance R of both s-SWNTs and m-SWNTs increases (from the quantum resistance R_0) with tube length L. In addition, the rate of resistance increase, dR/dL, becomes large with temperature, as the electron-phonon scattering increases with temperature. Moreover, the electric resistance of submicron-length m-SWNTs is much smaller than that of s-SWNTs. These simulation results are in agreements with previous results [1]. Thus, the new simulation method we developed can be applied to various transport features of SWNTs and other nanoscale materials.

[1] T. Ando, J. Phys. Soc. Jpn. **74**, 777 (2005).

Corresponding Author: T. Yamamoto
Tel: +81-3-5876-1492
E-mail: takahiro@rs.tus.ac.jp

Development of Poly(vinylsulfonic acid) wrapped Multi-Walled Carbon Nanotube for Fuel Cell Electrode Catalyst

○Akiyo Nagashima[1], Tsuyohiko Fujigaya[1,2], Naotoshi Nakashima[1,2]

[1] *Department of Applied Chemistry, Kyushu University, Fukuoka 819-0395, Japan*
[2] *WPI-I2CNER, Kyushu University, Fukuoka 819-0395, Japan*

Polymer electrolyte fuel cells (PEFC) are considered as one of the promising power sources for automobile and house in near future due to their high energy conversion efficiency and compactness. Generally, Pt loading carbon black are used as catalyst due to low cost. However, the low durability due to its low chemical stability and introducing defect as Pt binding site was pointed out. To overcome this issue, we used multi-walled carbon nanotube (MWNT) as carbon support instead of carbon black since MWNT is superior in terms of electrochemical durability. In our group, MWNT are wrapped with anchoring polymer, polybenzimidazole (PBI), to load Pt without defect sites[1]. We found PBI-wrapped MWNT has high durability due to homogeneous and stable Pt nanoparticles as well as their structural intactness. Although this PEFC showed high durability, this catalyst had large overvoltage, probably because the low ionic conductivity of proton transporting material, poly(vinylphosphonic acid) (PVPA)[2]. Therefore, in this study, we introduced poly(vinylsulfonic acid) (PVSA) having higher proton conductivity than PVPA as new proton transporting material to increase ionic conductivity instead of PVPA (**Fig.1**).

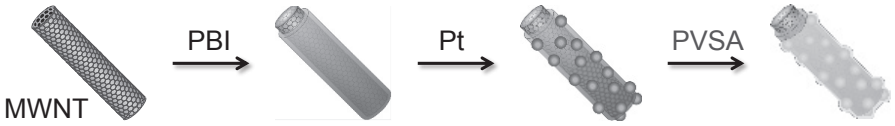

Fig.1 Illustration of the method of synthesis PVSA-coated catalyst.

Single cell tests were performed using three Membrane Electrode Assembly (MEA) containing the PVPA-, PVSA- and Nafion- coated catalysts in the gas diffusion electrode, where Nafion117 were used as the membrane. The performance of MEAs was measured at 80 ºC with humidification and atmospheric pressure using H_2 at the anode and air at the cathode. As shown in **Fig. 2**, PVSA-coated catalyst showed higher I-V performance than PVPA coating catalyst. We assumed that higher ionic conductivity of PVSA than PVPA lead the low overvoltage. However, it revealed that the diffusion overvoltage of PVSA-coated catalyst was larger than that of Nafion-coated catalyst.

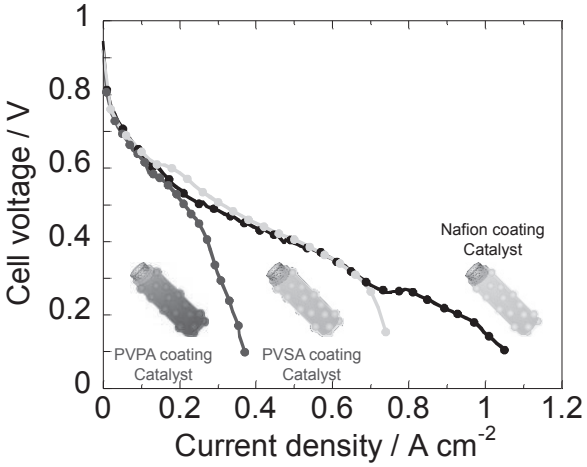

Fig.2 I-V curves of the MEAs having PVPA-, PVSA- and Nafion-coated catalysts measured at 80 ˚C under 100%RH, using H_2 and air anode and cathode, respectively.

[1] T. Fujigaya, N. Nakashima, Adv. Mater. 25, 1666 (2013).
[2] N. Nakashima et al, Sci. Rep. 3, 1764 (2013).

Corresponding Author: T. Fujigaya
Tel: +81-92-802-2842, Fax: +81-92-802-2842
E-mail: fujigaya-tcm@mail.cstm.kyushu-u.ac.jp

Flexible and semi-transparent film heater for temperature range higher than 100 °C using single-wall carbon nanotube film

○Daiki Kobayashi, Kuniharu Takei, Takayuki Arie, Seiji Akita

Department of Physics and Electronics, Osaka Prefecture University, Sakai, Osaka 599-8531 Japan

Transparent electronics device is one of emerging fields of recent electronic devices. A flexible and semi-transparent heater with quick response is an important component for this application. The flexible heater with transparency would provide visibility for heating process which might be useful for material science for investigation of temperature dependence of micro scale structural change such as phase transition of polymer. Here, we report on a flexible and semi-transparent film heater for temperature range higher than 100 °C using single-wall carbon nanotubes and polyimide film.

A single-wall carbon nanotube ink (0.1 wt% in water, WaterSolutionGen 2.3 (KH Chemicals)) was used for fabrication of CNT film heater, which was formed by spray coating method onto polyimide film (1.5×1.5 cm^2, 50 μm) at 180 °C. Note that the polyimide film was coated with 15-nm-thick SiO_2 layer for hydrophilicity. The transient response of surface temperature of the heater was measured using thermography in ambient air. We have prepared 3 film heaters with different electrical resistivity of 134, 250, and 412 Ω, where the optical transparencies were varied from 71 to 82.1%, where the light absorption of the polyimide film was corrected.

Figure 1 shows the electro-thermal response of the film heaters under the application of 15 V. The surface temperature of the film with a resistivity of 134 Ω reaches to 160 °C within 5 s. Although the temperature response at rise includes information not only of the thermal properties of the film but also of the temperature dependence of the electrical resistance, the temperature response at fall-down only depends on the thermal properties of the film such as thermal conductivity, heat capacity and heat conduction to ambient air. At fall-down response, all of the film heaters show the almost identical time constant. The heat flow analysis using finite element method with heat losses to ambient air and support of the heater revealed that the obtained heater response is governed by the thin polyimide film, which gives the same time constants for fall-down response.

Thus, we have successfully fabricated the semi-transparent film heater for temperature range higher than 100 °C through simple fabrication process using spray coating method.

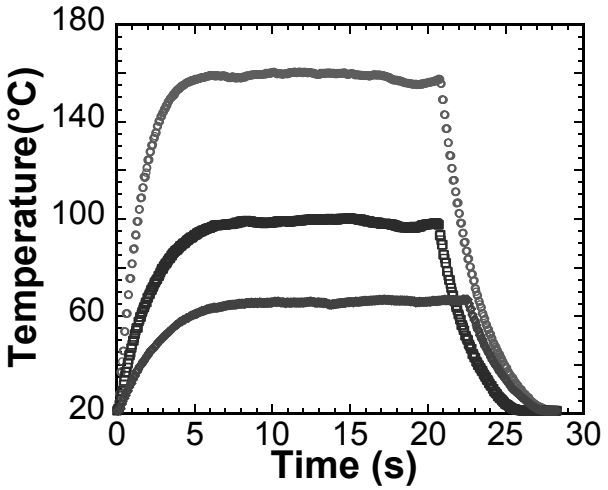

Fig.1 Electro-thermal response of film heaters with different electrical resistivity.

Corresponding Author: S. Akita
Tel: +81-72-254-9261
E-mail:akita@pe.osakafu-u.ac.jp

Ultra-high sensitivity carbon nanotube biosensors based on redox cycle process

○Takuya Ushiyama[1], Nguyen Xuan Viet[1], Shigeru Kishimoto[1], and Yutaka Ohno[1, 2]

[1]*Graduate School of Engineering, Nagoya University, Nagoya 464-8603, Japan*
[2]*EcoTopia Science Institute, Nagoya University, Nagoya 464-8603, Japan*

Carbon nanotube (CNT) is useful electrode material for electrochemical biosensors because of its wide potential window and rapid electron transfer kinetics [1]. Excellent electrochemical properties [2] and ultra-high sensitivity in biomolecule detection [3] of CNT microelectrodes have been reported. In the previous reports, however, measured signal current was quite small as ~nA, so that, highly-sensitive galvanometer or potentiometer was necessary to ensure sufficient signal-to-noise ratio for the analysis. The signal current density, hence the sensitivity can be increased drastically by introducing redox cycle in detection process [4]. In this work, we have fabricated interdigitated electrodes with a CNT thin film to realize high-sensitivity electrochemical biosensors based on the redox cycle.

Figure 1 shows a fabricated CNT interdigitated electrode (CNT-IDE) consisting of two working electrodes. The redox cycle, i.e., repetitive oxidation and reduction reactions of analyte molecules, are caused between two working electrodes. The CNT thin film was formed by the dry transfer process based on floating-catalyst CVD, and then patterned by conventional micro-process. A PMMA cover layer was formed on the sample surface, except for the CNT-IDE region, so that, gold interconnections are electrically separated from analyte.

The electrochemical property of the CNT-IDE was evaluated by measuring cyclic voltammetry of $K_4[Fe(CN)_6]$ with four-electrode configuration. The CNT-IDE showed very high collection efficiency of 95%. Measured signal current was about 1000 times larger than the previous CNT microelectrodes [3]. The current density was also about 10 times larger. This is probability due to the effect of redox cycle.

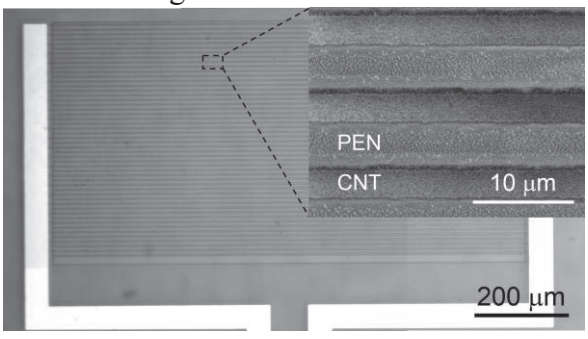

Fig. 1 Fabricated CNT-IDE.

[1] I. Dumitrescu *et al*, Chem. Commun., **45**, 6886 (2009)
[2] W. Harreither *et al*, Anal. Chem., **85**, 7447 (2013)
[3] N.X. Viet *et al*, The 47th FNTG general symposium 3P-4 (2014)
[4] D.G. Sanderson and L.B. Anderson, Anal. Chem., **57** 2388 (1985)
Corresponding Author: Y. Ohno
Tel: +81-52-789-5387, Fax: +81-52-789-5387
E-mail: yohno@nagoya-u.jp

Highly thermal durable fluorinated rubber and CNT composite

○Seisuke Ata[1,2], Ayummi Nishizawa[1], Takaaki Mizuno[2], Eiichi Usuda[1], Shigeki Tomonoh[1,2], Takeo Yamada[1,2] and Kenji Hata[1,2]

[1] Nanotube Research Center, National Institute of Advanced Industrial Science and Technology (AIST), Tsukuba 305-8565, Japan
[2] Technology Research Association for Single Wall Carbon Nanotubes (TASC), Tsukuba, 305-8565, Japan

Elastomer and rubber have soft and elastic properties, therefore one of their main application is sealing materials for connection part. However, elastomer is weak for heat derived by thermal degradation of polymer chain with heat-radical. The low-heat resistance of elastomer limits the wide-range application of elastomers. The key to increasing thermal resistance of elastomer is quenching heat-radical in elastomer at high temperature. CNT have been known as a radical scavenging material. We provide high-thermal resistance elastomer by adequately adding small amount of carbon nanotubes for elastomer. The heat resistance was estimated by time dependence of storage modulus under isothermal condition (200 ^{o}C). The high thermal resistance of CNT/rubber composite have achieved by excellent radical scavenging effect of CNT. By adding 1 wt% of CNT, the heat resistance of elastomer increase in 100K compared with pure elastomer. This CNT/elastomer composite have large possibility for oil-sealing material in oil drilling, sealing material of gas engine as a private power generator and sealing materials for automobiles.

This presentation is based on results obtained from a project commissioned by the New Energy and Industrial Technology Development Organization (NEDO).

Corresponding Author: S.Ata
Tel: +81-22-861-4654, Fax: +81-22-861-4851,
E-mail: ata-s@aist.go.jp

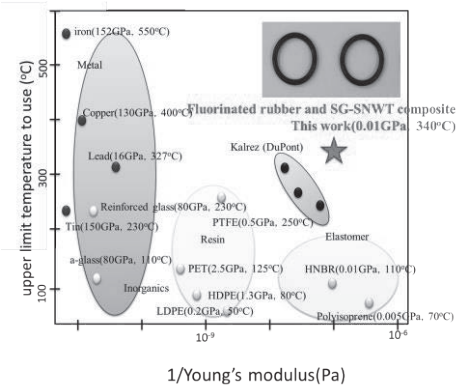

Figure. Inverse number of Young's modulus versus upper limit temperature to use.

Highly stable carbon nanotube/ultrathin cross-linked polymer hybrids for biomedical applications

○Yusuke Tsutsumi[1], Tsuyohiko Fujigaya[1,2], Naotoshi Nakashima[1,2]

[1]Department of Applied Chemistry, Graduate School of Engineering, Kyushu University, 744 Motooka, Fukuoka 819-0395, Japan
[2]WPI I[2]CNER, Kyushu University, 744 Motooka, Fukuoka 819-0395, Japan

Single-walled carbon nanotubes (SWNTs) are attracting increasing attention in biological applications because of their unique thermal, physical and optical properties. As-produced SWNTs are not soluble in many solvents and form aggregation due to the strong intertube van der Waals interactions. Since the aggregation of SWNTs has a risk of toxicity in vivo, a functionalization of SWNT surfaces is important in biological applications. Here, as a novel functionalization method, we demonstrate a method to prepare SWNTs/ultrathin cross-linked polymer hybrids by the polymerization in the interior of surfactant micelle encapsulating around SWNTs (Fig. 1) [1].

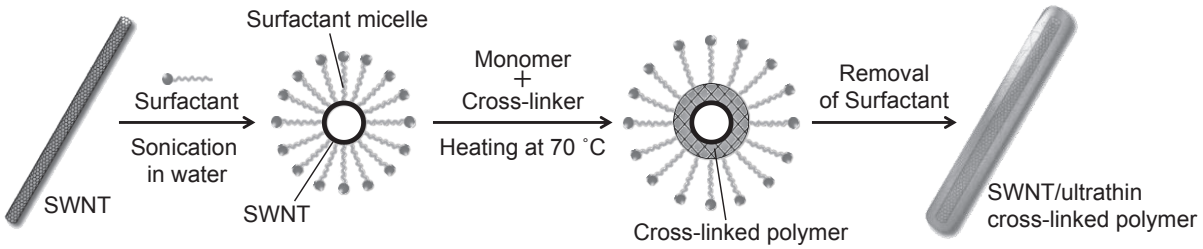

Fig. 1. Schematic illustration showing the preparation of SWNT/ultrathin cross-linked polymer.

Poly(*N*-isopropylacrylamide) was used as a polymer for SWNT-wrapping and the composites were synthesized by radical polymerization. Fig. 2 shows AFM image of the obtained composites. In this AFM image, many needle-like structures were observed and the average diameter of the needle-like structures was found to be 3.05 nm (N=59). Considering that the average SWNT diameter in this study is ~1 nm, the thickness of the cross-linked PNIPAM was determined to be ~1 nm. Furthermore, from the absorption and emission measurement of the composite materials, the absorption and emission peaks of the isolated SWNTs were observed in the near-IR region. These results show that SWNT structures are kept almost intact. Since the composites also have high stability in aqueous solution upon heating, freeze-drying and the addition of a large amount of surfactant, we expect the composites are attractive materials for biomedical applications.

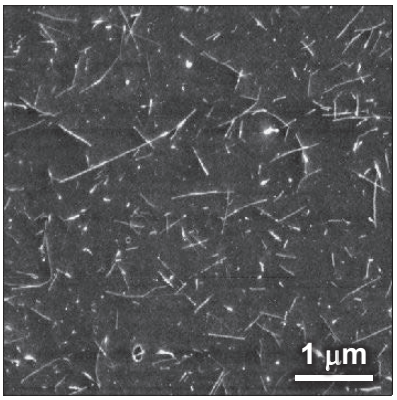

Fig.2: AFM image of the SWNT after the polymerization.

[1] Y. Tsutsumi, T. Fujigaya, N. Nakashima, *RSC. Adv.,* **2014**, *4*, 6318.

Corresponding Author: N. Nakashima
Tel: +81-92-802-2840, Fax: +81-92-802-2840, E-mail: nakashima-tcm@mail.cstm.kyushu-u.ac.jp

Purification of metal/semiconductive single-wall carbon nanotubes in two immiscible aqueous solution phase

Ryo Ishida[1], Marin Ohtsuka[1], Naoki Kanazawa[1], ○Shinzo Suzuki[1], Akira Ono[2]

[1]*Department of Physics, Kyoto Sangyo University, Kyoto 603-8555, Japan*
[2]*Department of Engineering, Kanagawa University, Yokohama 221-8686, Japan*

In 2013, C.Y. Khripin et al. first reported about spontaneous partition of single-wall carbon nanotubes (SWNTs) in polymer-modified aqueous solution phase [1], where metal/ semiconductive SWNTs of large diameter (> 1.2 nm) were shown to be successfully separated in two immiscible aqueous solution (i.e., in polyethylene glycol (PEG) and dextran (DX) solution). After that, this technique has been extensively used for not only for SWNTs dispersed in sodium (SC) solution, but those dispersed in DNA solution as well, by using slightly modified combination of two immiscible aqueous solution [2, 3].

In the previous symposium, we reported about the application of Raman spectroscopy in order to evaluate the ratio of metal/semiconductive single-wall carbon nanotubes in these immisible solution by changing excitation photon energy (532 nm and 633 nm) [4]. In this presentation, several experimental findings obtained by Raman spectroscopy in order to find the best experimental condition for the separation of metal/semiconductive carbon nanotubes dispersed in sodium cholate (SC) solution were summarized, and discussed in comparison with the experimental condition described in the Khripin's paper [1].

References:

[1] C.Y. Khripin et al., *J. Am. Chem. Soc.*, **135**, 6822-6825(2013).
[2] G. Ao et al., *J. Am. Chem. Soc.*, **136**, 10383-10392(2014).
[3] H. Gui et al., *Nano Lett.*, **15**, 1642-1645(2015).
[4] N. Kanazawa et al., *Proc. of the 46th Fullerene-Nanotube-Graphene General Symposium.* 1P-27(2014).

Corresponding Author: Shinzo Suzuki
Tel: +81-75-705-1631, Fax: +81-75-705-1631,
E-mail: suzukish@cc.kyoto-su.ac.jp

Synthesis of Single-Walled Carbon Nanotubes from Rh Catalysts at Low Temperature by Alcohol Gas Source Method in High Vacuum

○Akinari Kozawa[1], Hoshimitsu Kiribayashi[1], Seigo Ogawa[1], Takahiro Saida[2], Shigeya Naritsuka[1], Takahiro Maruyama[1,2]

[1] Department of Materials Science and Engineering, Meijo Univ., 1-501 Shiogamaguchi, Tempaku, Nagoya 468-8502, Japan
2 Department of Applied Chemistry, Meijo Univ., 1-501 Shiogamaguchi, Tempaku, Nagoya 468-8502, Japan

Single-walled carbon nanotubes (SWNTs) have been anticipated for application in a lot of future nanodevices. To fabricate SWNT electronics devices, it is important to grow SWNTs with uniform chirality and diameter at low temperature. So far, we have reported SWNT growth using Pt catalysts and succeeded in obtaining SWNTs with small diameters below 1.2 nm [1]. This suggests that metal catalysts with high-melting points are effective to grow SWNTs with small and uniform diameters. However, SWNT yield from Pt catalysts was small at a growth temperature of less than 600ºC. In this study, we carried out SWNT growth by CVD using Rh catalysts, whose melting point is 1966°C. By optimizing growth conditions, we obtained SWNTs with narrow diameter distribution at a growth temperature of 400ºC.

After deposition of Rh catalyst on $Al_2O_3/SiO_2/Si$ substrates, SWNT growth was carried out using the alcohol gas source method in a high vacuum [1]. The growth temperature was set between 400ºC and 600ºC, and the ethanol pressure was varied between 1×10^{-5} Pa and 1×10^{-2} Pa. The grown SWNTs were characterized by FE-SEM, TEM and Raman spectroscopy.

Fig. 1 shows the Raman spectra of SWNTs grown from Rh catalysts on $Al_2O_3/SiO_2/Si$ substrates. The growth temperature is between 400 and 600ºC, and ethanol pressure is optimum. When the growth temperature was decreased to 400ºC, the G band intensity was reduced, but the RBM peaks were still observed. As the growth temperature decreased, the SWNT yield decreased, but their diameter distribution became narrower. Our results indicate that Rh catalyst is suitable for low temperature growth of SWNTs with the smaller-diameter and the narrower diameter distributions.

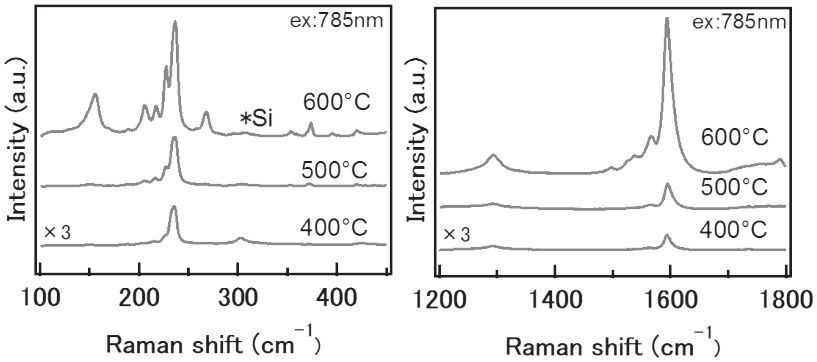

Fig.1 Raman spectra of SWNTs grown at 400～600℃

[1] T. Maruyama *et al*. Mater. Express **1** (2011) 267.

Corresponding Author: T. Maruyama
Tel: +81-52-838-2386, Fax: +81-52-832-1179,
E-mail: takamaru@meijo-u.ac.jp

A Growth Mechanism of (6,5)-Nanotube Cap on the Basis of Vibronic Coupling Density Analysis

○ Naoki Haruta[1], Tohru Sato[1,2], Yohji Achiba[3], Takeshi Kodama[3], Hirofumi Sato[1,2], Haruo Shiromaru[3]

[1] *Department of Molecular Engineering, Graduate School of Engineering, Kyoto University, Kyoto, 615-8510, Japan*
[2] *Unit of Elements Strategy Initiative for Catalysts & Batteries, Kyoto University, Nishikyo-ku, Kyoto 615-8510, Japan*
[3] *Department of Chemistry, Tokyo Metropolitan University, Hachioji 192-0397, Japan*

Carbon nanotubes (CNTs) have received much attention in the field of material chemistry because of their unique electronic, mechanical, and structural properties [1]. Although the chirality control of CNTs is important for their potential applications, it is still difficult because the growth mechanism of CNTs has not been decisively clarified. Achiba *et al.* have proposed a possible growth model of CNTs by the laser ablation method with metal-carbon composites [2,3]: (1) carbon caps are produced in gas phase at high temperature; (2) the caps are adsorbed onto metal/metal-carbon nanoparticles; (3) small carbon clusters such as C_2 are inserted successively into edges of the caps on the nanoparticles, leading to tube-like structures.

On the basis of this model, C_{43}(**1**) [Fig. 1 (a)] is considered to be one of the typical cap structures yielding an abundant CNT, (6,5)-CNT [4]. A question arises: what is the precursor of C_{43}(**1**)? In this study, we discuss the final step to yield C_{43}(**1**). If the C_2 insertion is assumed, five types of C_{41} isomers can be candidates for the precursor of C_{43}(**1**) [Fig. 1 (b–f)]. The most likely precursor can be determined by considering whether the regioselectivity of each C_{41} isomer gives C_{43}(**1**) or not.

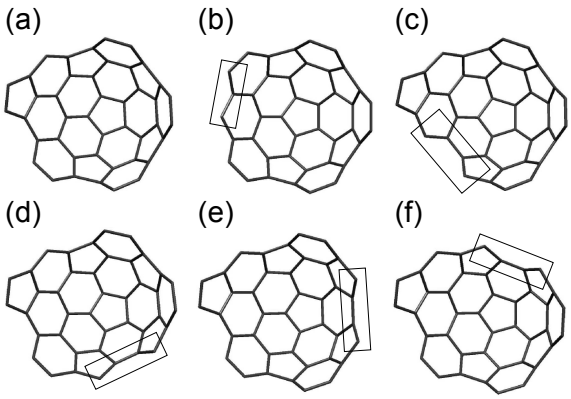

Fig. 1: (a) C_{43}(**1**), (b–f) C_{41}(**1**–**5**).

The frontier orbital theory has a difficulty in predicting the regioselectivities of π-conjugated nanocarbons including fullerenes and graphene fragments because their frontier orbitals are sometimes strongly delocalized [5,6]. One way to overcome this difficulty is the use of vibronic coupling density (VCD) theory [5–7], in which not only electronic structures but also vibrational ones are taken into account. In this study, in order to determine the precursor of C_{43}(**1**), we apply the VCD analysis to the five C_{41} isomers which are hydrogen-terminated as theoretical models of the C_{41} isomers supported by nanoparticles. According to our results, C_{41}(**5**) has a large VCD distribution localized around the bay region leading to C_{43}(**1**). This is in contrast to the other C_{41} isomers. Moreover, the C_2 attack on C_{41}(**5**) gives larger stabilization due to vibronic couplings. C_{41}(**5**) is therefore considered to be the most likely precursor of C_{43}(**1**).

[1] R. H. Baughman *et al.*, Science **297**, 787 (2002). [2] H. Kataura *et al.*, Carbon **38**, 1691 (2000). [3] Y. Achiba, Mol. Sci. **6**, A0055 (2012). [4] Q. Wang *et al.*, ACS Nano **4**, 939 (2010). [5] T. Sato *et al.*, Chem. Phys. Lett. **531**, 257 (2012). [6] N. Haruta *et al.*, Tetrahedron Lett. **56**, 590 (2015). [7] T. Sato *et al.*, J. Phys. Chem. A **112**, 758 (2008).

Corresponding Author: T. Sato
Tel: +81-75-383-2803, Fax: +81-75-383-2555
E-mail: tsato@moleng.kyoto-u.ac.jp

Metallic/Semiconducting Separation by Electric-Field-Induced Layer Formation Method Applied to SWCNTs Purified for Removal of Catalysts

○Fusako Sasaki[1], Fumiyuki Nihey[2], Yuki Kuwahara[1,3], Takeshi Saito[1,3], Hiroyuki Endoh[2], Shinichi Yorozu[2]

[1] *Technology Research Association for Single Wall Carbon Nanotubes, Tsukuba 305-8565, Japan*

[2] *Smart Energy Research Laboratories, NEC Corporation, Tsukuba 305-8501, Japan*

[3] *National Institute of Advanced Industrial Science and Technology, Tsukuba 305-8565, Japan*

We had proposed a method to separate metallic and semiconducting SWCNT solution with nonionic surfactant by Electric-Field-induced Layer formation (ELF) method [1]. In this presentation, we report the results of ELF separation applied to SWCNTs purified for the removal of metal catalysts. SWCNTs synthesized by using eDIPS method [2] were purified by the procedure that consists of low temperature activation, soaking in HCl solution, and vacuum annealing (Fig. 1). The purified SWCNTs were dispersed in aqueous solution of polyoxyethylene (100) stearyl ether by sonication and ultracentrifugation. After the treatment, metallic and semiconducting SWCNTs were separated by ELF method (Fig. 2 (a)). The optical-absorbance spectra of separated fractions showed the enrichment of metallic/semiconducting peaks (Fig. 2 (b)). We found that 500°C-or-higher vacuum annealing plays an important role to achieve successful separation with this method applied to the purified SWCNTs[3]. This presentation is based on results obtained from a project subsidized by the New Energy and Industrial Technology Development Organization (NEDO).

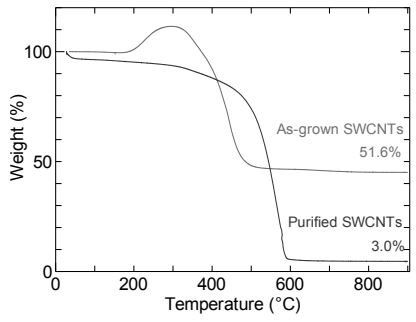

Fig. 1 Thermogravimetric analysis results of SWCNTs.

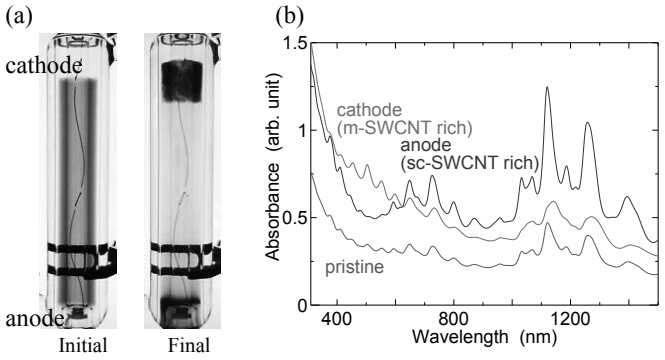

Fig. 2 (a) Initial and final images of a separation cell. (b) Absorption spectra of the separated SWCNTs.

References:

[1] K. Ihara et al., J. Phys. Chem. C 115, 22827 (2011).

[2] T. Saito et al., J. Nanosci. Nanotechnol. 8, 6153 (2008).

[3] F. Sasaki et al., NT15 Abstract, p.99 (2015).

Corresponding Author: F. Sasaki, Tel: +81-29-861-3778

Fax: +81-29-858-6330, E-mail: f_sasaki@tasc-nt.or.jp

Time evolution study of narrow-chirality distributed single-walled carbon nanotubes synthesis during pulse plasma CVD

○Bin Xu, Toshiaki Kato, and Toshiro Kaneko

Department of Electronic Engineering, Tohoku University, Sendai 980-8579, Japan

Single-walled carbon nanotubes (SWNTs) are potential materials for future high performance opto-electric device application. Since the energy state of SWNTs depends on the chirality, it is important to control the chirality of SWNTs [1-3]. Based on our previous study, we developed novel plasma CVD named pulse plasma CVD, which can grow SWNTs with narrow chirality distribution. To improve the purity of chirality species, it is important to understand the effects of pulse plasma on the growth of SWNTs. In this study, we have investigated the correlation between pulse on/off time parameters and chirality-distribution of SWNTs. It is found that SWNTs chirality-distribution is influenced by the balance of pulse effect and Ostwald ripening effect, which is decided by pulse on/off ratio and total process time, respectively. The carbon concentration in each catalysts controlled by pulse time parameters is believed to be the critical factor to explain the pulse effects. Furthermore, we investigate the length distribution of SWNTs as a function of pulse times by atomic force microscope (AFM) measurement (Fig. 1), reveling that SWNTs growth can be continued by repeating pulse plasma CVD.

Through the fine tuning of growth conditions following this growth mechanism, we have succeeded in synthesizing SWNTs with very narrow chirality distribution, where only three chirality species ((6,4), (7,3), (6,5)) are dominant.

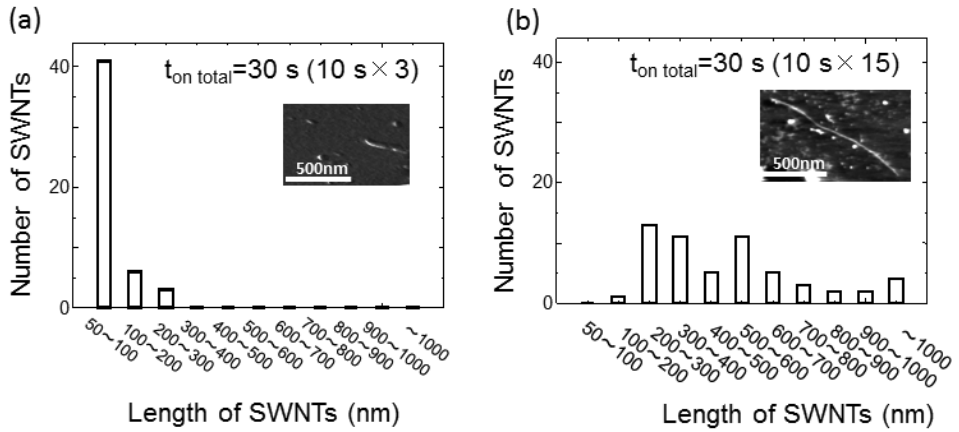

Fig.1: Length distribution of SWNTs measured by AFM. The pulse time parameters are (a) 10s×3 and (b) 10s×15.

[1] Z. Ghorannevis, T. Kato, T. Kaneko, and R. Hatakeyama, J. Am. Chem. Soc. **132**, 9570 (2010).
[2] T. Kato and R. Hatakeyama, ACS Nano **4**, 7395 (2010).
[3] B. Xu, T. Kato, K. Murakoshi, and T. Kaneko, J. Plasma Fusion Res. **9**, 1206075 (2014).

Corresponding Author: B. Xu
Tel: +82-22-795-7046
E-mail: xu12@ecei.tohoku.ac.jp

Selective synthesis of single-walled carbon nanotubes using sputtered W/Co

Hua An[1], Rong Xiang[1], Taiki Inoue[1], Shohei Chiashi[1], Shigeo Maruyama[1,2]

1. Department of Mechanical Engineering, the University of Tokyo, 7-3-1 Hongo, Bunkyo, Tokyo, 113-8656, Japan

2. National Institute of Advanced Industrial Science and Technology (AIST), 1-2-1 Namiki, Tsukuba, 305-8564, Japan

Direct growth of single-walled carbon nanotubes (SWNTs) with a single chirality is highly desired in the applications. Unfortunately, the as-grown SWNTs are always obtained with a mixture of various chiralities, which limits the performance of SWNTs-based nanoelectronics. Extensive researches have focused on the catalyst structure, growth conditions and initial nucleated cap to realize the selective growth of SWNTs. W/Co catalyst has been reported to grow a single chirality SWNT, (12, 6), with over 90% abundance via a high-temperature (1030^{o} C) reduction and growth. [1].

In this study, we used sputtered W/Co as catalyst to grow SWNTs by alcohol catalytic chemical vapor deposition (ACCVD) [2]. The catalyst was prepared on the Si/SiO_2 substrate and annealed at a much lower temperature than that of originally reported tungsten-cobalt clusters [1]. SWNTs with high-quality and uniformity were obtained with this bimetallic sputtered W/Co. The narrow (*n, m*) distribution was confirmed by Raman spectroscopy with four different excitation wavelengths. Most of the peaks centers at 197 cm^{-1} in Fig. 1, which suggests the high quantity of (12, 6). The absorption spectroscopy also shows the dominant (12, 6) peak. Further parametric study reveals that the annealing temperature before growth is critical for the selectivity. More details will be discussed on the chirality distribution and growth mechanism.

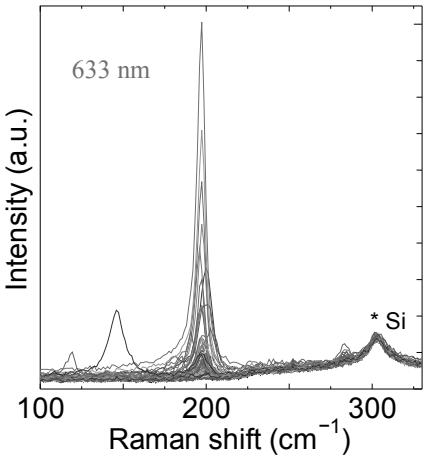

Fig.1: Raman spectra of SWNTs with the corresponding excitation wavelength.

[1] F. Yang et al., Nature **510**, 522, (2014).

Corresponding Author: Shigeo Maruyama
Tel: +81-3-5841-6421, Fax: +81-3-5800-6983
E-mail: maruyama@photon.t.u-tokyo.ac.jp

Preparation and Characterization of Fibrous Aggregates of Single-Walled Carbon Nanohorns

○Ryota Yuge[1], Fumiyuki Nihey[1], Kiyohiko Toyama[1], and Masako Yudasaka[2, 3]

[1]*Smart Energy Research Laboratories, NEC Corporation, Tsukuba 305-8501, Japan*
[2]*National Institute of Advanced Science and Technology (AIST), Tsukuba, 305-8565, Japan*
[3]*Graduate School of Science and Technology, Meijo University, Nagoya 468-8502, Japan*

Single-walled carbon nanohorns (SWCNHs) [1] are a type of nano-carbon materials such as carbon nanotubes and graphenes, which are attractive having the high dispersibility and large specific surface area. As a result, the gas adsorbents [2], compound materials [3], electrochemical capacitors [4], and carriers of drug delivery systems [5] are expected as promising applications. The preparation of SWCNHs with good conductivity is the hopeful strategy to obtain further outstanding performance. In this study, we succeeded in preparing fibrous aggregate of SWCNHs (Fibrous SWCNHs) for the first time and characterize the structure and electronic properties.

Fibrous SWCNHs were prepared by CO_2 laser ablation of an iron-contained graphite target at room temperature. The CO_2 laser was operated in the continuous-wave mode. The gas pressure in the growth chamber was sustained at 760 Torr by controlling the evacuation rate while the flow rate of buffer gas of N_2 was kept at 10 L/min.

From SEM and TEM observation of the obtained samples, the individual SWCNH was 2-5 nm in diameter and 40-50 nm in length. The SWCNHs have been assembled fibrously with 30 -100 nm in diameter and grown in several micro-meters in length, which is different entirely from general spherical aggregates of SWCNHs. The fibrous SWCNHs were prepared simultaneously with the spherical SWCNHs. From EDX and XPS measurements, the catalyst contained in fibrous and spherical SWCNHs after CO_2 laser ablation existed mainly as Fe metal particles. In a four-point-probe resistivity measurements, the electrical resistivity of the mixture of fibrous and spherical SWCNHs was 0.99 Ωcm, 33% lower than that of spherical SWCNHs. The details will be shown in the presentation.

[1] S. Iijima *et al*. Chem. Phys. Lett. **309**, 165 (1999).

[2] E. Bekyarova, *et al*. J. Phys. Chem. B, **107**, 4681 (2003).

[3] A. Tanaka, *et al*. Tribol. Lett. **19**, 135 (2005).

[4] C. M. Yang *et al*. J. Am. Chem. Soc. **129**, 20 (2007).

[5] T. Murakami *et al*. Mol. Pharm. **1**, 399 (2004).

Corresponding Author: R. Yuge

Tel: +81-29-850-1566, Fax: +81-29-856-6137,

E-mail: r-yuge@bk.jp.nec.com

Electrochemical Exfoliation of Graphite Intercalation Compounds Encapsulated in Polymer

○Yasunaga Tan-no, Haruya Okimoto, Masahito Sano

Department of Polymer Science and Engineering, Yamagata University
Yonezawa, Yamagata 992-8510, Japan

A graphene intercalation compound (GrapheneIC) is a graphite intercalation compound (GIC) consisting of a few layer graphene sheets. Having doped by the intercalants, GrapheneIC possesses high electric conductivity with optical transparency of graphene. So far, GrapheneICs have been fabricated by treating a few layer graphene sheets with the intercalants in the vapor phase. We are interested in developing a technique to exfoliate GIC in the liquid phase. In particular, electrochemical exfoliation has an advantage of minimizing oxidation by controlling electrolytes and potentials. This new technique may lead to cost-effective, mass productions of GrapheheICs.

The most common intercalants that are capable of doping graphene are metal halides. Although their GICs are relatively stable in air, they are immediately disintegrated in aqueous phases. Thus, a means to protect metal halides is required to exfoliate GIC in solution. In this study, a polymer is used to offer a protective layer around GrapheneIC during electrochemical exfoliation.

$FeCl_3$-GIC was made by heating graphite with $FeCl_3$ in vacuum. It was, then, used as an anode for electrochemical exfoliation in H_2SO_4 solution with carboxymethyl cellulose (CMC) as a protective polymer. Figure 1 shows that, prior to exfoliation, in the acidic solution without CMC (left), the metal chloride from $FeCl_3$-GIC was dissociated into the solution and a graphite Raman spectrum is recovered. In contrast, CMC reacts with the dissociated metal ions to form gel around the GIC (right) and a GIC Raman spectrum is retained in the acidic solution. After electrochemical exfoliation, $FeCl_3$-GrapheneIC was successfully obtained from the solution with CMC. An excellent ability to be adsorbed on graphitic compounds as well as its characteristic to form cross-links with metal cations allow CMC to encapsulate $FeCl_3$-GrapheneIC in solution.

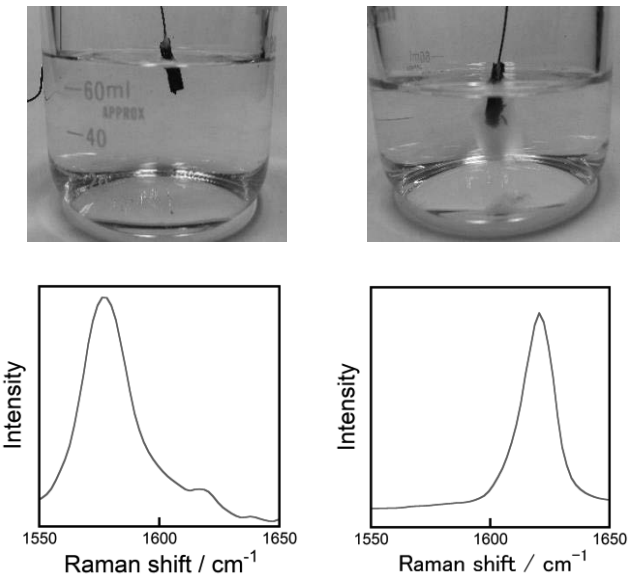

Fig.1: The electrochemical solutions (top) and Raman spectra (bottom) of $FeCl_3$-GIC in the acid solution with (right) and without (left) CMC.

Corresponding Author: H. Okimoto
Tel: +81-238-26-3074,
E-mail: haruya@yz.yamagata-u.ac.jp

Fabrication of clean graphene/BN heterostructures by metal melting transfer

○Ryosuke Inoue[1], Kenji Watanabe[2], Takashi Taniguchi[2],
Yutaka Maniwa[1], Yasumitsu Miyata[1,3]

[1]*Department of Physics, Tokyo Metropolitan University, Hachioji, 192-0397, Japan*
[2] *National Institute for Materials Science, Tsukuba 305-0044, Japan*
[3]*JST, PRESTO, Kawaguchi, 332-0012, Japan*

Chemical vapor deposition (CVD) are widely used for the growth of large-area, uniform monolayer graphene films. Generally, CVD graphene is grown on metal substrates such as Cu and Ni foil, and thus graphene films should be transferred from metal substrates to insulating substrates such as SiO_2 and boron nitride (BN) for electronics applications. Conventional transfer process uses polymer coating to support graphene films during etching metal substrates, and then, the polymer is washed by organic solvent [1]. This process, however, includes several unavoidable issues such as remaining polymer and solvent on the graphene surface and at the graphene/substrate interface. The improvement of transfer process is, therefore, still highly desired to realize intrinsic transport properties of CVD graphene.

In this study, we have developed a clean, direct transfer process (Direct transfer) of CVD graphene under inert atmosphere at very high temperature over 1100°C. Graphene was grown on Cu foil, and then was fixed on BN substrates. For the transfer, the samples were annealed at 1150°C to melt Cu foil under Ar/H_2 atmosphere. During the Cu melting, the graphene films can be directly transferred on the BN substrates. The presence of graphene on BN was confirmed by optical microscope, atomic force microscope (AFM), and Raman spectra (Fig. 1). It is noteworthy that the graphene on BN has highly-clean surface like BN surface and one-atom-thick height profile (Fig.1b,c). Furthermore, 2D band of the graphene shows relatively narrow full width at half maximum (fwhm) of 19 cm^{-1} compared to that of graphene transferred on BN by conventional polymer-assisted process (Fig.1d). In the presentation, we will report the details of process and properties of the present graphene/BN heterostructures.

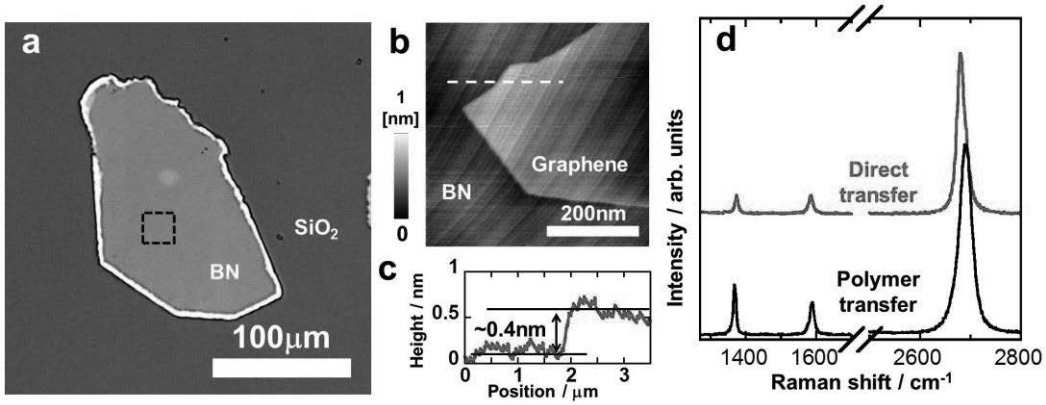

Fig.1 (a) Optical microscope, (b) AFM images, and (c) height profile of the graphene on BN. (d) Raman spectra of graphene on BN obtained by the present direct transfer and conventional polymer transfer processes.

[1] X. Li, *et al*., Science **324**, 1312 (2009).

Corresponding Author: Yasumitsu Miyata, Tel: +81-42-677-2508, E-mail: ymiyata@tmu.ac.jp

Graphene Etching Reaction Analyzed by a Time-Reversed Crystallization Theory

○Yu-uto Watanabe, Yu-usuke Ikemura, Masahito Sano

Department of Polymer Science and Engineering, Yamagata University
Yonezawa, Yamagata 992-8510, Japan

For semiconducting and magnetic applications of graphene, it is important to fabricate small graphene flakes with controlled shapes and edge structures. In this study, a wet-etching reaction of graphene by piranha solution at a mild condition is examined to see if it is suitable for shape- and edge- controls. In particular, it is of our interest to know whether the etching reaction proceeds along zigzag edges (at perimeters or 1D) or it enlarges pits or holesexisting within a graphene plane (2D). It is also our aim to gain information on if the reaction produces additional defects during etching.

In order to analyze the kinetic data, we have noted that graphene etching is a removal process of identical carbon hexagons from the honeycomb lattice. When viewed backward in time (i.e. with time-axis reversed), it is an addition of hexagons to the lattice. This has suggested us that the etching kinetics may be analyzed by a time-reversed crystallization theory with "etching" replaced by "growth" and "initiation" by "nucleation". In particular, Avrami theory is appropriate to resolve our interests. It is based on a problem of expanding waves produced by randomly falling raindrops on water. The Kolmogorov-Johnson-Mehl-Avrami (KJMA) equation describes a fractional space occupied by all expanding waves at time *t*.

Confocal Raman microscopy was employed to follow the etching kinetics of single-layer graphene and multi-layer graphene oxide. The KJMA equation in the present case is given by

$$-\ln\left(\frac{G}{G_0}\right) = kt^n$$

where G is the G-band intensity at t, k is a rate constant, and n is the Avrami exponent that equals the dimension in heterogeneous (constant number of nucleus) nucleation and the dimension + 1 in homogeneous (increasing number of nucleus) nucleation.

A mild piranha solution was made and reacted at a low temperature. Figure 1 shows the Avrami plot for single-layer graphene. The exponents indicate that, at the early stage of the reaction, etching proceeds along zigzag edges without creating additional defects. The study demonstrates that the piranha etching at the mild condition can be applied to produce shape- and edge- controlled graphene flakes.

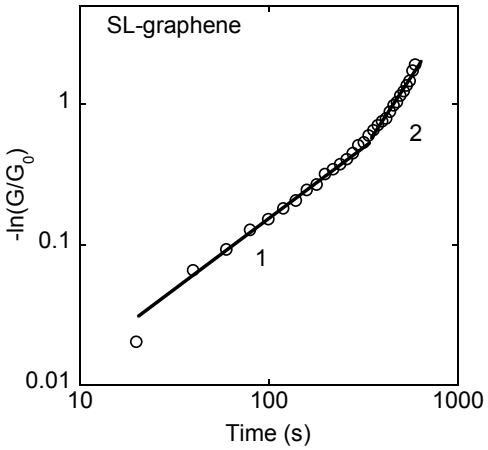

Fig.1: Log-log plot of the KJMA equation. The number indicates the slope of a straight segment.

Corresponding Author: M. Sano
Tel: +81-238-26-3072,
E-mail: mass@yz.yamagata-u.ac.jp

Raman spectroscopy of graphene in magnetic field

Toshiya Shirakura[1], Riichiro Saito[1]

[1] *Department of Physics, Tohoku University, Sendai 980-8578, Japan*

In this work, we calculate the Raman spectra of graphene in magnetic field in which the optical phonon and the inter Landau-level (LL) electronic transitions are coupled together. The physics of graphene in the presence of the magnetic field can be studied by the magneto Raman spectroscopy [1,2,3]. The high quality of graphene samples are reflected by the long lifetime of the Dirac fermions and the narrow spectral widths of the LL [4]. For evaluating the in-plane crystal size, the defects, the LL spectral width can be compared by using Raman spectroscopy in magnetic field [4,5].

A previous theoretical work has calculated the Raman spectra of graphene under the magnetic field by using fitting parameter which relating to G-peaks from experiment of Raman spectra in their formula [6]. However, they did not consider the microscopic picture of interference of the peaks. In this work, we directly calculate the G-band Raman spectra by considering electron-photon and electron-phonon interaction. In order to get the result, we consider time-dependent perturbation theory, and we adapt dipole approximation for electron-photon matrix element. Dipole approximation means that wave length of laser is sufficient long compared with atomic bond length of graphene, and it is important point to satisfy selection rule of transition probability, that is $|n'| - |n| = \pm 1$(n is the index of LL) [7]. In the case of electron-phonon interaction, we consider the deformation potential which is given by a sum over atomic screened ion potential, and we use Gaussian fitting parameter in calculation of atomic orbital [8]. We will compare the calculation and experimental result.

[1] M. O. Goerbig, *et al.*, Phys. Rev. Lett. **103**, 087402 (2009).
[2] T. Ando, *et al.*, J. Phys. Soc. Jpn. **76**, 024712 (2007).
[3] C. Faugeras, *et al.*, Phys. Rev. Lett. **103**, 186803 (2009).
[4] J. Yan, *et al.*, Phys. Rev. Lett. **105**, 227401 (2010).
[5] C. Faugeras, *et al.*, Phys. Rev. Lett. **107**, 036807 (2011).
[6] C. Qiu, *et al.*, Phys. Rev. B. **88**, 165407 (2013).
[7] M. Arikawa, *et al.*, Phys. Rev. B. **78**, 205401 (2008).
[8] A. Gruneis, PhD Thesis. (2008).

Corresponding Author: T. Shirakura
E-mail: shirakura@flex.phys.tohoku.ac.jp

Photoluminescence properties of thin layer black phosphorene

○Takashi Nakamura, Shinichiro Mouri, Yuhei Miyauchi, and Kazunari Matsuda

Institute of Advanced Energy, Kyoto University, Kyoto, Japan

Recently, the atomically thin layered two-dimensional (2D) materials have attracted much interest from the viewpoints of fundamental physics and applications. The black phosphorus is also capable of being mechanically exfoliated to single or several atomic layers, which are called as "phosphorene". Although the phosphorene is spotlighted as the new material for 2D semiconductor [1], the detail electronic and optical properties have not been fully understood. Thus, we studied single- and multi-layer black phosphorene by using optical spectroscopy, Raman, photoluminescence (PL), and differential reflectivity to understand their characteristic optical and electronic properties.

Our previous work shows the linearly polarized differential reflectivity spectra corresponding to absorption spectrum of black phosphorene with different thickness [2]. The differential reflectivity spectrum of thick phosphorene shows the peak at 0.37 eV, which is almost consistent with the previously reported value of bulk phosphorus [3]. In contrast, the differential reflectivity spectrum of thinner phosphorene shows a peak at 0.55 eV, which is assigned as the exciton absorption peak. The energy of absorption peak increases with decreasing of layer thickness due to quantum confinement effect. However for more thinner layers (single- and bi-layer), the absorption peaks would exist in far beyond the near-infrared region, therefore we have studied optical properties in thin-layer phosphorene with different methods. Figure 1 (a) and (b) show optical and PL image of phosphorene flakes. The PL spectrum in Fig, 1 (c) shows the broad features of 1.3, and 1.55 eV from bi- and single-layer black phosphorene, where the layer numbers of black phosphorene was confirmed from the optical contrast and Raman spectra [3,4]. In the conference, we will discuss the detail optical and electronic structure of thin layer black phosphorene based on the experimental results of Raman and PL spectroscopy.

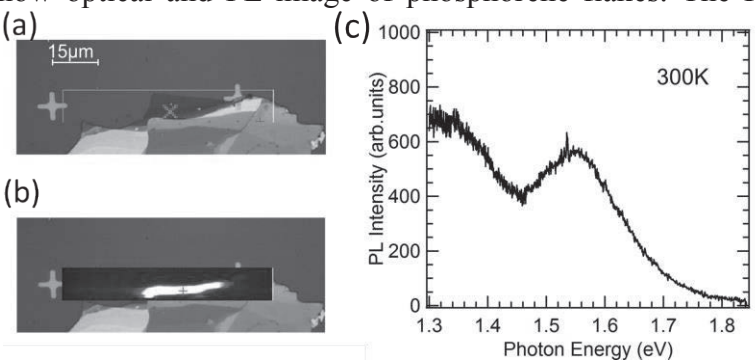

Fig, 1: Optical and PL image of flakes of phosphorene. PL spectra of single- and bi-layer phosphorene.

[1] Likai Li *et al., Nat. Nanotech.* **9,** 372-377 (2014).

[2] Takashi Nakamura *et al.,* 48th *Fullerene-nanotube-graphene conference*. 3-5

[3] Wanglin Lu *et al, Nano Research* **7**, 853-859 (2014).

[4] Han Liu *et al, ACS Nano* **8**, 4033-4041 (2014).

Corresponding Author: Takashi Nakamura
Tel: +81-774-38-3463, Fax: +81-774-38-4567,
E-mail: nakamura.takashi.23z@st.kyoto-u.ac.jp

Magnetic properties of graphene quantum dots embedded in h-BN

○Mina Maruyama and Susumu Okada

Graduate School of Pure and Applied Sciences, University of Tsukuba, Tsukuba 305-8571, Japan

Because of structural similarity between graphene and h-BN, they can form in-plane hetero structures in which h-BN and graphene are connected each other via C-B and N-C hetero chemical bonds at their borders. Recently, these in-plane hetero sheets of graphene and h-BN have been synthesized experimentally. In an early theoretical calculation predicted that these hetero sheets exhibit the magnetic ordering in graphene domain depending on the domain shapes and the border arrangements. In the case of the graphene dot with a triangular shape embedded in h-BN, the dots exhibit spin polarization induced by the half-filled non-bonding states at the Fermi level. For the practical application of the graphene dots in h-BN for spin devices, it is important to elucidate the fundamental magnetic properties of both within and between the dots. Therefore, in this work, we aim to investigate that energetics and spin-spin interaction J between graphene dots with the triangular shape embedded into h-BN using density functional theory.

Figure 1 shows isosurfaces of spin densities of graphene dots in h-BN with the inter-dots spacing of 1nm. Spin densities are localized on C atoms situated at the border between graphene dots and h-BN. We find the singlet and triplet spin arrangements as their stable spin configurations. By taking the energy difference between the singlet and triplet states, we can estimate the spin-spin interaction J between dots. Figure 2 shows the J between two graphene dots. The J possesses a minimum value of J = 25 meV at the inter-dot spacing of 0.5 nm, indicating that the flakes prefer the singlet spin arrangement to the triplet spin arrangement. The J rapidly approaches zero with increasing the inter-dot spacing. The fact indicates that the spin interaction J is the short-range interaction of which interaction range is less than 1 nm.

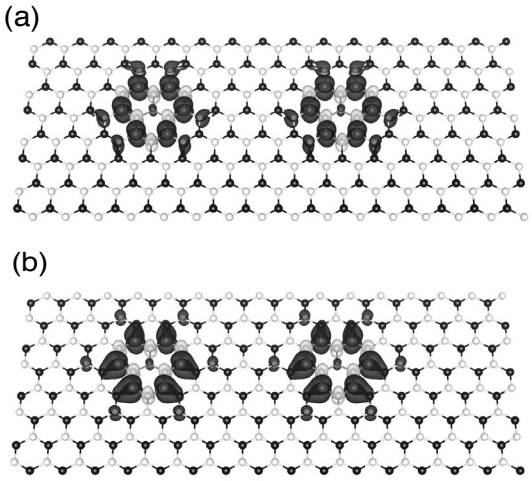

Fig.1: Isosurfaces of spin densities of (a) C/N and (b) C/B borders of graphene dots embedded into h-BN with inter-dots spacing of 1 nm in a triplet spin coupling.

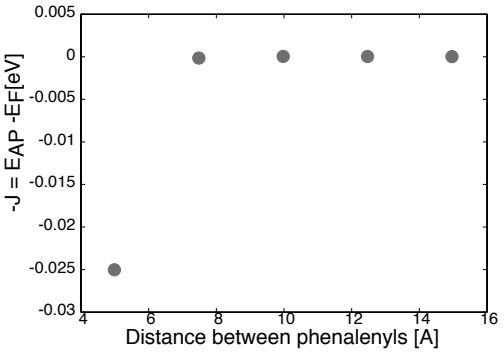

Fig. 2: The spin-spin interaction J between graphene dots as a function of the inter-dots spacing.

Corresponding Author: M. Maruyama
Tel: +81-29-853-5600 (ext. 8233), Fax: +81-29-853-5924,
E-mail: mmaruyama@comas.frsc.tsukuba.ac.jp

A durable Pt electrocatalyst supported on a polybenzimidazole wrapped 3D nanoporous carbon shows a high fuel cell performance

Zehui Yang[1], Tomohiro Shiraki[1], Isamu Moriguchi[2] and Naotoshi Nakashima *[1,3]

[1] *Department of Applied Chemistry, Kyushu University, Fukuoka 819-0395, Japan*
[2] *Division of Chemistry and Materials Science, Graduate School of Engineering, Nagasaki University, 1-14 Bunkyo-Machi, Nagasaki 852-8521, Japan*
[3] *WPI-I2CNER, Kyushu University, Fukuoka 819-0395, Japan*

Polymer electrolyte fuel cells (PEFCs) have the potential to alleviate major problems associated with the production and consumption of energy, considered as promising, attractive, reliable and clean energy generation for automotive and stationary applications; thus considerable attention has been focused on the high-temperature PEFCs (> 100 ^{o}C), due to their benefiting PEFCs with higher carbon monoxide (CO) tolerance, faster electrochemical kinetics, and better water management than those of conventional PEFCs. However, the high-temperature PEFCs also suffer from their low durability in terms of carbon corrosion and platinum nanoparticles (Pt-NPs) aggregation resulting in the detachment of the Pt-NPs from the catalysts and loss in electrochemical surface area (ECSA) as well as the degradation of FC performance. Thus, enhancement in durability is highly demanded for the commercialization of the next-generation PEFCs.

Nanoporous carbon (NanoPC) has a porous structure with a higher surface area that has a high potential to be a supporting carbon of PEFCs. In this study, we used PyPBI to wrap nanoporous carbon (NanoPC) before Pt-loading as schematically shown in Figure 1 in order to obtain a NanoPC/PyPBI/Pt electrocatalyst. The electrochemical surface area (ECSA), durability and high temperature fuel cell performance of the prepared electrocatalyst have been measured and compared its performance to the conventional CB/Pt and CB/PyPBI/Pt electrocatalysts.

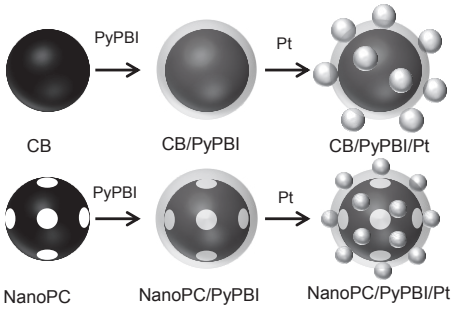

Figure 1. Schematic illumination of preparation of CB/PyPBI/Pt and NanoPC/PyPBI/Pt electrocatalysts.

As shown in Figure 2, the power density of NanoPC/PyPBI/Pt (342 mW/cm^2) was almost 2 times higher than that of the CB/PyPBI/Pt.

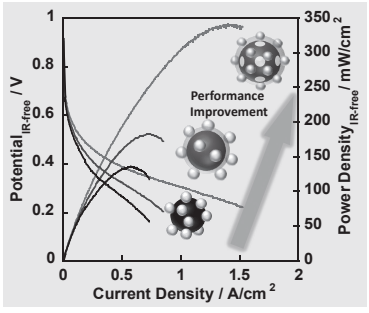

Figure 2. I-V and power density polarization curves of different MEAs based on CB/Pt (black line), CB/PyPBI/Pt (blue line) and NanoPC/PyPBI/Pt (red line) at 120 ^{o}C under non-humidified atmosphere.

Reference

[1] N. Nakashima et al. *ACS Appl. Mater. Interfaces*, **2015**, *7*, 9800-9806.

Corresponding Author: N. Nakashima
Tel: 092-802-2840, Fax: 092-802-2840,
E-mail: nakashima-tcm@mail.cstm.kyushu-u.ac.jp

Synthesis of carbon nanopot with Fe catalyst supported on graphene oxide

○Hiroyuki Yokoi[1], Kazuto Hatakeyama[1], Michio Koinuma[1], Takaaki Taniguchi[2], Yasumichi Matsumoto[1]

[1] *Graduate School of Science and Technology, Kumamoto University, Kumamoto 860-8555, Japan*

[2] *International Center for Materials Nanoarchitectonics, National Institute for Materials Science, Tsukuba 305-0044, Japan*

Carbon nanopot, a novel material developed recently[1], is a pot-shaped material composed with multi-layered graphene sheets, and is produced in series to form fibers (nanopot fibers). The typical size of carbon nanopot is 20-40 in diameter and 100-200 nm in length. Its narrow and deep mesopore is closed on one end, which suggests that this material could be applied as nano-container.

In the previous syntheses of carbon nanopot, we used iron acetate and cobalt acetate as precursors of catalyst and mixed them with aqueous dispersion of graphene oxide to mount catalyst on graphene oxide. However, UV-VIS absorption measurements and XRF and XPS analyses have revealed recently that cobalt is not mounted on graphene oxide as much as prepared. In order to investigate the effect of cobalt on the growth of carbon nanopot, we first conducted the synthesis experiments with using iron acetate as a single precursor of catalyst. In the synthesis conditions same as the previous growth conditions except for the catalyst, we obtained carbon nanopot similarly as in the previous synthesis (Figs. 1 and 2). However, the amount of products decreased greatly compared with the previous ones, as one observes in Fig. 1 that nanopot fibers were produced sparsely. This result suggests that cobalt can enhance the formation of carbon nanopot though it may not be essential to that. Control of cobalt content on graphene oxide could be one of key factors in producing carbon nanopot effectively.

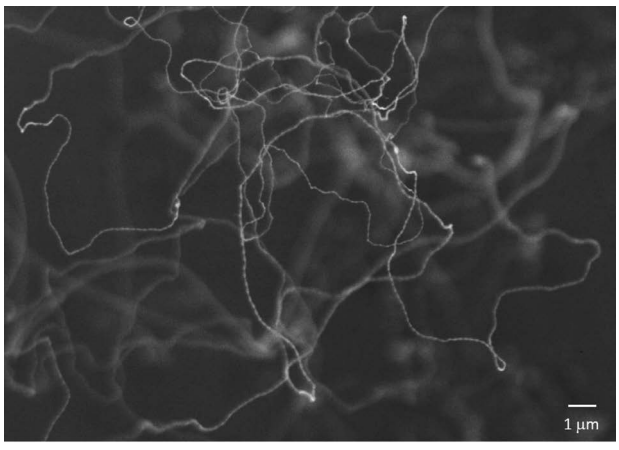

Fig. 1: SEM image of carbon nanopot fibers produced in this study.

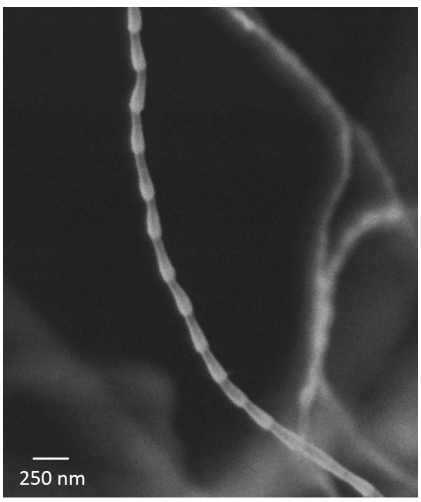

Fig. 2: Enlarged SEM image of one of carbon nanopot fibers in Fig. 1.

[1] H. Yokoi *et al*. submitted.

Corresponding Author: H. Yokoi
Tel: +81-96-342-3727, Fax: +81-96-342-3710,
E-mail: yokoihr@kumamoto-u.ac.jp

Bound Exciton Emission in Photoluminescence Spectrum of Monolayer WSe_2

○N. Baizura Mohamed, Feijiu Wang, Shinichiro Mouri, Koirala Sandhaya, Yuhei Miyauchi, and Kazunari Matsuda

Institute of Advanced Energy, Kyoto University, Uji, Kyoto 611-0011, Japan

The atomically thin transition metal dichalcogedes (TMDCs) have been attracted much interests from viewpoint of fundamental physics and applications. The optically generated electron-hole pair forms two-dimensional (2D) exciton in atomically thin TMDCs, such as MX_2 (M=Mo, W, X=Se, S). Recently, the spatially localized exciton in semiconductor materials have become a hot topic for the quantum scientific field, because single impurities could be used as the qubits of quantum computation, as well as nonclassical light sources, in quantum information science [1]. In particular, it is expected that the bound exciton to well-defined single impurity (defect) in TMDCs are promising system for these target [2,3].

In this study, we investigated the nature of bound exciton emission in WSe_2 by photoluminescence (PL) spectroscopy from 5 to 300 K. Figure 1(a) shows the optical microscope image of WSe_2 flake with monolayer thickness. We obtained the PL image of the WSe_2 flakes, monitored in the PL intensity of 1.55 eV at low temperature. The strong PL intensity is observed from monolayer region in the PL image. Moreover, the bright PL spot is observed in the edge of monolayer WSe_2 (figure 1(b)). Figure 1(c) exhibits temperature dependence of PL spectra at the bright PL spot. The PL spectra at 5 K shows broad peak around 1.65 eV due to the defects (or vacancies) related emission of WSe_2. Very sharp emissions appear at 1.55 eV in the PL spectra from 5 to 40 K, which depicts the bright spot in the PL image. This very sharp peak might originate from bound exciton emission to well-defined point defect of WSe_2. This type of spatially localized bound exciton behaves as 0D-like exciton in 2D WSe_2. We will discuss the natures of 0D-like exciton in monolayer WSe_2 for future development of TMDCs-based quantum optical science and its applications.

References

[1] T. Kato *et al.,* ACS Nano, 8, 12777, (2014).

[2] P. Tonndorf *et al.*, Optica, 2, 347, (2014)

[3] A. Srivastava *et al., Nature Nanotech*,doi:10.1038/nnano.2015.60 (2015).

Corresponding Author: Prof. Kazunari Matsuda
Tel: +81-774-38-3460
Fax: +81-774-38-3460
E-mail: matsuda@iae.kyoto-u.ac.jp

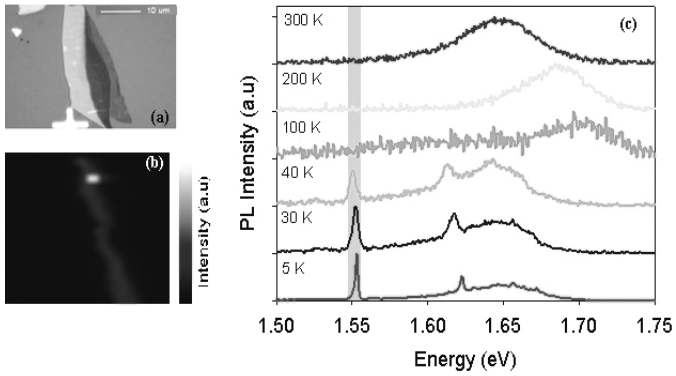

Figure 1 (a) Optical image of monolayer WSe_2, (b) PL intensity map integrated at 1.55 eV, (c) PL spectra of WSe_2 from 5 to 300 K.

In-situ electrochemical Raman Spectroscopic Studies of MoS_2 grown on Au(111)

○Ryosuke Takahashi, Ryota Kumagai, Satoshi Yasuda, Kei Murakoshi

Department of Chemistry, Hokkaido University, Sapporo 060-0810, Japan

Molybdenum disulfide (MoS_2) has extensively studied in recent years due to its various electronic properties. To maximize their properties, precise understanding of an influence of carrier doping on phonon properties is required. In this study, single crystalline monolayer MoS_2 was synthesized by PVD process, and in-situ Raman spectroscopy (532nm, 1mW) was carried out to investigate the potential dependent change of monolayer MoS_2 on Au(111) under electrochemical potential control in aqueous solution.

Fig. 1 shows an optical image of a large area MoS_2 grown on Au(111) substrate, and monolayer MoS_2 with rectangular shaped MoS_2 patterns could be produced. Raman measurement found that both E^1_{2g} and A_{1g} were clearly observed, however, A_{1g} mode split two peaks. Observed splitting of A_{1g} mode is attributed to be a modulation effect by interacting with Au(111) surface. Electrochemical potential dependence of Raman spectra was also found that both phonon modes soften with electron doping (Fig. 2), suggesting weakening of the bonds due to an occupation of the antibonding states in the conduction band. These results demonstrated detail evaluation of the influence of carrier doping on MoS_2 phonon properties.

Corresponding Author: S. Yasuda
TEL & FAX: +81-(0)11-706-4811
E-mail: satoshi-yasuda@sci.hokudai.ac.jp

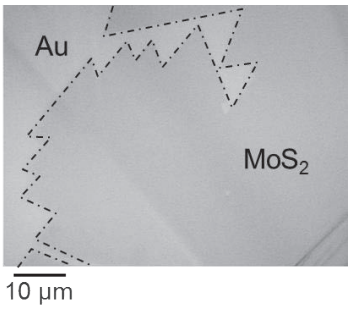

Fig.1 A representative Photograph of monolayer MoS_2 grown on Au(111).

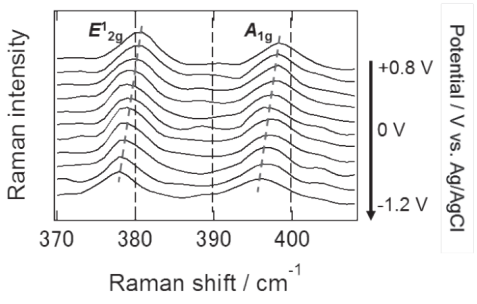

Fig.2. Electrochemical Raman spectra of monolayer MoS_2 grown on Au(111) 0.5 M Na_2SO_4 aqueous solution.

First-principles study of the morphology of MoS_2 on $Al_2O_3(0001)$

○Hideyuki Jippo, Kenjiro Hayashi, Shintaro Sato, Mari Ohfuchi

Fujitsu Labs. Ltd., 10-1 Morinosato-wakamiya, Atsugi, Kanagawa 243-0197, Japan

An increasing interest has emerged in transition metal dichalcogenides (TMDCs) such as MoS_2 owing to their unique properties. Chemical vapor deposition (CVD) is a promising method to synthesize large-scale monolayer MoS_2, which is crucial for device applications. Sapphire (α-Al_2O_3) has been explored as one of the substrates for such large-scale CVD growth; however, recently it was reported that triangular MoS_2 islands have two preferential orientations on α-$Al_2O_3(0001)$ substrates [1], possibly causing grain boundaries. We have also obtained similar experimental results. In this work, to understand this phenomenon, we perform first-principles calculations of MoS_2 on α-$Al_2O_3(0001)$, using the density functional theory (DFT) code, OpenMX [2].

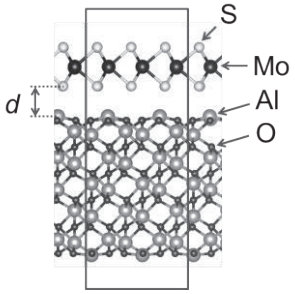

Fig. 1: Side view of the most stable structure (Structure A) of MoS_2 on Al-terminated $Al_2O_3(0001)$. The rectangle shows the unit cell. The interlayer distance *d* was determined to be 2.4 Å.

The surface condition of α-$Al_2O_3(0001)$ has not been identified in our CVD experiments. For example, DFT calculations have revealed that two orientations of MoS_2 on O-terminated α-$Al_2O_3(0001)$ produce a small total energy difference (2.2 meV per MoS_2) [3]. Although OH terminations may also exist on the surface, we here investigate MoS_2 on Al-terminated α-$Al_2O_3(0001)$ surface. This Al-terminated surface is observed under UHV conditions and considered to be the most stable. Figures 1 and 2(a) show the most stable structure (Structure A) among the examined models. Three topmost Al atoms per unit cell make bonds with S atoms of MoS_2. After rotation of MoS_2 by 60° and geometric optimization, we obtained the second most stable structure (Structure B) shown in Fig. 2(b). We have found that "Structure B" is less stable than "Structure A" only by 0.7 meV per MoS_2, which is smaller than that for the O-terminated surface.

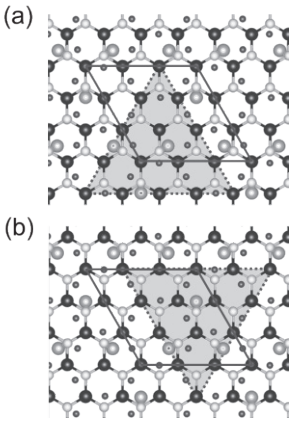

Fig. 2: Top views of (a) the most and (b) the second most stable structures (Structures A and B). The atoms of MoS_2 and top two layers of Al_2O_3 are shown. The rhombus represents the unit cell. The gray triangle indicates the MoS_2 island with Mo edges.

Our CVD experiments were performed under S-rich conditions, where Mo edges with S terminations are the most stable [4], leading to triangle islands as illustrated in Fig. 2. If the orientation of the triangles is determined at the early stage of islands with approximately ten MoS_2 units, the probability ratio of two orientations of the triangles is estimated to be 1.1 at our growth temperature of 800° C. This suggests that it is essentially difficult to align the orientation of triangular MoS_2 islands on α-$Al_2O_3(0001)$ substrate.

[1] D. Dumcenco *et al*., ACS Nano 9, 4611 (2015). [2] http://www.openmx-square.org/
[3] Q. Ji *et al.*, Nano Lett. 15, 198 (2015). [4] D. Cao *et al.*, J. Phys. Chem. C 119, 4294 (2015).

Corresponding Author: H. Jippo, Tel: +81-46-250-8843, E-mail: jippo.hideyuki@jp.fujitsu.com

Preparation of iron oxide nanotubes with spectral sensitivity peak at red light region and its application to photo-voltaic device

○ Yuta Kosugi[1], Takuya Tomiyasu[1], Shunji Bandow[2]

Department of Materials Science & Engineering[1] and of Applied Chemistry[2], Meijo University, Nagoya 468-8502, Japan

Magnitude of optical band gap for various iron oxides materials are at around 2.2 eV, which corresponds to the light wavelength of ~520 nm. This wavelength is much longer than that of TiO_2 (~3 eV; ~380 nm) which is used for various photo-energy conversion applications. However the maximum of the radiation intensity of sunlight is around 500 nm and it rapidly drops in UV region. Regarding the radiation intensity of sunlight, iron oxide is much effective for the sunlight harvesting when the HOMO and LUMO level matchings are solved. To modify the energy levels, we conducted several trials such as nano-tubulization, thermal treatment and zinc doping.

Fig. 1 indicates a dependence of thermal treatment on the optical band gap (top abscissa) evaluated by a Tauc plot method, together with that on zinc doping (bottom abscissa). One can see clearly that the thermal treatment and zinc doping decrease the band gap. Former one is associated with the lattice relaxation effect and latter one with widening the LUMO level.

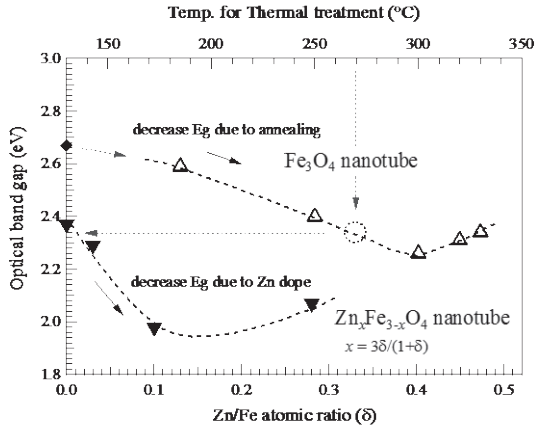

Fig. 1. Thermal treatment and Zn/Fe atomic ratio dependence of the optical bad gap.

Obtained nanotubes were spin coated onto FTO glass from an aqueous suspension of Fe-ox-NT (or ZnFe-ox-NT) powder which was grounded by adding a small amount of acetylacetone. Film thickness was controlled by the quantity of droplets. Then the spectral sensitivity was measured in the electrolyte of $LiClO_4/LiI/I_2$/acetonitrile by irradiating the band-pass filtered light of 390, 420, 480, 510, 540, 600, 660 and 710 nm. Fig. 2 is the results of spectral sensitivity. Thicker Fe-ox-NTs has much better characteristic than that of thin one, and the zinc doping was invalid for improving the spectral feature.

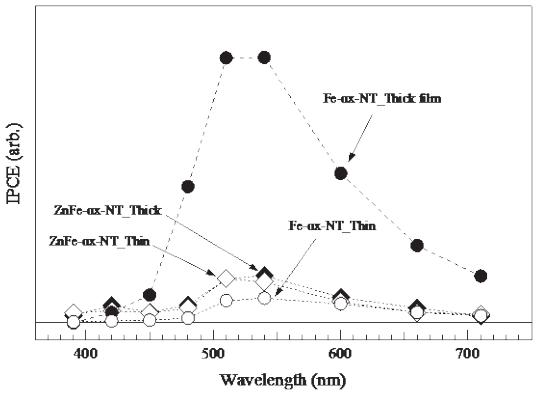

Fig. 2. Thickness dependence of spectral sensitivity for Fe-ox-NTs and ZnFe-ox-NTs.

Corresponding Author: S. Bandow
E-mail: bandow@meijo-u.ac.jp, Tel: +81-52-838-2404

Fabrication and Brightness Evaluation of Nano-Carbon Field Emission Electron Source

Hitoshi Nakahara, Shinichi Ito, Yahachi Saito

Department of Quantum Engineering, Nagoya University, Nagoya 464-8603, Japan

We have studied nano carbon field emitters fabricated by field emission induced growth (FEIG) for high brightness electron source of electron microscopy. It has been already reported [1] that the FEIG nano emitters were easy for gun alignment and obtained better SEM images than carbon nanotube (CNT) emitters. However, its detailed structure and brightness has not been obtained so far. Thus in this study, we observed transmission electron microscopy (TEM) images of the grown emitter. In addition, evaluation of brightness was carried out by means of computer simulations of electric fields and electron trajectories.

Fig. 1 is a TEM image of a FEIG fabricated emitter. As shown in the figure, amorphous layer and graphitic layer (which has 0.35 nm of lattice spacing) were formed on a tungsten needle. In addition, capsule like particles (which has about 1 nm of diameter) formed a nano protrusion as a nano emitter. These capsules were considered to be carbon nano capsules transformed from the graphitic carbon by Joule heat caused by field emission electric current at an emission site.

Fig. 2 shows calculated brightness for growing emitter as a function of growing radius of nano emitter (r). The radius of base tungsten needle (R) used in the calculation was 50.7 nm. Both radii were estimated from I-V measurements during FEIG experiment. As shown the figure, it has been confirmed that the brightness of FEIG emitter was about 10 times higher than that of conventional single crystalline tungsten field emission electron source.

[1] H. Nakahara, S. Ito, S. Ichikawa and Y. Saito: e-J. Surf. Sci. Nanotech. 12 (2014) 192.

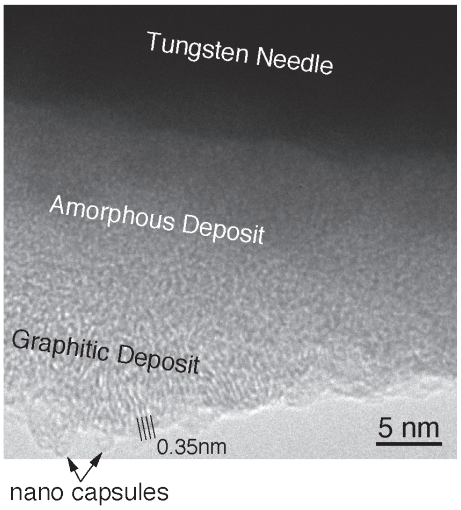

Fig. 1: TEM image of FEIG fabricated emitter tip.

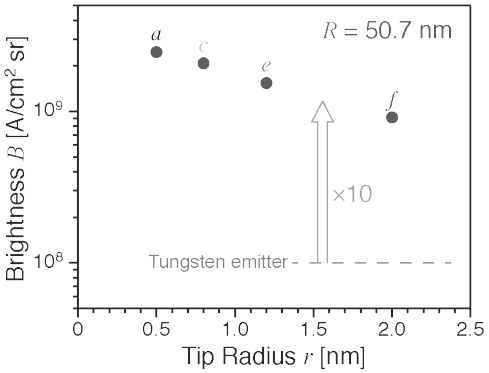

Fig. 2: Calculated brightness for growing emitter. *a* to *f* in the figure correspond to growth stages, and horizontal axis shows growing radius of nano emitter during the growth (estimated from I-V measurements).

Preparation of [C_{60}]Fullerene Nanowhiskers-Gold Nanoparticles Composites and Their Catalytic Activity for Reduction of 4-Nitrophenol

○Jeong Won Ko[1], Jiulong Li[1], Weon Bae Ko[1,2*]

[1]*Department of Convergence Science, Graduate School, Sahmyook University, Seoul 139-742, South Korea*
[2] *Department of Chemistry, Sahmyook University, Seoul 139-742, South Korea*

Gold nanoparticles solution which was synthesized by adding trisodium citrate dihydrate($C_6H_5Na_3O_7 \cdot 2H_2O$), sodium borohydride($NaBH_4$), cetyltrimethyl ammonium bromide($(C_{16}H_{33})N(CH_3)_3Br$), ascorbic acid and potassium gold(Ⅲ) chloride($KAuCl_4$) into distilled water and then, the resulting solution was stirred for 15 min. [C_{60}]Fullerene nanowhiskers-gold nanoparticles composites were synthesized using C_{60}-saturated toluene, gold nanoparticles solution and isopropyl alcohol by liquid-liquid interfacial precipitation(LLIP) method. The product of [C_{60}]fullerene nanowhiskers-gold nanoparticles composites was characterized by X-ray diffraction, Raman spectroscopy, scanning electron microscopy and transmission electron microscopy. Catalytic activity of [C_{60}]fullerene nanowhiskers-gold nanoparticles composites as a catalyst was confirmed in the reduction of 4-nitrophenol by UV-vis spectroscopy.

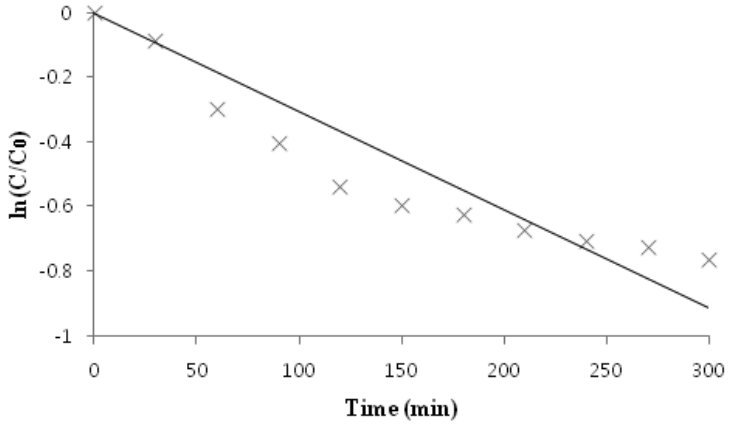

Fig.1 Kinetics for reduction of 4-nitrophenol by first-order reaction equation with the [C_{60}]fullerene nanowhiskers-gold nanoparticles composites

[1] S. K. Hong, J. H. Lee, J. M. Kim and W. B. Ko, *J. Nanosci. Nanotechnol*., **11,** 734 (2011).
[2] K. Miyazawa, *J. Nanosci. Nanotechnol*., **9,** 41(2009).

* Corresponding Author: Weon Bae Ko
Tel: +82-2-3399-1700, Fax:, +82-2-979-5318
E-mail: kowb@syu.ac.kr

Development of *O*-acetylated sugar substituted fullerenes for solution-processed organic field-effect transistors and photovoltaics

○Yu Uemura[1,2,3], Akifumi Yagami[1], Masayoshi Yoshitake[1], Yuta Murakami[1], Yoshihiko Nishihara[3], Masayuki Chikamatsu[3], Keiji Mizuki[1,2], Taizo Hatta[1,2]

[1] Department of Nanoscience, Sojo University, Kumamoto 860-0082, Japan
[2] Kumamoto Institute for Photo-Electro Organics (PHOENICS), Kumamoto 862-0901, Japan
[3] Research Center for Photovoltaics (RCPV), National Institute of Advanced Industrial Science and Technology (AIST), Ibaraki 305-8565, Japan

Soluble fullerene derivatives have been highly required to realize solution-processed organic field-effect transistors (OFETs) and organic photovoltaics (OPVs) with low-cost, large-area, light-weight and flexibility.

In this study, highly organic solvent-soluble fulleropyrrolidines having *O*-acetylated glucoside or galactoside units in the phenyl group (**1a**-**1c**, **2a**-**2c**) were developed. In addition, their fluorinated ones (**3**, **4**) and *N*-phenyl isomer (**5**) were also synthesized. These derivatives and a reference material (**PCBM**) were applied to the solution-processed OFETs and OPVs, and the influence of the chemical structures on the characteristics of the OFETs and the OPVs was investigated.

Moreover, diastereoresolution of **2c** was succeeded by using a chiral column chromatography. The resolved diastereomers (**2c-fwd**, **2c-bwd**) were applied to OFETs and OPVs, and their performances were compared to those of the diastereo-mixture (**2c**).

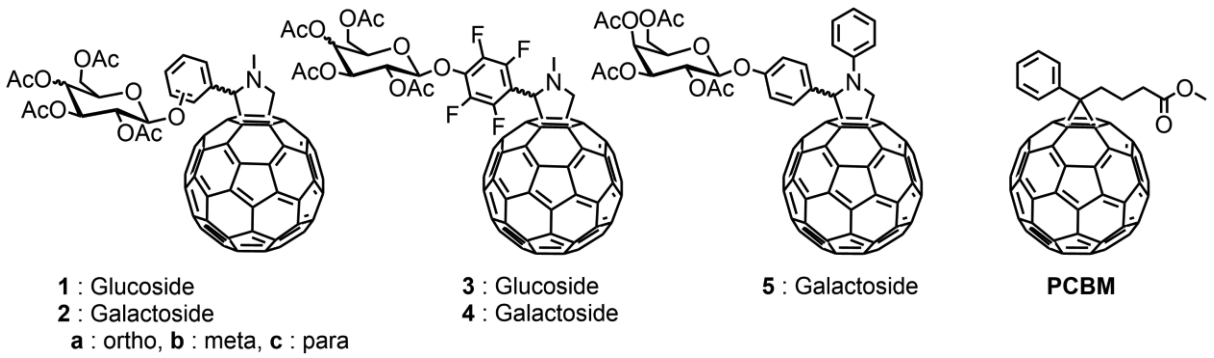

Figure 1. Molecular structures of fulleropyrrolidine derivatives having *O*-acetylated glucoside or galactoside units (**1a**-**1c**, **2a**-**2c**, **3**, **4**, **5**) and **PCBM**.

Corresponding Author: T. Hatta
Tel: +81-96-326-3745, Fax: +81-96-326-3000,
E-mail: hatta@nano.sojo-u.ac.jp

Curvature Effect on Wettability of Carbon Nanotubes

○Konan Imadate[1], Kaori Hirahara[1, 2]

[1] *Department of Mechanical Engineering, Osaka University, Osaka, 565-0871, Japan*
[2] *Center for Atomic and Molecular Technologies, Osaka University, Osaka, 565-0871, Japan*

It is well known that nanometer-scale morphology of the solid surface often affects to the wetting characteristics [1]. It is interesting question how a single carbon nanotube (CNT) gets wet by liquid, since its surface consists of highly-curved graphene due to cylindrical feature with nanometer scale diameter. CNTs usually show hydrophobic nature, but Homma *et al.* have reported the existence of water layer surrounding the CNTs surfaces in humid atmosphere [2].

In this study, we examined the correlation between wettability and curvature of individual CNTs experimentally. Evaluation of single-CNT level wettability was carried out by means of force measurement using isolated CNTs with various diameters from 1.4 to 22nm based on Wilhelmy's balance method. In this method, force applied to a cylindrical solid material due to wetting usually measured, and contact angle is evaluated with Wilhelmy's balance equation $F=\pi d\gamma\cos\theta$, where F, d, γ and θ are the force due to wetting, diameter of cylinder, surface tension, and contact angle, respectively. Note that γ and θ are assumed to be constant on macroscale measurement.

Figure 1 shows a schematic of force measurement performed in this study. A CNT attached to a cantilever tip was contacted to the liquid surface and the force due to wetting was measured by using atomic force microscope (AFM). Diameter dependence of the measured values of force obtained with ionic liquid as the liquid specimen is shown in Fig. 2, where the force is normalized by circumference of individual CNTs ($F/\pi d$). The value of $F/\pi d$ is equal to $\gamma\cos\theta$ and therefore should be constant on macroscale, but we can see that the measured value for CNTs with diameter less than 5nm were significantly deviated. This finding indicates the curvature affects the wettability of CNTs. Details will be discussed on poster.

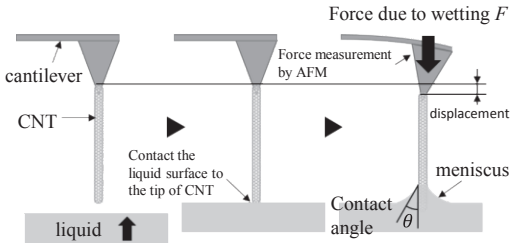

Fig. 1. Schematic image of force measurement in AFM.

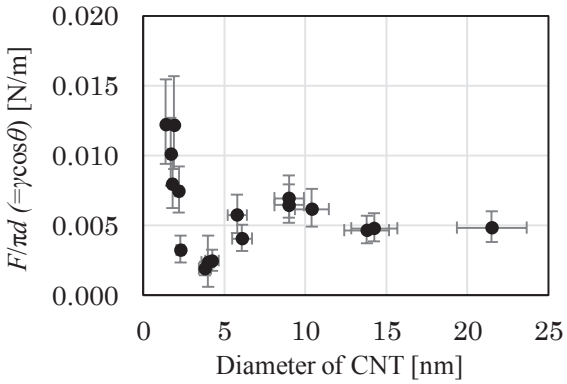

Fig. 2. Diameter dependence of $F/\pi d$

[1] S. Imabayashi, Review of Polargraphy, **54**, 115, 2008 (in Japanese)
[2] Y. Homma *et al.*, Phys. Rev. Lett., **110**, 157402, 2013

Corresponding Authors: Konan Imadate, Kaori Hirahara
Tel: +81-06-6879-7815, Fax: +81-06-6879-7815,
E-mail: imadate@ne.mech.eng.osaka-u.ac.jp, hirahara@mech.eng.osaka-u.ac.jp

Activity and Durability Evaluation of Non-Precious Metal Electrocatalyst for Oxygen Reduction Reaction in Fuel Cell

○Yosuke Uchibori[1], Atom Furuya[1], Satoshi Yasuda[1,2], Kei Murakoshi[1]

[1] *Department of Chemistry, Faculty of science, Hokkaido University, Sapporo, 060-0810, Japan*
[2] *JST-PRESTO, Kawaguchi, Saitama 332-0012, Japan*

Non-precious metal-nitrogen-carbon (M-N-C) catalysts has been attracted much attention as alternatives to costly and limited reserves Pt-based catalysts for oxygen reduction reaction (ORR) on cathodes of polymer electrolyte membrane fuel cells (PEMFC). Among the various Pt replaced candidates, Fe coordinated to nitrogen functionalized graphitic carbon (Fe-N-C) catalyst produced by pyrolysis of composites with nitrogen, Fe and carbon precursors, have been attracted much attention due to their ORR activities in acid solution. Even though various approaches have been performed to enhance ORR activity, the resultant catalysts still suffers from limited activity presumably due to low immobilization of the catalytic sites. In this study, we developed facile but abundant active Fe-N-C immobilized on CNT catalyst by pyrolyzing iron phthalocyanine (FePc) molecules adsorbed on vertically aligned carbon nanotube (VA-CNT). VA-CNTs have a feature of high specific surface area (~ 1000 cm^2/g) in contrast to conventional CNT represented by HiPco nanotube (~ 600 cm^2/g).

Simply mixing VA-CNTs and FePc were produced FePc wrapped CNT composites due to strong affinity by π – π interaction, and the pyrolysis (~900 ^oC under Ar atmosphere) efficiently translated the adsorbed FePc molecules into Fe-N-C active structure on VA-CNTs (Fig. 1). Ring rotating disk electrode (RRDE) voltammetry in oxygen saturated 0.5 M H_2SO_4 solution was performed to evaluate ORR activities (Fig. 2). The catalyst exhibited high ORR activity of an onset and half-wave potentials of 0.97 and 0.79 V versus the reversible hydrogen electrode, high selectivity of 3.94 ~ 3.98 electron transferred number and high electrochemical durability of 17 mV negative shift of $E_{1/2}$ for 10,000 cycles, respectively, in oxygen-saturated 0.5 M H_2SO_4 solution. The catalyst demonstrated one of the highest ORR performance in previously reported any nanotube based catalysts in acid medium. Such excellent ORR performance was attributed to its high surface area and efficient mass transport by its mesoporous nature.

Corresponding Author: K. Murakoshi
TEL: +81-(0)11-706-2704 , FAX: +81-(0)11-706-4810
E-mail: kei@sci.hokudai.ac.jp

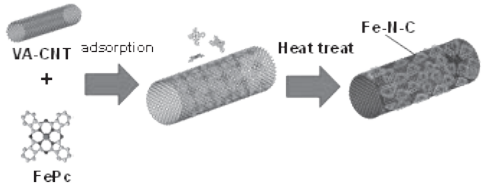

Fig. 1 Schematic illustration of fabrication of the Fe-N-C/VA-CNT.

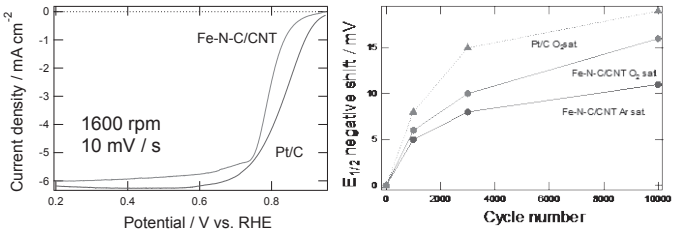

Fig. 2 RRDE polarization curves (left) and durability of Fe-N-C/VA-CNT in an O_2-saturated 0.5 M H_2SO_4 solution (right).

Laccase bioelectrocatalytic high potential oxygen reduction at steroid-type biosurfactant-modified carbon nanotube interface

○Aiko Sasaki[1], Makoto Togami[1], Masato Tominaga*[1,2]

[1] *Graduate School of Science and Technology, Kumamoto University, Kumamoto 860-8555, Japan*
[2] *Kumamoto Institute for Photo-Electro Organics (Phoenics), Kumamoto 862-0901, Japan*

Many redox enzymes operate very close to the thermodynamic potential of their substrate/product couple. Multicopper oxidases, especially laccase (Lac) and bilirubin oxidase, have been widely studied as fuel cell catalysts for oxygen reduction in enzymatic biocathodes, where oxygen is fully reduced to water without releasing H_2O_2 as an intermediate [1-3]. The multicopper oxidases have four copper atoms in their active sites, which are classified as type-1 (T1), type-2 (T2), and type-3 (T3) Cu sites. The mechanism of the function of multicopper oxidase includes three major steps: reduction of the T1 Cu site by electron transfer from a reduced substrate, intramolecular electron transfer between the T1 Cu site and T3 Cu site over a distance of ca. 1.3 nm, and reduction of O_2 to two H_2O molecules at the T2/3 Cu site.

The performance of multicopper enzymes in electrochemical oxygen reduction compares favorably with that of Pt. The turnover frequency, which is the maximum rate at which the catalyst can reduce oxygen, can exceed $>10^3$ s^{-1} for Lac and bilirubin oxidase, while the equivalent turnover frequency of Pt is limited to approximately 15 s^{-1} per Pt atom. However, the reported values of the heterogeneous electron transfer rate with electrodes are still far from the expected value ($>10^3$ s^{-1}), although the electrode surface function has been developed. We present the interface of single-walled carbon nanotubes (SWCNTs) modified with a steroid-type biosurfactant that give very fast heterogeneous electron transfer rates (3000 s^{-1}) between the T1 Cu site of Lac and the SWCNTs. The onset potential for starting the reduction reaction of O_2 was very close to the equilibrium redox potential of the oxygen/water couple. The electron transfer reaction behaviors were very sensitive to the side-chain of the steroid biosurfactant.

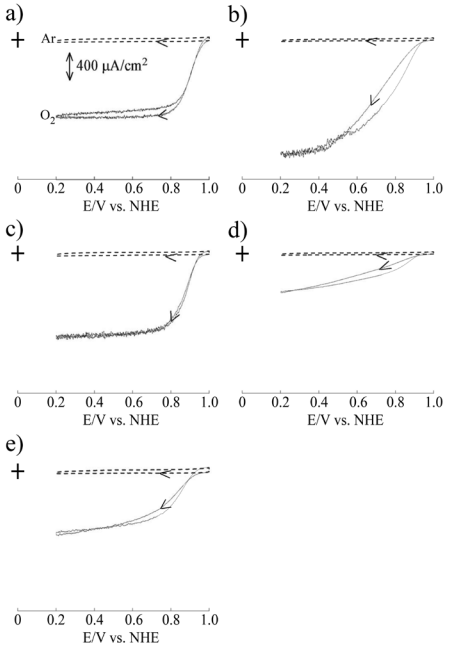

Fig. 1 Cyclic voltammograms of the bioelectrocatalytic current of O_2 reduction from the direct electron transfer reaction of Lac immobilized on a) SC-, b) SD-, c) ST- and d) STdx-SWCNTs, and e) unmodified SWCNTs in the presence of O_2 (solid line) and Ar gas (broken line). The potential sweep rate was 10 mV s^{-1} and the electrode surface area was 0.25 cm^{-1}. SC: sodium cholate; SD: sodium deoxycholate; ST: sodium taurocholate; STdx: sodium taurodeoxycholate.

[1] M. Tominaga *et al*. Anal. Chem., **87**, 5417 (2015).
[2] M. Tominaga *et al*. Anal. Chem., **86**, 5053 (2014).
[3] M. Tominaga *et al*. Electrochem. Commun, **59**, 32 (2015).

*Corresponding Author: M. Tominaga
Tel: +81-96-342-3655, F+81-96-342-3655,
E-mail: masato@gpo.kumamoto-u.ac.jp

Application of diameter-tunable single-walled carbon nanotubes to CNT-silicon solar cells

○Yang Qian[1], Kehang Cui[1], Rong Xiang[1], Shohei Chiashi[1], Shigeo Maruyama[1, 2]

[1] *Department of Mechanical Engineering, The University of Tokyo, Tokyo 113-8656, Japan*
[2] *National Institute of Advanced Industrial Science and Technology (AIST), Tsukuba, 305-8564, Japan*

Single-walled carbon nanotubes (SWNTs) have been a promising material for solar cell applications due to its wide range absorption spectrum, high electrical conductivity and transparency, as well as chemical stability. CNT-Si solar cell has shown a power conversion efficiency beyond 10% [1]. Despite the two crucial properties of SWNT film, conductivity and transmittance, the other effects of starting SWNTs, e.g. diameter, on CNT-silicon solar cells has not been investigated sufficiently.

Recently, our laboratory has successfully synthesized SWNTs on the flat substrate with diameter tunable from 2.5 to sub-nm, through alcohol catalytic chemical vapor deposition (ACCVD) [2,3]. With the decreasing diameter of SWNTs, the band gap of SWNTs could become larger and exceeding 1 eV with regard to sub-nm diameter. As a result, SWNTs with average diameter smaller than 1 nm are expected to have promising applications in photoelectronic devices. In our investigation, we will discuss the results of CNT-silicon solar cells utilizing different average diameters of SWNTs. These SWNT films are synthesized by Co-Cu and Co-Mo catalysts that have obvious differences in the resulting average diameters. Regarding CNT-silicon solar cells, the fabrication process is a systematic process which contains photolithography and sputtering that are capable of large scale applications. Our investigation could shed some light into the mechanism of CNT-silicon solar cells.

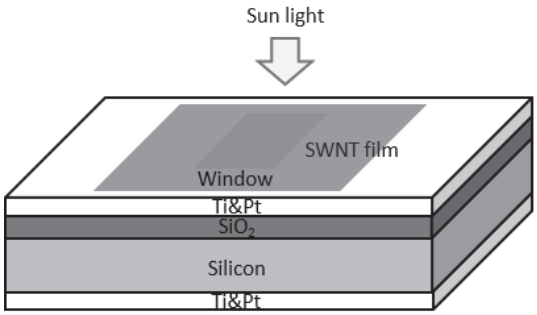

Fig.1: Schematic of CNT-silicon solar cell.

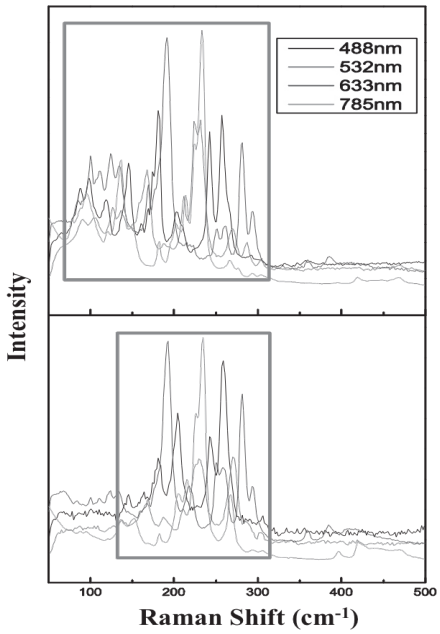

Fig.2: Raman Spectrum of SWNTs that possess different diameters.

[1] K. Cui *et al*. J. Mater. Chem. A. **2**, 11311 (2014).
[2] S. Maruyama *et al*. Chem. Phys. Lett. **360**, 229 (2002).
[3] K. Cui *et al*. In preparation.

Corresponding Author: S. Maruyama
Tel: +81-3-5841-6421, Fax: +81-3-5800-6983, E-mail: maruyama@photon.t.u-tokyo.ac.jp

Carbon Nanotube Thin-Film Transistor for Flexible Biosensor Applications

○Nguyen Xuan Viet[1], Shigeru Kishimoto[2], and Yutaka Ohno[1,3]

[1] *Department of Electrical Engineering and Computer Science, Nagoya University, Nagoya 464-8603, Japan*
[2] *Department of Quantum Engineering, Nagoya University, Nagoya 464-8603, Japan*
[3] *EcoTopia Science Institute, Nagoya University, Nagoya 464-8603, Japan*

Carbon nanotubes (CNTs) are promising materials for biosensors due to the ultra-high mobility, giving high transconductance and sensitivity [1]. From the point of view of practical use, FETs based on a random network CNT thin film is advantageous, compared to FETs based on individual CNTs. In our previous work, CNT thin-film transistors (TFTs) with a high-mobility more than 1,000 $cm^2/V.s$ have been realized on a flexible plastic film [2]. In this study, we demonstrate sensor behavior of CNT TFTs.

CNT were grown by the floating-catalyst CVD, collected on membrane filter, and then transferred on a polyethylene naphthalate (PEN) substrate. This method has advantages over conventional solution process, i.e., the CNT film is composed of long and clean CNTs with a controllable density [3]. The device was fabricated by conventional photolithography process covered by PMMA, except for CNT channel.

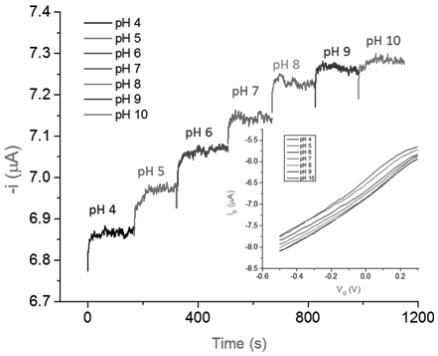

Fig. 1 Response of CNT TFT to 1 mM PBS with 10 mM NaCl solutions of various pH from 4 to 10. (Inset) I_D-V_{GS} characteristics of CNT TFT measured in solution of pH from 4 to 10.

To examine the sensitivity of the CNT TFT sensors to the change of pH of medium, we conducted a series of pH detection experiments. The different pH solutions were put in the PDMS pool formed on the substrate by using a pipette. Figure 1 shows the response of a CNT TFT to buffer solutions of various pH ranging from 4 to 10. The drain current (hole current) increased and the positive shift of threshold voltage (inset of fig 1) with the increase in pH, however transconductance was kept unchanged. This behavior can be explained by the presence of surface charges on the CNT surface. The surface charge density can be modified by changing of electrolyte pH. De-proton process (pH increase) makes the surface more negatively charged, resulting in a positive shift of threshold voltage as experimentally observed. In addition, we have also demonstrated the detection of dopamine (DA), an important neurotransmitter in the central brain, with a high sensitivity.

[1] B.L. Allen, *et al.*, Advanced Materials, **19** (2007) 1439-1451.

[2] D.-M. Sun, *et al.*, Nature communications, **4** (2013).

[3] A. Kaskela, *et al.*, Nano letters, **10** (2010) 4349-4355.

Corresponding Author: Y. Ohno
Tel: +81-52-789-5387, Fax: +81-52-789-5387,
E-mail: yohno@nagoya-u.jp

Temperature dependence on the synthesis of Pt nanoclusters on polybenzoimidazole-wrapped carbon nanotubes for use in oxygen reduction reaction catalyst

○Yuki Hamasaki[1,2], Tsuyohiko Fujigaya[1,2], Naotoshi Nakashima[1,2]

[1] *Department of Applied Chemistry, Kyushu University, Fukuoka 819-0395, Japan*
[2] *WPI-I2CNER, Kyushu University, Fukuoka 819-0395, Japan*

Oxygen reduction reaction (ORR) has been realised existing in polymer electrolyte membrene fuel cells (PEMFCs). Currently, most popularly used catalysts for ORR are platinum (Pt)-based catalysts. However, Pt is a very expensive metal, hinders wide use of such catalyst in the global commercialization.

In this study, we fabricated sub-nanosized Pt nanoclusters on polybenzoimidazole (PBI)-wrapped multi-walled carbon nanotubes (MWNT) based on i) a coordination step and ii) a reduction step (Figure 1). The MWNTs and PBI work as the carbon support and the Pt coordination site, respectively. [1,2] The use of a polyelectrolyte (here PBI) as an anchoring unit for the metal is advantageous in view of the practical applications in the PEFCs.

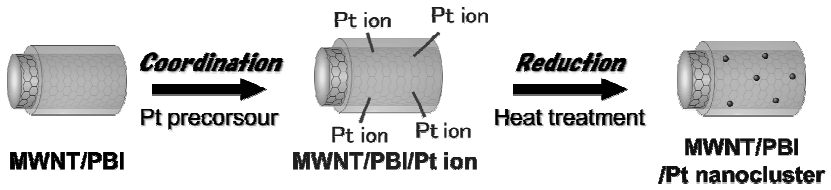

Figure 1 Synthesis routs of Pt nanoclusters on MWNT/PBI.

MWNT/PBI composites were added into a deionized water, then dispersed by sonication. H_2PtCl_6 as a precursor was added into the solution. After stirring over night at room temperature, the composites were filtered by a PTFE, which were reduced by H_2 gas at giving temperatures (200, 300 and 400 °C). The obtained materials were characterized by transmission electron microscope (TEM), thermogravimetric analyses (TGA) and X-ray photoelectron spectroscopy (XPS). ORR activity was measured in 0.1 M $HClO_4$ saturated with oxygen.

TEM images of the catalysts revealed that mean diameters of the Pt synthesized at 200, 300 and 400 °Cwere 1.0±0.5, 1.6±0.4 and 4.6±2.4 nm, respectively, indicating that the size of Pt nanoclusters can be regulated simply by changing the reaction temperature.

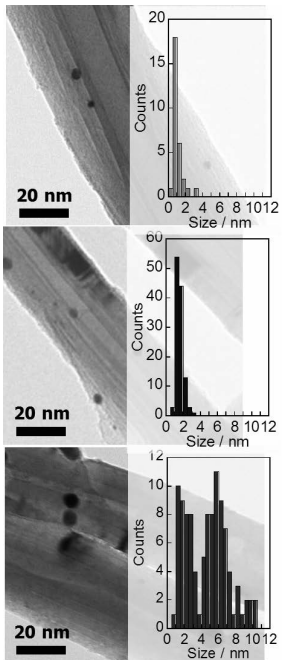

Figure 2 TEM images and their size distributions of Pt nano clusters on MWNT/PBI synthesized at 200 (a), 300 (b) and 400 °C (c).

[1] N. Nakashima *et al*. Small **5**, 735 (2009).
[2] N. Nakashima *et al*. Sci. Rep. **4**, 6295 (2014).

Corresponding Author: Naotoshi Nakashima
Tel&Fax: +81-92-802-2840
E-mail: nakashima-tcm@mail.cstm.kyushu-u.ac.jp

Sub-millimeter-tall vertically-aligned CNT arrays directly grown on Al foils

°Yu Yoshihara,[1] Kei Hasegawa,[1] Suguru Noda[1,*]

[1] *Department of Applied Chemistry, Waseda University, Tokyo 169-8555, Japan*

Vertically-aligned carbon nanotubes (VA-CNTs) have attracted great interests due to their rich opportunities for applications, however, direct growth on device substrates is important to fully utilize such a unique structure. Most studies have been made on silicon substrates with surface insulator, but growth on inexpensive Cu or Al foils is highly demanded such for batteries/capacitors and thermal interface materials (TIMs). Several groups have succeeded in growing VA-CNTs on Cu foils due to the relatively high melting point of Cu (1085 °C), often with a help of insulating Al_2O_3 underlayer to suppress the catalyst deactivation due to alloying with the foils. Recently, we realized tens-micrometer-tall, 0.2−0.3 g cm^{-3}-dense VA-CNTs on Cu foils at 700 °C with conductive TiN/Ta underlayer and Fe catalyst, which showed TIM-performance closed to an indium sheet [1]. In this work, we targeted at the growth of sub-millimeter-tall VA-CNTs on Al foils that have a melting point as low as 660 °C.

Tall VA-CNTs are normally synthesized at a temperature around 750 °C [2]. At lower temperatures, suppressed carbon feed and oxidative additives are the key for tall VA-CNTs so as not to kill the catalyst by carbonization [3]. Fe with a gradient thickness profile was prepared on an Al foil by sputtering with a physical filter [4]. Then the Al foil with Fe catalyst was set in a tubular quartz glass reactor (34 mm in inner diameter and 300 mm in heating zone length), heated to 600 °C under a 10 vol% H_2/Ar flow at 500 sccm, and CNTs were grown at 600 °C under a 0.06 vol%C_2H_2/1.8 vol% CO_2/Ar flow at 500 sccm.

CNTs grew taller with the addition of CO_2 and the optimum CO_2/C_2H_2 ratio (v/v) was 30. CNTs stopped growing within 20−40 min with a maximum height of ~80 μm without the addition of CO_2 while stopped growing within 20 min with a maximum height of ~50 μm with the excess addition of CO_2. At the optimum CO_2/C_2H_2 ratio, CNTs kept growing for 4 h to reach ~650 μm in height (Figs. 2,3).

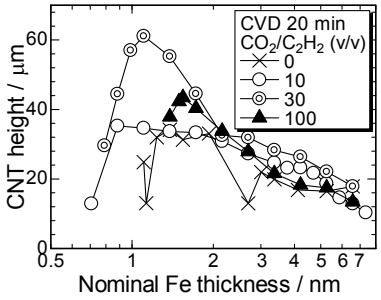

Fig. 1 Height of CNT arrays grown with and without addition of CO_2

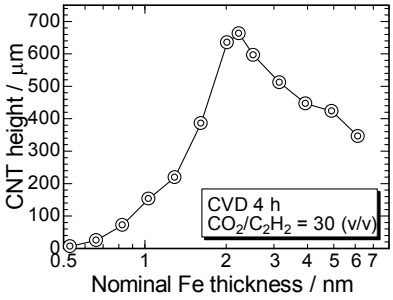

Fig. 2 Height of CNT arrays grown on an Al foil at 600 °C for 4 h.

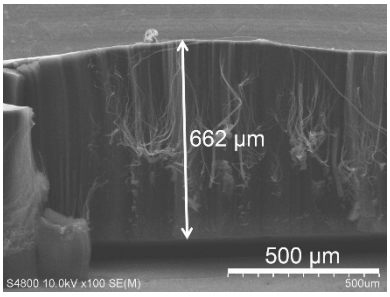

Fig. 3 SEM image of CNT grown on an Al foil at 600 ℃ for 4 h.

[1] N. Na, *et al.,* Jpn. J. Appl. Phys., in press.
[2] K. Hata, *et al.,* Science **306**, 1362 (2004).
[3] K. Hasegawa and S. Noda, Carbon **49**, 4497 (2011).
[4] S. Noda, et al., Carbon **44**, 1414 (2006).

Corresponding Author: S. Noda
Tel: +81-3-5286-2769, Fax: +81-3-5286-2769, E-mail: noda@waseda.jp

Bulk separation of (6,5) single-wall carbon nanotube enantiomers

○Takeshi Tanaka, Takuya Hirakawa, Xiaojun Wei, Yohei Yomogida, Atsushi Hirano, Shunjiro Fujii, and Hiromichi Kataura

Nanosystem Research Institute, National Institute of Advanced Industrial Science and Technology (AIST), Ibaraki 305-8562, Japan

Single-wall carbon nanotubes (SWCNTs) are produced as a mixture of various structures, and the inhomogeneity hinders their basic research and applications. We have reported (n,m) and enantiomer separation of SWCNTs by overloading or temperature-control gel column chromatography [1]. Recently we have developed another separation method for (n,m) enantiomers of SWCNTs at very high purities using a mixed surfactant system [2]. In this presentation, we show large-scale (6,5) enantiomer separation of SWCNTs using the system. CoMoCAT SWCNTs (SG65) dispersion in sodium dodecyl sulfate (SDS) and sodium cholate (SC) was prepared by sonication and ultracentrifugation and was separated by using a chromatography system equipped with 430 ml column. Adsorbed SWCNTs to the column were eluted by stepwise increasing concentration of sodium deoxycholate in SDS/SC. Fig. 1a shows circular dichroism spectra of separated (6,5) SWCNT enantiomers. After a few separation cycles, we could obtain milligrams of (6,5) enantiomers of SWCNTs. Bucky papers of (6,5) enantiomers were prepared from the separated solutions (Fig. 1b).

This work was supported by KAKENHI No. 25220602

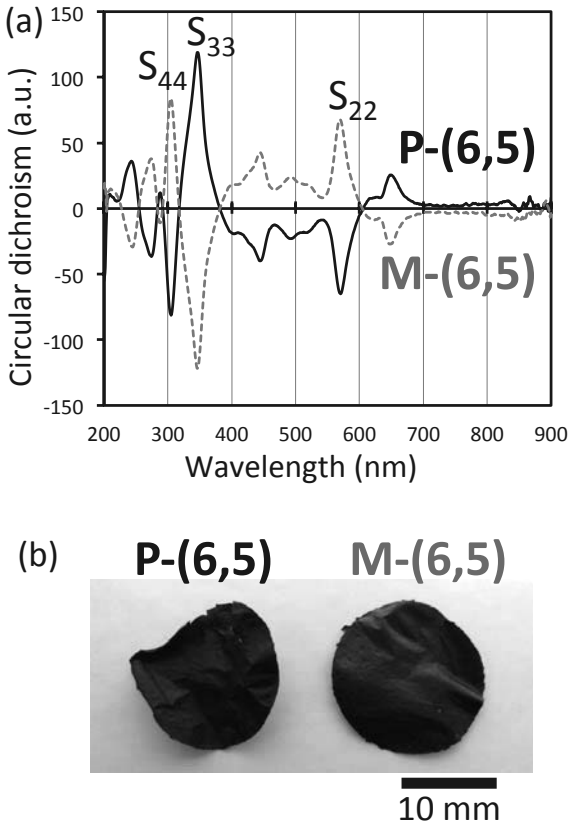

Fig. 1. (a) Circular dichroism spectra of separated (6,5) SWCNT enantiomers. (b) Bucky papers of (6,5) SWCNT enantiomers.

[1] H. Liu *et al.*: Nature Commun., 14, 309 (2011), Nano Lett., 13, 1996 (2013), Nano Lett., 14, 6237 (2014).
[2] X. Wei *et al.*, The 48th FNTG general symposium, 1P-14 (2015) Tokyo, Japan.

Corresponding Author: T. Tanaka
Tel: +81-29-861-2903, Fax: +81-29-861-2786
E-mail: tanaka-t@aist.go.jp

Synthesis and characterization of SWNTs from activated nanotube edges

○Hiroki Takezaki[1], Keigo Otsuka[1], Taiki Inoue[1],
Shohei Chiashi[1] and Shigeo Maruyama[1, 2]

[1] *Department of Mechanical Engineering, The University of Tokyo, Tokyo 113-8656, Japan*
[2] *Energy NanoEngineering Lab. National Institute of Advanced Industrial Science and Technology (AIST), Ibaraki. 305-8564, Japan*

To realize the application of single-walled carbon nanotubes (SWNTs), it is required to establish the method of chirality-controlled synthesis of SWNTs. Recently, the concept of cloning [1,2], in which SWNTs are grown using SWNTs as templates without using metal catalysts, was reported. In this study, we grew SWNTs using open-end SWNTs as templates to obtain the knowledge of the growth mechanism as well as to increase the growth yield.

We grew horizontally aligned SWNTs on quartz substrates using patterned metal catalyst. Then the grown SWNTs were partially etched by photolithography and oxygen plasma treatment to prepare open-end SWNTs. Figure 1 (a) shows the scanning electron microscopy (SEM) image of partially etched SWNTs. We annealed the partially etched SWNTs in air and in water vapor to activate the edges of the open-end SWNTs, and then grew SWNTs via ethanol chemical vapor deposition (CVD). Figure 1 (b) shows the image of the SWNTs, which were annealed in water vapor at 900 °C and were heated in ethanol vapor at 900 °C. SWNTs grown from activate nanotube edges was observed. We found that the yield of SWNTs grown from the open-end SWNTs was varied by changing the condition of water vapor treatment. Raman mapping images showed the chirality of the grown SWNTs was the same as that of the corresponding template SWNTs. Figure 2 shows RBM distribution of (a) template SWNTs and (b) grown SWNTs, indicating that the average SWNT diameter of grown parts was a little smaller than that of template SWNTs. This reveals that cloning growth of smaller-diameter SWNTs occurs more preferably in this condition.

[1] J. Liu *et al*. Nat. Comm. **3**, 1199 (2012).
[2] Y. Yao *et al*. Nano Lett. **9**, 1673 (2009).
Corresponding Author: Shigeo Maruyama
TEL: +81-3-5841-6421, FAX: +81-3-5800-6983
E-mail: maruyama@photon.t.u-tokyo.ac.jp

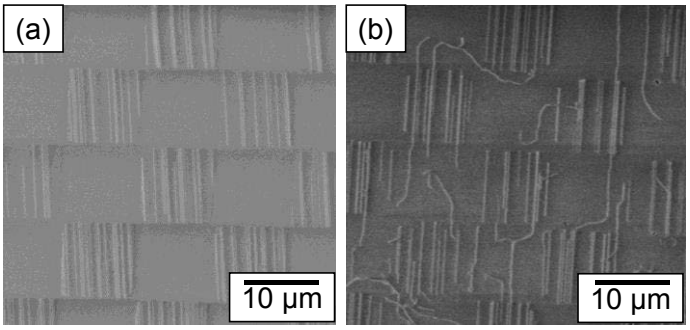

Fig. 1 SEM images of (a) partially etched SWNTs and (b) SWNTs after the growth process.

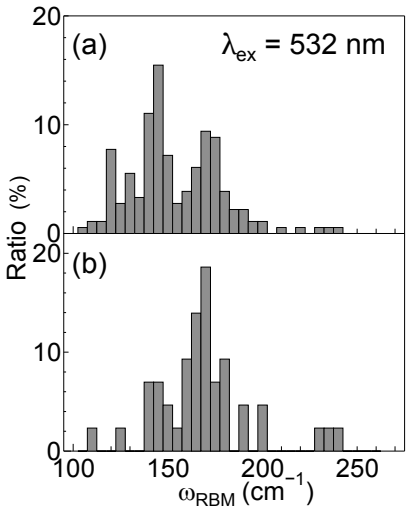

Fig. 2 RBM distribution of (a) template SWNTs and (b) grown SWNTs.

Control of diameter and chirality of single-walled carbon nanotubes due to magnetic field

○Yasumasa Takashima, Atom Hamasaki, Jin Uchimura, Ayumi Sakaguchi, Sumio Ozeki

Department of Chemistry, Faculty of Science, Shinshu University
Matsumoto, Nagano 390-8621, Japan

Single-walled carbon nanotube (SWCNT) has a cylindrical structure comprised of rolled graphene monolayer and its conjugate system brings about various novel properties. Since the electrical properties of SWCNT as a metal or semiconductor depends strongly on its structure, the chirality should be controlled for applications.

Graphitic layers having large magnetic anisotropy may be controlled by magnetic fields to lead to new structures and functions. We constructed an electric furnace system available in a superconducting magnet and found structural changes of various carbon materials such as activated carbon, multi-walled CNT, and SWCNT prepared under magnetic fields [1-2]. In this study, the magnetic fields of up to 10 T was applied to SWCNT growth processes in two kinds of synthetic methods of chemical vapor deposition (CVD) and liquid decomposition (LD). We investigated magnetic field effects on structures of SWCNT and their mechanism.

Fig. 1 shows Raman spectra of SWCNT prepared with the LD method under magnetic fields of up to 6 T. Methanol dissolving Cobalt (II) acetate tetrahydrate was used as a carbon source. SWCNT grew on carbon paper during electric heat at 1053 K. Peak intensity around 230-250 cm^{-1} increased with increasing magnetic field, which indicated that metallic SWCNT of small diameter grew more preferentially than semiconducting one. SWCNT prepared by the CVD method [2] showed similar tendency to the LD method. Therefore, no magnetic field effect on SWCNT structures depended on the preparation methods.

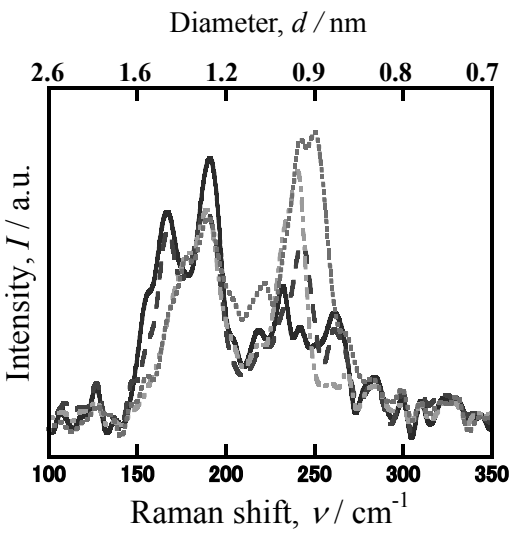

Fig.1: Raman spectra of SWCNT prepared under various magnetic fields, excited with 532 nm laser. 0 T (solid) ; 1 T (dashed) ; 4 T (dashed and dotted) ; 6 T (dotted)

Reference

[1] A. Sakaguchi, *et. al.*, *Chem. Lett.,* **2012**, *41*, 1576.
[2] A. Sakaguchi, *et. al*., *Chem. Lett.*, **2013**, *42*, 304.

Corresponding Author: Atom Hamasaki
Tel: +81-263-37-2467, Fax: +81-263-37-2559, E-mail: atom@shinshu-u.ac.jp

Solubilization of Single-Walled Carbon Nanotubes Using Riboflavin and Analysis of Temperature Dependent Solubilization Behavior

Wataru Ishimaru[1], Fumiyuki Toshimitsu[1], Naotoshi Nakashima[1,2]

[1] *Department of Applied Chemistry, Kyushu University, Fukuoka 819-0395, Japan*
[2] *WPI-I^{2}CNER, Kyushu University, Fukuoka 819-0395, Japan*

Single-walled carbon nanotubes (SWNTs) are carbon cylinders as rolled up graphene. Due to their remarkable properties, such as mechanical strength and electron mobility, they are expected as nanomaterials for the next generation devices like solar cell and nano wiring materials. For application of SWNTs, solubilization of the materials is needed and many reports about this including its mechanism have been published. However, further understanding on the solubilization mechanism is still important.

In this study, we report i) the finding that riboflavin (Fig.1) can solubilize SWNTs and ii) analysis of temperature dependence on this solubilization behavior. Flavin derivatives have been reported to form specific adsorption structures [1, 2].

SWNTs and riboflavin in water were sonicated, then centrifugated to obtain a supernatant, which was collected and used for measurements. The MD simulation was conducted in two temperatures, 283 K (low) and 313 K (high). To analyze the absorbance of SWNTs, we decomposed the spectra of the SWNTs, then analyzed the results using the regression curve. Fig.2 shows the plot of the area of the peaks at 0.75-nm diameter of the SWNTs vs. solubilization temperature, in which LogNormal and Linear plots suggest a specific adsorption of riboflavin at lower temperatures, and non-specific temperature dependent adsorption at higher temperatures. From the MD simulation, we evaluated the number of adsorbed riboflavin increased with temperature.

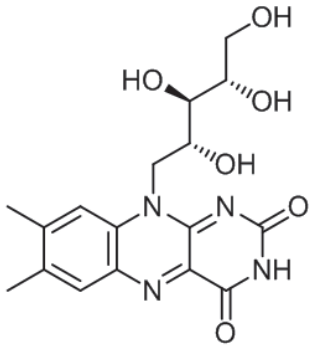

Fig.1 Chemical structure of riboflavin.

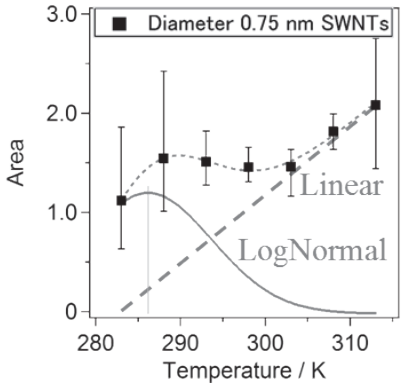

Fig.2 Plot of the area of peaks at 0.75-nm diameter of the SWNTs vs. solubilization temperature.

[1] F. Papadimitrakopoulos et al, *Science* **2009**, *323*, 1319.
[2] N. Nakashima et al, *Chem. Lett.* **2015**, *44*, 566.

Corresponding Author: N. Nakashima
Tel: +81-92-802-2840, Fax: +81-92-802-2840,
E-mail: nakashima-tcm@mail.cstm.kyushu-u.ac.jp

Synthesis and Characterization of Single-Molecule Magnet Encapsulated in Carbon Nanotube

Mudasir Ahmad Yatoo[1], ○Ryo Nakanishi[1,2], Keiichi Katoh[1,2], Takeshi Saito[3], Masahiro Yamashita[1,2]

[1] Department of Chemistry, Tohoku University, Sendai 980-8578, Japan
[2] JST-CREST, Chiyoda-ku, Tokyo 102-0075, Japan
[3] National Institute of Advanced Industrial Science a d Technology (AIST), Tsukuba 305-8565, Japan

Single-molecule magnet (SMM) is a molecule which shows slow relaxation of the magnetization of purely molecular origin due to the large ground spin state with a uniaxial magnetic anisotropy. On the basis of their unique magnetic properties, SMM is investigated vigorously these days for potential applications in the fields of molecular spintronics, data storage devices and quantum computing. However, any real application of SMM requires their communication with the outside macroscopic world, to allow read-and-write processes. Simultaneously, smaller spin-spin interaction between each molecule is important in order to use the SMMs as isolated magnets. Here, we focused on carbon nanotube (CNT) because of the high electric conductivity which offers a unique solution to linking SMM to the outside world [1], and the internal nano-space in which the intermolecular interaction can be reduced from three- to one-dimensionally. Given the vast potentials of this field, we are working on synthesizing CNT-SMM hybrids in which SMM is encapsulated into CNT.

In this work, We used Dysprosium(III) acetylacetonate complexes [$Dy(acac)_3$] which show SMM-like behavior when they are diluted [2]. Firstly, we have synthesized CNT-SMM hybrid using multi-walled CNT (MWCNT; Aldrich) by soaking cap-opened CNT into 1,2-dichloroethane solution of $Dy(acac)_3$. From transmission electron microscope (TEM) observation, we observed the stark contrast inside CNT and further presence of dysprosium could be confirmed by energy dispersive X-ray (EDX) spectroscopy (Fig. 1). From AC magnetic susceptibility measurements, frequency dependence could be confirmed, which suggests the $Dy(acac)_3$ still retain the SMM properties even in MWCNT. The relaxation time of this hybrid could be estimated as 5.3×10^{-9} s, this number is smaller than that of before the encapsulation, which may indicate the spin-spin interaction of each SMM become strong. $Dy(acac)_3$ could also be introduced in single-walled CNT (which is produced by enhanced direct injection pyrolytic synthesis method) by sublimation method, then the detailed characterization and comparison are in progress.

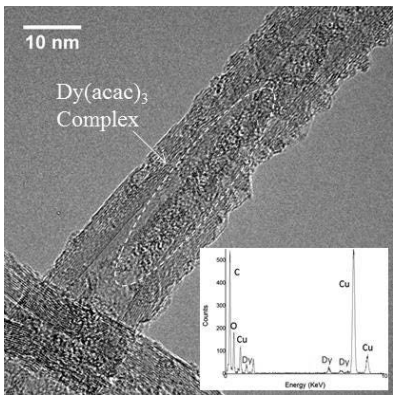

Fig. 1 TEM image of $Dy(acac)_3$ @MWCNT. Inset shows the EDX spectrum.

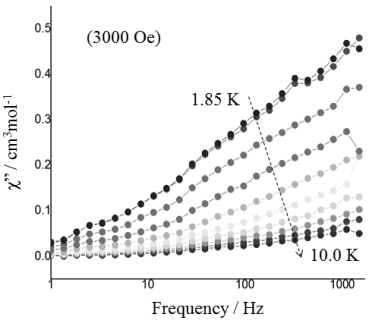

Fig. 2 AC magnetic susceptibility (out of phase) of $Dy(acac)_3$@ MWCNT.

[1] M. C. Giménez-López. *et al. Nat. Comm.*, **2011**, 407, 1415.
[2] S.-D. Jiang, *et. al*, *Angew. Chem. Int. Ed.* **2010**, 49, 7448 –7451.

Corresponding Author: M. Yamashita
Tel: +81- 22-795-6544, Fax: +81- 22-795-6548, E-mail: yamasita@agnus.chem.tohoku.ac.jp

Metalorganic chains assambled inside single-wall carbon nanotubes

∘Oleg Domanov[1], Markus Sauer[1], Michael Eisterer[2], Takashi Saito[3], Herwig Peterlik[1], Thomas Pichler[1], Hidetsugu Shiozawa[1]

[1]*Faculty of Physics, University of Vienna, Boltzmanngasse 5, 1090 Vienna, Austria*
[2]*Institute of Atomic and Subatomic Physics, Vienna University of Technology, Stadionallee 2, 1020 Vienna, Austria*
[3]*National Institute of Advanced Industrial Science and Technology (AIST), 1-1-1 Higashi, Tsukuba 305-8565, Japan*

Molecular chains are of great interest due to their unique magnetic and structural properties which stem from intermolecular interactions. The confined nanospace of single-wall carbon nanotubes (SWCNT) allow molecules to be arranged in one dimensional chains (see Fig. 1)[1-2]. Our research is focused on the structural and magnetic properties of such 1D magnetic systems investigated by means of X-ray diffraction(XRD), superconducting quantum interference device (SQUID), X-ray/UV Photoemission Spectroscopy (XPS, UPS) and X-ray Absorbtion Spectroscopy (XAS). XRD data suggest unique 1D molecular arrangements with the lattice constant that varies with the host SWCNT's diameter. On the basis of SQUID data, we will discuss the magnetic ground states and possible bulk magnetic ordering.
Our study provides insight into the magnetic and structural properties of 1D molecular chains that would pave the way towards advanced metalorganic-based magnets.
We acknowledge financial support from the Austrian Science Fund (FWF).

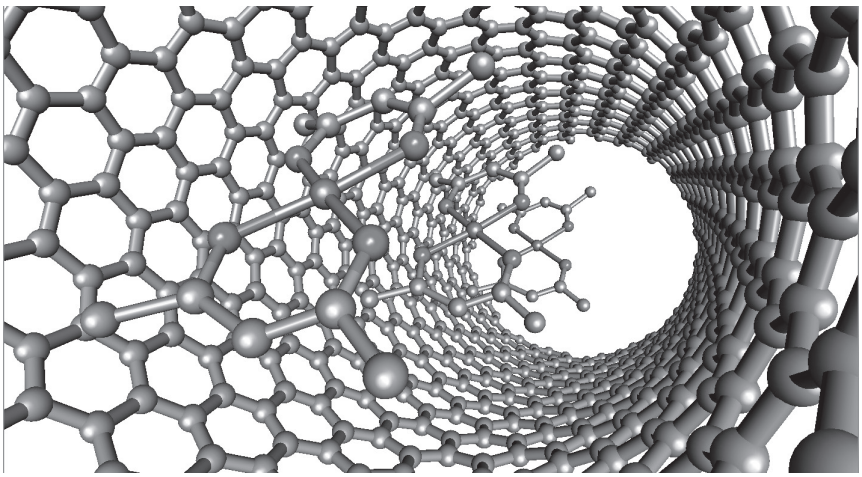

Figure 1: 1-D Nickel(II) acetylacetonate ($C_{10}H_{14}NiO_4$) chain structure inside SWCNT.

[1] M. Kharlamova et al. Nanoscale 7, 1383 (2015).
[2] A. Briones-Leon et al. Phys. Rev. B 87, 195435 (2013).
Corresponding Author: O.Domanov
Tel: +43-1-4277-72628, Fax: +43-1-4277-9726,
E-mail: oleg.domanov@univie.ac.at

Synthesis and electronic evaluation of bilayer graphene

○Ryo Hoshino, Yutaro Hayashi, Nozomi Suzuki, Kentaro Imai,
Tomoko Nagata, Nobuyuki Iwata, Hiroshi Yamamoto

College of Science &Technology, Nihon University, 7-24-1 Narashinodai, Funabashi-shi, Chiba 274-8501 japan

In order to realize superconductivity at room temperature, we fabricate metal intercalated bilayer graphene. The electron-exciton coupling is expected to generate high temperature superconductivity [1]. In this study, we report the growth of bilayer graphene and its electric property.

The single-layered graphene sheet was synthesized on Cu foil by chemical vapor deposition (CVD) method, using CH_4, H_2 and Ar as process gases. After etching of Cu foil by $Fe(NO)_3$ aqueous solution, the single-layered graphene was transferred on SiO_2/Si substrate. The bilayer graphene was prepared by transferring the single-layered graphene twice.

Figure1 shows the temperature dependence of the resistance of bilayer graphene, detected by traditional four wire resistance measurement. The bilayer graphene showed metallic property in the wide temperature range of 300 to 40K. A small increase was observed below 40K. In general, pure bilayer graphene is a semiconductor, while metal-intercalation makes bilayer graphene metal [2]. The metallic behavior of our bilayer graphene suggests the metal-intercalation. The Fe ion may be intercalated during the Cu etching process. The details will be discussed.

[1] Akimitsu, Parity. MARUZEN. **05**, 6-12 (2008).

[2]Yan-Feng, Appl. Phys. Lett. **102**, 231906(2013)

Corresponding Author: Nobuyuki Iwata
Tel: +81-47-469-5457
E-mail: iwata.nobuyuki@nihon-u.ac.jp

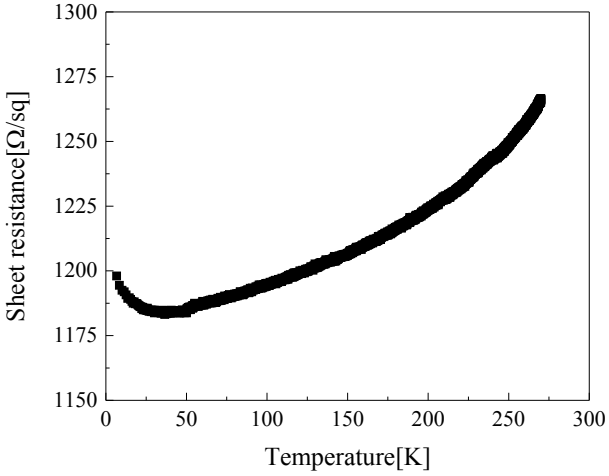

Figure-1. Temperature dependence of the sheet resistance of the bilayer graphene

Growth temperature dependence of CVD-growth of highly uniform multilayer graphene using Au/Ni catalyst

○Yuki Ueda[1], Jumpei Yamada[1], Itsuki Uchibori[1], Masashi Horibe[1], Shinichi Matsuda[1], Takahiro Maruyama[2], and Shigeya Naritsuka[1]

[1] *Department of Materials Science and Engineering, Meijo University, Nagoya 468-8502, Japan*
[2] *Department of Applied Chemistry, Meijo University, Nagoya 468-8502, Japan*

Graphene possesses special electrical characteristics, such as, low resistivity, high tolerance for the current flow. The number of the layer is a key parameter of the performances of the multilayer graphene (MLG) because they are largely depend on the number of the layers. Metal catalyst with a high solubility of carbon such as Ni, Co, and Fe are usually used to synthesize MLG by CVD, while precipitation method is also employed to grow MLG. The uniformity of the layer is very important for the applications of MLG. However, it is quite difficult to control the uniformity of MLG especially for the precipitation method. In this paper, the uniformity of the MLG by CVD is tried to improve by the use of the Au/Ni catalyst and the optimization of growth temperature.

MLG was grown by CVD using Au/Ni catalyst. Ethanol kept at 5 ^{o}C was bubbled for suppling it in the CVD furnace. The MLG was grown with flowing the mixture gas of H_2, N_2, and ethanol for 5 min at 0.5 atm. The growth temperature was changed between 850-1050 ^{o}C. The layer number of the graphene was studied using Raman spectroscopy [1].

Differential interference contrast microscope (DICM) images and Raman spectra of the MLG grown at 950 ^{o}C, and 1050 ^{o}C are shown Fig.1. The figure shows that the MLG only exists around the grain boundaries of the Au/Ni catalyst on the sample grown at 950 ^{o}C. On the other hand, MLG covers the whole surface and about 70 % of them are 2-5 layers graphene on the sample grown at 1050 ^{o}C. The very low D peak suggests the high quality of the grown MLG. It is probably because the nucleation of graphene was largely suppressed by the low amount of the dissolved carbon from the low solubility of the carbon in the Au/Ni catalyst and the long diffusion length of the carbons on the surface from the high growth temperature. Consequently, the uniformity MLG was successfully improved.

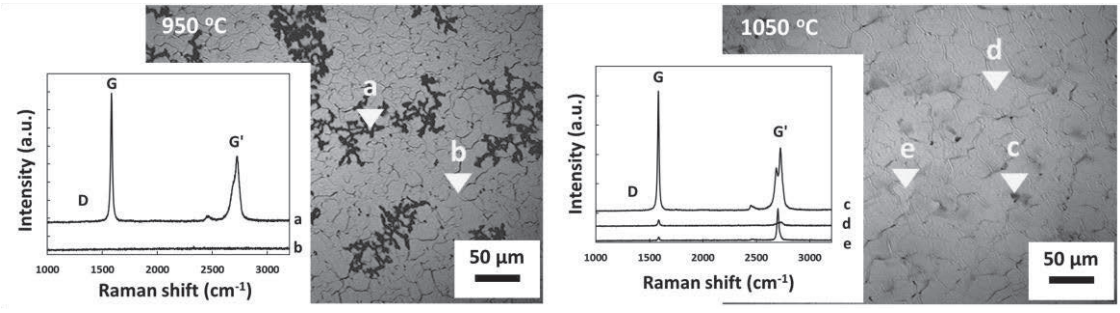

Fig.1 DICM images and Raman spectra of MLG grown at 950 ^{o}C (left) and 1050 ^{o}C (right), respectively.

Acknowledgment: This work was supported in part by JSPS KAKENHI Grant Numbers 2660089, 15H03558, 26105002, 25000011.

Reference: [1] A.C. Ferrari. Solid State Commun., **143** (2007) 47.

Corresponding Author: Y. Ueda, Tel: +81-52-838-2387, E-mail: 153434003@ccalumni.meijo-u.ac.jp

Synthetic Studies toward BN-Doped Graphene/Nanographene Using the Borazine Derivatives

○Yasuyo Ishio, Haruka Omachi, Ryo Kitaura, and Hisanori Shinohara*

Department of Chemistry & Institute for Advanced Research, Nagoya University, Nagoya 464-8602, Japan.

Heteroatom-doped graphene is attractive as the candidates for various device applications in electronics and optics because of its semiconductive character in addition to the properties from graphene, such as high carrier mobility and optical transparency. Recently, boron/nitrogen co-doped graphene (BN-doped graphene) has been investigated as one of the heteroatom-doped graphene. It is obtained by chemical vapor deposition (CVD) using carbon source and BN source [1] and solvothermal reaction [2]. However, these reported approaches are limited to control the positions and amounts of doped B and N atoms. Therefore, synthesis of the well-defined BN-doped graphene has never been achieved.

To develop a method of the synthesizing well-difeined BN-doped graphene, we focused on using a BN-doped nanographene, borazine substituted hexa-*peri*-hexabenzocoronene (BN-HBC)[3], as a feedstock of BN-doped graphene in CVD-growth (Scheme 1). A novel borazine derivative, chlorine-substituted hexaphenylborazine (Cl-HPB) was synthesized as a precursor of BN-HBC through one-pot procedure[4,5]. We tackled to planarize Cl-HPB to BN-HBC via intramolecular C–C bond formation and also attempted direct CVD growth of BN-doped graphene by using Cl-HPB.

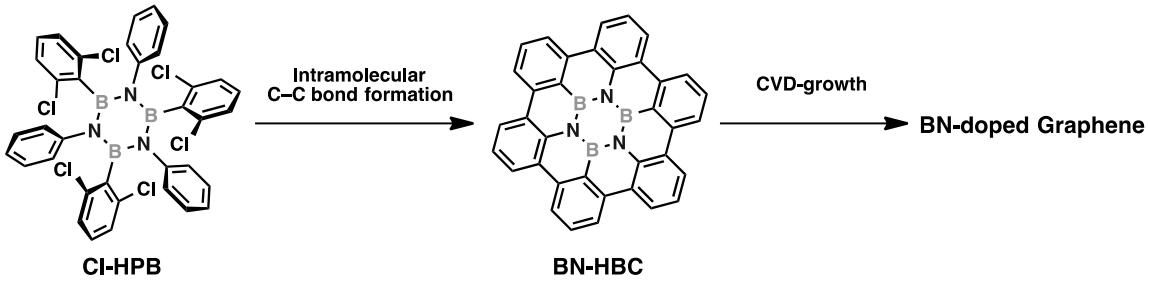

Scheme 1. Synthetic strategy of BN-doped graphene in this work.

[1] P. M. Ajayan *et al*. Nat. Mater., **9**, 430 (2010).
[2] J. Baek *et al.* Angew. Chem., Int. Ed., **53**, 2398 (2014).
[3] H. F. Bettinger *et al*. Angew. Chem., Int. Ed., **54**, 8284 (2015).
[4] S. Yamaguchi *et al.* J. Am. Chem. Soc., **127**, 14859 (2005).
[5] D. Bonifazi *et al.* Chem.– Eur. J., **19**, 7771 (2013).

Corresponding Author: H. Shinohara
Tel: +81-52-789-2482, Fax: +81-52-747-6442,
E-mail: noris@nagoya-u.jp

Residual particles on transferred CVD graphene

○Tomohiro Yasunishi[1], Yuya Takabayashi[2], Shigeru Kishimoto[1],
Ryo Kitaura[2], Hisanori Shinohara[2], and Yutaka Ohno[3]

[1]*Depertment of Quantum Engineering, Nagoya University, Nagoya 464-8603, Japan*
[2]*Department of Chemistry, Nagoya University, Nagoya 464-8602, Japan*
[3]*EcoTopia Science Institute, Nagoya University, Nagoya 464-8603, Japan*

Graphene is attracting much attention because of the various unique properties such as mechanical flexibility, excellent electrical conductivity, gas impermeability, and so on. By exploiting the exclusive properties, graphene is considered to be useful for flexible electron devices [1]. A large-area single-layered graphene can be grown on a Cu foil by the chemical vapor deposition (CVD) technique [2]. For the device application, the graphene is needed to be transferred from the Cu foil onto a target substrate. In the transfer process, the Cu foil is normally etched away by wet etching process [3]. However, there are often residues observed on the transferred graphene as shown in the AFM image of Fig. 1. Such residues are seriously problematic in device applications; not only a failure in complete transfer of the graphene, but also current leakage between the graphene and electrodes through an insulator layer in the devices may be caused by the residual particles. In this work, we have investigated the composition of residual particles on graphene after Cu etching by energy-dispersive X-ray spectrometry (EDX) to find out the origin of the particles and a method to remove them.

Graphene was grown by CVD on a Cu foil at 1050°C using CH_4 as a carbon source. After covering the graphene with a PMMA layer, a thermal release tape was attached on top to support the PMMA/graphene film mechanically. Then, the Cu foil was etched by soaking into ammonium persulfate ($(NH_4)_2S_2O_8$) solution (0.5 M) [4] for 1 h. The graphene surface was washed by HCl solution (10 wt%) for 30 min. We observed the graphene surface by SEM/EDX (Hitachi, S-5200 equipped with HORIBA, E-MAX).

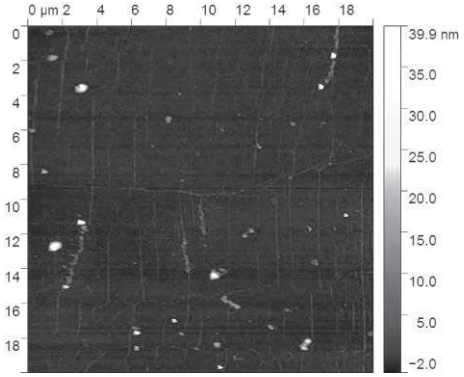

Fig. 1 AFM image of transferred graphene.

Figure 2 shows an EDX spectrum measured in the region indicated by the white square in the inset SEM image. Several peaks were observed in the EDX spectrum, corresponding to C (0.28 eV), O (0.53 eV), Mg (1.30 eV), Al (1.56 eV), Si (1.84 eV), and Ti (4.56, 4.96 eV). We also observed particles consisting of C, O and Si. These particles may be attributed to the impurities contained in the Cu foil and/or the quartz tube of the CVD furnace.

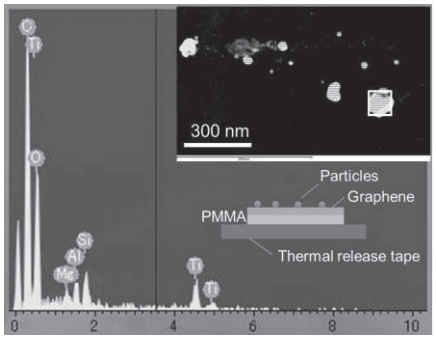

Fig. 2 EDX spectrum of a particle on graphene in white square region of inset SEM image.

[1] K. S. Kim *et al.* Nature **457**, 706 (2009).
[2] X. Li *et al.* Science **324**, 1312 (2009).
[3] Y. Lee *et al.* Nano Lett. **10**, 490 (2010).
[4] J. W. Suk *et al.* ACS Nano **5**, 6916 (2011).

Corresponding Author: Y. Ohno
Tel&Fax: +81-052-789-5387,
E-mail: yohno@nagoya-u.jp

Electron confinement in graphene-based junction

∘Yuya Inoue[1], Riichiro Saito[1]

[1] *Department of physics, Tohoku University, Sendai 980-8578, Japan*

Graphene is a material attracting big attentions for applications because of the great physical property such as high mobility. However, it has a big problem that we can not make devices such as field effect transistor (FET) of graphene unless we make a bandgap. The Klein tunneling gives rise to 100% tunneling probability of incident electrons going perpendicular to the potential barrier [1]. This means that we can not confine an electron on the monolayer graphene by applying any potential. We also can not control current by electrostatic gates. However, in the case of bilayer graphene (AB stacking), complete reflection against the barrier is realized.

Some previous works show that FET using bilayer graphene can be realized by applying electric fields perpendicular to the bilayer graphene, which brake the symmetry between the two layers and result in opening the energy gap [2,3]. In this work, we consider the following effects to confine electrons, 1) connecting single- and bilayer graphene and 2) applying the electrostatic potential for bilayer graphene. We calculate the electron structure by tight-binding method and show the possibilities of electron confinement in such a device.

[1] M. I. Katsnelson *et al.* Nature Physics **2**, 620 (2006).
[2] Y. Zhang, *et al.* Nature **459**, 820 (2009).
[3] S-L. Li *et al.* Acs Nano **5**, 500 (2011).

Corresponding Author: Y. Inoue
Tel: +81-22-795-6442, Fax: +81-22-795-6447,
E-mail: inoue@flex.phys.tohoku.ac.jp

pH Dependence of the Electrochemical Reaction of Graphene Oxide Evaluated by SEIRAS

○Katsuhiko Nishiyama[1,3], Yasuhiro Yoshimura[1], Yusuke Hayashi[1], Kazuto Hatakeyama[1,4], Michio Koinuma[1,4] Soichiro. Yoshimoto[2,3], and Yasumichi Matsumoto[1,4]

[1]*Graduate School of Science and Technology and* [2]*Priority Organization for Innovation and Excellence, Kumamoto University Kumamoto 860-8555, Japan*

[3]*Kumamoto Institute for Photo-Electro Organics (Phoenics), Kumamoto 862-0901, Japan*

[4]*JST CREST*

Graphene oxide (GO) prepared by oxidation of graphite have advantages such as low-cost, mass-productive, and various applications. By reducing GO by chemical and electrochemical, reduced grapheme oxide (rGO) is prepared. In this study, by surface enhanced infrared spectroscopy (SEIRAS)[1, 2], the electrochemical, adsorption, and desorption processes were studied in aqueous solution.

A Bio-Rad FTS-6000 FT-IR spectrometer equipped with an MCT detector and a single-reflection accessory was used to record spectra. The spectrometer was operated in rapid scanning mode with a resolution of 4 cm^{-1}. Au thin film electrodes for surface enhanced infrared spectroscopy (SEIRAS) were prepared by vacuum evaporation onto a Si prism with a deposition rate of ca. 0.67 nm s^{-1}. Sample solution containing GO (4 mg ml^{-1}) was injected into a SEIRAS cell ([GO] in the cell = 0.4 mg ml^{-1}) and change in FT-IR spectra for adsorption and electrochemical process were recorded.

Fig. 1 shows change in SEIRA spectra, applying potential from 0, -0,2, -0,4, and -0.6 V after injection of GO dispersed solutions containing 0.1 M $HClO_4$. Here, the spectrum at an open circuit potential was taken as a reference spectrum. When - 0.6 V was applied, a broad band around 1500 -1700 cm^{-1} was appeared. The observed band in the region might correspond to the in-plane vibration mode for the aromatic hydrocarbon caused by the reduction and change in the adsorption state of GO. In addition, the decrease in absorbance around 1200 cm^{-1} was clearly observed. This band is attributed to the epoxy group of the GO, which indicates that the epoxy group of the GO was reduced at -0.6 V. To ensure the reversibility of the reaction in 0.1 M $HClO_4$, the electrode potential was back to 0 V, however, no change in the spectrum was observed. Similar experiments have been conducted in 0.1 M $NaClO_4$ and 0.1 M NaOH. The reduction of the epoxy group was also observed in the neutral and alkaline solution, however, no reversible changes in absorption band attributed to the electrochemical reaction were observed.

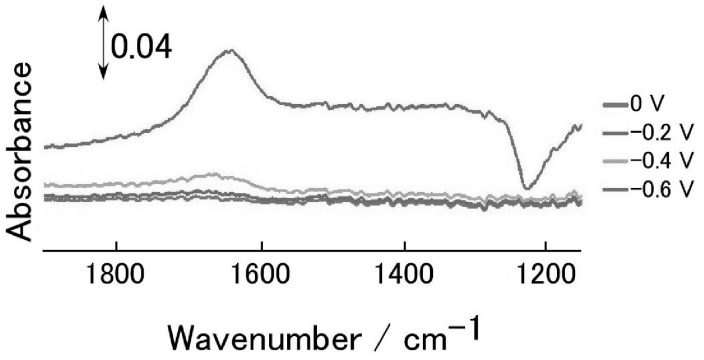

Fig. 1 Potential dependence of SEIRA spectra of GO in 0.1 M $HClO_4$.

[1] K. Nishiyama *et al*. 4th Graphene Oxide Symposium, in Kumamoto (2015).

[2] K. Nishiyama *et al*., 7th International Surface Science Symposium, Matsue (2014).

Corresponding Author: K. Nishiyama
Tel&Fax: +81-96-342-3657,
E-mail: nisiyama@kumamoto-u.ac.jp

Comprehensive Study of Edge-Disordered Graphene Nanoribbons

○K. Takashima[1], T. Yamamoto[1, 2]
[1] *Department of Electrical Engineering, Tokyo University of Science, Japan*
[2] *Department of Liberal Arts, Tokyo University of Science, Japan*

Graphene is expected to be a channel material of field effect transistors (FETs) because of its high carrier mobility. However no band gap of the graphene is a serious problem for its FET application. One possible way to overcome the gap-opening problem is to process it in the form of a nanometer width ribbon, referred as graphene nanoribbons (GNRs). They have been successfully applied to FETs with high on-off ratio. A recent experiment reported that the resistance of GNRs increases exponentially with their length even at the room temperature [1]. This non-Ohmic behavior is due to the edge-vacancy of GNRs. The effects of edge-vacancy become more remarkable when the ribbon width becomes narrower in the future. However the electronic transport properties of such narrow GNRs have not been clarified yet.

In this study, we have investigated the coherent electronic transport in edge-disordered armchair GNRs (ED-AGNRs) using the nonequilibrium Green's function method combined with a tight-binding model. In our simulation model, the edge vacancy is modeled by adding or removing pairs of carbon atoms at the edges. We calculated electrical conductances of ED-AGNRs by changing the roughness concentration from 0% to 30% and the ribbon-width from 1.48nm to 2.95nm. We confirmed that the electrical conductances G of ED-AGNRs decrease exponentially with their lengths L, *i.e.*, $G \propto \exp(-L/\xi)$, where ξ is the localization length [2]. Moreover, we numerically determined the vacancy-concentration dependence of ξ and the ribbon-width dependence of ξ. In addition, we gave a physical interpretation of these dependences through theoretical analysis based on the perturbation theory. This result provides a guideline for developing GNR-based FETs.

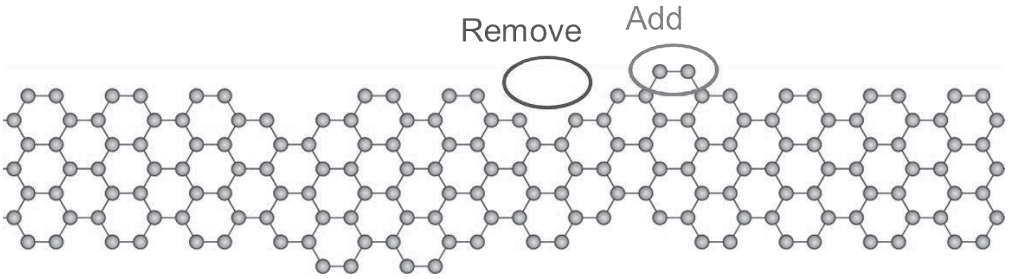

Fig.1: Schematic picture of edge-disordered graphene nanoribbon model

References:
[1] Xu *et al*., Nano Lett. **11**, 1082 (2011).
[2] K. Takashima and T. Yamamoto., APL, **104**, 093105 (2014).

Corresponding Author: T. Yamamoto
E-mail: takahiro@rs.tus.ac.jp

Photocurrent spectroscopy in monolayer WSe_2 p-n junction

○S. Kimura[1], D. Kozawa[1], T. Fujimoto[1], Y. Wada[1], J. Pu[1], K. Matsuki[1], L. J. Li[2], T.Takenobu[1]

[1] *Department of Applied Physics, Waseda University, Shinjuku 169-8555, Japan*

[2] *Physical Sciences and Engineering Division, KAUST, Thuwal 23955-6900, Saudi Arabia*

Transition metal dichalcogenide (TMD) monolayers are ultimately thin two-dimensional materials and therefore have intriguing optical properties, such as strong enhancement of Coulomb interactions of photoexcited electron-hole pair (or exciton). The spectrum of excited exciton states, one of focused topics, has been observed by optical measurements [1-3]. Although the fine structures of the excited exciton states are observable via photocurrent spectroscopy, the exciton fine structure has not yet been observed due to difficulties of p-n junction formation. Here, we address these problems by introducing p-n junction into WSe_2 monolayers with electric double layers and investigate their photocurrent spectra, realizing the observation of exciton fine structure, accompanied with the information on charge-separation properties, which is the key factor for exciton energy harvesting.

We formed the p-n junctions on CVD-grown large area WSe_2 monolayers using the freezing-while-gating technique, as previously reported by Zhang *et al.*[4]. Figure 1 shows the photoresponsivity as a function of excitation photon energy, and is reasonably explained by absorption spectrum. Lower-energy two peaks (at 1.73 eV and 2.15 eV) are corresponding to direct excitonic transitions with the spin-orbit splitting. We note that higher-energy two peaks (at 2.53 eV and 2.97 eV) are contribution from hot carrier. Moreover, as shown in Fig. 2, we found weak fine spectrum structure between 1st and 2nd peaks, and we can assign these three peaks as excited states of exciton (2s, 3s and 4s), indicating relatively high charge-separation rate in these states.

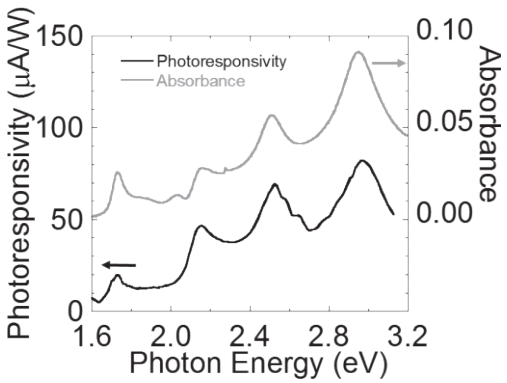

Fig.1 Photocurrent spectrum of WSe_2 p-n junction at 85K.

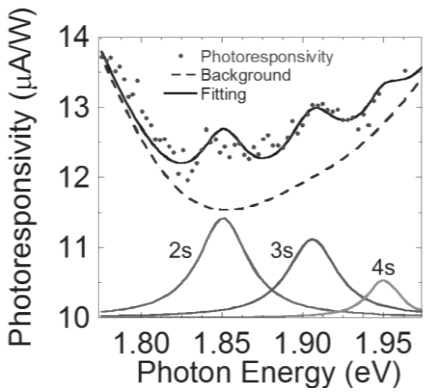

Fig.2 Fine spectral structures due to excited states.

[1] A. Chernikov, et al. PRL 113, 076802 (2014). [2]H. M. Hill et al, Nano Lett. 15, 2992 (2015).

[3] J. Shan, et al. PRL 113, 026803 (2014). [4] Y. J. Zhang, et al. Nano Lett., 13(7), 3023-3028 (2013).

Corresponding Author: Taishi Takenobu, Tel&Fax: +81-3-5286-2981, E-mail: takenobu@waseda.jp

Band-gap tuning of bilayer graphene by defects and inter-layer spacing

○Ken Kishimoto and Susumu Okada

Graduate school of Pure and Applied Sciences, University of Tsukuba, Tsukuba 305-8571, Japan

Electronic structures of graphene are fragile against the external environment, such as atoms, molecules, and substrates, because the electron states near the Fermi level are exposed to such foreign materials. Indeed, graphene adsorbed on the α-quartz is not metal but semiconductor with a few tens meV band gap because of the modulation of electrostatic potential on graphene layer induced by the substrate. In our previous work [1], we shows that bilayer graphene, one of which layer possesses atomic and topological defects, no longer possesses pairs of linear dispersion bands at or near the Fermi level, but instead has quadric dispersion bands together with the states associated with the defects, even though one of two layers retains their hexagonal atomic network because of the substantial interlayer interaction. In this work, we further investigate the influence of the defects in the graphene layer on the electronic structure of the other pristine graphene layer in terms of the interlayer spacing and the number of graphene layers using first principles total energy calculations within the framework of density functional theory.

Our DFT calculations show that the energy gap between the bonding and antibonding π states of pristine graphene layer in the bilayer structures monotonically decrease with increase of the interlayer spacing. Figure 1 shows the energy gap of the bilayer graphene, one of which layers possesses monovacancies per 4×4 lateral periodicity, as a function of the interlayer spacing: The gap vanishes at the critical interlayer spacing of 0.5 nm. The fact indicates that the influence of the defect on electrostatic potential of pristine graphene layer is negligible under the interlayer spacing of 0.5 or wider. Further calculations on the bilayer graphene with other defects, we find that the critical interlayer spacing strongly depends on the defect species. We also check how the gap depends on the number of layers.

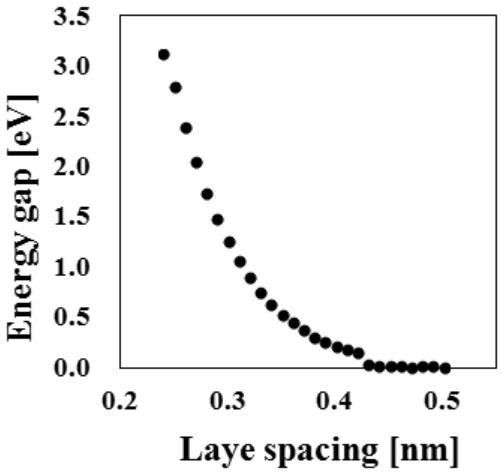

Fig. 1, Energy gap between π and π* states of pristine layer of bilayer graphene as a function of the interlayer spacing.

Table 1 The critical interlayer spacing at which the pristine layer possesses Dirac cone..

Defect species	Spacing [nm]
Monovacancy (per 4x4)	0.50
Divacancy	0.43
Hexagonal vacancy (V6)	0.51
Topological defect	0.46

[1] K.K, S.O in Abstracts of the 48th FNTG General Symposium (February 2015) p.127

Corresponding Author: K. Kishimoto
Tel: +81-29-853-5600(ext.; 8233)
E-mail: kkishimoto@comas.frsc.tsukuba.ac.jp

Magnetic properties of graphene flakes connected via sp^3 C atoms

Susumu Okada

Graduate School of Pure and Applied Sciences, University of Tsukuba, Tennodai, Tsukuba 305-8577, Japan

Graphene flakes with zigzag edges and a triangular shape exhibits spin polarization because of the number of non-bonding states arising from the imbalance between two sublattices of graphitic network. Phenalenyl ($C_{13}H_9$: fused three benzene rings) is the one of smallest example that exhibits spin polarization. In the case, the molecule possesses a singly occupied state at the Fermi level leading to the radical spin with S=1/2 ground state. By assembling phenalenyl molecules with appropriate intermolecular connections, we can design various hydrocarbon networks possessing interesting spin states as their ground and metastable states. In this work, we aim to explore the possible radical spin configurations on three phenalenyl units connected via sp^3 C atoms as the structural model of graphene nanoflakes with intersectional lines using density functional theory with generalized gradient approximation. Our calculations showed that the phenalenyl trimmers possess three possible spin states with the moment of S=1/2 and 3/2. Among the three states, one of the states with S=1/2 is found to be the ground state spin configuration, in which the two of three radical spins pairs exhibit the antiparallel coupling while the remaining one exhibit the parallel coupling. Our findings show that the intersectional sp^3 C atoms could not perfectly terminate the spin interaction among the graphene flakes.

Corresponding Author: Susumu Okada
Tel: +81-29-853-5921, Fax: +81-29-853-5924,
E-mail: sokada@comas.frsc.tsukuba.ac.jp

Measurement of powder resistivity of carbon nanomaterials with different geometries and graphitic structures

○Y. Suda[1], K. Mizui[1], T. Ohiro[1], Y. Shimizu[1], T. Harigai[1], H. Takikawa[1], H. Ue[2]

[1] *Department of Electrical and Electronic Information Engineering, Toyohashi University of Technology, Toyohashi, Aichi 441-8580, Japan*
[2] *Fuji Research Laboratory, Tokai Carbon Co., Ltd., Oyama, Shizuoka 410-1431, Japan*

1. Introduction

Carbon black, nanometer-size carbon particles, is commercially used as the catalyst support in fuel cell owing to its high surface area, porosity, electric conductivity, low density, and low cost. In previous work, we have used various carbon nanomaterials as catalyst supports for direct methanol fuel cell (DMFC) [1]. In this study, we measured the powder resistivity of carbon nanomaterials with different geometries and graphitic structures.

2. Experimental

The carbon nanomaterials were characterized using scanning electron microscopy (SEM; S-4500II and SU8000, Hitachi) and compressive resistivity measurements. The powder resistivity of compressed carbon nanomaterials is the result of a combination of the number of factors, including the resistivity of the individual particles, the degree of contact between the particles, and their packing density.

3. Results

The compressive resistivity of different carbon nanomaterials are listed in Table 1. From Table 1, carbon nanoballoon (CNB), which was prepared by heat treatment of Arc black (AcB), showed comparable powder resistivity to commercial Vulcan XC-72R (Vulcan). Moreover, in the comparison of fibrous carbon nanomaterials, carbon nanocoil (CNC) and vapor-grown carbon fiber (VGCF-X), VGCF-X showed lower resistivity.

Table 1. Compressive resistivity of different carbon nanomaterials

	Sample mass, g	Compression pressure, MPa	Area of base, cm^2	Compression bulk, cm	Current, mA	Voltage, V	Resistance, Ω	Resistivity, Ω cm
CNB	0.30	1.01	1.50	0.81	300.00	0.07	0.23	0.43
Vulcan	0.30	1.01	1.50	0.56	300.00	0.04	0.13	0.36
CNC	0.30	1.01	1.50	0.53	300.00	0.20	0.67	1.89
AcB	0.30	1.01	1.50	0.39	300.00	0.58	1.93	7.44
VGCF-X	0.30	1.01	1.50	1.15	300.00	0.12	0.40	0.52

This work has been partly supported by the EIRIS Project from Toyohashi University of Technology (TUT); JSPS KAKENHI Grant Number 24360108 and 15K13946; and the Toyota Physical and Chemical Research Institute, “Scholar Project”.

[1] Yoshiyuki Suda, Yoshiaki Shimizu, Masahiro Ozaki, et al. Materials Today Communications, 3 (2015) 96-103

Corresponding Author: Y. Suda
Tel: +81-532-44-6726, Fax: +81-532-44-6757
E-mail: suda@ee.tut.ac.jp

Evaluation of catalytic activity of fuel cell catalyst nanoparticles loaded on carbon nanoballoon

○Y. Suda[1], T. Ohiro[1], K. Mizui[1], T. Harigai[1], H. Takikawa[1], H. Ue[2]

[1] *Department of Electrical and Electronic Information Engineering, Toyohashi University of Technology, Toyohashi, Aichi 441-8580, Japan*
[2] *Fuji Research Laboratory, Tokai Carbon Co., Ltd., Oyama, Shizuoka 410-1431, Japan*

1. Introduction

Carbon black, nanometer-size carbon particles, is commercially used as the catalyst support in fuel cell owing to its high surface area, porosity, electric conductivity, low density, and low cost. In previous work, we have used various carbon nanomaterials as catalyst supports for direct methanol fuel cells (DMFC) [1]. In this study, we used carbon nanoballoon (CNB) as a catalyst support and measured the catalytic activity of CNB-supported PtRu catalyst.

2. Experimental

The twin-torch arc discharge apparatus was used for AcB synthesis. CNB was prepared by a heat treatment in Ar gas at 2600°C [2]. The particle shape of CNB is hollow. CNB is graphitic and has high conductivity. We prepared PtRu catalysts for the DMFC anode. The PtRu catalysts were loaded onto CNB by the reduction method using sodium boron hydrate ($NaBH_4$).

3. Results

Table 1 shows the electrochemically active surface area (ECSA) and the potential at peak current density during methanol oxidation reaction (MOR) of the PtRu catalysts with different loadings. The highest ECSA was observed at a loading of 15 wt.%, while they decreased with the catalyst loading. The PtRu catalysts supported on CNB showed highest current density of 2.07 mA cm^{-2}, when the catalyst loading was 30 wt.%.

Table 1. Electrochemical properties of PtRu catalyst particles loaded on carbon nanoballoon.

	ECSA / m^2 g^{-1}	Potential at peak current density / V (vs Ag/AgCl)	Peak current density / mA cm^{-2}
PtRu/CNB (15wt.%)	131.1	0.64	0.49
PtRu/CNB (30wt.%)	53.8	0.61	2.07
PtRu/CNB (45wt.%)	45.3	0.67	2.05

This work has been partly supported by the EIIRIS Project from Toyohashi University of Technology (TUT); JSPS KAKENHI Grant Number 24360108 and 15K13946; and the Toyota Physical and Chemical Research Institute, "Scholar Project".

[1] Y. Suda *et al*. Materials Today Communications. Vol 3, pp. 96-103 (2015).
[2] T. Ikeda *et al*. Japanese Journal of Applied Physics Vol 50, 01AF13 (2011).

Corresponding Author: Y. Suda
Tel: +81 532 44 6726, Fax: +81 532 44 6757
E-mail: suda@ee.tut.ac.jp

Structure of amorphous carbon deposited on nanometer-seized nickel particles under ultrahigh vacuum at room temperature

○Koji Asaka, Yahachi Saito

Department of Quantum Engineering, Nagoya University, Nagoya 464-8603, Japan

We studied the structures of amorphous carbon (a-C) films deposited on nickel (Ni) nanoparticles with clean surfaces at room temperature by transmission electron microscopy (TEM) and Raman spectroscopy. The a-C films on the surfaces of the nanoparticles have already been transformed into disordered graphitic layers without annealing.

The Ni nanoparticles were prepared on NaCl substrates by electron-beam deposition at a base pressure of less than 3×10^{-7} Pa at 673 K, and successively a-C was deposited onto the nanoparticles at room temperature without exposing the nanoparticles to the atmosphere. The structures of the a-C films were observed by high-resolution TEM operated at 120 kV. Raman spectra were measured using a laser excitation source with a wavelength of 532 nm.

Figures 1(a) and 1(b) show a TEM image of the Ni nanoparticles on the a-C film which was successively deposited without exposing the nanoparticles to the atmosphere and its selected-area electron diffraction pattern, respectively. The diameter distribution of the Ni nanoparticles is shown in Fig. 1(c). The surfaces of the nanoparticles are surrounded by defined facets and the [001] direction of the nanoparticles is perpendicular to the a-C film plane. The average diameter of the nanoparticles is 5.74 ± 0.02 nm. Figure 2 shows a high-resolution image of the Ni nanoparticles. On the surfaces of the nanoparticles, disordered graphitic layers similar to the structure of carbon black are already formed without annealing. The spacing of the layers shown by the arrows in Fig. 2 is about 0.36 nm, which is 4 % times as large as that of graphite. On the other hand, in the case where a-C was deposited at room temperature after the nanoparticles were exposed to the atmosphere, no graphitic layer was formed on the nanoparticles. When the samples were heat-treated at more than 873 K for 10 min in argon gas flow ambience, a few graphitic layers on the nanoparticles were formed. These results suggest that the Ni nanoparticles with the clean surfaces cause a decrease in graphitization temperature of a-C.

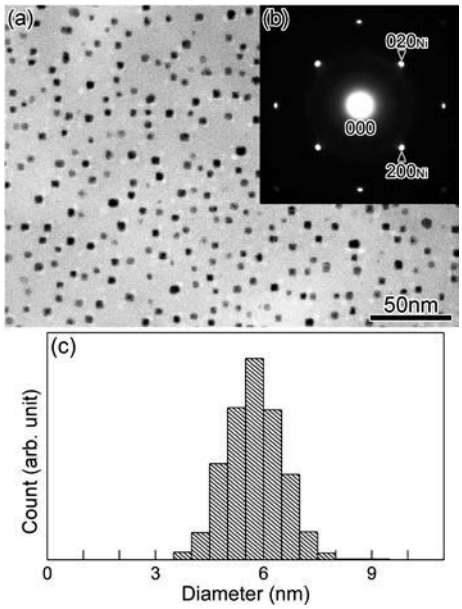

Fig.1 (a) TEM image, (b) its selected-area electron diffraction pattern, and (c) diameter distribution of Ni nanoparticles on the a-C film.

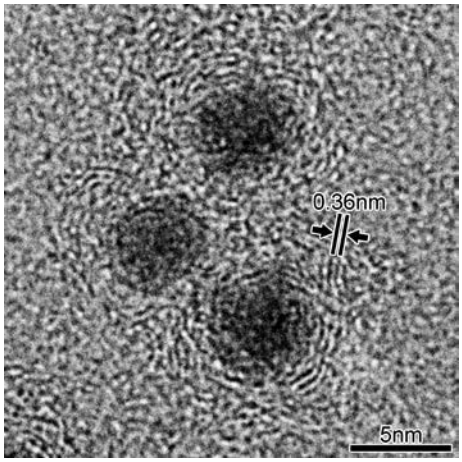

Fig.2 High-resolution image of Ni nanoparticles.

Corresponding Author: K. Asaka
Tel: +81-52-789-4464, Fax: +81-52-789-3703, E-mail: asaka@nuqe.nagoya-u.ac.jp

Conducting one-dimensional interface in an atomic-layer semiconductor heterojunction

○Yu Kobayashi[1], Yutaka Maniwa[1], and Yasumitsu Miyata[1,2,*]

[1]*Department of Physics, Tokyo Metropolitan University, Hachioji, 192-0397, Japan*
[2]*JST, PRESTO, Kawaguchi, 332-0012, Japan*

So far, semiconductor heterojunction interfaces with two-dimensional (2D) electron gas have played an important role in condensed-matter physics and electronics. Recent progress of atomic layer research provides an opportunity to realize novel, one-dimensional (1D) electronic system at heterojunction interface of atomic layers. For this purpose, atomically thin transition metal dichalcogenides (TMDCs) are an ideal material because of their tunable electronic properties. In recent studies, several groups including ours have reported the direct synthesis of TMDC-based heterojunctions by vapor-phase growth techniques [1-4]. However, 1D interface state at the heterojunction has never observed probably due to the problems in sample quality and/or alloying at interface.

Here, we report on the first observation of highly-conductive 1D interface state in a 2D semiconductor heterojunction. The present heterojunction consists of lateral and vertical heterostructure based on bilayer MoS_2/WS_2 and grown by chemical vapor deposition as reported previously [5]. In the present work, the graphite substrate also allows us to probe electronic properties around the interface by conductive atomic force microscopy. Unlike a simple monolayer WS_2/MoS_2 heterojunction, the present bilayer-based heterojunction has highly-conductive region along the interface (Fig.1). This conductivity enhancement can be understood as the result of carrier accumulation due to quantum confinement at the interface. The present results pave the way for understanding and applications of novel 1D electronic system.

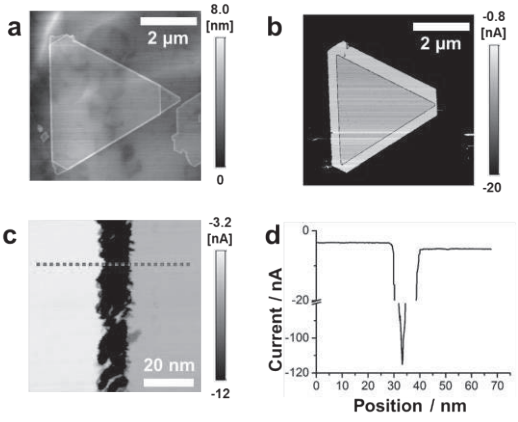

Fig.1 (a) Height and (b) current images of the bilayer heterostructure. (c) The magnified current image at the interface in b. (d) Current profile at the red dotted line in c.

[1] Y. Gong, *et al.* ***Nat. Mater.*** 13, 1135 (2014)., [2] X. Duan, *et al.* ***Nat. Nanotechnol***, 9, 1024 (2014).,
[3] C. Huang, *et al*. ***Nat. Mater.*** 13, 1096 (2014). [4] Y. Kobayashi, *et al.,* ***Nano Res.*** in press.
[5] Y. Kobayashi *et al.,* ***ACS Nano*****,** 9, 4056 (2015).
Corresponding Author: Yasumitsu Miyata, Tel: 042-677-2508, E-mail: ymiyata@tmu.ac.jp

CVD growth and characterization of monolayer $Nb_{1-x}W_xS_2$ alloys

○Shogo Sasaki[1], Yu Kobayashi[1], Yutaka Maniwa[1], Yasumitsu Miyata[1,2]

[1] *Department of Physics, Tokyo Metropolitan University, Hachioji 192-0397, Japan*
[2] *JST, PRESTO, Kawaguchi 332-0012, Japan*

Atomic-layer transition metal dichalcogenides (TMDCs) are attractive components for two-dimensional layered heterostructures because of their tunable electronic properties. To control their bandgap and carrier densities, there are several approaches such as chemical doping and alloying. In our previous works, we reported the growth of bandgap-tunable $Mo_{1-x}W_xS_2$ alloys [1] and highly-conductive $Nb_{1-x}W_xS_2$ alloys [2] using thin-film sulfurization. However, it is difficult to obtain large-area crystals using thin film sulfurization probably due to the limitation of nucleation densities. To solve this issue, we have developed a growth method of large-area, monolayer TMDC alloys using chemical vapor deposition (CVD) because of its tunability of supplying rate of precursors.

In this presentation, we report the growth and characterization of monolayer Nb-doped WS_2. Nb-doped WS_2 were grown on graphite and sapphire substrates by CVD method using WO_3 and Nb_2O_5 powders at 1100℃ under argon/sulfur atmosphere. Figure 1a shows an optical image of a typical triangle-shaped crystal with a size of 50 μm on the sapphire substrate. The crystals have two characteristic small Raman peaks at 380 cm^{-1} and 400 cm^{-1} between WS_2-E_{2g} and WS_2-A_1' peaks (Fig. 1b). Photoluminescence spectra show two broad peaks at 1.96 eV and 1.70 eV for the doped samples (Fig. 1c). These results suggest that the present approach enables large-area growth of Nb-doped WS_2 monolayers, and could provide an effective way to produce carrier-controlled TMDC-based heterostructures.

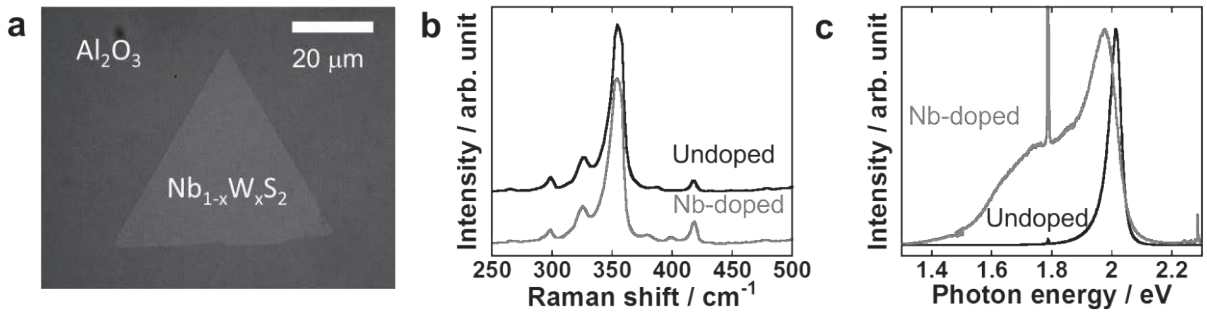

Fig. 1 (a) Optical image of a typical monolayer Nb-doped WS_2 crystal grown on a sapphire substrate. (b) Raman and (c) photoluminescence spectra of undoped and Nb-doped WS_2 monolayers.

[1] Y. Kobayashi *et al*. Nano Res. (2015) in press.
[2] S. Sasaki *et al*. The 48th FNTG symposium.

Corresponding Author: Yasumitsu Miyata, Tel: +81-42-677-2508, E-mail: ymiyata@tmu.ac.jp

In-Plane Heterostructures of Graphene and MoS_2

○Yoshihiro Shiratsuchi,[1] Hiroko Endo,[2] Masaharu Tsuji,[3] Hiroki Hibino,[4,5] Hiroki Ago[1,2,6]

[1]Grad. Schl. Eng. Sci., Kyushu Univ., Fukuoka 816-8580, Japan, [2]Inst. Mater. Chem. Eng., Kyushu Univ., Fukuoka 816-8580, [3]Center Carbon Res., Kyushu Univ., Fukuoka 8165-0943, Japan, [4]Kwansei Gakuin Univ., Hyogo 669-1337, Japan, [5]NTT Res. Lab., Kanagawa 243-0198, Japan, [6]PRESTO-JST, Saitama 332-0012, Japan

Heterostructures of atomically thin, layered materials offer unique electronic and photonic properties together with high mechanical flexibility. Graphene shows extraordinary high carrier mobility, while monolayer MoS_2 has a finite band gap of 1.9 eV with high optical absorption for the visible light. Therefore, the combination of these two materials as well as their Schottky junction is expected to offer unique devices with high optical response [1-4]. However, most of these devices are made with exfoliated films [1,5] so that the device size is limited and not suitable for large-scale devices. Here, we demonstrate direct CVD growth of MoS_2-graphene in-plane heterostructures, as well as their structural characterization and carrier transport properties.

To synthesize MoS_2-graphene heterostructures, hexagonal graphene domains grown by ambient pressure CVD on Cu foil were transferred onto a sapphire substrate, followed by the second CVD process to grow MoS_2 using MoO_3 and S as feedstock. Figure 1a shows an SEM image of the in-plane graphene-MoS_2 heterostructure. It is seen that MoS_2 domains preferentially grow from sides of graphene domains. Raman mapping image and spectrum (Fig. 1b,c) support the formation of monolayer MoS_2 at the sides of CVD graphene. Interestingly, the selected-area diffraction measured by low-energy electron microscope (LEEM) shown in Fig. 1d indicates that some of the MoS_2 domains have the identical orientation with the neighboring graphene domains, signifying *the lateral epitaxy*. We will also present transport properties in these unique heterostructures.

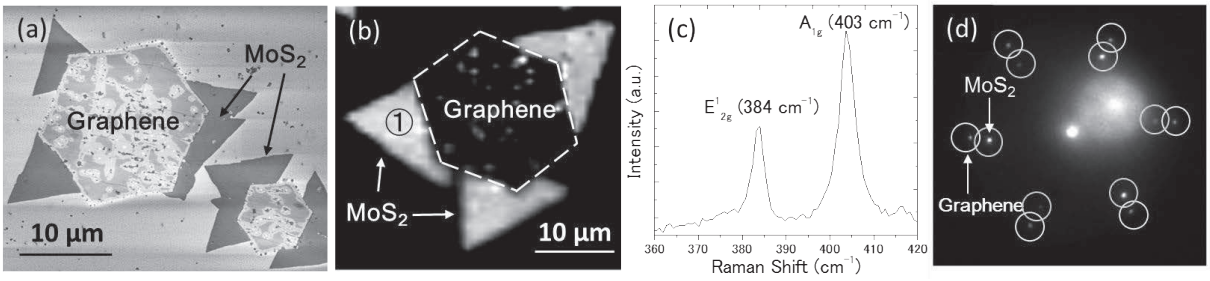

Figure 1. (a) SEM image of the graphene-MoS_2 in-plane heterostructure. (b) Raman mapping image of the A_{1g} intensity of MoS_2. (c) Raman spectrum measured at the point 1 of (b). (d) Selected-area electron diffraction pattern obtained from the heterostructure.

References: [1] K. Roy et al., *Nat. Nanotech.*, **8**, 826 (2013). [2] H. Tian et al., *Sci. Rep.*, **4**, 5951 (2014). [3] H. Ago et al., *ACS Appl. Mater. Interfaces*, **7**, 5265 (2015). [4] J. Y. Kwak et al., *Nano Lett.*, **14**, 4511 (2014). [5] G. H. Lee et al., *ACS Nano*, **7**, 7931 (2013).

Corresponding Author: Hiroki Ago (Tel&Fax: +81-92-583-7817, E-mail: ago@cm.kyushu-u.ac.jp)

Functionalization of few-layer tungsten diselenide with mild O_2 plasma treatment

○Reito Nagai, Toshiaki Kato, Tomoyuki Takahashi, and Toshiro Kaneko

Department of Electronic Engineering, Tohoku University, Sendai 980-8579, Japan

Atomically-thin two-dimensional (2D) sheets attract intense attention for their superior electrical and optical features. Transition metal dichalcogenide (TMD) is known as a 2D material with excellent semiconducting properties. Optical and electrical properties of TMD strongly depend on its number of layer. Monolayer TMD has strong photoluminescence (PL) intensity due to their direct band gap [1]. Although multi-layer (2～5 layers) TMDs don't show bright PL for its indirect band structure, the carrier mobility is higher than that of monolayer one. For the fabrication of high performance optoelectrical device, it is required to combine these optical and electrical properties of mono- and multi-layer TMD, respectively.

In this study, we investigated the electrical and optical properties of few-layer tungsten diselenide (WSe_2) before and after mild plasma treatment [2,3] (Fig.1). We found that mild O_2 plasma treatment can drastically enhance PL intensity of WSe_2, whereas the initial electrical properties of WSe_2 can be maintained even after the mild plasma treatment. This result indicates the mild O_2 plasma treatment can fabricate functionalized TMD including better optoelectrical features.

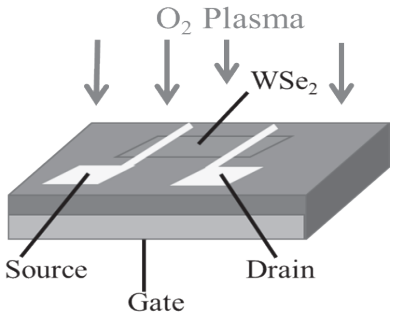

Fig.1: Schematic illustration of WSe_2-FET device structure

[1] T. Kato and T. Kaneko, ACS Nano **8**, 12777 (2014).

[2] T. Kato, L. Jiao, X. Wang, H. Wang, X. Li, L. Zhang, R. Hatakeyama, and H. Dai, Small **7**, 574 (2011).

[3] T. Kato and R. Hatakeyama, Nature Nanotechnology **7**, 651 (2012).

Corresponding Author: R. Nagai

Tel: +81-22-795-7046

E-mail: nagai14@ecei.tohoku.ac.jp

Local Optical Absorption Spectra of Transition Metal Dichalcogenide Monolayer by Scanning Near-field Optical Microscopy Measurements

○Junji Nozaki[1], Shohei Mori[1], Yasumitsu Miyata[1,2], Yutaka Maniwa[1], Kazuhiro Yanagi[1*]

[1] *Department of Physics, Tokyo Metropolitan University, Hachioji, Tokyo 192-0397, Japan*
[2] *PRESTO, JST, Kawaguchi, Saitama 332-0012, Japan*

Transition metal dichalcogenide (TMDCs) have attracted a lot of interest due to their remarkable physical properties. [1,2] Here, we investigated local optical absorption spectra of MoS_2 thin sheet by combining scanning near-field optical microscopy (SNOM) and super-continuum laser light source. And we revealed local optical absorption spectra of MoS_2 thin layer in high resolution which overcomes diffraction limit of excitation laser wavelength.

We connected super-continuum laser light source to monochromator, and wavelength of excitation light is selected. Then, selected visible excitation laser light ranging from 450 to 740 nm wavelength is introduced to our SNOM system. In SNOM system, laser light is focused on the SNOM cantilever (aperture diameter: ~90nm) to make evanescent light field on the far side of the aperture. The sample is scanned, transmitted far-field is detected through the inverted objective lens at the bottom. We determined the absorbance of single layer MoS_2 as follows. The transmitted light intensity at sapphire substrate was I_0, and the transmitted light intensity at the sample was I, and the absorbance was determined as $-\log(I/I_0)$

The local optical absorption spectra, obtained from SNOM, at sites P and Q corresponding to the center and edge of the crystal, respectively, are shown in Figure 1. The sampling area of P and Q are shown in the inset of Fig. 1, and their sizes were 1 μm^2. The spectra clearly exhibit the A and B exciton peaks, suggesting the validity of optical absorption evaluation using SNOM. However, detailed spectral structures are shown in Fig. 1b and there exists a slightly difference between the line-shapes of P (center) and Q (edge) sites. As shown here, the line-shape of the A peak at site Q was a little broader than the same peak observed at site P. When we analyzed the line-width of the A peak using a Gaussian function, its band-width of A peak at Q was (0.048 ± 0.013) eV and that at P was (0.034 ± 0.005) eV.

We identified the slightly difference of the local absorption structure between the different parts of MoS_2 monolayer by combination of SNOM and super-continuum light source. We will analyze other different parts of the crystal, and will proceed further study to investigate the detail of local absorption spectra.

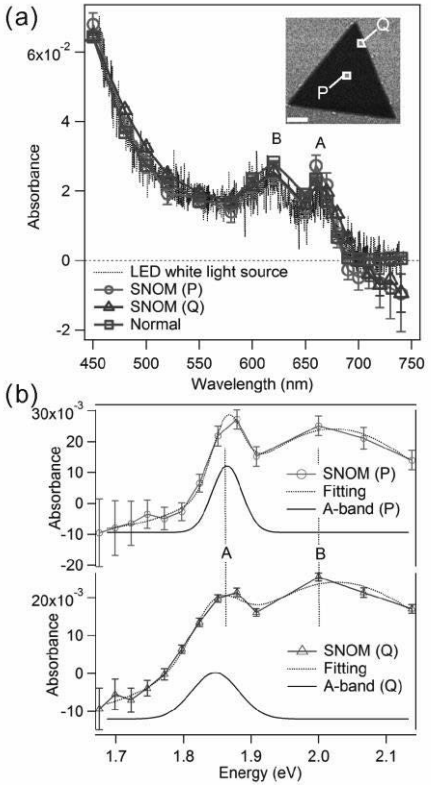

Fig.1: (a) Local absorption structure of single layer MoS_2 measured by SNOM with super-continuum laser light source (b) detailed structure of center (P) and edge (Q) part.

[1] Qing Hua Wang *et al*., Nature Nanotech. **7**, 699 (2012).

[2] Yu-Ming He *et al*., Nature Nanotech. **10**, 497 (2015).

Corresponding Author: K. Yanagi
Tel: +81-42-677-2494, Fax: +81-42-677-2483,
E-mail: yanagi-kazuhiro@tmu.ac.jp

The topological and electronic structure of Starfish nanocarbon

○Natsuki Namba, Yukihiro Takada and Kyoko Nakada

College of Science and Engineering, Aoyama Gakuin University,
5-10-1, Fuchinobe, Chuo-ku Sagamihara 252-5258, Japan

We proposed new sp^2 carbon structures named "starfish nanocarbon" (SFNC, Fig 1) and analyzed the relationships between their structures and electronic states.

We found 12 SFNCs and all of them have 6N heptagons (N is number of arms). We proved this by topological consideration. SFNCs have common axis at its center. The axis is composed of 2N heptagons and 4N hexagons. Removing 2 heptagons that are used for the axis , SFNCs have 4 heptagons per arm. The structures and electronic states of 12 SFNCs are identified by the configuration of 4 heptagons per arm.

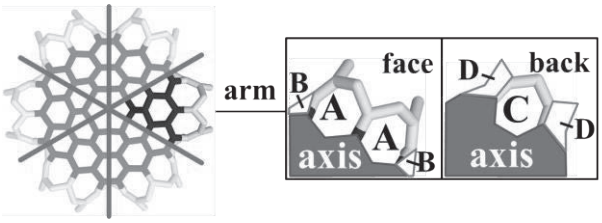

Fig 1 Name of the parts of SFNC.

We made 2D periodic system of each SFNC (Fig 2). To make this system, we connected various types of SFNCs with various types of tubes. Fig 3 shows the electronic states of them calculated by Hückel method. We focused on the location of DOS peak and divided 12 starfish nanocarbons. SFNCs with (2N, 0)tubes shows peaks at E=±1 like van Hove singularity of graphene.

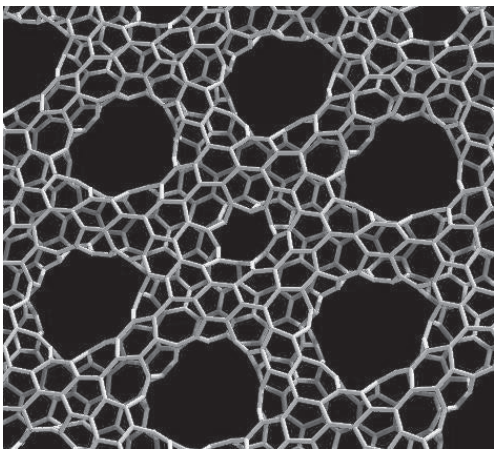

Fig 2 A periodic system of SFNC .

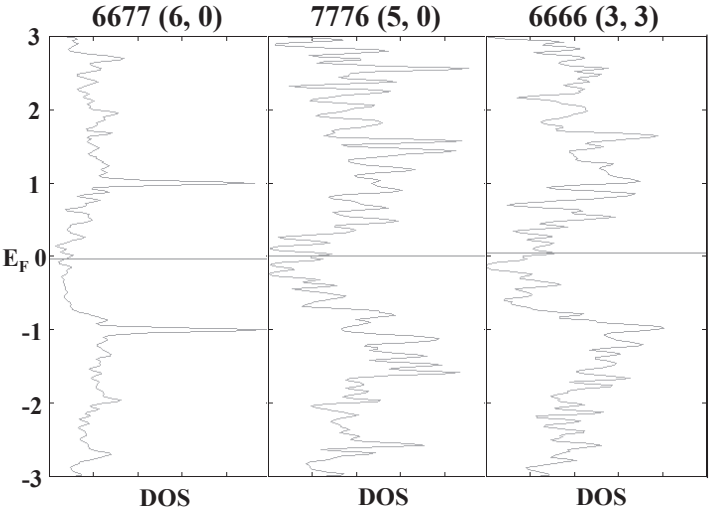

Fig3 DOS of the periodic system.

Corresponding Author: K. Nakada
Tel: +81-42-759-6219 Fax: +81-42-759-6493 E-mail: nakada@chem.aoyama.ac.jp

Room temperature synthesis of two-dimensional organic framework materials

○Gayoung Kim[1], Tomohiro Shiraki[1], Naotoshi Nakashima[1,2]

[1] *Department of Applied Chemistry, Kyushu University, Fukuoka 819-0395, Japan*
[2] *WPI-I2CNER, Kyushu University, Fukuoka 819-0395, Japan*

Dimensionally-controlled organic architectures are attracting great attentions due to their unique structures and functions. In particular, two-dimensional organic frameworks with crystalline structures are known as covalent organic frameworks (COFs), [1] which are expected as a promising material for further applications such as gas storage, optoelectronic devices and catalysis due to their porous and highly-ordered molecular structures. Synthesis of high quality COFs is still challenging, since COFs are generally mixtures of crystalline and amorphous domains. Here we report the room temperature synthesis of an imine-linked COF. Compared with a COF synthesized by a conventional solvothermal reaction[2], our COF has a highly crystalline structure and shows remarkable gas uptake and high thermal stability.

Benzene-1,3,5-tricarboxylate (**1**, 24 mg) and phenylendiamine (**2**, 24 mg) were dissolved in dioxane (2.5 ml), respectively. The molar ratio of aldehyde and amino groups was 1:1. After mixing the solutions, 3 M aqueous acetic acid (0.25 ml) was added. Two-day storage at 25 °C was found to generate a precipitate, which was collected by filtration, then washed with acetone. The obtained solid was dried overnight in vacuo at 80 °C to provide a pale yellow powder (**COF1**, Fig. 1).

The XRD pattern (Fig. 2) shows obvious diffraction peaks at 4.8, 8.1, 9.3, 12.4, and 25.8 degrees, which are attributed to the (100), (110), (200), (210), and (001) facets of the two dimensional crystal structure with an eclipsed arrangement[2]. The N_2 adsorption measurement for the sample was conducted. Based on the BET analysis, the surface area was determined to be 1528 m^2/g, which was 3.7 times higher than that of the solvothermally synthesized COF (410 m^2/g). The TGA analysis identified that the **COF1** has a better thermal stability (degradation temperature: 450°C) compared to that (310°C[2]) synthesized by the solvothermal method. Synthesis of a nitrogen-doped graphitic carbon based on carbonization of the highly crystalline COF will be reported at the meeting.

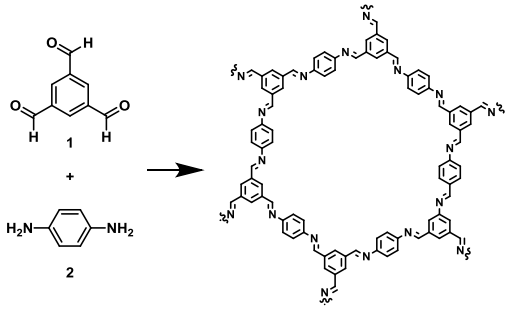

Fig.1 Schematic representation of **COF1** synthesis.

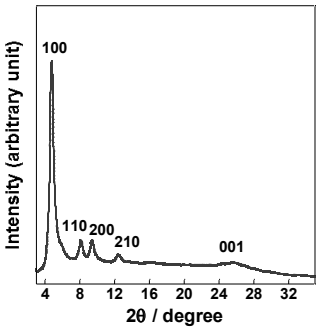

Fig.2 XRD pattern of **COF1**.

[1] O. M. Yaghi *et al*. Science **310**, 1166 (2005), [2] W. Wang *et al*. J. Am. Chem. Soc. **133**, 19816 (2011).

Corresponding Author: N. Nakashima
Tel: +81-92-802-2840, Fax: +81-92-802-2840,
E-mail: nakashima-tcm@mail.cstm.kyushu-u.ac.jp

Thermal [2+2] cycloaddition of $[Li^+@C_{60}]NTf_2^-$ with anethole via single electron transfer process

○Yu Yamazaki, Ken Kokubo, Ikuma Naohiko, Hidehiro Sakurai

Division of Applied Chemistry, Graduate School of Engineering, Osaka University, Suita 565-0871, Japan

Lithium-ion-encapsulated fullerene $Li^+@C_{60}$ exhibits ionic property and stronger electron acceptability than pristine C_{60}. Our previous report revealed that [4+2] Diels-Alder reaction of $Li^+@C_{60}$ with 1,3-cyclohexadiene was ca. 2400-fold accelerated than that of C_{60}, giving a novel product [1].

On the other hand, the thermal [2+2] cycloaddition of C_{60} with alkene is thermally forbidden and photo-induced cycloaddition with anethole through single electron transfer process has been reported [2]. Only highly electron-rich alkenes such as enamine and dienamine can undergo thermal [2+2] cycloaddition via single electron transfer [3].

In this study, we report a [2+2] cycloaddition of $[Li^+@C_{60}]NTf_2^-$ with anethole via single electron transfer process under thermal condition. The obtained [2+2] cycloadduct was fully characterized by ^1H, ^{13}C, ^7Li-NMR and MALDI-TOF MS, and the stereochemistry was determined as (*E*)-isomer by means of NOESY measurement. The electronic properties of the product were compared with those of both parent $Li^+@C_{60}$ and the corresponding [2+2] adduct with pristine C_{60}.

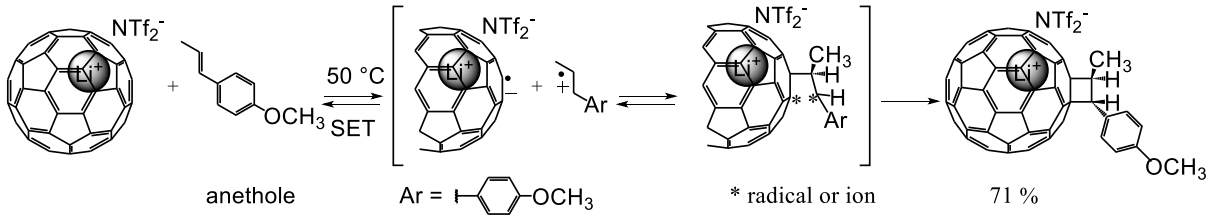

[1] (a) H. Ueno, K. Kokubo, Y. Nakamura, K. Ohkubo, N. Ikuma, H. Moriyama, S. Fukuzumi, T. Oshima, *Chem. Commun.* **2013**, *49*, 7376; (b) H. Ueno, H. Kawakami, K. Nakagawa, H. Okada, N. Ikuma, S. Aoyagi, K. Kokubo, Y. Matsuo, T. Oshima, *J. Am. Chem. Soc.* **2014**, *136,* 11162.

[2] G. Vassilikogiannakis, M. Orfanopoulos, *Tetrahedron lett*. **1997**, *38*, 4323.

[3] T. Mikie, H. Asahara, K. Nagao, N. Ikuma, K. Kokubo, T. Oshima, *Org. Lett*. **2011**, *13*, 4244.

Corresponding Author: K. Kokubo
Tel: +81-6-6879-4592, Fax: +81-6-6879-4593, E-mail: kokubo@chem.eng.osaka-u.ac.jp

Energetics of fullerenes under an external electric field

○Jun-ya Sorimachi, Susumu Okada

Graduate school of Pure and Applied Sciences, University of Tsukuba, Tsukuba 305-8571, Japan

Because of the hollow-cage structures of pentagons and hexagons, electronic states of fullerenes can be approximately regarded as the electron system confined in the quantum well with spherical shell. Accordingly, the electronic energy levels of π electrons are bunched up each other characterized by the spherical harmonics Y_{lm} corresponding to the electrons confined in a spherical shell or a sphere: It has been known that the highly degenerated states emerge in the electronic energy level of an isolated C_{60} molecule. In this work, we clarify the energetics and electric field response of fullerenes under the constant electric field between two parallel planar electrodes using density functional theory (DFT) with the effective screening medium (ESM) method.

Figure 1 shows the total energy of fullerenes, C_{60}, C_{70} and $C_{78}(C_{2v}')$, as a function of the electric field. In the case of C_{60} and C_{70}, the energy exhibits quadric behavior with respect to the external field. Thus, the electron system of these fullerenes can be regarded as the spherical electron system, since the total energy of dielectric spherical shell is proportional to the square of the external parallel electric field. Indeed, the induced carriers by the external field exhibit symmetric feature along the field direction (Fig. 2). In contrast, the total energy of $C_{78}(C_{2v}')$ does not exhibit quadric relation under the electric field. We further investigate the total energy of fullerenes with various molecular orientation under the electric field.

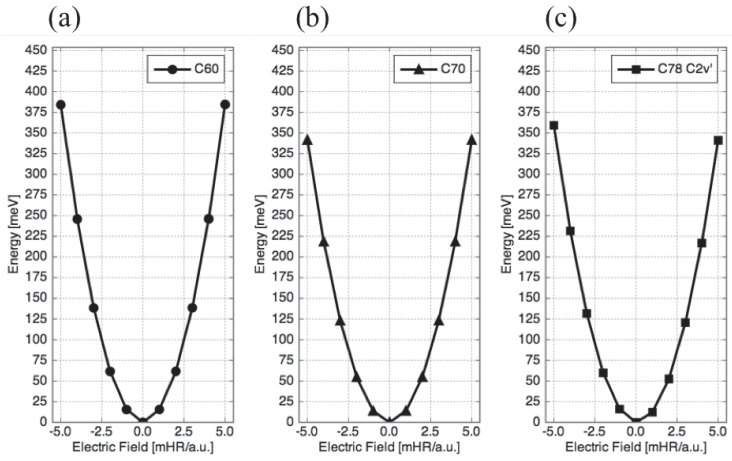

Fig. 1; Correlation between energy and electric field about (a) C_{60}, (b) C_{70} and (c) C_{78} (C_{2v}').

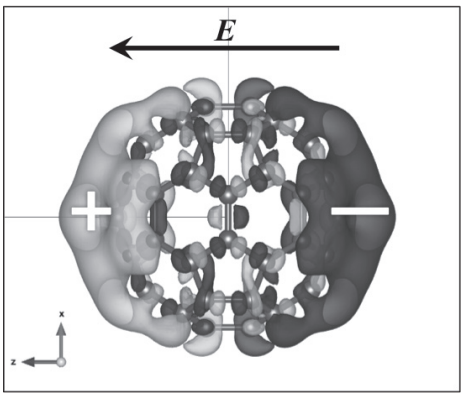

Fig. 2; Isosurfaces of the induced charge by the electric field.

Corresponding Author: J. Sorimachi
Tel: +81-29-853-5600(ext.; 8233)
E-mail: jsorimachi@comas.frsc.tsukuba.ac.jp

Low temperature Raman measurements of iodine molecules encapsulated in single-walled carbon nanotubes

○Shinji Kawasaki, Y. Ishii, Y. Yoshida, Y. Taniguchi, M. Yamada

Nagoya Institute of Technology, Nagoya 466-8555, Japan

We developed very simple method to encapsulate iodine molecules into single-walled carbon nanotubes (SWCNTs) by electro-oxidation of iodine ions. It was found that the electric conductivity of SWCNTs is drastically improved by iodine encapsulation because large hole careers are introduced. It was also found that the SWCNTs encapsulating iodine molecules (I@SWCNTs) are well dispersed in water at low temperature.[1] However, the reason why the dispersibility of I@SWCNTs changes with temperature has not been understood well. In order to clarify the reason, we performed Raman measurements of I@SWCNTs at several temperatures from -100ºC to +70 ºC.

SWCNTs (Meijo Nano-Carbon, SO type) having mean tube diameter of ca. 1.5 nm were used. Iodine encapsulation treatments were done in an electrochemical cell consisting of SWCNT electrodes and NaI aq. electrolyte. Low temperature Raman measurements were performed using a JASCO NRS-3300 spectrometer and a Linkam 10036L temperature control stage. As shown in Fig. 1, relative intensity of iodine Raman peaks observed in low wavenumber region to G-band peak of SWCNT at around 1600 cm^{-1} increased with decreasing temperature. It indicates that the reaction ($I_2 + I_3^- \rightarrow I_5^-$) would be promoted at low temperature. This hypothesis is supported by that the G-band peak position at low temperature was shifted toward higher wavenumber side.

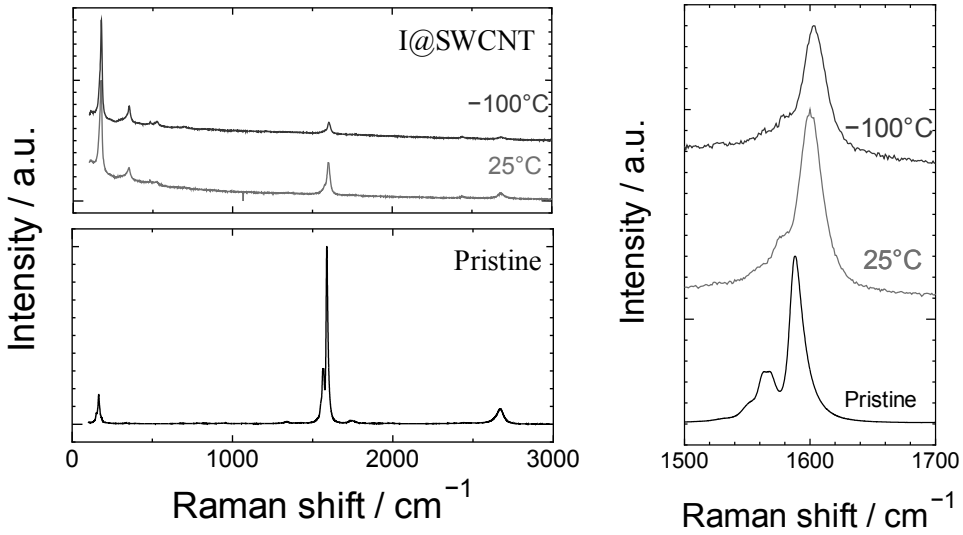

Fig. 1 Raman spectra of pristine SWCNT and I@SWCNT at room temperature

[1]H. Song, Y. Ishii, A. Al-zubaidi, T. Sakai, S. Kawasaki, Temperature-dependent water solubility of iodine-doped single-walled carbon nanotubes prepared using an electrochemical method, Phys. Chem. Chem. Phys. 15, 5767-5770 (2013).

Corresponding Author: S. Kawasaki
Tel: +81-52-735-5221, E-mail: Kawasaki.shinji@nitech.ac.jp

Rayleigh Scattering Spectroscopy of Single-Walled Carbon Nanotubes in Various Condition

○Toru Osawa[1], Takeshi Okochi[1], Yoritaka Furukawa[1],
Taiki Inoue[1], Shohei Chiashi[1], Shigeo Maruyama[1, 2]

[1]*Department of Mechanical Engineering, The University of Tokyo, Tokyo 113-8656, Japan*
[2]*Energy NanoEngineering Laboratory, National Institute of Advanced Industrial Science and Technology (AIST), Ibaraki, 305-8564, Japan*

Single-walled carbon nanotubes (SWNTs) are one of the most promising materials for electronic devices such as a field effect transistor because of its high mobility and its nanostructure. However, it is known that electronic structures of SWNTs depend not only on their structures, known as a chirality, but also on their surrounding environment. Therefore, understanding actual electronic structures of SWNTs is important to evaluate the performance and reliability of SWNT devices. Recently, Rayleigh scattering spectroscopy has attracted much attention as an efficient method to investigate the 1D electronic structure of SWNTs [1].

In this study, we constructed the measurement system and observed Rayleigh scattering spectra and images of various SWNTs. The schematic diagram of our optical system is shown in Fig. 1. The attenuated continuum laser (the range of wavelength is 400 - 2500 nm) was focused on SWNTs. Scattered light was measured with CCD array and InGaAs detectors for spectroscopy and with 2D CCD camera for imaging. In order to avoid influence by the stray light, we adopted a confocal system. We measured Rayleigh scattering from dispersed SWNTs in the surfactant solutions [2], dry-deposited SWNT films [3], suspended SWNTs and so on. As one example, Fig. 2 and Fig. 3 show SEM image of suspended SWNTs and its Rayleigh scattering image, respectively. From these observations, we compared characteristic features of SWNT electronic structures depending on surrounding environments.

[1] M. Y. Sfeir *et al*., Science **306**, 1540 (2004).
[2] H. Liu *et al*., Nat. Commun. **2**, 309 (2011).
[3] A. Kaskela *et al*., Nano Lett. **10**, 4349 (2010).
Corresponding Author: S. Maruyama
Tel: +81-3-5841-6421, Fax: +81-3-5841-6421,
E-mail: maruyama@photon.t.u-tokyo.ac.jp

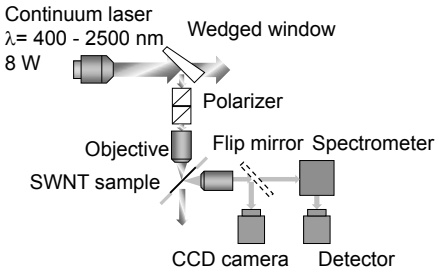

Fig. 1: Schematic diagram of Rayleigh scattering measurement system.

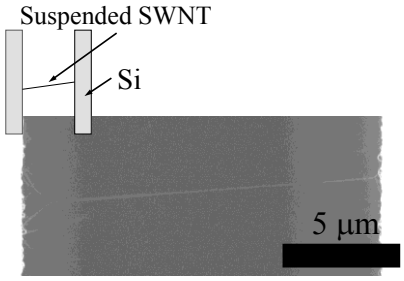

Fig. 2: SEM image of suspended SWNTs.

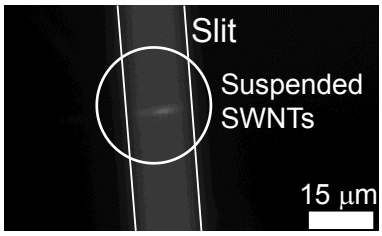

Fig. 3: Rayleigh scattering image of suspended SWNTs.

Variety of structural modulations in bridged carbon nanotubes under joule heating

○Yuki Araki[1], Kaori Hirahara[1, 2]

[1] *Department of Mechanical Engineering, Osaka University, Osaka 565-0871, Japan*
[2] *Center for Atomic and Molecular Technologies, Osaka 565-0871, Japan*

Since carbon nanotubes (CNTs) generally show excellent elastic property, their machining process requires inducing structural anomalies to obtain the deformed features. In-situ transmission electron microscopy (TEM) has investigated plastic deformation process of individual CNTs under various deformation modes such as cutting, bonding, bending, sharpening etc. [1-8] by applying mechanical stress with joule heat. Joule heating is effective to apply energy for cutting or switching carbon-carbon bonds at the local area of CNTs. In case of joule heating of a straight CNT bridged between electrodes, usually its central portion has highest temperature, and various types of structural modulations have been observed there. In some cases voids [2] or kinks [2] firstly formed, or sometimes its diameter partially decreased [3]. When voids formed, their expansion and/or traveling resulted in cutting of CNTs [2], but sometimes repair of voids with reducing tube diameter has been observed [4]. Furthermore, when it comes to multi-walled CNTs, some papers reported that sublimation of carbon atoms started from outer shells [5] or from inner shells [6]. There is a question how such a variety arises to Joule-heated CNTs. Our previous studies have shown that shapes of thinning CNTs depend on the temperature increase [7], energy barriers for coalescence, kink formation and sublimation in a CNT has been also discussed[8]. In this study, we experimentally examined the difference in conditions for occurring the other various deformation modes by using TEM equipped with a nanomanipulator. By operating the nanomanipulator, an isolated double-walled CNT (DWNT) was bridged between two electrodes, and voltage was applied. The changes in the shape of DWNTs with increasing current were monitored. As the result, formation of voids and kinks, and reducing diameters promoted by travelling and/or repairing voids or by migration of kinks were observed in tens of DWNTs. Sorting these by critical current applied revealed an energetic trend in the deformation process of bridged DWNTs; formation and migration of voids requires lower energy than kink formation. Those voids can be repaired by applying energy comparable to that for sublimation of carbon atoms or form kinks reduce diameters.

[1] C. Jin et al., Nat. Nanotech. **3**, pp. 17-21, (2008)
[2] C. Jin et al., Nano Lett. **8** 4, pp. 1127-1130, (2008)
[3] T. D. Yuzvinsky et al., Nano Lett. **6** 12, pp. 2718-2722, (2006)
[4] T. Nishijima et al., MICROELECTRON. ENG. **88**, pp. 2519-2523, (2011)
[5] Y. Nakayama et al., Jpn. J. Appl. Phys. **44** 23, pp. 720-722, (2005)
[6] C. Jin et al., J. Am. Chem. Soc. **2** 6, pp. 1275-1279, (2008)
[7] H. Maruyama et al., Appl. Phys. Express **3**, 025101, (2010)
[8] H. Somada et al., Jpn. J. Appl. Phys. **46** 44, pp. 1055-1057 (2007)

Corresponding Authors: Yuki Araki, Kaori Hirahara
Tel: +81-06-6879-7815
E-mail: araki@ne.mech.eng.osaka-u.ac.jp, hirahara@mech.eng.osaka-u.ac.jp

Structure and solid state properties of hydroxylated single-walled carbon nanotubes and related materials

○Yoshiaki Sano[1] and Hironori Ogata [1, 2]
[1]*Graduate School of Engineering, Hosei University, Koganei, Tokyo 184-8584, Japan*
[2]*Research Center for Micro-Nano Technology, Hosei University, Koganei, Tokyo, 184-0003, Japan*

It has been reported that polyhydroxylated fullerene (fullerenol: $C_{60}(OH)_{12}$) solids [1] have proton conductivity in a dry atmosphere. On the other hands, $C_{60}(OH)_{24}$ solids have no proton conductivity[1]. We previously reported the proton dynamics in fullerenol solids studied by solid-state ^{1}H NMR. Local structures, motion of hydroxyl groups and proton dynamics of the hydroxyl groups on carbon solid surfaces is considered to be very interesting.

It is reported that the dispersibility in ethanol[2] of CNTs is increased by hydroxylation. However, it has not been fully elucidated the structure and solid state properties of hydroxylated CNTs. In this study, SWNTs modified with hydroxyl groups (SWNT-OH) were prepared and characterized their structures with FT-IR spectroscopy, Raman spectroscopy, X-ray photoelectron spectroscopy and transmission electron microscope (TEM) and solid-state NMR spectroscopy.

Synthesis SWNT-OH were performed by using H_2SO_4/HNO_3 and HCl[3]. Figure 1 shows XPS spectrum of SWNT-OH and peak fitting conclusion. The ratio of OH-groups of SWNT-OH was evaluated to be 24.5 atm%. Detailed results on the properties of proton motions in SWNT-OH and related materials will be presented.

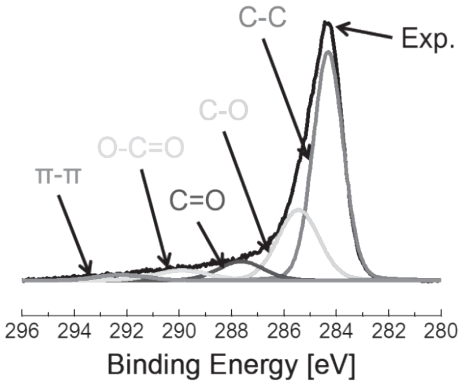

Figure 1 XPS spectrum of SWNT-OH

References:
[1] K. Hinokuma *et al., Chem. Phys. Lett.,* **341**, 442 (2001).
[2] S.Z. Kang, *et al.*,*Colloids Surf.* A. **384**, 363‑367 (2011).
[3] A.G. Osorio, *et al*., *Applied Surface Science* 255, 2485–2489, **2008**
Corresponding Author: Hironori Ogata
Tel: +81-42-387-6229, Fax: +81-42-387-6229, E-mail: hogata@hosei.ac.jp

Interfacial Engineering of Epoxy Composite Reinforced by Polybenzimidazole-wrapped Carbon Nanotubes

○Tsuyohiko Fujigaya[1,2], Yusuke Saegusa[1], Shogo Momota[3], Nobuhide Uda[3], Naotoshi Nakashima[1,2,]

[1] Department of Applied Chemistry, Graduate School of Engineering. Kyushu University, 744, Motooka Nishi-ku Fukuoka, 819-0395, Japan
[2] WPI I²CNER. Kyushu University, 744 Motooka, Nishi-ku, Fukuoka, 819-0395, Japan
[3]Department of Aeronautics and Astronautics, Graduate School of Engineering. Kyushu University, 744, Motooka Nishi-ku Fukuoka, 819-0395, Japan

Carbon fiber reinforced plastics (CFRP), typically composed of carbon fiber (CF) and epoxy resin, have been attracting enormous attentions as an alternative material of metal-based materials because of their remarkable mechanical properties with lightweight. One of the promising strategy is to replace the CF with stronger materials. In this target, carbon nanotubes (CNTs) having higher Young's modulus of 270-950 GPa and tensile strength of 11-63 GPa than those of CF (typically, 200-700 GPa and 3-7 GPa for Young's modulus and tensile modulus, respectively) are emerged as a promising substitution.

However, unlike the CF, it is well recognized that CNTs form strong bundle structures, which hinder homogeneous mixing with an epoxy matrix. When CNT's dispersion in epoxy matrices is poor, the CNT bundles tend to induce a stress concentration, which hampers effective reinforcement of the composites. And the interfacial adhesion between the CNTs and matrix is very weak, thus resulting insufficient load transfer to CNTs in the composites.

We describe a novel strategy to reinforce an epoxy resin using carbon nanotubes (CNTs) as the material, in which polybenzimidazole (PBI) was used as the glue to enable an effective adhesion between the epoxy matrix and CNT surfaces (Fig. 1). Since the PBI strongly interacts with the surfaces of the CNTs and reacts with epoxy matrices to form covalent bonding, the PBI-wrapped CNTs are a promising material for a novel epoxy-CNT hybrid. Indeed, the PBI-wrapped CNTs (CNT/PBI) exhibited an effective reinforcement of the epoxy resin hybrid by +28.1% and +8.8% for the tensile strength and Young's modulus, respectively, which are much higher (+18.6% and −4.8% reinforcement for tensile strength and Young's modulus, respectively) than those of the hybrid using oxidized CNTs in place of PBI-wrapped CNTs. Scanning electron microscope (SEM) measurements of the fracture surfaces of CNT/PBI-epoxy hybrid revealed that only very short CNTs were observed for the CNT/PBI-epoxy hybrid due to an effective load transfer by the formation of the covalent bonds between the PBI on the CNTs and the epoxy, which showed a sharp contrast to that of the oxidized CNT-epoxy exhibiting long CNTs in the fracture surfaces due to the slippage at the interfaces [1].

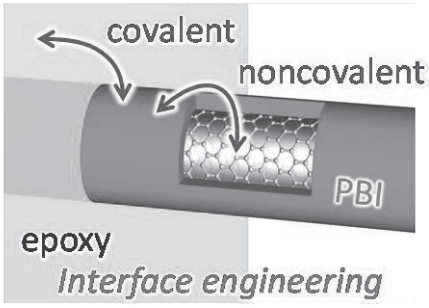

Fig.1: Schematic of interfacial engineering of CNT/PBI-epoxy composite.

[1] T. Fujigaya *et al*. submitted.

Corresponding Author: T. Fujigaya
Tel: +81-92-802-2842, Fax: +81-92-802-2842,
E-mail: fujigaya-tcm@mail.cstm.kyushu-u.ac.jp

Selective Electrochemical Reduction of CO_2 to CO with a Cobalt Chlorin Complex Adsorbed on Multi-Walled Carbon Nanotubes in Water

○Shoko Aoi[1], Kentaro Mase[1], Kei Ohkubo[1,2], Shunichi Fukuzumi[1,2]

[1] *Department of Material and Life Science, Graduate School of Engineering, Osaka University, ALCA and SENTAN, Japan Science and Technology Agency (JST), Suita, Osaka 565-0871, Japan*
[2] *Faculty of Science and Technology, Meijo University and ALCA and SENTAN, Japan Science and Technology Agency (JST), Tempaku, Nagoya, Aichi 468-8502, Japan*

Electrocatalytic two-electron reduction of CO_2 to CO has merited significant interest, because CO can be converted to liquid hydrocarbon fuels using H_2 by Fischer-Tropsch processes. There have been extensive studies on the electrocatalytic reduction of CO_2 with cobalt macrocycles. Cobalt macrocycles can also act as good electrocatalysts for selective CO_2 reduction to CO in organic solvents. In water, however, cobalt macrocycles have lacked the selectivity for CO. We report herein the selective electrocatalytic reduction of CO_2 to CO using a glassy carbon electrode modified with a cobalt(II) chlorin complex (Co^{II}(Ch), Fig. 1 (a))[1] adsorbed on multi-walled carbon nanotubes (MWCNTs) in water.[2] In addition, we have examined photocatalytic reduction of CO_2 to CO with Co^{II}(Ch) adsorbed on MWCNTs as a catalyst.

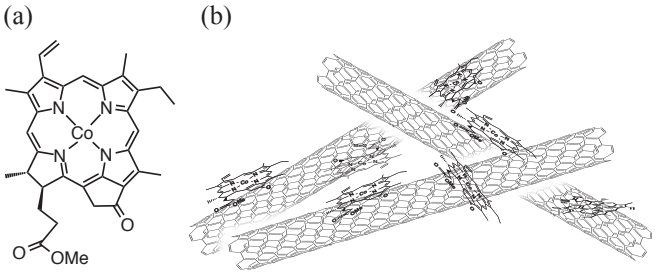

Fig. 1 (a) Structure of Co^{II}(Ch) and (b) schematic image of Co^{II}(Ch) on MWCNTs

A Co^{II}(Ch)-modified electrode was prepared by drop casting a sonicated acetonitrile (MeCN) solution containing Co^{II}(Ch) (1.0 mM), MWCNTs (1.3 mg) as a support material and 5% Nafion (12 μL) as a proton exchange membrane and stabilization agent of Co^{II}(Ch) on MWCNTs to a glassy carbon electrode. Controlled-potential electrolysis of a CO_2-saturated aqueous solution was performed and the formation of CO and H_2 was confirmed. The Faradaic efficiency at pH 4.6 was 89% for CO production under applied potential at –1.1 V *vs*. NHE with H_2 production accounting for the remaining 11%. No CO formation in the electrolysis was observed without MWCNTs or Co^{II}(Ch). An EPR spectrum of a frozen MeCN solution containing Co^{II}(Ch) on MWCNTs exhibited a signal at g = 4.203. The g = 4.203 signal is a triplet marker of two molecules of cobalt(II) complexes (S = 1/2) located close to each other. When MWCNTs were replaced by reduced graphene oxide (rGO), which is planar, as a support material of Co^{II}(Ch), the CO yield became much smaller. These results indicate that the three dimensional assembly of MWCNTs with Co^{II}(Ch) (Fig. 2 (b)) provides a suitable hydrophobic environment for binding of CO_2 instead of proton and the proximity of two Co^{II}(Ch). Such situations may not be attained by a large two-dimensional π-system such as rGO. Photoirradiation (λ > 420 nm) of a CO_2-saturated MeCN (5% water) solution containing Co^{II}(Ch) adsorbed on MWCNTs, $[Ru^{II}(Me_2phen)_3]^{2+}$ (Me_2Phen = 4,7-dimethyl-1,10-phenanthroline) as a photocatalyst and triethylamine as a sacrificial reductant resulted in CO evolution.

[1] Mase, K.; Ohkubo, K.; Fukuzumi, S. *J. Am. Chem. Soc.* **2013**, *135*, 2800.
[2] Aoi, S.; Mase, K.; Ohkubo, K. *Chem. Commun*. **2015**, *51*, 10226.
Corresponding Author: S. Fukuzumi, Tel: +81-6-6879-7369, Fax: +81-6-6879-7370
E-mail: fukuzumi@chem.eng.osaka-u.ac.jp

Enhanced Thermoelectric Properties of Single-walled Carbon Nanotubes with Ionic Liquid-Derived Polymers

○Motohiro Nakano, Yoshiyuki Nonoguchi, Takuya Nakashima, Tsuyoshi Kawai

Graduate School of Materials Science, Nara Institute of Science and Technology, Nara 630-0192, Japan

Single-walled Carbon Nanotubes (SWNTs) are low-dimensional materials exhibiting relatively high conductivity and are thus promising candidates for thermoelectric materials. In the low-dimensional materials such as SWNTs, the electric density of state (DOS) at the Fermi level becomes narrower with decrease in size and dimensionality, which leads to an enhancement in thermoelectricity. [1] In the previous study, we focused on the dispersion of SWNTs using ionic liquids (ILs) [2] to enhance their thermoelectric properties. The composite containing individually-isolated SWNTs in ionic polymers exhibited the Seebeck coefficient up to 150 μV/K, which is comparable to those of a single semiconducting SWNT. We here demonstrate the remarkable thermoelectric properties of SWNT composites with cationic polymers, providing an efficient strategy to enhance the thermoelectric power of SWNT materials.

The composites were prepared by infiltrating cationic methacrylates into SWNT buckypapers, followed by the radical polymerization for the IL-derived polymers (**PIL**s) (**Fig. 1**). The electrical conductivity was enhanced from 550 S/cm to 1100 S/cm as the loading level of **PIL**s increased to ~30 wt%. SWNT/**PIL** composites showed a 1.7-fold increase in the Seebeck coefficients compared to those of SWNT buckypapers. The unique simultaneous improvement of electrical conductivity and Seebeck coefficient led the remarkable thermoelectric power factor over 500 μW/mK^2. There was no significant change in thermoelectric properties when methanol or methanol/AIBN were added to SWNT buckypapers.

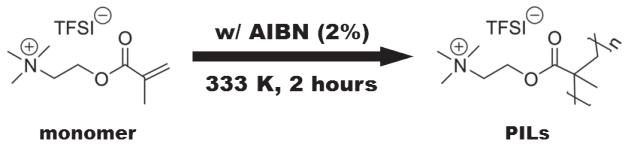

Fig. 1: Molecular structures of PILs and corresponding monomer. TFSI: bis(trifluoro methanesulfonyl) imide.

We attributed the enhancement in the Seebeck coefficient to the partial dispersion of SWNTs filled in ILs. **PIL**s can easily contact with the SWNTs surface because of a porous structure of the buckypapers. Majumdar *et al.* reported that, as a bundle became thinner, the Seebeck coefficient of the fiber became larger. [3] This previous report agreed to our results that partial SWNT exfoliation leads to an enhancement in the Seebeck coefficient of the bulk film. Another possible explanation may also arise from the appropriate insertion of organic compounds at the inter-SWNT junctions. When the diameter of SWNT bundles becomes smaller, the density of point sections between SWNTs are expected to increase, resulting in an increase in electrical conductivity. [4]

[1] N. F. Mott *et al.*, Phys. Rev. **131**, 1336 (1969).
[2] T. Aida *et al.*, Science **300**, 2072 (2003).
[3] A. Majumdar *et al.*, J. Heat Transfer. **125**, 881 (2003).
[4] K. Suemori *et al.*, Appl. Phys. Lett. **106**, 113902 (2015).

Corresponding Author: Y. Nonoguchi
Tel: +81-743-72-6028 E-mail: nonoguchi@ms.naist.jp

High performance micro-supercapacitors with carbon nanotubes and flexible components

○Fumiaki Tanaka[1], Atsuko Sekiguchi[2], Karolina U. Laszczyk[1], Kazufumi Kobashi[2], Shunsuke Sakurai[2], Don N. Futaba[2], Takeo Yamada[2], Kenji Hata[2]

[1] *Technology Research Association for Single Wall Carbon Nanotubes (TASC), Tsukuba 305-8565, Japan*
[2] *National Institute of Advanced Industrial Science and Technology, Tsukuba 305-8565, Japan*

Micro-supercapacitors are attracting increasing attention as integratable energy devices on a silicon substrate, possessing safety, long cycle lifetimes, and high power density. Recently, our group succeeded in developing high-performance micro-supercapacitors [1], where long and pure single-walled carbon nanotubes (SWCNTs), synthesized by "Super-growth" method [2], were utilized as electrodes.

Here, to broaden their potential applications (in particular, to flexible electronics), we developed a reliable and stable fabrication process for high-performance micro-supercapacitors with SWCNTs and flexible components. To achieve this, we utilized Super-growth SWCNTs as electrodes and fillers for flexible current collectors.

As shown in Fig. 1, CNT micro-supercapacitors were designed as in-plane interdigital shapes and successfully fabricated with flexible current collectors (composite of SWCNT-fluorinated elastomer) on a flexible substrate (fluorinated elastomer). The performance of our device was evaluated through typical electrochemical analyses. Owing to the high specific surface area and electrical conductivity of SWCNT network, high volumetric capacitance and energy and power densities were achieved. When comparing the energy and power densities of our device with those of previously reported flexible micro-supercapacitors [3-6], our devices revealed nearly top-level performances, keeping flexibility and outstanding mechanical durability. These results prove our device could be stably fabricated with flexible components, broadening their potential applications such as energy devices for flexible electronics.

This presentation is based on results obtained from a project commissioned by the New Energy and Industrial Technology Development Organization (NEDO).

[1] K. U. Laszczyk *et al*., Adv. Energy Mater., doi: 10.1002/aenm.201500741 (2015).
[2] K. Hata *et al*., Science **306**, 1362 (2004).
[3] M. El-Kady and R. Kaner, Nat. Commun. **4** 1475 (2013).
[4] D. Kim et al., ACS Nano **7** 7975 (2013).
[5] B. Lim *et al*., ACS Nano **8** 11639 (2014).
[6] S. Hong *et al*., ACS Nano **8** 8844 (2014).

Corresponding Author: A. Sekiguchi
Tel: +81-29-861-4611, Fax: +81-29-861-4851,
E-mail: atsuko-sekiguchi@aist.go.jp

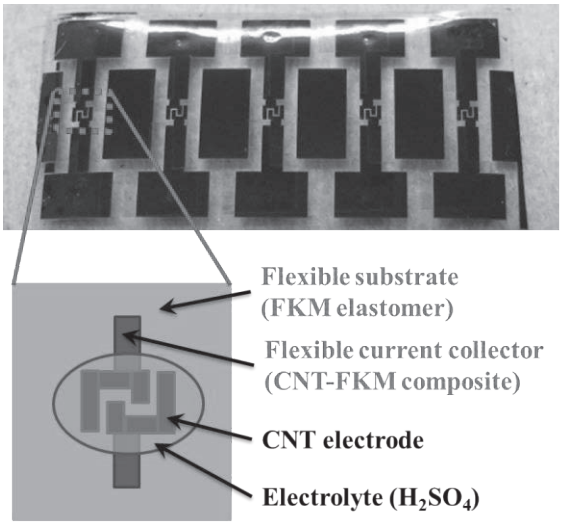

Fig. 1: Photograph and schematic illustration of CNT micro-supercapacitors with flexible components.

A durable Pt electrocatalyst with high performance based on poly(*para*-pyridine benzimidazole)-wrapped carbon nanotubes

Zehui Yang[1], Tomohiro Shiraki[1], Tsuyohiko Fujigaya[1,2] and Naotoshi Nakashima *[1,2]

[1] *Department of Applied Chemistry, Kyushu University, Fukuoka 819-0395, Japan*
[2] *WPI-I2CNER, Kyushu University, Fukuoka 819-0395, Japan*

Polymer electrolyte fuel cells (PEFCs) are considered as promising, reliable and sustainable next-generation energy source for stationary and portable power applications due to high energy conversion, high power density and zero-pollution under the operation of hydrogen as fuel in that the byproduct is water.

To make the most use of the Pt and reduce the Pt consumption, Pt is loaded on carbon supporting materials. However, the conventional electrocatalyst, CB/Pt, suffers from the low durability and performance in terms of fast carbon corrosion and Pt migration and dissolution.

Compared to the conventional CB, multi-walled carbon nanotubes (MWNTs) are recognized as a promising candidate for carbon supporting materials due to higher electrical conductivity, higher chemical stability, and lower impurities.

Here, we utilized poly[2,2'-(2,5-pyridine)-5,5'-bibenzimidazole] (*para*-PyPBI， Figure 1a) to disperse MWNTs and deposited Pt-NPs on the MWNTs/*para*-PyPBI. Based on our previous unique doping system, in which the electrocatalyst was doped with some polymer or molecular showed higher power density due to the introduction of ionomer to catalyst layer, the obtained electrocatalyst was doped with PA shown in Fig. 1b. Meanwhile, the PA-doped *para*-PyPBI membrane was utilized to identically sandwich the membrane electrode assembly (MEA) with PA-doped electrocatalyst and membrane. The durability and FC performance were investigated.

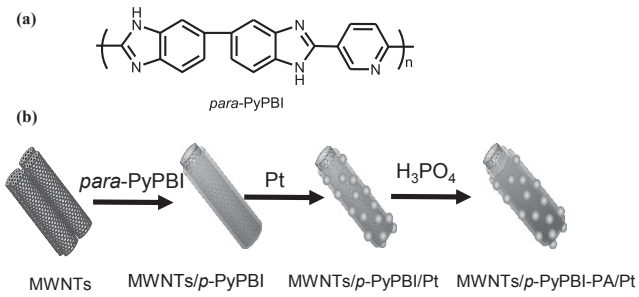

Figure 1 (a) The chemical structure of *para*-PyPBI. (b) Procedure of preparation of PA doped electrocatalyst.

As shown in Figure 2, the MWNTs/*para*-PyPBI-PA/Pt shows the highest power density of 414 mW cm^{-2}, which was ~2 times that of the non-doped electrocatalyst (208 mW cm^{-2}). Compared to our previous PBI system, the fuel cell performance was ~4-times higher due to the higher proton conductivity.

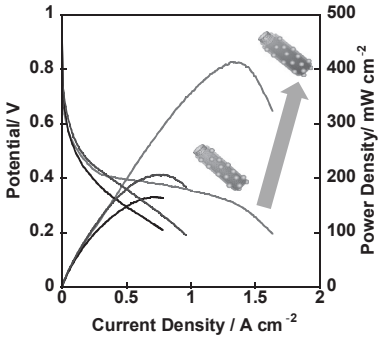

Figure 2. Polarization of I-V and power density curves of the different MEAs at 120 °C for the CB/Pt (black), MWNTs/*para*-PyPBI/Pt (blue) and MWNTs/*para*-PyPBI-PA/Pt (red).

Reference

[1] N. Nakashima et al. *J. Mater. Chem. A*, 2015, 3, 14318-14324.

Corresponding Author: N. Nakashima
Tel: 092-802-2840, Fax: 092-802-2840,
E-mail: nakashima-tcm@mail.cstm.kyushu-u.ac.jp

A very high methanol tolerant cathodic electrocatalyst for direct methanol fuel cell based on a polymer wrapped method

Zehui Yang[1], Tomohiro Shiraki[1] and Naotoshi Nakashima* [1,2]

[1] *Department of Applied Chemistry, Kyushu University, Fukuoka 819-0395, Japan*
[2] *WPI-I2CNER, Kyushu University, Fukuoka 819-0395, Japan*

Direct methanol fuel cells (DMFCs) are recognized as an ideal power source for mobile applications and have received considerable attention. One main issue affecting the efficiency and power density of the DMFCs is methanol crossover, because methanol can easily go through a Nafion membrane and be oxidized at the cathode, poisoning the electrocatalyst and degrading the FC voltage and power density; especially when a high concentration of methanol is fed to the anode side. Thus, the design of a new electrocatalyst with a methanol tolerance on the cathode side of the DMFCs is significantly required.

We here present the third trial for this issue (methanol tolerance) that shows a much higher performance than previous methods as well as an easy preparation based on a "polymer-coating" method as shown in Figure 1. We have reported that the electrocatalyst coated with PVPA showed an enhancement in its fuel cell durability and blocked methanol absorption on the active Pt nanoparticles (Pt-NPs), which are important parameters for the cathode side of the DMFC. In this study, we describe the results that after coating with a polymer, the electrocatalyst showed a very high methanol tolerance.

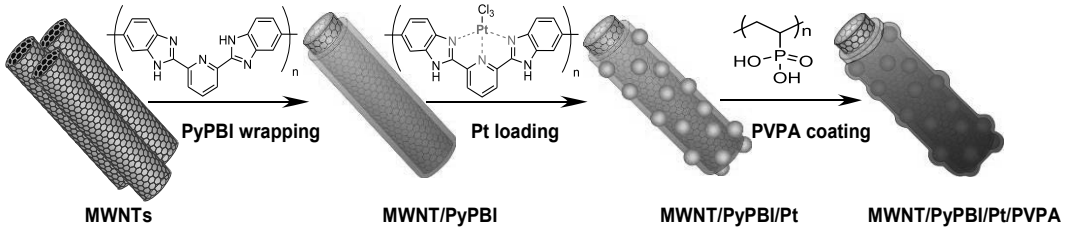

Figure 1 Schematic illustration for the preparation of the MWNT/PyPBI/Pt/PVPA.

Compared to a non-coated electrocatalyst, the polymer coated electrocatalyst showed an ~3.3 times higher oxygen reduction reaction activity compared to that of the commercial CB/Pt and methanol tolerance in the presence of methanol to the electrolyte due to a 50% decreased methanol adsorption on the Pt after coating with the PVPA.

Reference

[1] N. Nakashima et al. *Sci Rep.*, **2015**, *5*, art no. 12236.

Corresponding Author: N. Nakashima
Tel: 092-802-2840, Fax: 092-802-2840,
E-mail: nakashima-tcm@mail.cstm.kyushu-u.ac.jp

Channel length dependence of characteristic variations in carbon nanotube thin-film transistors

○Jun Hirotani[1], Shigeru Kishimoto[1], and Yutaka Ohno[1,2]

[1]*Graduate School of Engineering, Nagoya University, Nagoya 464-8603, Japan*
[2]*EcoTopia Science Institute, Nagoya University, Nagoya 464-8603, Japan*

Carbon nanotubes (CNTs) have been widely recognized as a promising material for various electron device applications because of their remarkable electrical and mechanical properties. CNT thin-film transistors (TFTs) are advantageous in simple and mass fabrication on various kinds of substrates including flexible plastic films. Therefore, CNT TFTs are promising active components for flexible and wearable devices. Though great efforts have been made to achieve medium-scale integrated circuits [1] and high-performance CNT TFTs [2], the large dispersion in their characteristics is still one of remaining issues for practical applications such as signal processing and active matrix for displays. We previously reported statistical investigation on characteristic variations for CNT TFTs with a channel length of 100 μm [3]. In this work, similar works have been carried out for devices with shorter channel length from 5 to 30 μm with the aim for obtaining higher current driving ability. Purified semiconducting single-walled CNTs were used to as the channel material. Schematic and optical micrographs of back-gate CNT TFTs fabricated on a SiO_2/Si substrate are shown in Fig. 1. More than 3000 CNT TFTs were measured to investigate statistically on-current, on/off ratio, and mobility for CNT TFTs with various channel lengths.

As the channel length decreased, the device-to-device dispersion in device characteristics increased. There were some CNT TFTs with degraded on/off ratio. This trade-off between on-current and on/off ratio was significant for short channel devices. The degradation of on/off ratio is probably due to bundled CNTs causing leakage current flowing through the inner CNTs at off-state.

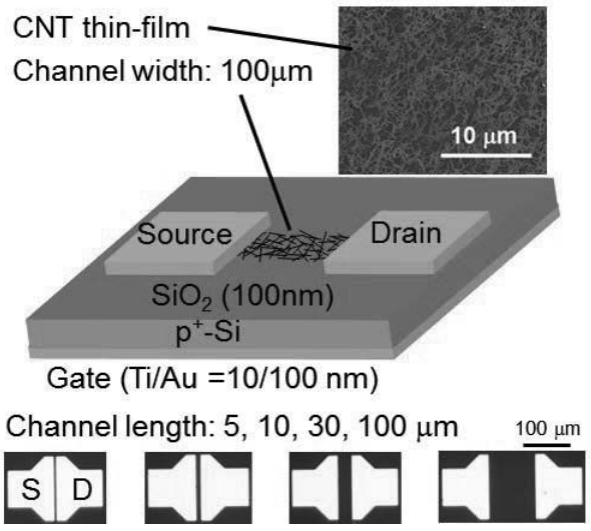

Figure. Schematic and optical images of CNT TFT and SEM image of CNT network.

Acknowledgements: The semiconducting SWNTs were provided by TASC. This work was partially supported by Grant-in-Aid by MEXT, JST/SICORP, and JST/ALCA.

[1] Q. Cao *et al*., *Nature* **454**, 495 (2008).
[2] D.-M. Sun *et al*., *Nature Nanotechnol*. **6**, 156 (2011).
[3] J. Hirotani et al., *The 48th FNTG symposium*, 3P-12

Corresponding Author: Yutaka Ohno
Tel & Fax: +81-52-789-5387, E-mail: yohno@nagoya-u.jp

Effect of Free Electron Laser Irradiation on the Chirality of In-Plane Oriented Single-Walled Carbon Nanotubes

○Daiki Kawaguchi, Keisuke Yoshida, Miu Kobayashi, Shinnosuke Harumiya, Tomoko Nagata, Nobuyuki Iwata and Hiroshi Yamamoto

College of Science & Technology, Nihon University
7-24-1 Narashinodai, Funabashi, Chiba 274-8501 Japan

Single-walled carbon nanotube (SWNT) has many advantages for application, such as high electric conductivity, high allowable current density and mechanical strength. On the other hand, SWNTs can be both metal and semiconductor, depending on their chirality. Thus the control of the chirality is required for the application. The *in-plane* orientation of the SWNTs is also essential for the electric devices. We have succeeded in obtaining all semiconductive SWNTs having random directions by irradiation of free electron laser (FEL) during growing process [1]. The irradiation of FEL may enhance the growth of SWNTs having specific bandgap, which corresponds to the photon energy of the FEL. In this presentation, we report the simultaneous control of the chirality and *in-plane* orientation.

The SWNTs were grown by alcohol catalyst chemical vapor deposition (ACCVD) method. Co/Fe nano-particles were deposited on ST-cut quartz substrate by evaporation as the catalyst. The 800 nm FEL was irradiated during growth. Figure 1(a) shows the surface image obtained by dynamic force microscopy (DFM). The SWNTs were well-aligned along the [100] direction. Figure 1(b) shows the Raman spectra of the SWNTs grown with 800 nm FEL (thick solid line) and without FEL (solid line). The observed radial breathing mode (RBM) without the FEL indicated the growth of SWNTs with the diameter of 1.07 nm (◎) and 1.59 nm (●) using 532 and 785 nm excitation laser. With 800 nm FEL irradiation, the observed RBM indicated the growth of diameter of about 1.59 nm (▲) and 1.07 nm (△) using only 785 nm excitation laser. Bandgap corresponding to the energy of FEL. The details will be reported in the poster.

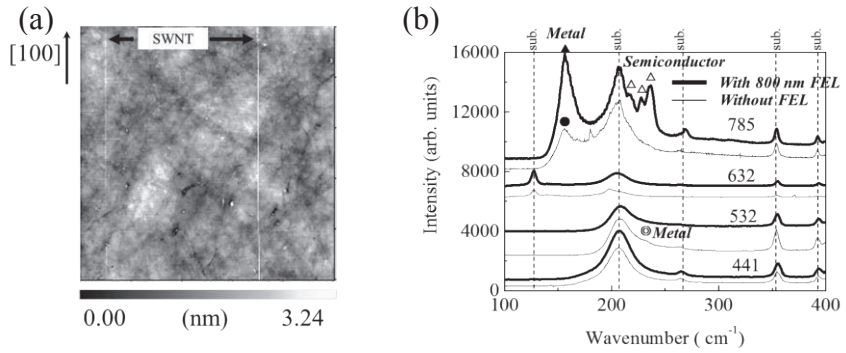

Fig. 1 (a) DFM image 5 μm× 5 μm and (b) Raman spectra. Used excitation lasers were 785 nm, 632 nm, 532 nm and 441 nm. The notation of △ and ▲ mean with FEL RBM peaks, ● and ◎ mean without FEL RBM peaks. △ symbols indicate semiconductor. ▲, ● and ◎ symbols indicate metal. Dotted line indicate substrate peaks.

[1] K. Sakai *et al.* IEICE Trans. Electron. **E94-C**, 1861 (2011)

Corresponding Author: Nobuyuki Iwata
Tel: +81-47-469-5457, Fax: +81-47-469-5457,
E-mail: iwata.nobuyuki@nihon-u.ac.jp

Single-Walled Carbon Nanotube Synthesis using $Al_2O_x/Pd/Al_2O_x$ multilayer catalyst by alcohol Gas Source Method in High Vacuum

○Hoshimitsu Kiribayashi[1], Akinari Kozawa[1], Seigo Ogawa[1], Takahiro Saida[2], Shigeya Naritsuka[1] and Takahiro Maruyama[1,2]

[1]*Department of Materials Science and Engineering, Meijo University, Aichi 468-8502, Japan*

[2]*Department of Applied Chemistry, Meijo University, Aichi 468-8502, Japan*

Single-walled carbon nanotubes (SWNTs) are anticipated to be applied to the field of electronics. For application to LSI device process, it is necessary to grow SWNTs at low temperature and under high vacuum. Previously, using Pt catalysts, we reported SWNT growth in a high vacuum, however, the yield below 700°C was not high[1]. In this study, we used Pd as a catalyst for low temperature growth.

Using rf-sputtering and electron beam depositions, $Al_2O_x/Pd/Al_2O_x$ structures were formed on SiO_2(100nm)/Si substrates. SWNT growth was carried out on them using the alcohol gas source method. The grown SWNTs were characterized by SEM, TEM, and Raman spectroscopy.

Figure 1 shows RBM region of Raman spectra for the samples which were grown at 500ºC. When the ethanol pressures were 1×10^{-4} ~ 1×10^{-3} Pa, both G band and RBM peaks were observed in Raman spectra, indicating that SWNTs grew even at low temperature. From the wavenumbers of RBM peaks, SWNT diameters were estimated to be distributed between 1.2 and 1.8 nm. Figure 2 shows a TEM image of the sample grown at 500ºC. It was found that most of Pd catalyst particle sizes were smaller than 2nm, which would lead to SWNT growth. Our results showed that SWNTs grow from Pd catalysts by optimizing the ethanol pressure during the CVD growth.

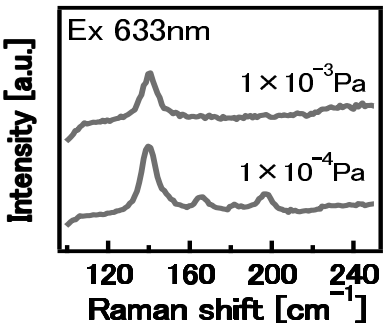

Figure 2 Raman spectra

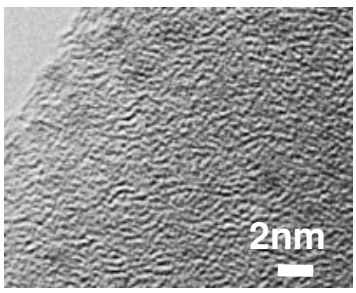

Figure 2 TEM image

[1] H. Kondo et al. J. Nanotechnol. **2012** (2012) 690304.

Corresponding Author: T. Maruyama
Tel: +81-52-838-2386, Fax: +81-52-832-1179,
E-mail: takamaru@meijo-u.ac.jp

Water-assisted burning of metallic single-walled carbon nanotubes triggered by Joule heating or field-emission electron

○Keigo Otsuka[1], Yuuki Shimomura[1], Taiki Inoue[1], Shohei Chiashi[1], Shigeo Maruyama[1,2]

[1] *Department of Mechanical Engineering, The University of Tokyo, Tokyo 113-8656, Japan*
[2] *Energy NanoEngineering Lab. National Institute of Advanced Industrial Science and Technology (AIST), Ibaraki. 305-8564, Japan*

Despite ideal properties of semiconducting (s-) single-walled carbon nanotubes (SWNTs) as channel materials of field-effect transistors (FETs), selective growth techniques have not attained a required purity of s-SWNTs. Hence, selective removal of metallic (m-) SWNTs after lattice-oriented growth is necessary to create densely-packed s-SWNT arrays for logic circuit application. We recently reported organic film-assisted electrical breakdown [1] as a tool to burn full-length of m-SWNTs, but burning length widely varied among an SWNT array, also depending on seasons. Here, we investigated the effect of water vapor pressure on the burning length, and discussed SWNT re-burning initiated by field-emission electron after nanogap formation, which resulted in half-length burning.

Horizontally-aligned SWNTs grown on crystal quartz were transferred onto SiO_2/Si substrates, followed by photolithographically-defined metal electrode deposition and PMMA thin film coating (~50 nm). A drain voltage was ramped up from 0 V until all m-SWNTs were broken, while positive gate voltage was applied. This process was performed in ambient air or oxygen saturated with water vapor (wet oxygen). Histograms of SWNT burning length (L_B) obtained in both condition (Fig. 1) indicate that SWNT burning was highly enhanced by water vapor. Therefore the burning length variation depending on the seasons and the weather can be explained as the result of humidity change of ambient air.

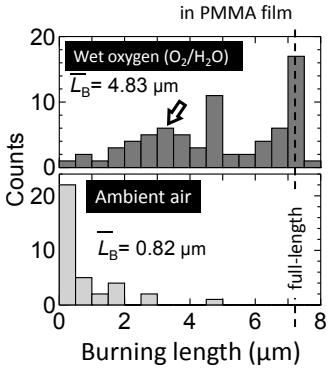

Fig.1: Histogram of SWNT burning length, performed in wet oxygen (upper) or ambient air (lower).

Focusing on a broad peak at ~3.5 μm denoted by an arrow in Fig. 1 and the fact that more SWNTs remained near cathode metal electrodes, we studied field-induced gap extension of SWNTs [2]. After SWNT gaps were fabricated by conventional electrical breakdown [3], voltage was further applied in PMMA films. Figure 2a shows applied voltage vs. gap size extended in pure oxygen or wet oxygen. While the gaps were slightly extended in pure oxygen depending on voltage, the SWNTs on anode side to the gaps were completely burned out in wet oxygen, probably ignited by field-emission electron (Fig. 2b) after first voltage application (40 V). This re-burning phenomenon from the gaps might also occur in the experiment shown in Fig. 1 and result in the broad peak at the center.

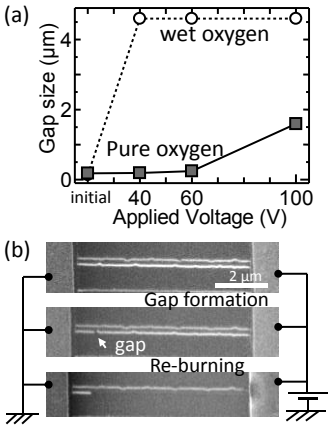

Fig. 2: (a) Applied voltage vs. gap size, performed in pure oxygen or wet oxygen. (b) SEM image of a re-burned SWNT.

[1] K. Otsuka *et al*., Nanoscale **8**, 8831 (2014).
[2] K. Otsuka *et al*., The 48th FNTG general symposium, 1P-11 (2015)
[3] P. G. Collins *et al*., Science **292**, 706 (2001).

Corresponding Author: S. Maruyama
Tel: +81-3-5841-6421, Fax: +81-3-5800-6983,
E-mail: maruyama@photon.t.u-tokyo.ac.jp

Local structure and properties of the alkali halide crystals encapsulated in single-walled carbon nanotubes studied by molecular dynamics simulations and solid-state NMR spectroscopy

○Eita Yokokura [1], Yosuke Kataoka [1] and Hironori Ogata[1,2]

[2] *Graduate School of Engineering, Hosei University, Koganei, 184-8584, Japan*
[3] *Research Center for Micro-Nano Technology, Hosei University, Koganei, 184-0003, Japan*

Single-walled carbon nanotubes (SWNTs) have a hollow space in the nanometer size that can be encapsulated various functional molecules. The confined molecular assemblies may exhibit unique low-dimensional structures and solid state properties that can not be realized in the bulk. Synthesis and structure of alkali halide encapsulated SWNTs have been reported [1-2]. However, the systematic studies of tube diameter dependence, chirality dependence and temperature dependence on the local structure and properties (ionic conductivity, melting point etc.) of alkali halides encapsulated SWNTs have not been reported. In this study, we report the effects of the diameter and chirality of SWNTs on the local structures of the encapsulated alkali halides including temperature dependence by using molecular dynamics (MD) simulations.

In the MD simulation, we used the Born-Mayer-Huggins-Tosi-Fumi intermolecular potential between the alkali halide ions and the Dreiding potential between carbon atoms in SWNT. One SWNT and any number of alkali halide ion pairs(Cs-I, K-I) around SWNT were set in a rectangular cell as initial configuration. Stable structure at 300 K was calculated with the NVT ensemble after the relaxation calculation at 1000 K. Stable structures was calculated to raise the temperature by 20 K from 300 K to 1000 K. The detailed results on the local structures of encapsulated KI or CsI crystals and the values of the melting points will be presented.

In addition, their experimental results obtained by TEM and solid-state NMR spectroscopy will be also presented.

References:

[1] J. Sloan, M.C. Novotny, *Chem. Phys. Lett.*, **329** (2000)61.
[2] M. Wilson, P.A. Madden, *J. Am. Chem. Soc.,* **123** (2001)2101.
[3] Ryosuke Senga, Hannu-Pekka Komsa, Zheng Liu, Kaori Hirose-Takai, Arkady V. Krasheninnikov and Kazu Suenaga, *Nature Materials,*13(2014)1050.

Corresponding Author: H. Ogata Tel: +81-42-387-6229, Fax: +81-42-387-6229, E-mail: hogata@hosei.ac.jp

Molecular structure of chalcogen encapsulated in single-walled carbon nanotubes studied by molecular dynamics simulations(II)

○[1]Yutaka Sato, [2]Yousuke Kataoka, and [1,2,3]Hironori Ogata

[1] Graduate School of Science and Engineering, Hosei University, Koganei 184-8584, Japan
[2]Department of Faculty of Bioscience and Applied Chemistry, Hosei University, Koganei, 184-8584, Japan
[3]Research Center for Micro-Nano Technology, Hosei University, Koganei 184-0003, Japan

Single-walled carbon nanotubes(SWNTs) have a hollow space in the nanometer size that can be encapsulated various functional molecules. Recently, sulfur and selenium encapsulated DWNTs are synthesized and one-dimensional conductive sulfur chain structure and double-helices selenium structure were reported, respectively. In this study, we report the effects of chirality and tube diameter of SWNTs on the local structure and molecular mobility of the chalcogen by using molecular dynamics(MD) simulations.

In our MD simulations using scigressVer2.6.1(Fujitsu). We applied the GEAR method of the fifth order in the numerical integration method and the speed scaling method in the temperature control method. By placing the CNT and arbitrary number of slufur atoms or selenium atoms in rectangular cell, and using NTV ensemble. First, we went the relaxation calculated at 1K. Then, the temperature was raised to 800K. Finally, the temperature was lowered to 297K, I got a stable structure.

Figure1 shows the structure of sulfur encapsulated in (a) (7,0) and (b) (6,6) carbon nanotubes at 298K. Sulfur encapsulated in SWNT shows one-dimensional linear or zig-zag chain structure depending on the tube diameter. Figure2 shows the chairal vector dependence of second-neighbor peaks of S – S pair correlation functions at room temperature. Detailed results on the encapsulated sulfer structures will be presented.

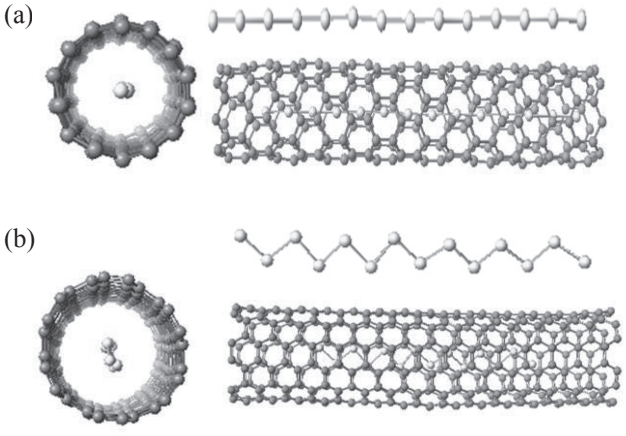

Fig.1 The structure of (a)S@(7,0)SWNT , (b)S@(6,6)SWNT.

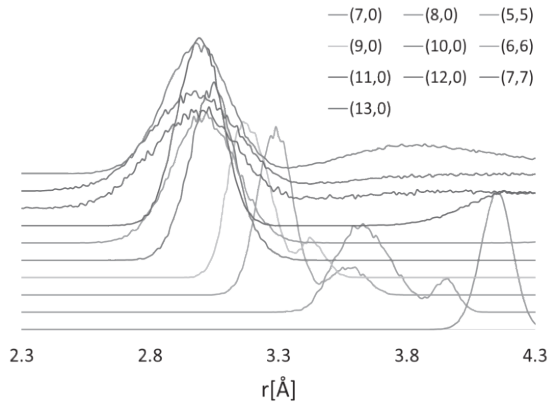

Fig.2 Chairal vector dependence of
second-neighbor peaks of S – S pair correlation functions.

[1] Toshihiko Fujimori et al. Nature Communications4(2013)2162.
[2]Frank H.Stillinger et al. J.Phys.Chem85, 6460 (1986)
[3]Frank H.Stillinger et al. J.Phys.Chem.1987, 91 (19), pp4899-4907

In situ SEM/STM observations of monolayer graphene growth on SiC (0001) wide terraces

○Chenxing Wang, Hitoshi Nakahara, Koji Asaka, and Yahachi Saito

Department of Quantum Engineering, Nagoya University, Furo-cho, Nagoya 464-8603, Japan

High quality epitaxial few layer graphene has been formed by thermal decomposition of SiC due to sublimation of Si atoms during heat treatment. However, morphology of SiC substrate surfaces after graphene growth is complicated and depends on the annealing conditions. Several divergent growth models had been proposed in previous studies [1, 2, 3], which still confused us. Especially, we noticed that a fingerlike buffer layer usually remains during monolayer graphene forming from step edges, which may prevent graphene from growing with large size on terraces. V. Borovikov et al. [3] explained such phenomenon as the result of a curvature driven mechanism for step edge stability.

In this work, in order to have a better knowledge of graphene growth processes on SiC surface, different stages of graphene growth processes on 6H-SiC (0001) on-axis substrates at various anneal conditions were observed by in situ SEM/STM. We succeed in recording the growth process of monolayer graphene from step edges without forming pits on wide terraces. Fig.1 shows SEM images of monolayer graphene growth process from step edges at the same portion of SiC surface, which was heated at 1550ºC for 90 min in 1-atm-Ar atmosphere. Graphene firstly formed from step edges uniformly (fig.1a), and then a fingerlike morphology of buffer layer remained when graphene growing to terraces (Fig. 1b). After that, fingers shrank and disappeared when the front of graphene reached next step (Fig. 1c, d). Such observations are against the description of fingerlike morphology in previous study [3]. In addition, monolayer graphene grown from the same step edge likely formed in one domain, confirmed by STM images. Fig.2 shows a high resolution STM image of monolayer graphene. Clear Moiré pattern was observed in graphene area (fig.3 insert) and no boundary was detected.

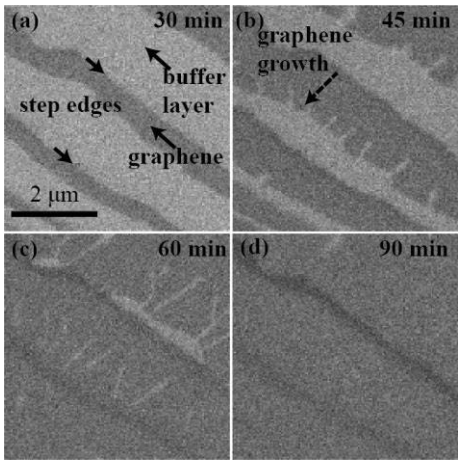

Figure 1 A series of SEM images of graphene growth at 1550℃.

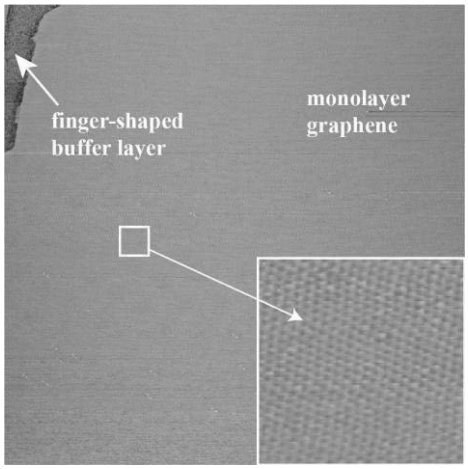

Figure 2 STM image of monolayer graphene formed from step edge (800×800 nm). The insert is an enlarged image (50×50 nm) of graphene area.

[1] P. Sutter, Nat. Mater. 8 (2009) 171-172.
[2] C. Held et al., Beilstein J. Nanotechnol. 3 (2012) 179–185.
[3] V. Borovikov et al., Phys. Rev. B 80 (2009) 121406.

Corresponding Author: Chenxing Wang
Tel: +81-52-789-4464, Fax: +81-52-789-3703,
E-mail: cx-wang@surf.nuqe.nagoya-u.ac.jp

Visualization of Grain Structure of Polycrystalline Graphene by Transition Metal Dichalcogenide

○Satoru Fukamachi,[1] Hiroko Endo,[1] Rozan Mohamad Yunus,[2]
Masaharu Tsuji,[1,2] and Hiroki Ago[1,2,3]

[1]*Institute for Materials Chemistry and Engineering, Kyushu University, Fukuoka 816-8580*
[2]*Graduate School of Engineering Sciences, Kyushu University, Fukuoka 816-8580*
[3]*PRESTO-JST, Saitama 332-0012*

Recently, large-area graphene sheets synthesized by CVD on Cu catalyst have been widely used for many practical applications. However, the CVD-grown single-layer graphene is polycrystalline with many grain boundaries (GBs), and the presence of GBs deteriorates the physical properties of graphene by reducing its carrier mobility and mechanical strength. Therefore, the visualization of the grain structure of graphene is important, and several methods, such as TEM and low-energy electron microscope (LEEM), have been used to analyze the grain structure [1,2]. However, TEM requires the graphene transfer process on a TEM grid, while LEEM can measure only on metallic substrates.

In this presentation, we demonstrate a novel method to visualize the grain structure of CVD-grown polycrystalline graphene by the post-growth of transition metal dichalcogenides. Recently, we reported the epitaxial CVD growth of MoS_2 on graphene, in which the orientation of triangular MoS_2 grains is well matched with the hexagonal lattice of underlying graphene [3]. By utilizing this relationship, we succeeded in visualizing the grain structure of polycrystalline graphene (synthesized on Cu foil) from the orientation of MoS_2 grains, as shown in Figure 1 [4]. Moreover, this method can be applied to graphene transistors fabricated on Si wafers, which revealed the multi-grain structure in the graphene channels. Furthermore, we could observe the GBs, because MoS_2 tends to nucleate along the GBs. Our finding offers a facile and transfer-free labeling technique that can be applied to various two-dimensional materials.

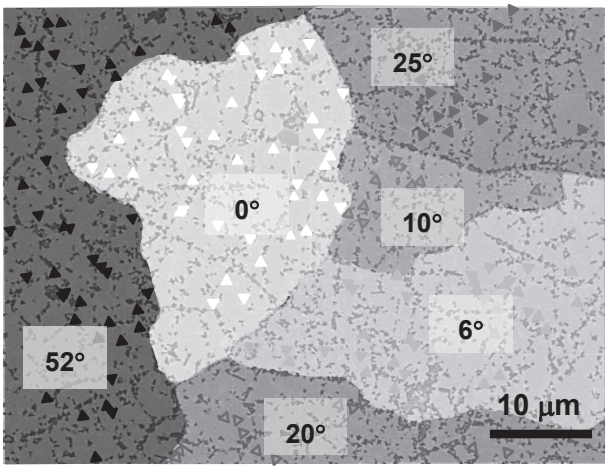

Figure 1 Grain structure of the graphene determined from the orientation of MoS_2 grains. The angles show the relative orientation with respect to the white grain.

References: [1] Huang, P. Y. *et al. Nature* **469**, 389 (2011). [2] Ogawa, Y. *et al. Nanoscale* **6**, 7288 (2012). [3] Ago, H. *et al. ACS Appl. Mater. Interfaces* **7**, 5265 (2015). [4] H. Ago et al. to be submitted.
Corresponding Author: Hiroki Ago (Tel&Fax: +81-92-583-7817, E-mail: ago@cm.kyushu-u.ac.jp)

Polymer-free transfer of CVD graphene to boron nitride substrates

○Miho Fujihara[1], Shun Ogawa[2], Ryosuke Inoue[2], Yutaka Maniwa[2], Kenji Watanabe[3], Takashi Taniguchi[3], Hisanori Shinohara[1], Yasumitsu Miyata[2,4]

[1] *Department of Chemistry, Nagoya University, Nagoya 464-8602, Japan*
[2] *Department of Physics, Tokyo Metropolitan University, Hachioji 192-0397, Japan*
[3] *National Institute for Materials Science, Tsukuba 305-0044, Japan*
[4] *JST, PRESTO, Kawaguchi, 332-0012, Japan*

Hexagonal boron nitride (hBN) has been widely used as a substrate for graphene because the carrier mobility of graphene can be drastically enhanced on hBN.[1] Usually, such graphene/hBN heterostructures are prepared by transferring graphene onto hBN flakes. For exfoliated graphene, all the processes are conducted without solution treatment, and thus, clean samples can be obtained. In contrast, for graphene grown by chemical vapor deposition (CVD), conventional transfer process requires polymer coating to support graphene during wet etching of metal substrates. However, the complete cleaning of polymer coated is quite difficult and the remaining polymer residues degrade carrier transport properties of graphene. It is, therefore, highly desired to develop a method for clean, controlled transfer of CVD graphene on hBN.

In this work, we have developed the polymer-free transfer method of CVD graphene onto hBN. CVD Graphene on Cu foil was fixed on the small hBN flakes directly, and then Cu foil was etched with iron nitride solution. Atomic force microscope observations reveal that the graphene obtained by the present method has highly clean surface compared to the samples of polymer-assisted method (Fig.1a,b). Unlike the polymer-transfer sample, the electric double layer transistors of the present samples exhibit symmetric curves and the disappearance of hysteresis in I_d-V_{gs} characteristics (Fig. 1c). These results indicate the suppression of carrier scattering and impurity levels in the polymer-free samples. The present method provides a simple and effective way to prepare clean heterostructures of graphene and other two dimensional materials.

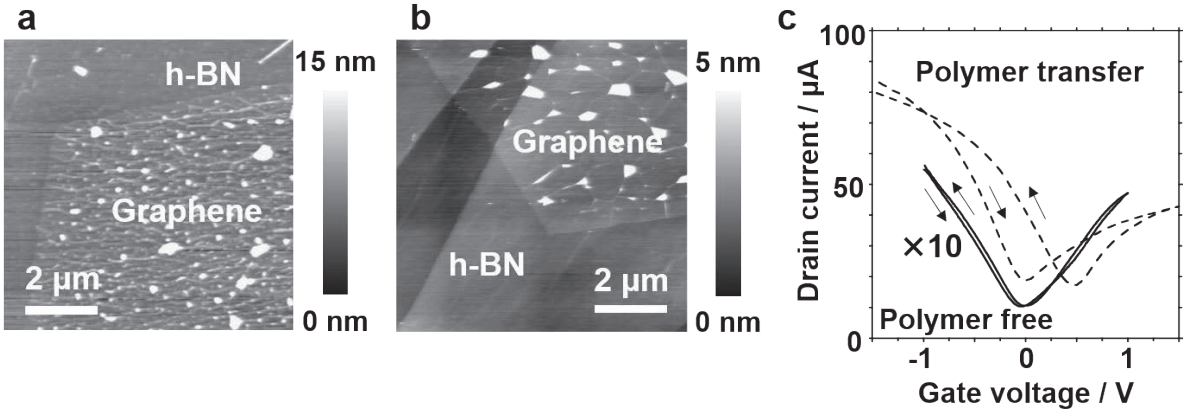

Fig.1: AFM images of graphene transferred on hBN by (a) conventional polymer-assisted method and (b) polymer-free method. (c) I_d-V_{gs} curves of the electric double layer transistors of these samples.

[1] C. R. Dean *et al*. Nat. Nanotech. **5**, 722 (2010).

Corresponding Authors: Y. Miyata, H. Shinohara

Tel:+81-42-677-2508, +81-52-789-2482, E-mail:ymiyata@tmu.ac.jp, noris@nagoya-u.jp

Study of direct growth mechanism of multi-layer graphene by precipitation method using W capping layer

○Jumpei Yamada[1], Yuki Ueda[1], Takahiro Maruyama[2], and Shigeya Naritsuka[1]

[1]Department of Materials Science and Engineering, Meijo University, Nagoya 468-8502, Japan
[2]Department of Applied Chemistry, Meijo University, Nagoya 468-8502, Japan

Because of its superior characteristics, graphene is highly expected to apply in various fields, such as electrical wiring, transparent electrodes. Graphene is usually grown by CVD method using Cu or Ni as a catalyst. However, the transfer process of the graphene makes it not suitable to the mass production of devices. Recently, a direct growth of graphene on a substrate has been often studied as an alternative method for the transfer process. We have been studying the precipitation method for forming high-quality multilayer graphene [1] and have succeeded in the direct growth of multilayer graphene using a W capping layer. In this paper, the annealing temperature and time is varied to study the mechanism of direct growth of graphene by precipitation method using W capping layer.

W(25nm) / Ni(300nm) / a-C(5nm) layers deposited on a sapphire substrate using electron-beam deposition were prepared as the samples. These were annealed by changing annealing temperature from 700 to 900 °C for 30min in vacuum. The annealing time was also varied from 1 to 60 minutes for the annealing at 900 °C.

The Raman spectra in Fig.1 show that the D peak intensity decreased with increasing the annealing temperature while no conspicuous difference was observed on the Raman spectra of various annealing time in Fig.2. The result suggests that the major part of graphene precipitated during the cooling process after the annealing. Therefore, the annealing temperature only effects the quality and the thickness of the precipitated graphene.

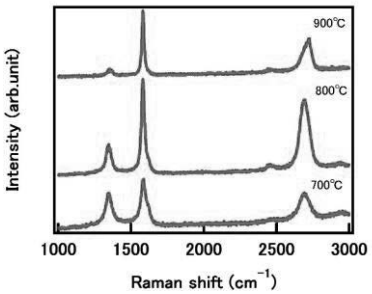

Fig.1 Raman spectra for annealing temperature dependence.

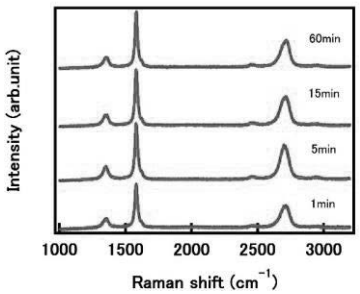

Fig.2 Raman spectrum for annealing time dependence.

Reference: [1] Jumpei Yamada et al., MRS spring Meeting & Exhibit., (2015) T14.03.

Acknowledgement: This work was supported in part by JSPS KAKENHI Grant Numbers 2660089, 15H03558, 26105002, 25000011.

Corresponding Author: J.Yamada **E-mail**:jjjjjjyyyyyy119@gmail.com

Edge-Disorder Engineering on Thermoelectric Performance of Graphene Nanoribbons: Theoretical and Computational Prediction

○Tetsumi Izawa, Kengo Takashima, Takahiro Yamamoto

Department of Electrical Engineering, Tokyo University of Science, Tokyo 125-8585, Japan

Since waste heat occupies about 66 % in total primary energy, we have increasingly paid attention to importance of waste heat. Nearly 70 % of the entire waste heat is below 200 degrees Celsius and dispersed. Large-scale equipment such as heat engines are not proper for recycling low-temperature waste heat. Thermoelectric materials can convert useless low-temperature waste heat into useful electrical energy anywhere. Thermoelectricity technology contributes to energy harvesting for achieving IoT (Internet of Things).

Existing thermoelectric materials generally consist of rare metals, are toxic and fragile. Graphene nanoribbons (GNRs), a single-layered graphene in the shape of a nanometer-width ribbon, will solve the all problems. Moreover, due to high electrical conductivity and large Seebeck coefficient, GNRs are expected to be a candidate for a new thermoelectric material. However, thermoelectric efficiency of GNRs is suppressed by high thermal conductivity. To reduce the thermal conductivity without reduction of thermoelectric power factor (PF), we have proposed to introduce edge disorder into GNRs (ED-GNRs).

In this study, we have theoretically investigated PF of sub-micrometer ED-GNRs with various concentrations of edge disorder using the non-equilibrium Green's function method combined with the Tight-Binding method.

A right figure shows ribbon-length dependence of room-temperature PF of zigzag-edged GNRs (ZGNRs) with various edge-disorder concentrations at Fermi energy. We found that PF of ED-GNRs increase in the presence of the edge-disorder compared with pristine. The maximum value of PF in 10 % edge-disorder concentration at 97 nm is almost 250 μW/(cm･K^2) that is 5 times larger than that of pristine, indicating that enough thermoelectric ability is realized by ED-GNRs. Furthermore, in 20 and 30 % edge-disorder concentrations each PF has a maximum value at a certain ribbon length. Edge-disorder concentrations give an optimum ribbon length for PF of ZGNRs. Thus, controlling edge-disorder concentrations enables us to enhance thermoelectric performance of GNRs.

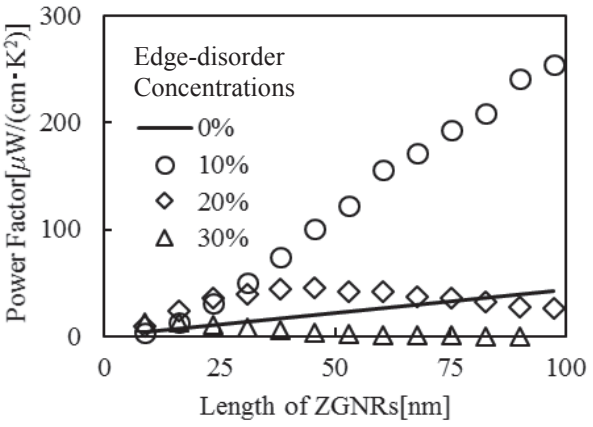

Fig. Length dependence of room-temperature PF of ZGNRs with various edge-disorder concentrations at Fermi energy

Corresponding Author: T. Yamamoto
Tel: +81-03-5876-1717, Fax: +81-03-5876-1717
E-mail: takahiro@rs.tus.ac.jp

CVD Growth of MoS_2-Graphene Nanoribbon Heterostructures and High Gain Photodetectors

○Rozan Mohamad Yunus[1], Hiroko Endo[2], Masaharu Tsuji[1,2], Hiroki Ago[1,2,3]

[1] Graduate School of Engineering Sciences, Kyushu University, Fukuoka 816-8580, Japan
[2] Institute for Materials Chemistry and Engineering, Kyushu University, Fukuoka 816-8580, Japan [3]PRESTO, Japan Science and Technology (JST), Saitama 332-0012, Japan

Heterostructures of 2D layered materials have attracted great interest due to their electronic and optical properties, which are expected by combining different types of 2D materials [1]. On the other hand, reduction of the dimensionality from 2D to 1D, such as graphene nanoribbons (GNRs), is also interesting due to the electron confinement and unique edge effects [2]. Here, we demonstrate bottom-up growth of MoS_2/GNR heterostructures by a two-step chemical vapor deposition (CVD) method. It is a unique growth process because 2D materials of MoS_2 could grow in 1D direction by following the 1D nature of our GNRs. The GNRs were first grown by ambient pressure CVD on an epitaxial Cu(100) film as reported previously [3]. After transferring on SiO_2, the GNRs were subjected to the second CVD to grow MoS_2 using MoO_3 and S powder as feedstock. The MoS_2 layer was found to grow preferentially on the surface of the GNRs, while the coverage could be further tuned by adjusting the growth conditions. Figure 1a,b shows the SEM images after the second CVD with a substrate temperature of 900 ºC for 30 min, where the dark contrast corresponds to the MoS_2 grown on the GNR. Raman spectra confirmed a single-layer MoS_2 grown on GNR, while from the comparison with the single-layer MoS_2 domains grown on sapphire, we found that the PL quenching effect by GNRs. Furthermore, the transport properties under light illumination were measured, as illustrated in Figure 1c, and high photoinduced current modulation for the heterostructures were observed upon illumination with visible light (Figure 1d). This optical response is higher than that of the heterostructure of MoS_2/graphene sheet [4]. The ability to grow a novel 1D heterostructure of layered materials by bottom-up CVD approach will open a new avenue to expand the dimensionality of the material synthesis and applications [5].

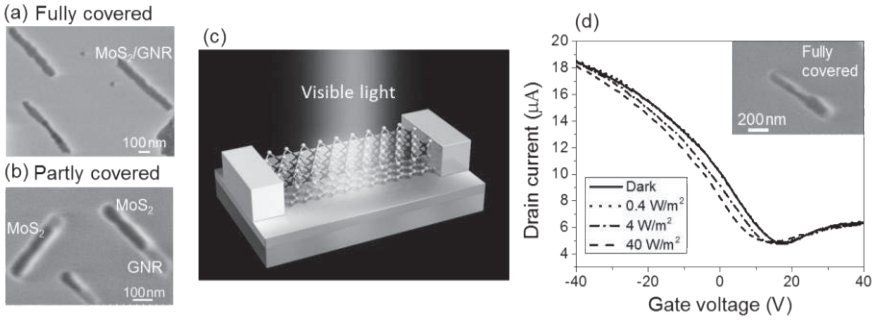

Fig 1: (a,b) SEM images of as-grown MoS_2/GNR heterostructures. (c) Schematic diagram of the FET for fully covered MoS_2 on GNR with visible light illumination. (d) Transfer curves of the fully covered MoS_2/GNR device measured in dark and under illumination with different power densities. Inset shows a SEM image of fully covered MoS_2 on GNR, which is the identical sample used to measure the transfer curve.

[1] H. Lim et al., Chem. Mater. **26,** 4891 (2014). [2] X. Li et al., Science **319,** 1229 (2008). [3] R. Mohamad Yunus et al., Chem. Mater. **26,** 5215 (2014). [4] H. Ago et al., ACS Appl. Mater. Interfaces **7,** 5265 (2015). [5] R. Mohamad Yunus et al., submitted.

Corresponding Author: Hiroki Ago (Tel & Fax: +892-583-7817, E-mail: ago@cm.kyushu-u.ac.jp)

Gate-Tunable Doping Level of Molecular Doped Graphene

○Pablo Solís-Fernández[1], Masaharu Tsuji[1], Hiroki Ago[1,2]

[1] *Institute for Materials Chemistry and Engineering, Kyushu Univ., Fukuoka 816-8580, Japan*
[2] *PRESTO, Japan Science and Technology Agency (JST), Saitama 332-0012, Japan*

Control of the charge carrier type and concentration in graphene can be attained with an applied external electric field, as in graphene field-effect transistors (FETs) [1]. However, implementation of graphene in some current technologies, such as complementary metal-oxide-semiconductor (CMOS) logic structures or optoelectronic devices, require an intrinsic and controllable doping of the graphene [2]. Here, we report the gate-tunable doping effect on graphene of absorbed piperidine (schematics of the piperidine molecule can be seen in Fig. 1a) [3].

Electric measurements showed that the doping level of graphene can be varied from an unintentional p-type to n-type, by gradually increasing the amount of adsorbed piperidine (Fig. 1a). For intermediate coverages of piperidine, the coexistence of covered and uncovered areas of graphene induces the formation of p-n junctions (dotted line in Fig. 1a). Interestingly, the doping effect of the piperidine can be further increased by the application of negative back-gate voltages, evidenced by the shift of the charge neutrality point (*CNP*) (Fig. 1b). This is attributed to the interaction between the piperidine molecules and the electric field generated by the gate, which in turn will tune the charge transfer between the piperidine and the graphene. Given the non-covalent nature of the bonding, the electronic properties of graphene result well preserved, resulting in an easy, controllable, and nonintrusive method to alter the electronic structure of graphene, which can be interesting for the fabrication of memory devices.

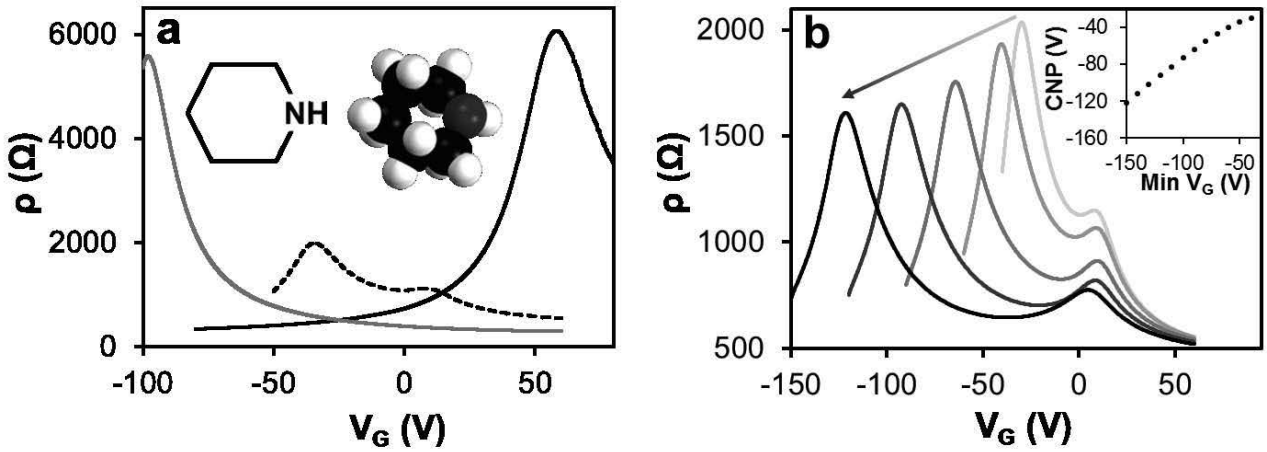

Fig.1: a) Resistance versus gate voltage of a same FET before (black), and after mild (dotted) and large (grey) exposures to piperidine. Inset shows the structure of piperidine. b) Gate-tuned doping in the graphene FET exposed to a mild dose of piperidine. Doping level increases (light gray to black curve) as the minimum applied voltage decreases. Inset shows the variation of the CNP with the minimum applied gate voltage.

[1] K.S. Novoselov *et al*., Science **306**, 666 (2004).
[2] F. Schwierz, Nat. Nanotechnol. **5**, 487 (2010).
[3] P. Solís-Fernández, M. Tsuji, H. Ago, submitted.

Corresponding Author: P. Solís Fernández and H. Ago
Tel: +81-92-583-7817, Fax: +81-92-583-7817,
E-mail: ps-fernandez@cm.kyushu-u.ac.jp, ago@cm.kyushu-u.ac.jp

Highly stable and sensitive graphene photosensor realized by thermally oxidized Au electrodes

○Shohei Ishida[1], Yuki Anno[1], Masato Takeuchi[2], Masaya Matsuoka[2], Kuniharu Takei[1], Takayuki Arie[1], Seiji Akita[1]

[1] *Department of Physics and electronics, Osaka Prefecture University*
[2] *Department of Applied Chemistry, Osaka Prefecture University*

Graphene is expected for optical sensors with ultra-wide wavelength region from ultraviolet to terahertz which originates from zero-gap band structure. Recently, we reported highly photosensitive graphene filed-effect transistor (G-FET) with the native Au oxide layer on Au electrodes [1], where stable and controlled formation of Au oxide layer is still open subject. In this study, we investigated the formation of Au oxide layer using thermal oxidation process.

Source and drain electrodes consisting of Cr/Au (5nm/30nm) were fabricated on highly doped Si substrate with a 300nm thick SiO_2 layer. The oxidation of the Au electrode was performed by annealing at 100 ^oC in O_2 (1 atm) for 4 hours. Then a monolayer graphene was transferred onto to the substrate and trimmed by using oxygen plasma etching to form an FET channel (width x length = 5 x 4 μm^2), where the graphene was synthesized using low pressure chemical vapor deposition at 1000 ^oC using Cu foil as catalyst.

Figure 1 shows transfer characteristics of the G-FET measured under dark and illumination (510nm, ~228mW/cm^2) conditions in vacuum at ~10^{-3} Pa. The shift of Dirac point (V_{Dirac}) is well suppressed in the case of the thermal oxidation of Au electrodes, where the photosensitivity appears only at $V_{GS} > V_{Dirac}$. Note that no further shift of V_{Dirac} is also observed for the repetitive measurements. The faster sweep rate of V_{GS} is favorable for the photosensitivity owing to the lower dark current. At the sweep rate of V_{GS} = 14V/s, high photoresponse of ~ 1.7 x 10^5 AW^{-1} is achieved. These results are comparable to the G-FET with native Au oxide layer on electrodes [1]. Note that the G-FET with Au oxide layer formed at 150 ^oC showed poor photosensitivity with shift of V_{Dirac}, because the Au_2O_3, which is most stable Au oxide, is dissolved higher than 150 ^oC.

Thus, the thermal oxidation process is efficient for formation of the Au oxide layer for the highly photosensitive G-FET.

Acknowledgement

This work was partially supported by JSPS KAKENHI Grant Number 25286010, by the Osaka Prefectural Government and by the Iketani Science and Technology Foundation.

Reference

[1] S. Ishida et al, submitted

Corresponding Author: S. Akita
Tel: +81-72-254-9261
E-mail:akita@pe.osakafu-u.ac.jp

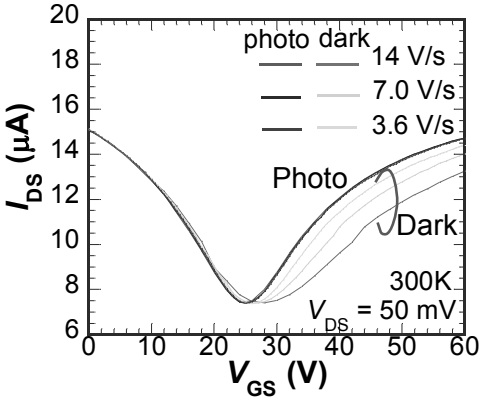

Fig.1: Transfer characteristics of the G-FET with thermally oxidized Au layer on the electrodes with various sweep rate of V_{GS}.

Evaluation of pyrene density on graphene films: toward sensor applications

○Yuji Matsui, Ryota Negishi and Yoshihiro Kobayashi
Department of Applied Physics, Osaka University, Suita 565-0871, Japan

Reduced graphene oxide (rGO) is one of promising candidates as the channel materials in field effect transistor which can be applied to highly sensitive biosensors. Pyrene functionalized by succinimidyl group is widely used as anchor molecule which links biomolecule-recognizing materials such as aptamers to the rGO surface [1]. Evaluation and control of pyrene density adsorbed on the rGO surfaces are essential issues for optimizing the sensor structures with desired sensitivity and stability. In this study, we evaluate the pyrene density adsorbed on GO and rGO using ultraviolet visible (UV) absorption spectroscopy, and find that the pyrene density is dominated by oxygen-related groups slightly remaining on the rGO surfaces, rather than restoration of π-conjugated system in graphitic structure of the rGO.

Uniform GO thin film was prepared by electrostatic adsorption of GO from its aqueous dispersion on transparent quartz substrate modified with a self-assembled monolayer. The GO film was thermally treated in inert (Ar) and reactive (ethanol) environments for reduction and structural restoration. Pyrene was adsorbed by immersing the samples in pyrene solutions with various concentrations for the time sufficient to achieve adsorption equilibrium. Pyrene density was evaluated from the UV spectra of the samples, especially focusing the absorbance at 350 nm in the spectra, which is the wavelength of a marker signal for pyrene.

Figure 1 analyzes the relation between the pyrene densities obtained from the UV spectra and the pyrene concentrations used for the sample preparation. The pyrene density can be fitted well by Langmuir isotherm (dash lines) for relatively dilute concentration range (10μM-500μM), indicating Langmuir-type monolayer adsorption. For relatively higher concentration (1mM), however, it significantly deviates from the fitting curves, suggesting gradual transfer from monolayer to multilayer adsorption. These results indicate that the pyrene density can be controlled by the concentration of pyrene solution used for sample preparation. Figure 1 also indicates that the thermal treatments drastically improve the pyrene density from that of the pristine GO. The pyrene densities are slightly affected by the temperatures of the thermal treatments, and are not virtually influenced by the environment (Ar/ethanol). As indicated by the analysis using X-ray photoelectron spectroscopy, oxygen-containing groups are efficiently removed from GO for higher temperature [2]. We have reported that the thermal treatments in ethanol lead to the remarkable restoration of graphitic structure in addition to removal of oxygen containing groups [3]. Therefore, the observed results in this study indicate that residual oxygen-related groups on the rGO after the thermal treatments dominate the pyrene density, and the restoration of π-conjugated system in rGO, which should be intuitively a dominant factor of the pyrene adsorption on rGO, has only minor effects to the pyrene density. This unexpected phenomenon suggests that pyrene molecule only interacts with very narrow area of π-conjugated system on rGO, which is hardly detectable in Raman spectroscopy.

[1] J. P. Kim et al., Biosens. Bioelectron. **24**(2009)3372.
[2] D.Yang et al., Carbon. **47**(2009)147-152
[3] R. Negishi et al., The 66th JSAP,18p-E2-11(2014).

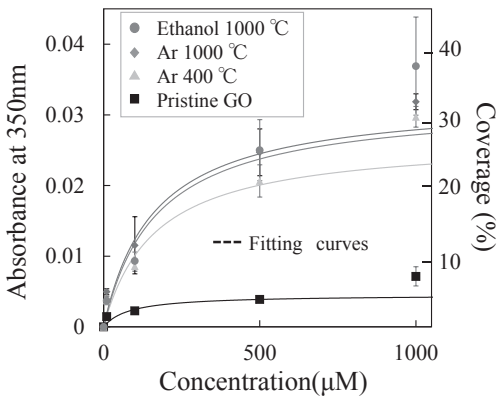

Pyrene density on GO and rGO analyzed from UV spectra of the samples prepared using pyrene solutions with various concentration.

Effects of electrodeposition conditions on the states of Pt-Ru nanoparticles on nanocarbon materials and their electrocatalytic activities for methanol oxidation(II)

○[1] Haruhiko Yoshitake , [3]Eiichi Inami, [2]Wang Zhipeng and [1,3]Hironori Ogata

[1] *Graduate School of Science and Engineering, Hosei University Koganei 184-8584, Japan*
[2] *Institute of Carbon Science and Technology, Shinshu University, Nagano 380-8553, Japan*
[3]*Research Center for Micro-Nano Technology,Hosei University,Koganei 184-0003,Japan*

Direct methanol fuel cells (DMFCs) are one of the most promising transportable power sources which can be used in mobiles, laptops, and small power generation. The basic operation principle of DMFCs involves methanol oxidation and oxygen reduction on the precious metal catalysts, which are loaded on the support surfaces. As is well-known, the dispersion of Pt-based alloys on carbon supports as well as catalyst particle size and shape plays a dominant role in the electrochemical performance for fuel cells. We have explored the electrocatalytic properties of Pt-based nanoparticles supported on the carbon materials by one-step electrodeposition. In this study, we brought in pulsed electrodeposition method and investigated the effects of the electrodeposition conditions on the shape and dispersion state and electrocatalytic properties of Pt-based nanoparticles supported on the carbon materials, i.e. single-walled carbon nanotubes(SWNTs) or highly ordered pyrolytic graphite(HOPG) or carbon nanowalls(CNWs). Figure 1 shows the one example of the CV responses of Pt nanoparticles deposited on SWNTs at pulsed electrodeposition with potentials ranging of from 0 $V_{Ag/AgCl}$ (500 msec.) to -2.0 $V_{Ag/AgCl}$(500 msec.) for 250 cycles. Table.1 summarizes the electrochemical characteristics of methanol oxidation. The detailed results on the relationship between the deposition conditions, the shape and dispersion state of Pt nanoparticles and their electrocatalytic performance for methanol oxidation will be presented.

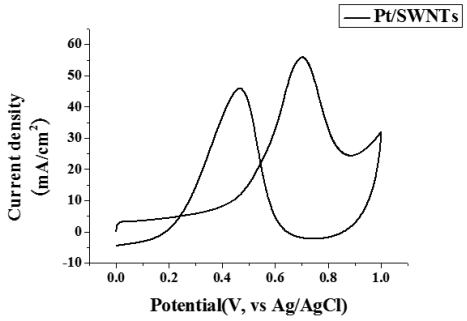

Figure 1. CV responses of Pt/SWNTs

Supported Carbon	Active area of S_{Pt} [cm^2]	J_f [mA/cm^2]	I_f/I_b	V_f [V]
SWMTs	2.30×10^3	55.8	0.78	0.697

Table 1. Electrochemical characteristics of methanol oxidation.

References:
(1)J.M.Sieben *et al., J. Appl. Electrochem.***38**(2008)483-490.
(2)Zhipeng Wang, Mao Shoji and Hironori Ogata, *Appl. Surf. Sci.***259**(2012)219-224.
(3)M.Tsai *et al., ElectroChemistry. Communication* **8**(2006)1445-1452.
(4)S.H.Ahn *et al., Chem. Eng .J. ,* (2012)**181-182** , 276-280.
Corresponding Author: Hironori Ogata,
Tel: +81-42-387-6229, Fax: +81-42-387-6229, E-mail: hogata@hosei.ac.jp

Fabrication of Graphene Nanoribbons by Unzip of Chirality-Selected Single-walled Carbon Nanotubes

○Minoru Fukumori,[1] Hirofumi Tanaka,[2,*] Takuji Ogawa[1,**]
[1]*Graduate School of Science, Osaka University, Osaka 560-0043, Japan*
[2] *Graduate School of LSSE, Kyushu Inst. Tech., Fukuoka 808-0196, Japan*

Graphene is attractive material for future nanoelectronics because of its high carrier mobility. Graphene nanoribbon (GNR) is a narrow and straight edged stripes of graphene. Electric properties of GNR depend on its width and edge structure. When the width is less than 10 nm, the GNR is semiconducting. In this work, we succeeded in fabricating GNR less than 10 nm width by applying the technique of unzipping reported by Jiao *et al.* [1] to single-walled carbon nanotube (SWNT). [2]

SWNT has variation of structure and the variation is expected to affect the ease of unzipping. Dependence of unzipping is important information to understand the unzipping process and to control GNR structure. To investigate the variation dependence, we performed experiment as described below.

A solution of (6, 5) SWNT was prepared by aqueous two-phase extraction [3]. Obtained SWNT was unzipped by annealing and sonication. Figure 1 shows an absorbance spectrum of the (6, 5) SWNT (dotted line), GNR unzipped from (6, 5) SWNT (solid line) and GNR unzipped from HiPco SWNT (dashed line). The (6, 5) SWNT shows E_{11} peak at 1020 nm (dashed arrow). After unzipping, this peak disappeared and a narrow new peak was found at 960 nm (solid arrow). The peak at shorter wavelength corresponds to narrower GNR [5]. Therefore, GNR unzipped form (6, 5) SWNT has narrower than that from HiPco SWNT and this is because the diameter of (6, 5) SWNT (0.75 nm) is smaller than that of HiPco SWNT (avg. 1.0 nm). The narrow peak implies that the distribution of width was very small and GNR from (6, 5) SWNT has single structure.

We will also report about GNRs unzipped from other chirality and the dependence of unzipping on chirality.

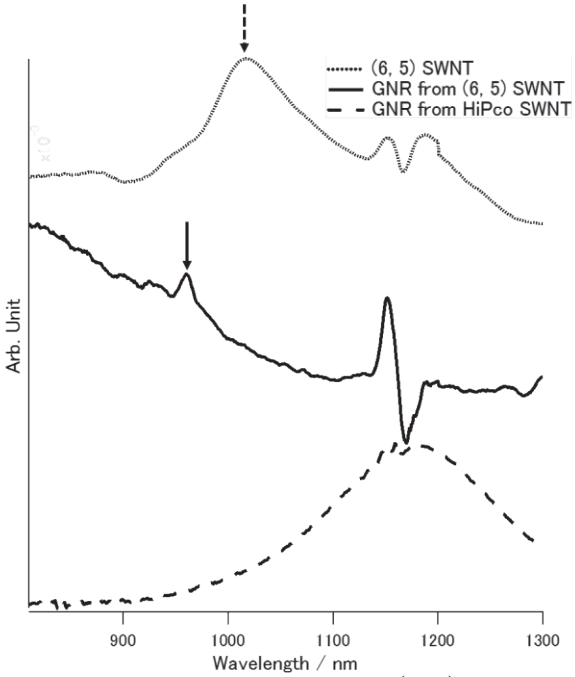

Fig. 1 Absorbance spectrum of (6, 5) SWNT (dotted line), GNR from (6, 5) SWNT (solid line), GNR from HiPco SWNT (dashed line)

[1] L. Jiao *et al.* Nat. Nanotechnol., **5**, 321 (2010).
[2] H. Tanaka *et al.* Sci. Rep., **5**, 12341 (2015).
[3] J. A. Fagan *et al.* Adv. Mater., **26**, 2800 (2014).
[4] L. Yang *et al.* Phys. Rev. B **99**, 186801 (2007)
[5] Y. Lu *et al.* J. Appl. Phys., **115,** 103701 (2014).

Corresponding Author: H. Tanaka
Tel&Fax: 093-695-6157
E-mail: *tanaka@brain.kyutech.ac.jp, ** ogawa@chem.sci.osaka-u.ac.jp

Evaluation of Electrochemical Characteristic of Graphene/Au(111) Electrode

○Koji Nakashima[1], Ryota Kumagai[1], Satoshi Yasuda[1, 2], Kei Murakoshi[1]

[1] *Department of Chemistry, Hokkaido University, Sapporo 060-0810, Japan*
[2] *JST-PRESTO, Kawaguchi, Saitama 332-0012, Japan*

Surface modification on metal electrode under electrolyte solution plays important role in tuning the electrochemical functionality and thus has been widely studied for developing novel applications such as protection of corrosion, sensing, energy storage and energy conversion systems. Graphene is one of the two dimensional materials and possesses not only high electronic conductivity, electrochemical stability but also selective proton permeability.[1] However, despite of the significant potential as surface modification material, there have been few experimental studies on electrochemical property of graphene grown on metal electrode. In this study, we investigated the first characterization of electrochemical behavior of monolayer graphene grown on Au(111) electrode. Monolayer graphene with high crystalline structure was synthesized on Au(111) single crystal by atmospheric CVD. Cyclic voltammetry measurement in 0.1M H_2SO_4 aqueous solution showed that the graphene blocks water molecule to access the underneath Au surface and result in effectively inhibition of the oxidation-reduction reactions of the Au (Fig. 1). Graphene coverage can be calculated by the reduction peak analysis and was estimated to 99.4 %. Interestingly, cathodic current with hysteresis loop resulting from hydrogen evolution reaction (HER) could be observed. It is strongly suggested that observed HER are attributed to be selective proton diffusion into the graphene/Au interface or the permeability.

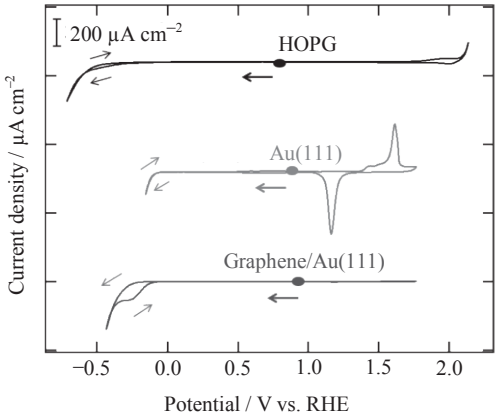

Fig.1. Cyclic voltammograms for freshly cleaved HOPG, bare Au(111) and monolayer graphene grown on Au(111) in 0.1 M aqueous H_2SO_4.

[1] S. Hu, A. K. Geim et al., *Nature*, **516**, 227 (2014).

Corresponding Author: K. Murakoshi
TEL & FAX: +81-(0)11-706-2704
E-mail: kei@sci.hokudai.ac.jp

Geometric and electronic structures of one-dimensionally polymerized coronene molecules

○Kohei Narita and Susumu Okada

Graduate School of Pure and Applied Sciences, University of Tsukuba
1-1-1 Tennodai, Tsukuba, Ibaraki 305-8571, Japan

Graphene nanoribbons (GNRs) have unique electronic properties depending on their edge shape and width. It has been pointed out that GNRs with armchair edges are metals or semiconductors depending on their width because of the discretization condition imposed on the two-dimensional energy bands of graphene. In contrast, GNRs with zigzag edges possess peculiar edge localized states known as the edge states, leading to the spin polarization near the edge atomic site. In addition, it has been pointed out that the edge roughness causes further variation in the electronic properties of GNRs. Recently, it has been experimentally demonstrated the origomerization and polymerization of coronene molecules ($C_{24}H_{12}$) inside carbon nanotubes, leading to the ultra narrow GNRs with edge roughness [1,2]. In this work, we study the geometric and electronic structures of 1D polymers of coronene molecules (Fig. 1) based on density functional theory with generalized gradient approximation.

Figure 1 shows the optimized structures of three coronene polymers with four-, five-, and six-membered intermolecular links. Among these polymers, the polymer with the six-membered link has the lowest total energy. Calculated total energies of the five- and four-membered link polymers are higher than the polymer with the six-membered link by 25 and 113 meV/atom, respectively. Thus, three structures may exist as energetically stable structure under ambient conditions once they are synthesized. Electronic structures of these polymers are semiconductors with energy gaps of 0.80, 1.54 and 0.85 eV for four-, five-, and six-membered links, respectively (Fig. 2). The four- and six-membered-link polymers possess direct band gap at the Γ point, while the five-membered link polymer possesses indirect gap between the Γ and X points.

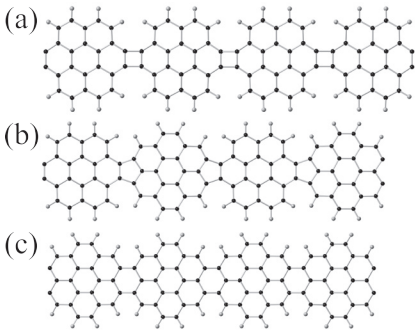

Fig. 1 Geometric structures of (a) the 4-polymer, (b) 5-polymer, and (c) 6-polymer.

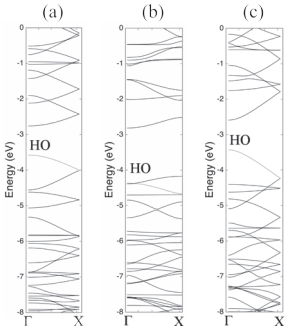

Fig. 2 Electronic structures of (a) the 4-polymer, (b) 5-polymer, and (c) 6-polymer.

[1] M. Fujihara, Y. Miyata, R. Kitaura, Y. Nishimura, C. Camacho, S. Irle, Y. Iizumi, T. Okazaki, H. Shinohara, J. Phys. Chem. C **116**, 15141 (2012).

[2] H.E. Lim, Y. Miyata, M. Fujihara, S. Okada, Z. Liu, Arifin, K. Sato, H. Omachi, R. Kitaura, S. Irle, K. Suenaga, H. Shinohara, ACS Nano, **9**, 5034 (2015).

Corresponding Author: K.− Narita
Tel: +81-29-853-5921, Fax: +81-29-853-5924,
E-mail: sokada@comas.frsc.tsukuba.ac.jp

Electronic properties of B/N-doped bilayer graphene

Yoshitaka Fujimoto[1], ○Susumu Saito[1-3]

[1]*Department of Physics, Tokyo Institute of Technology, Tokyo 152-8551, Japan*
[2]*International Research Center for Nanoscience and Quantum Physics, Tokyo Institute of Technology, Tokyo 152-8551, Japan*
[3]*Materials Research Center for Element Strategy, Tokyo Institute of Technology, Yokohama, Kanagawa 226-8503, Japan*

We study the energetics and the electronic properties of B-doped and N-doped bilayer graphene in the framework of the density functional theory [1]. As for the stacking of layers, we consider not only so-called "AB stacking" but also the "AA stacking" because the latter has been also observed experimentally [2]. In the case of the AB stacking, there are two kinds of doping sites as shown in the following figure ("AB1" and "AB2"). From the total energies obtained using the supercell calculation, it is found that the formation energy of B doping is relatively insensitive to the doping site, while that of N doping shows rather strong doping-site dependence with up to 44 meV difference.

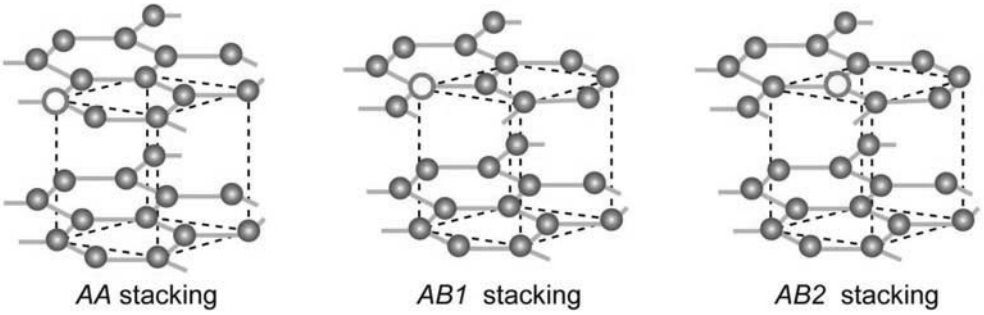

Polarities of the B-doped and N-doped systems are found to be p-type and n-type, respectively, with fully ionized dopant atoms. In addition, we report the calculated work function values for the doped systems studied. We also show the simulated STM images of the doped bilayer graphene to be used to identify them experimentally in the future.

[1] Y. Fujimoto and S. Saito, Surface Science **634**, 57 (2015).
[2] Z. Liu, K. Suenaga, P. J. F. Harris, and S. Iijima, Physical Review Letters **102**, 015501 (2009).

Corresponding Author: Y. Fujimoto
E-mail: fujimoto@stat.phys.ttiech.ac.jp
Fax: +81-3-5734-2368

Growth and characterization of single- and few-layer NbS_2 and $NbSe_2$

○Takato Hotta[1], Sihan Zhao[1], Kenji Watanabe[2], Takashi Taniguchi[2], Hisanori Shinohara[1], Ryo Kitaura[1]

[1] *Department of Chemistry, Nagoya University, Nagoya 464-8602, Japan*
[2] *National Institute for Materials Science, Tsukuba 305-0044, Japan*

Two-dimensional (2D) metal is an emerging material exhibiting unique properties. In particular, the recent research on superconductivity in 2D metals has provided great impacts and expanded the research on superconductors to various 2D materials[1,2]. Sample preparation however has been the serious bottle-neck for exploration of properties of 2D metal, which situation is in stark contrast to the well-studied 2D layered semiconductors.

We report here the successful growth of 2D metallic transition metal dichalcogenides (TMDCs), NbS_2 and $NbSe_2$, by respective chemical vapor deposition (CVD) and molecular beam epitaxy (MBE). In both methods, mono- and few-layer NbS_2 and $NbSe_2$ have been grown directly on atomically flat hexagonal boron nitride (hBN). Figure.1 shows a typical atomic force microscope (AFM) image of NbS_2 grown on hBN. As seen in the image, hexagonal and triangular NbS_2 crystals, whose lateral size is about 1~2 μm, are formed on hBN. Observed Raman spectra is layer-number dependent (Figure 2), where A_1 and E_2 modes have shown shift to the blue and red side, respectively. Figure 3 shows an AFM image of MBE-grown $NbSe_2$, whose thickness ranges from mono- to few-layer. In the presentation, in addition to further details on the growth method and structure of grown atomic layers, characterization including optical response and electronic transport will be discussed.

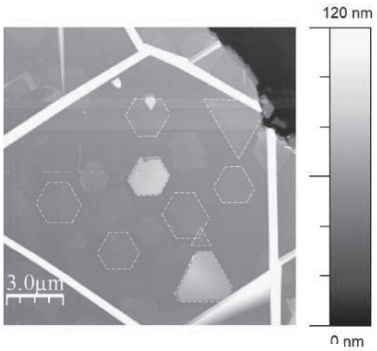

Fig. 1 An AFM image of NbS_2 grown on hBN. Dotted lines are eye-guides.

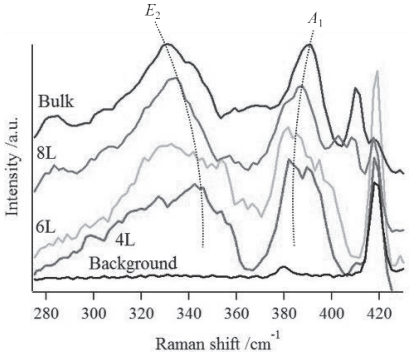

Fig. 2 Raman spectra of NbS_2 measured using excitation wavelength of 532 nm.

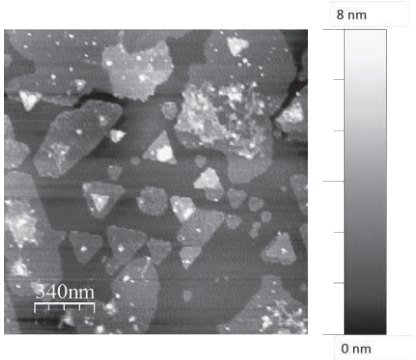

Fig. 3 An AFM image of $NbSe_2$ grown on hBN.

[1] Zhang, T. *et al.,* Nature Phys. **6,** 104-108 (2010). [2] Ge, J. *et al.*, Nature Mater. **14,** 285-289 (2015).

Corresponding Author: R.Kitaura and H.Shinohara Tel: +81-52-789-2477, Fax: +81-52-747-6442
E-mail: r.kitaura@nagoya-u.jp and noris@nagoya-u.jp

Anisotropy of optical absorption spectrum of phosphorene

○Yuki Tatsumi[1], Pourya Ayria[1], Huaihong Guo[2], Teng Yang[3], Riichiro Saito[1]

[1] *Department of Physics, Tohoku University, Sendai 980-8578, Japan*
[2] *College of Science, Liaoning Shihua University, Fushun, 113001, China*
[3] *Institute of Metal Research, CAS, Shenyang 110016, China*

Phosphorene, atomic layer of phosphorus, is a semiconducting material which has direct energy gap (~0.5eV). Owing to its characteristic structure [Fig. 1 (a)], phosphorene shows some anisotropic phenomena, such as in optical absorption[1] and electric conductivity[2]. However, the origin of the anisotropies is not interpreted clearly. In this work, we focus on the anisotropy of optical absorption of phosphorene. Our purpose of the present work is to reveal the origin of anisotropy of optical absorption and investigate which energy bands contribute to optical absorption. In order to investigate the polarization dependence of absorption of phosphorene, we perform two step calculations: (1) DFT calculation for obtaining the electronic energy bands of phosphorene, (2) Calculation of matrix elements of electron-photon interaction based on dipole approximation [3] by using the eigenfunctions of energy bands.

Figure 1 (b) shows calculated polarization dependence of absorption spectrum as incident photon energy. We can see x-y (in-plane) anisotropy around the gap energy (~0.5 eV). We can say that only y-polarization absorption can be observed around the gap energy. Such an in-plane anisotropy is in good agreement with the previous theoretical work [1]. Not only the in-plane anisotropy, we found that there is a large absorption peak at around 7 eV in the case of z- (out-of-plane) polarization. We can expect that selection rules of optical transition are associated with these anisotropic phenomena. We will show the origin of these anisotropies of phosphorene from dipole approximation approach.

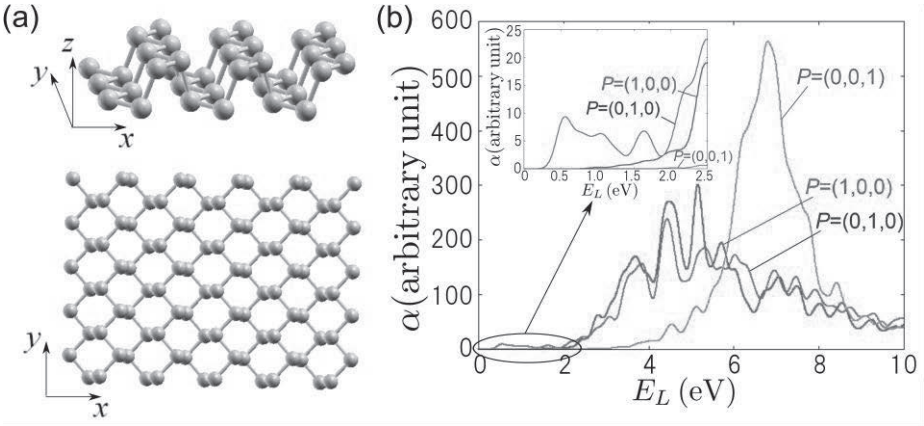

Fig.1: (a) Atomic structure of phosphorene (side view and top view). (b) Polarization dependence of absorption spectrum in phosphorene on incident photon energy.

[1] V. Tran, *et al*. Phys. Rev. B, **89**, 235319 (2014)
[2] F. Xia, *et al*. Nature Communications, **5**, 4458 (2014)
[3] A. Jorio, *et al*. *Raman Spectroscopy in Graphene Related Systems*, Wiley (2011)

Corresponding Author: Yuki Tatsumi
Tel: +81-22-795-6442, Fax: +81-22-795-6447,
E-mail: tatsumi@flex.phys.tohoku.ac.jp

Synthesis and characterization of $Mo_{1-x}Re_xS_2/MoS_2$ heterostructures

°Shohei Mori[1], Yutaka Maniwa[1], Yasumitsu Miyata[1,2]
[1]*Department of Physics, Tokyo Metropolitan University, Hachioji, 192-0397, Japan*
[2] *JST, PRESTO, Kawaguchi, 332-0012, Japan*

The heterostructures of two-dimensional semiconductors have attracted much attention for their potential applications in electronics and optoelectronic. Recently, several groups including ours have reported the vapor-phase growth of lateral and stacked heterostructures based on transition metal dichalcogenides (TMDCs) such as MoS_2, WS_2, and $Mo_{1-x}W_xS_2$ alloys [1-5]. In particular, the $Mo_{1-x}W_xS_2$ alloys have composition-dependent tunable bandgaps and could be useful for the fine tuning of electronic properties. In addition to the bandgap modulation, the control of carrier density is also one of the most important issue to be solved. In this study, we have focused our attention on the alloying of rhenium (Re) and molybdenum (Mo) for the carrier control of TMDC-based heterostructures.

$Mo_{1-x}Re_xS_2$ alloys were formed on sapphire substrates by chemical vapor deposition (CVD) method of sulfur, molybdenum oxide, and rhenium oxide. For the preparation of heterostructures, MoS_2 monolayers were firstly grown on a sapphire substrate, and then, $Mo_{1-x}Re_xS_2$ alloys were grown on the same substrate by two step CVD process. The formation of $Mo_{1-x}Re_xS_2$ alloys is probed through the changes in Raman spectra (Fig. 1a). For the heterostructures, atomic force microscope (AFM) observations (Fig. 1b,c) show the growth of monolayer $Mo_{1-x}Re_xS_2$ on monolayer MoS_2. In the presentation, we will report on the details of growth and properties of $Mo_{1-x}Re_xS_2$-based heterostructures.

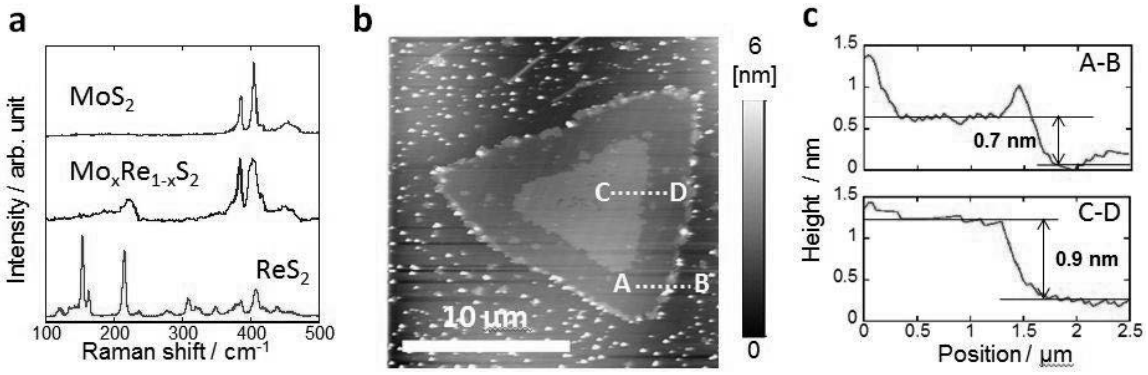

Fig.1 (a) Raman spectra of MoS_2, $Mo_xRe_{1-x}S_2$, and ReS_2 atomic layers. (b) AFM image and (c) height profiles of the $Mo_{1-x}Re_xS_2/MoS_2$ heterostructure.

[1] Y. Gong, *et al*., Nat. Mater. 13, 1135 (2014)., [2] X. Duan, *et al*., Nat. Nanotechnol, 9, 1024 (2014).,
[3] C. Huang, *et al.,* Nat. Mater. 13, 1096 (2014). [4] Y. Kobayashi, S. Mori, *et al*., Nano Res. in press,
[5] S. Mori, *et al.,* The 48th FNTG symposium.

Corresponding Author: Y. Miyata, Tel: +81-42-677-2508, E-mail: ymiyata@tmu.ac.jp

Exploring transport property of MoS_2 field effect transistor by scanning gate microscopy

○Masahiro Matsunaga[1], Ayaka Higuchi[1], Guanchen He[2], Jonathan P. Bird[2], Yuichi Ochiai[1] and Nobuyuki Aoki[1, 3]

[1] *Graduate School of Advanced Integration Science, Chiba University, Chiba 263-8522, Japan*
[2] *Department of Electrical Engineering, University at Buffalo, SUNY, Buffalo, New York 14260-1920, USA*
[3] *JST-PRESTO, Kawaguchi, Saitama 332-0012, Japan*

Scanning gate microscopy (SGM) is a category of scanning probe microscope techniques. SGM can explore local transport properties in semiconducting materials using a metallic coated cantilever as a mobile top gate [1]. Recently, transition metal dichalcogenides (TMDCs) have received remarkable attention as new 2d materials [2]. Molybdenum disulfide (MoS_2) is a typical example of TMDCs group.

In this report, we investigate local gate response within MoS_2 field effect transistor (FET) by SGM. The MoS_2 was directly grown on SiO_2 (285 nm)/Si substrate by chemical vapor deposition, supplied by the Ajayan group at Rice University [3]. Source-drain electrodes (Cr/Au) were deposited using electron beam lithography. Atomic force microscope (AFM) image of channel region within the FET is shown in Fig. 1 (a). After fabricating the FET, the SGM observation was performed at atmospheric conditions.

The SGM images were obtained at different tip voltages. Clear responses were observed at the edge between the grounded electrode and MoS_2 (Fig. 1 (b)). The peak height of responses vary according to the n-type characteristic at different tip voltages as shown in Fig. 2. These results indicate that the responses are attribute to control of Schottky barrier at the injection side, and the transport property of this MoS_2 FET is suffered by this effect.

The work was partially supported by KAKENHI Grant Number 26600009.

[1] X. Wei *et al*., Jpn. J. Appl. Phys. **51**, 04DN05 (2012).
[2] B. Radisavljevic *et al*., Nature Nanotech. **6**, 147 (2011).
[3] Y. Zhan *et al*., Small **8**, 966-971 (2012).

Corresponding Author: N. Aoki
Tel: +81-43-290-3430, Fax: +81-43-290-3427
E-mail: n-aoki@faculty.chiba-u.jp

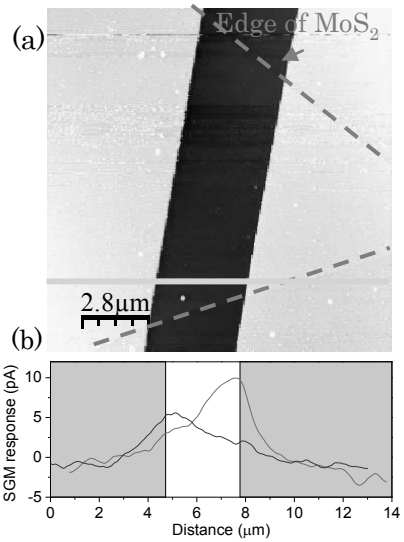

Fig.1 (a) AFM image of the MoS_2 FET. The broken lines correspond to the edges of the MoS_2 crystal. (b) Line profiles of SGM images along solid line in (a). Two curves are obtained at the different bias polarities. Shaded regions correspond to the electrodes.

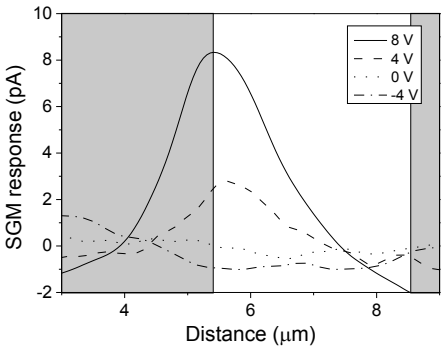

Fig. 2 Line profiles of SGM responses along the solid line in Fig. 1 (a) at different tip voltages. Shaded regions correspond to the electrodes.

発表索引
Author Index

Author Index

Bold number: Speaker

2015 年 9 月 7 日発行

第 49 回フラーレン・ナノチューブ・グラフェン総合シンポジウム
講演要旨集

＜フラーレン・ナノチューブ・グラフェン学会＞
〒113-8656 東京都文京区本郷 7-3-1
東京大学大学院工学系研究科　機械工学専攻
丸山研究室内
Tel：03-3830-4848
Fax：03-3830-4848
E-mail：fntg@photon.t.u-tokyo.ac.jp
URL：http://fullerene-jp.org
印刷　/　製本　門司印刷（株）

ALDRICH®
Materials Science

カーボンナノ材料新製品

蛍光ナノダイヤモンド

○ >1200NV/particle, 120 nm avg. part. size, 1 mg/mL in deionized water その他、>800, 500, 400, 300NV/particle 計 5 種	**798088-5ML**	**¥41,600**

グラフェン 分散液（グラフェン インク）

with ethyl cellulose in terpineol

○ スクリーン印刷用	**798983-10ML**	**¥64,000**
○ インクジェット印刷用	**793663-5ML**	**¥28,000**
○ グラビア印刷用	**796115-10ML**	**¥66,800**

酸化グラフェン

○ single layer sheet, 2 mg/mL, dispersion in H_2O	**795534-50ML**	**¥17,600**
	795534-200ML	**¥53,400**
○ 15-20 sheets, 4-10% edge-oxidized, 1 mg/mL, dispersion in H_2O	**794341-50ML**	**¥17,600**
	794341-200ML	**¥48,400**
○ powder, 15-20 sheets, 4-10% edge-oxidized	**796034-1G**	**¥16,700**

単層グラフェン フィルム

○ 1 in x 1 in on copper foil	**799009-1EA**	**¥25,000**
○ TEM グリッド (Quantifoil gold) , 膜厚 : 0.345nm	**798177-1PK**	**¥49,900**

グラフェン ナノプレート

○ 1 mg/mL, dispersion in H_2O	**799092-50ML**	**¥40,000**

カーボンナノチップス

○ Heat treated platelet graphite nanofibers	**799017-500MG**	**¥20,000**

カーボンナノホーン　近日発売予定！ NEW!

○ Carbon Nanohorns, As-grown	**804118-250MG**	価格未定
○ Carbon Nanohorns, Oxidized	**804126-250MG**	価格未定

www.aldrich.com/nano-jp

SIGMA-ALDRICH®

シグマ アルドリッチ ジャパン

〒140-0002　東京都品川区東品川2-2-24
天王洲セントラルタワー4階

■製品に関するお問い合わせは、弊社テクニカルサポートへ
TEL ： 03-5796-7330　FAX ： 03-5796-7335
E-mail ： sialjpts@sial.com

■在庫照会・ご注文方法に関するお問い合わせは、弊社カスタマーサービスへ
TEL ： 03-5796-7320　FAX ： 03-5796-7325
E-mail ： sialjpcs@sial.com

http://www.sigma-aldrich.com/japan

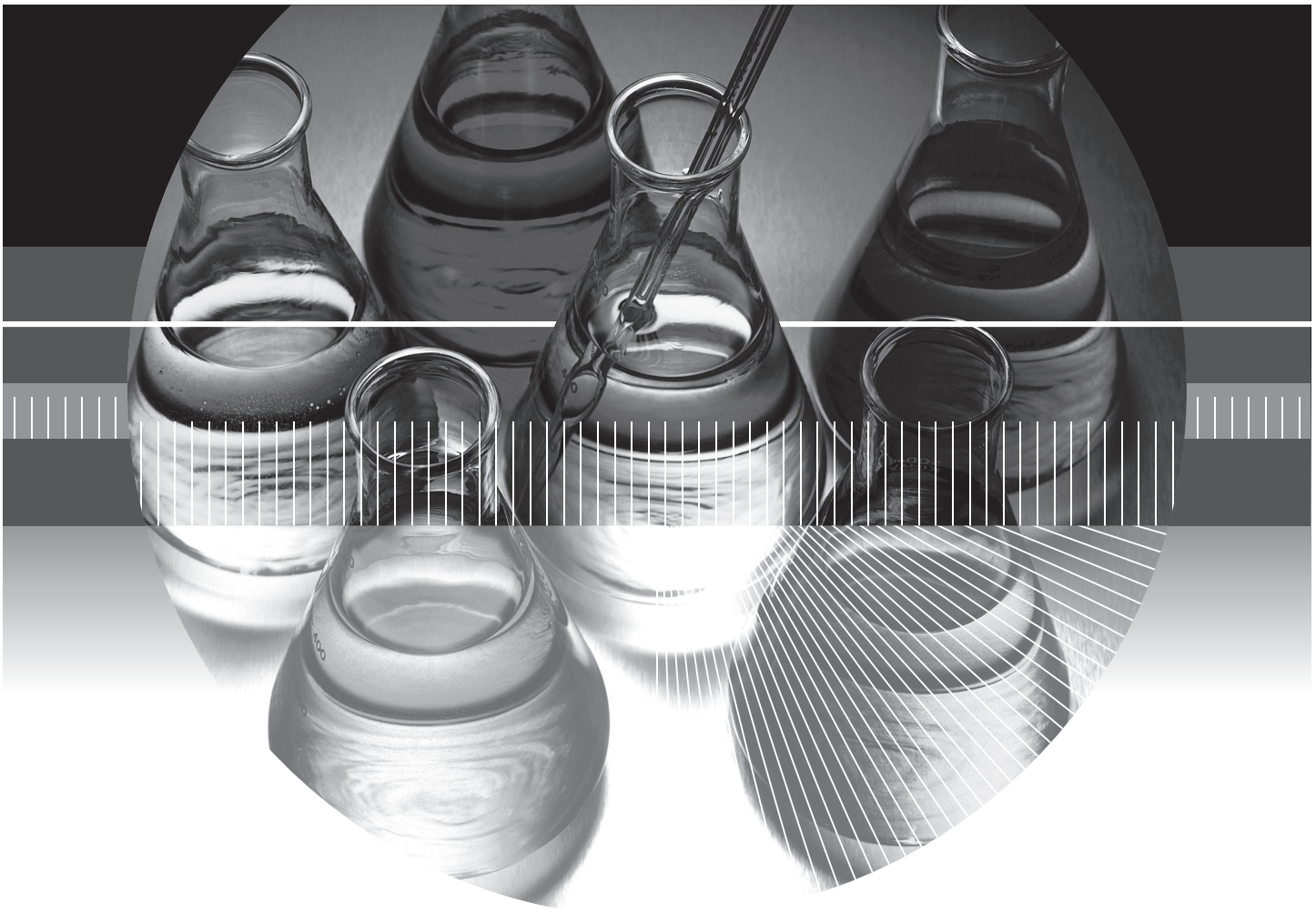

Think Perfection

お客様にとっての"パーフェクト"をめざして、正晃は常にユーザーの視点で考えています。

大学や官公立試験所、研究所をはじめ、各企業の研究に不可欠な試薬とそれに関連する最新の情報をタイムリーに提供しています。

病院臨床検査室や検査センターなどに、豊富な専門知識をベースに、最適な診断薬を最新の情報・技術とともに提供しています。

大学・官公庁・企業の試験研究機関へ国内外一流メーカーの最先端機器の販売と関連情報の提供およびメンテナンスを行っています。

高度化が進む医療現場に、診断に必要とされる各種検査機器と治療用機器などを専門的にサポート。また医療消耗品も提供しています。

大学・企業などの研究機関、病院・検査センターなどの医療機関での検体採取から保存までに必要な器材を扱っています。

産業や生活の幅広い分野で必要とされる化学工業製品や食品添加物およびIC生産に欠かせない洗浄剤・電子材料などを扱っています。

医療や研究分野向けに画像診断・データベースソフトや検査業務支援システムなどを開発・提供し、最先端の研究を支援しています。

「健康管理時代」のニーズに応えて、一般向けにオリジナルのフコイダン製品などの健康食品を開発・販売しています。

OA、AV機器、テレビや冷蔵庫からパソコン、デジカメなど、さまざまな一流メーカーの製品を取り扱っています。

ライフサイエンスをはじめとする科学技術は
私たちの生活と未来を大きくリードし続けています。
正晃は、医療・研究分野の総合商社として培ったノウハウを
お客様にとっての"パーフェクト"を起点に
多彩な分野へ柔軟な対応で貢献いたします。

正晃株式会社

www.seikonet.co.jp

本　社　福岡市東区松島3丁目34番33号
〒813-0062
TEL：092-621-8199(代)
FAX：092-611-4415

事業所　福岡第一　福岡第二　北九州
久留米　大　分　佐　賀
山　口　下　関　熊　本
沖　縄　宮　崎　鹿児島
東　京　長　崎　広　域

JEOL
Solutions for Innovation

GRAND ARM

Atomic Resolution electron Microscope

JEM-ARM300F

JEM-ARM300Fは、JEM-ARM200Fで培った高安定化技術を基に開発された装置です。
冷陰極電界放出電子銃を標準搭載し、STEMおよびTEMに球面収差補正装置が
搭載可能な最高加速電圧300 kVの世界最高峰の超高分解能電子顕微鏡です。

300 kV STEM Imaging（GaN[211]）
暗視野像　Ga-Ga 原子カラム

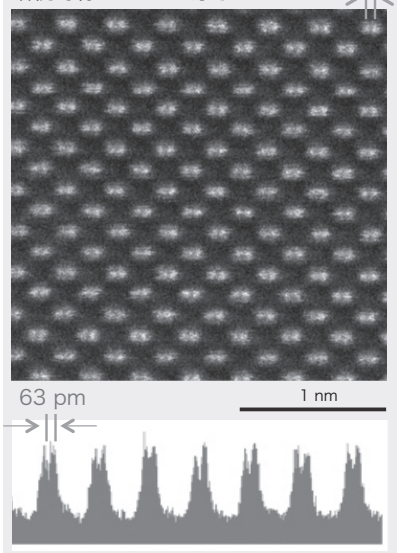

80 kV TEM Imaging（グラフェン）

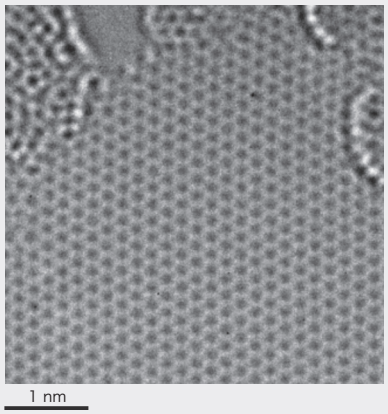

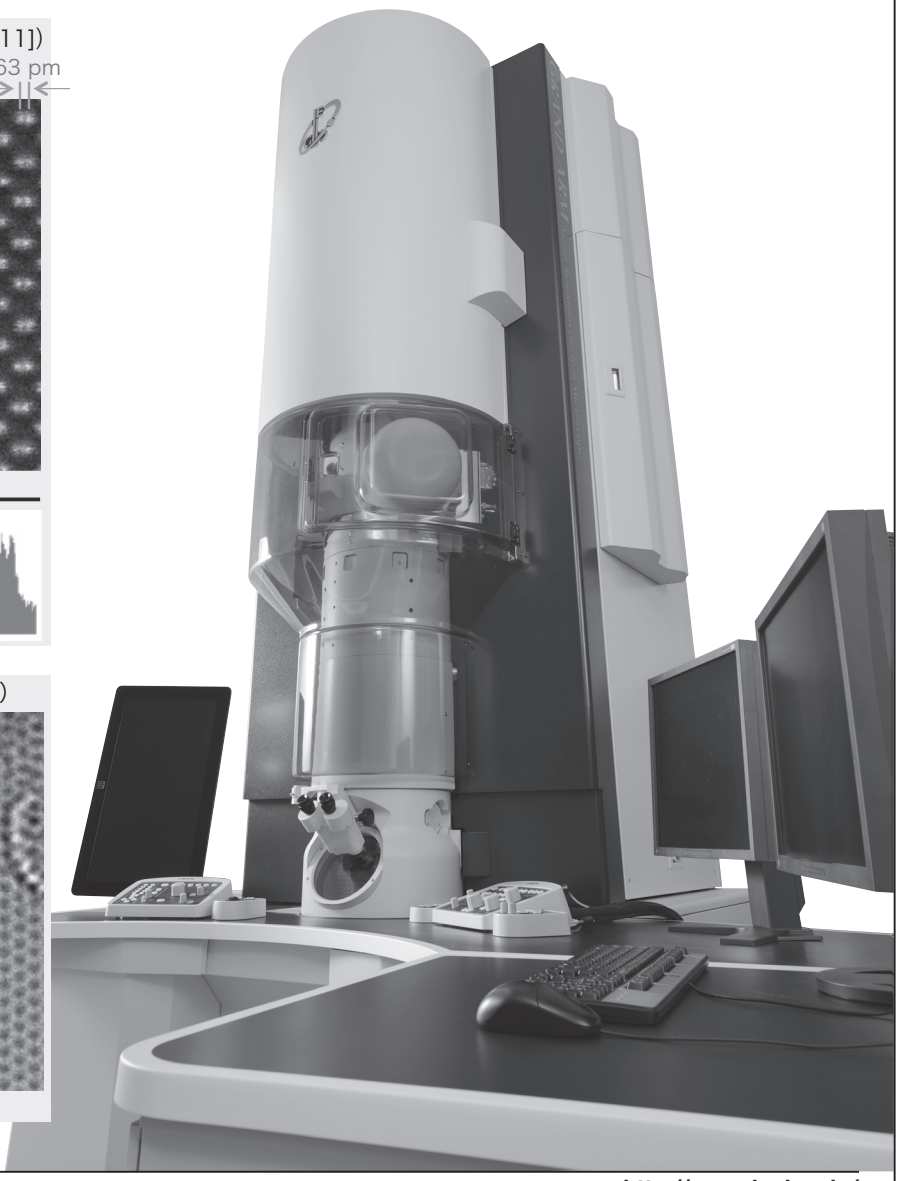

日本電子株式会社　本社・昭島製作所　東京都昭島市武蔵野3-1-2　TEL(042)543-1111　http://www.jeol.co.jp/
営業企画室　東京都千代田区大手町2-1-1　TEL(03)6262-3560 | 西日本ソリューションセンター　大阪市淀川区西中島5-14-5　TEL(06)6305-0121

■東　京　電子光学機器営業グループ　TEL(03)6262-3581 | 分析機器営業グループ　TEL(03)6262-3582 | 産業機器営業部　TEL(03)6262-3570
半導体機器営業部　TEL(042)528-3491 | 医用機器営業グループ　TEL(03)6262-3583

■札　幌　TEL(011)726-9680 | ■仙　台　TEL(022)222-3324 | ■筑　波　TEL(029)856-3220 | ■横　浜　TEL(045)474-2181 | ■名古屋　TEL(052)581-1406
■大　阪　TEL(06)6304-3941 | ■広　島　TEL(082)221-2500 | ■高　松　TEL(087)821-0053 | ■福　岡　TEL(092)411-2381

Single-walled Carbon Nanotube

単層カーボンナノチューブ

MEIJO eDIPS は国立研究開発法人産業技術総合研究所との共同研究による量産型高品質単層カーボンナノチューブ（SWNT）。不純物カーボンや欠陥が少なく高純度であり、結晶性が高い。直径分布が異なる３種類のSWNTを提供している。

MEIJO eDIPS

製品概要

■EC2.0

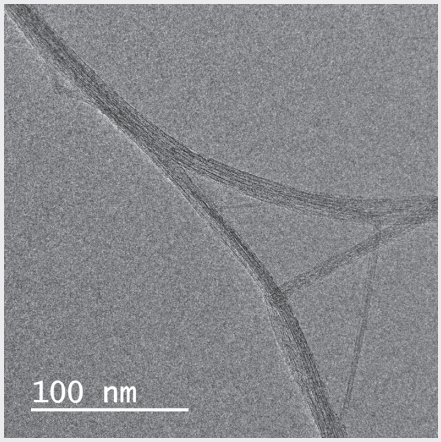

■×30 万倍 TEM(透過型電子顕微鏡) 写真

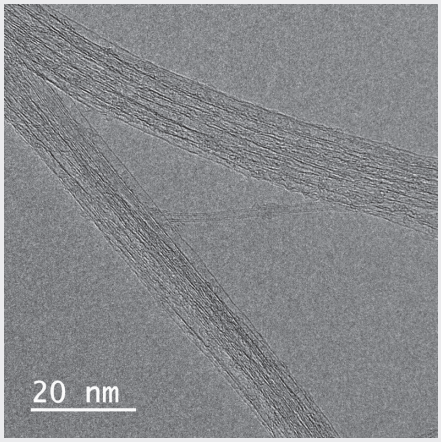

■×100 万倍 TEM(透過型電子顕微鏡) 写真

基本性能

品番	EC1.0	EC1.5	EC2.0
形状	綿状	綿状	綿状
製法	eDIPS 法	eDIPS 法	eDIPS 法
炭素純度	＞90%	＞90%	＞90%
直径	1±0.8nm	1.5±0.8nm	2±0.8nm

※値は保証値ではなく代表値

物性

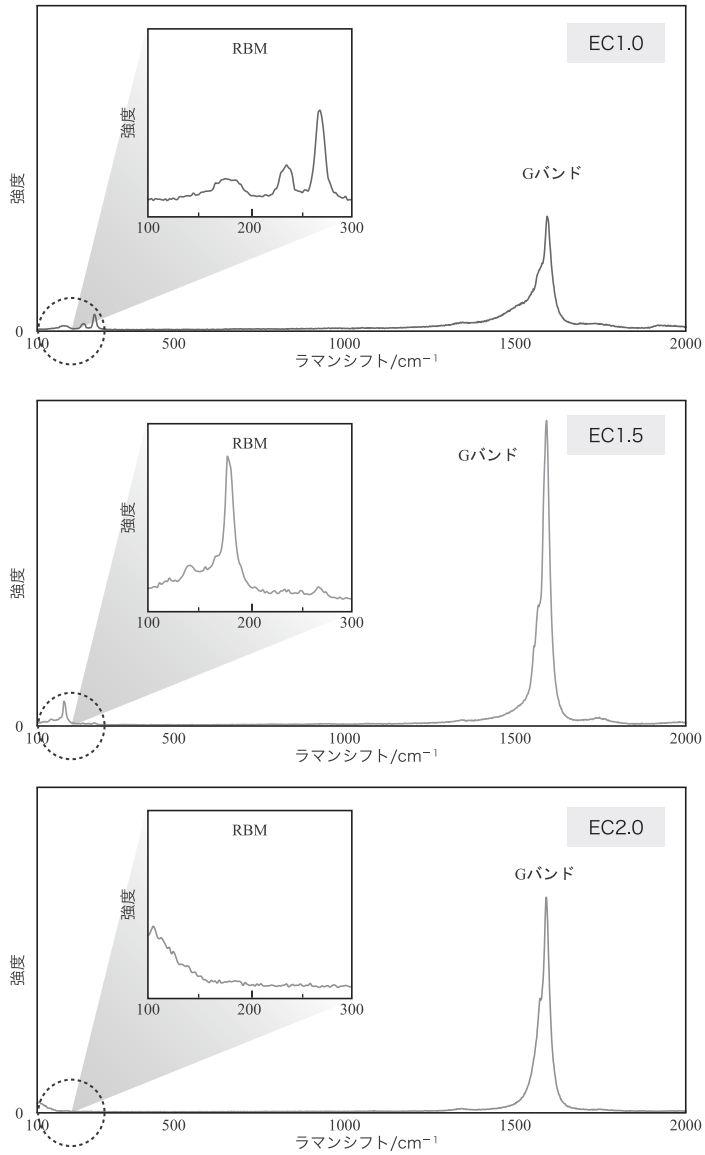

■ラマン分光（レーザー波長 532nm）上から EC1.0、EC1.5、EC2.0

株式会社 名城ナノカーボン　Web: www.meijo-nano.com　Tel: 052-736-2322　Fax: 052-736-5222

JASCO Corporation

Real Standard NRS series

レーザラマンの新たな時代

ラマン分光法は、赤外分光法と同じ振動スペクトル測定法ですが、サンプリングが赤外分光法に比べ容易で、赤外顕微鏡では不可能な微小部位の測定が可能などの特長がある反面、最適測定条件の検討や装置の光学調整等に、ある程度のスキルが要求されていました。NRS-5000/7000 シリーズは、顕微レーザラマン分光光度計に要求される性能・機能を網羅し、システムの制御や光学調整等を自動化することにより、精度の高いデータを安定して取得することができます。波数とラマン強度の自動補正、測定に関するアドバイス機能を搭載し、さらに高速イメージングへの拡張性も備えています

グラフェンの 2D イメージング

ラマン分光法により、2D/G バンド比にてグラフェンの層数を可視化できます。

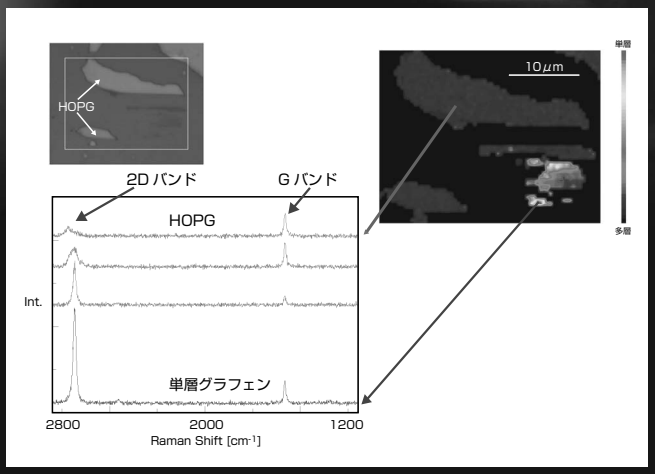

レーザラマン分光光度計／ Laser Raman Spectrometer

NRS-5000/7000series

NRS-5000series (5100/5200)
多彩なアプリケーションに対応した焦点距離300mmの高性能モノクロメータを採用し、グレーティングを最大3枚まで搭載できます。低波数測定ユニットを搭載したNRS-5200は、10cm^{-1}の低波数領域まで測定できます。

NRS-5000/7000series の特長

- 異物分析から構造解析まで幅広く対応
- スペクトルクオリティにこだわったハイエンドモデル
- 新世代 SPRIntSイメージングにより高速イメージング＆3D イメージング
- 1064nm レーザ＋InGaAs 検出器対応（デュアル検出器にも対応）
- 新機能 DSF（Dual Spatial Filtration）で空間分解能がさらにアップ
- 段違いの操作性、顕微スペクトル測定プログラム
- 1 クリックで蛍光除去、自動蛍光補正
- 誰でも楽々ラマン測定、ユーザーアドバイス機能＆フルオートシステム
- 容易に成分分析ができるイメージングモデル解析プログラム（オプション）

NRS-7000series (7100/7200)
500mmの焦点距離を持ち、高分解測定を実現しています。グレーティングは最大4枚まで搭載することができます。低波数測定ユニットを搭載したNRS-7200は、超低迷光により5cm^{-1}の低波数領域まで測定できます。

日本分光の最新情報はこちらから ***http://www.jasco.co.jp***

光と技術で未来を見つめる
日本分光
日本分光株式会社
〒192-8537　東京都八王子市石川町2967-5
TEL 042(646)4111㈹
FAX 042(646)4120

北海道S・C 011(741)5285　神奈川S・C 045(989)1711
北日本S・C 022(748)1040　名古屋S・C 052(452)2671
筑　波S・C 029(857)5721　大　阪S・C 06(6312)9173
東　京S・C 03(3294)0341　広　島S・C 082(238)4011
西東京S・C 042(646)7001　九　州S・C 092(588)1931

誘導体化フラーレン用HPLCカラム

COSMOSIL® Buckyprep-D

● 誘導体化フラーレン用HPLCカラム

● トルエン移動相中で誘導体化フラーレンが分離可能

■C60インデン付加体の分析例

C60インデンは誘導体化フラーレンの一種であり、有機薄膜太陽電池のn型半導体材料として注目されている化合物です。コスモシール Buckyprep-Dを用いることにより高い分離性能が得られます。

COSMOSIL Application Data

Column:
Column size: 4.6mmI.D.-250mm
Mobile phase: Toluene
Flow rate: 1.0 ml/min
Temperature: 30°C
Detection: UV 325nm

Sample: C_{60} [Indene]$_2$ (1.0mg/ml)
Inj.Vol.: 1.0µl

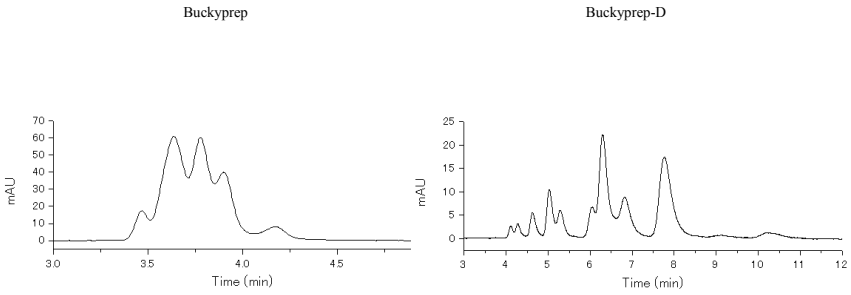

NACALAI TESQUE, INC

Data courtesy of Yusuke Tajima, Dr. Sci.
Organic Optoelectronics Laboratory, RIKEN (Institute of Physics and Chemistry)

■Buckyprepシリーズの用途

フラーレン分離のスタンダードカラム → COSMOSIL Buckyprep
誘導体化フラーレンの分離 → COSMOSIL Buckyprep-D
金属内包フラーレンの分離 → COSMOSIL Buckyprep-M

・誘導体化フラーレン (Buckyprep-D)

COSMOSIL Application Data

Column: Buckyprep-D
Column size: 4.6mmI.D.-50mm
Mobile phase: Toluene
Flow rate: 1.0 ml/min
Temperature: 30°C
Detection: UV325nm

Sample:
1; C_{60} (0.125mg/ml)
2; C_{70} (0.250mg/ml)
3; [*6,6*]-Phenyl-C_{61} Butyric Acid Methyl Ester [PCBM] (0.125mg/ml)
4; [*6,6*]-Phenyl-C_{71} Butyric Acid Methyl Ester [[70]PCBM] (0.375mg/ml)
Inj.Vol. 1.0µl

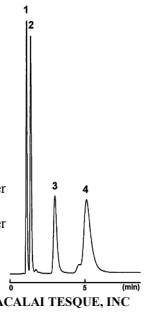

NACALAI TESQUE, INC

・金属内包フラーレン (Buckyprep-M)

COSMOSIL Application Data

Column: Buckyprep-M
Column size: 4.6mmI.D.-250mm
Mobile phase: Toluene
Flow rate: 1.0 ml/min
Temperature: 30°C
Detection: UV312nm

Sample:
$Sc_2@C_{76}$(I)
$Sc_2@C_{78}$
$Sc_2@C_{80}$(I)
C_{86}

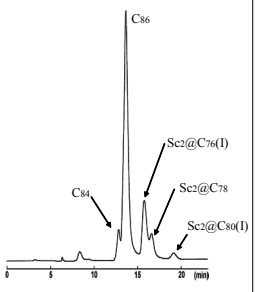

Sample courtesy of Prof. H.Shinohara,
Department of chemistry, Nagoya University

NACALAI TESQUE, INC

詳しい情報はWeb siteをご覧ください。

ナカライテスク株式会社
〒604-0855 京都市中京区二条通烏丸西入東玉屋町498

価格・納期のご照会 フリーダイヤル 0120-489-552
製品に関するご照会 TEL : 075-211-2746 FAX : 075-211-2710
Web site :http://www.nacalai.co.jp

LF プラズマクリーナー『CUTE・COVANCE』シリーズ：表面クリーニングに最適な LF 帯の周波数を使用したプラズマクリーナーです。UV オゾンクリーナーや RF プラズマ装置を使用している方やウエット処理で表面処理をしている方に最適です。主な用途:PDMS ポンディング・基盤洗浄、SEM/TEM 等の前処理

数十年の経験からついに誕生!

Genus_3D

全自動シリアルセクショニング３Ｄ顕微鏡

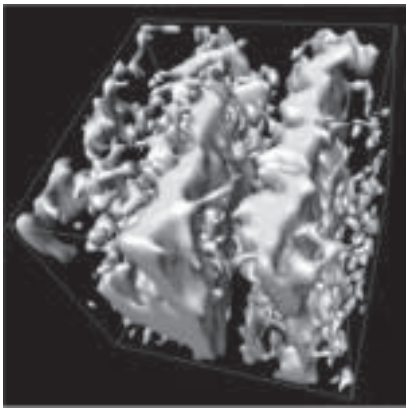

■主な用途：単相・複相組織解析、材料の破壊機構解明（ボイド・亀裂）、欠陥評価（介在物、空洞など）
材料内部面の解析（相界面、粒界）

株式会社 新興精機
Shinkouseiki.Co.,Ltd.

〒812-0054　福岡市東区馬出１丁目１８番３号

（TEL:092-641-8451･FAX:092-641-8786）http://www.shinkouseiki.co.jp

Hitachi Koki

HITACHI
Inspire the Next

カーボンナノチューブの分離・精製に

日立の超遠心機シリーズ!

バイオ研究 & ナノ粒子研究 の強い味方　世界トップクラスの高性能、床置き・卓上、日立なら選べます!

小形超遠心機

エコでスリムな床置きタイプ

himac CS-FNX Series

世界最高速150,000rpm* (CS150FNX)
世界最大遠心加速度1,050,000×g* (CS150FNX)
クラス最静音45dB(A)*
省スペース床置きタイプの小形超遠心機は日立だけ!

特長
- 世界標準の安全規格CEマーキング適合製品
- サンプルのバランスは目分量でOK!
- ロータは全て載せるだけ! (ロータクイックセッティング方式)
- エコ対応省エネモデル
- 7mlスイングロータ(S50ST)が回せます。
- 2012年度グッドデザイン賞 受賞!

■仕様

形　名	CS150FNX	CS120FNX	CS100FNX
最高回転速度 (rpm)	150,000	120,000	100,000
最大遠心加速度 (xg)	1,050,000	771,000	571,000
サイズ (W×D×H mm)	440×520×910		
質　量 (kg)	105		
標準価格 (税別)	￥5,500,000	￥4,900,000	￥4,300,000

卓上超遠心機

コンパクトなボディに世界トップクラスの性能

himac CS150NX

世界最高速150,000rpm*
世界最大遠心加速度1,050,000×g*
世界最小コンパクトサイズ*
クラス最静音45dB(A)*

特長
- 短い真空待ち時間
- サンプルのバランスは目分量でOK!
- ロータは全て載せるだけ!
- 7mlスイングロータが回せます。

■仕様

形　名	CS150NX
最高回転速度 (rpm)	150,000
最大遠心加速度 (xg)	1,050,000
サイズ (W×D×H mm)	590×582×408
質　量 (kg)	97
標準価格 (税別)	￥6,000,000

＊(2015年5月現在当社調べによる)

■ロータ仕様

形　名	S110AT	S50A	S50ST
最高回転速度 (rpm)	110,000	50,000	50,000
容量 (ml)×本数 (本)	5.0×8	30.0×6	7.0×4
標準価格 (税別)	￥1,100,000	￥950,000	￥1,500,000
形　名	S140AT	S58A	S55A2
最高回転速度 (rpm)	140,000	58,000	55,000
容量 (ml)×本数 (本)	2.0×10	13.5×8	1.5×12
標準価格 (税別)	￥1,290,000	￥1,000,000	￥750,000

バイオ研究 & ナノ粒子研究 のスタンダード

超遠心機

NEW

遠心分離が楽しくなる機能満載!

himac CP-NX Series

クラス最高速100,000rpm* (CP100NX)
クラス最大遠心加速度803,000×g* (CP100NX)
*(2015年5月 現在当社調べによる)

特長
- 離れていても運転状況がわかるLEDインジケーター搭載!
- ロータ寿命自動管理と寿命延長機能搭載 (RLMアダプタ付ロータ)
- カラー液晶タッチパネルを操作しやすい前面に配置
- ユーザー支援ソフト「 himac ***ASSIST*** 」標準装備
- 2014年度グッドデザイン賞受賞!

■仕様

形　名	CP100NX	CP90NX	CP80NX
最高回転速度 (rpm)	100,000	90,000	80,000
最大遠心加速度 (xg)	803,000	700,000	615,000
サイズ (W×D×H mm)	790×690×880 (テーブルまでの高さ863)		
質　量 (kg)	390		
標準価格 (税別)	￥11,000,000	￥9,500,000	￥8,000,000

■ロータ仕様

形　名	P70AT	P45AT	P21A2	P40ST	P28S	P100AT2
最高回転速度 (rpm)	70,000	45,000	21,000	40,000	28,000	100,000
容量 (ml)×本数 (本)	40×8	94×6	230×6	13×6	40×6	6.5×8
標準価格 (税別)	￥2,200,000	￥2,350,000	￥1,800,000	￥2,490,000	￥2,350,000	￥2,250,000

※本広告に掲載した以外にもロータを取り揃えております。最寄りの営業所へお気軽にお問い合せください。

【製造・販売・保守】
日立工機株式会社 ライフサイエンス機器事業部
東日本地区　03-6738-0860　　西日本地区　0798-23-4125

日立遠心機お客様相談センター　0120-024125
受付時間 9:00～12:00 / 13:00～17:00 (土・日・祝日・弊社休業日除く)
URL http://www.hitachi-koki.co.jp/himac/

Kanto Reagents

高純度溶媒 Primepureシリーズ

これまでにない最高品位を誇る新しい試薬の誕生です。

Primepureの特徴

30項目を超える保証スペック
- ◆金属不純物（20元素以上）をppbレベルで保証
- ◆有機不純物を低減

最高品位

▶製品例

	包 装	純 度
アセトン	1L	＞99.9% (GC)
アセトニトリル	1L	＞99.9% (GC)
ジクロロメタン	1L	＞99.9% (GC)
N,N-ジメチルホルムアミド	1L	＞99.9% (GC)
エタノール	1L	＞99.9% (GC)
ヘキサン	1L	＞96.0% (GC)
2-プロパノール	1L	＞99.9% (GC)
トルエン	1L	＞99.9% (GC)

関東化学株式会社 試薬事業本部
〒103-0022 東京都中央区日本橋室町2-2-1 (03) 6214-1090
〒541-0048 大阪市中央区瓦町2-5-1 (06) 6231-1672
〒812-0007 福岡市博多区東比恵2-22-3 (092) 414-9361
≪ http://www.kanto.co.jp　E-mail;reag-info@gms.kanto.co.jp ≫

Nikon

先進をゆく顕微鏡が、生体/ライブセルイメージングの新時代を切り拓く。

微細な世界を見る技術が、また新たな次元に到達しました。
常に頂点を目指して挑戦し続けるニコンの高度な顕微鏡技術が、生命科学の明日を揺り動かします。

共焦点レーザー顕微鏡システム A1R＋

■ガルバノ・高速レゾナントの2種類のスキャナーを搭載し、
高速＆高画質なイメージングが可能に。

高速多光子共焦点レーザー顕微鏡システム A1R MP+

■独自の高速スキャニング技術と高感度受光技術により、600μm以上の深部からの画像を420枚/秒(512×32画素)で可視化します。

広帯域・高解像対物レンズ λS対物レンズ

■超低屈折率を誇るニコン独自の薄膜技術、ナノクリスタルコートを採用。
■広範囲波長での高い透過率と同時に、広い色収差補正を実現しています。

λS対物レンズ

N-STORM

N-SIM

超解像顕微鏡　N-SIM/N-STORM

■115nmの解像度で、0.6秒/枚*での連続画像取得が可能な「N-SIM」
■従来製品の約10倍（約20nm）の分解能を実現した「N-STORM」
＊2D-SIM/TIRF-SIMモードで最速の場合。

販売元
株式会社ニコン／株式会社ニコン インステック

カタログ・パンフレット等のご請求は、（株)ニコンインステック　バイオサイエンス営業本部へ
108-6290 東京都港区港南2-15-3（品川インターシティC棟）　電話(03)6433-3982

■フリーダイヤル　0120-586-617
www.nikon-instruments.jp/

溶液中の物質のナノレベル微細化・分散

BRANSON 超音波ホモジナイザー

昨今のナノ・テクノロジーの発展及び粉体関連技術の発展により、
より微細な粒子に対する分散処理の要望が増えてまいりました。
超音波ホモジナイザーを使用し、均質な乳化分散処理を行い、安定させることにより製品の機能は向上します。一次粒子の凝集力にも拠りますが概ね 100nm 程度までの分散力があります。
ブランソン社の超音波ホモジナイザーは、コンバーター部での超音波振動変換効率が 98%以上ある為、ホーン先端部の振幅の安定性が高く、強力なキャビテーションが得られ、高効率で、再現性の高い破砕・分散処理が可能です。
ブランソン社では卓上型実験用 20kHz 機・40kHz 機、及び 1,100W～3,300W の高出力機で大量処理も可能なシステムも用意しております。

超音波ホモジナイザー（20kHz）
BRANSON　SONIFIER シリーズ

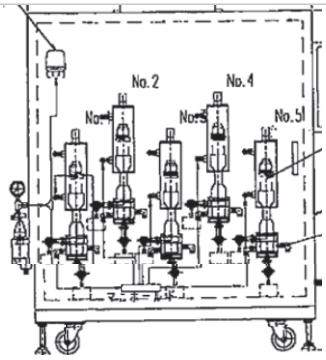

大量処理システム

微量用・超音波ホモジナイザー
BRANSON　SLPe　（40kHz）

主なアプリケーション

分散

カーボンナノチューブ　有機・無機顔料　感光体　記録材料　磁性粉　シリカ　アルミナ　セラミック　ポリマー　ラテックス　製紙　ファンデーション　光触媒　触媒　半導体　電子基盤　液晶　セメント　ワクチン　体外診断薬　歯磨き粉　貴金属　金属　宝石　タイヤ　発酵菌類　その他

乳化

エマルジョン製剤　農薬　トナー　ラテックス　界面活性剤　クリーム　乳液　クリーム　等

株式会社 セントラル科学貿易
本社：111-0052 東京都台東区柳橋 1-8-1
Tel 03-5820-1500 Fax 03-5820-1515
URL http://www.cscjp.co.jp/

大阪支店：　Tel 06-6325-3171 Fax 06-6325-5180
福岡営業所：Tel 092-482-4000 Fax 092-482-3797
札幌出張所：Tel 011-764-3611 Fax 011-764-3612

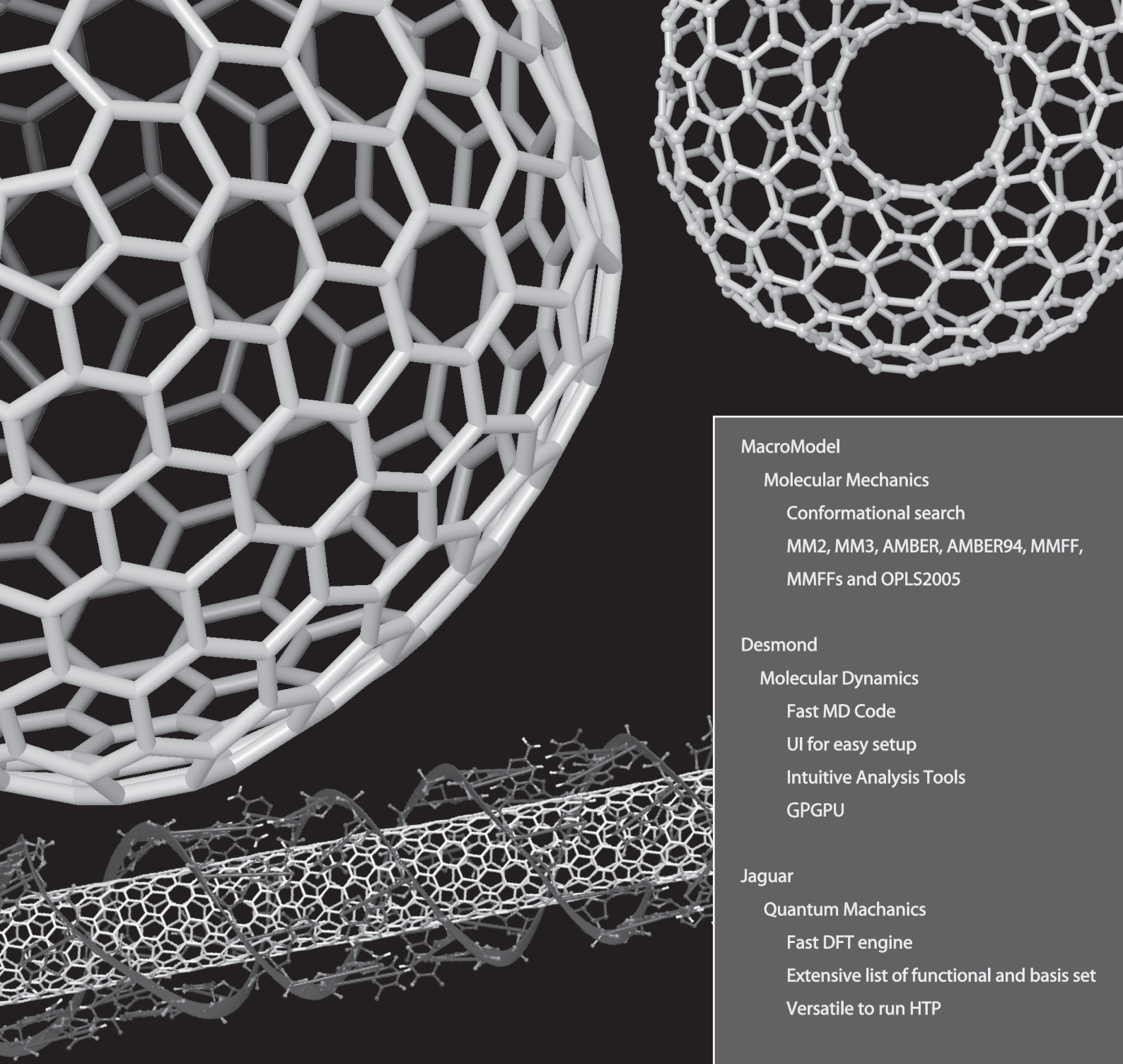

MacroModel
- Molecular Mechanics
  - Conformational search
  - MM2, MM3, AMBER, AMBER94, MMFF, MMFFs and OPLS2005

Desmond
- Molecular Dynamics
  - Fast MD Code
  - UI for easy setup
  - Intuitive Analysis Tools
  - GPGPU

Jaguar
- Quantum Machanics
  - Fast DFT engine
  - Extensive list of functional and basis set
  - Versatile to run HTP

Structure Builder
- Nanostructure Builder
- Complex Builder
- Nanoparticle Builder
- Crystal Builder

Materials Science Suite は材料設計のための分子モデリングプログラムです。炭素材料に対応したビルダー機能、高速アルゴリズムによる量子化学計算、豊富な力場パラメーターと多彩な手法による分子力学計算、並列化効率の高い分子動力学計算のプログラム等を搭載しています。各種プロパティの自動計算と解析機能により、研究目的にあわせた分子デザインを可能にします。

MATERIALS SCIENCE SUITE

日本国内お問い合わせ先
シュレーディンガー株式会社
〒100-0005 東京都千代田区丸の内1-8-1
丸の内トラストタワーN館　17階
Tel: 03-6860-8316 Fax: 03-6273-4722
Email: info-japan@schrodinger.com URL: http://www.schrodinger.com/jp
SCHRÖDINGER

開発・販売元
Schrödinger LLC
101 S.W. Main Street Suite 1300,
Portland, OR, U.S.A
Tel: +1-503-299-1150 Fax: +1-503-299-4532
Email: info@schrodinger.com URL: http://www.schrodinger.com

～輝く未来のために～

私達は、全ての研究者のサポートを致します。

●研究用試薬●理化学機器●工業薬品の総合商社

サンケイ化学薬品株式会社

福岡県福岡市南区大楠 2-6-24

TEL(092)531-2735・FAX(092)522-0768

E-mail：sankyakuhin@rio.odn.ne.jp

高分解能 s-SNOM（散乱型走査近接場顕微鏡）

see the nanoworld
neaspec

neaSNOM — 10nmに迫る高分解能での赤外イメージングと分光

Graphene on SiC substrate

測定概念図

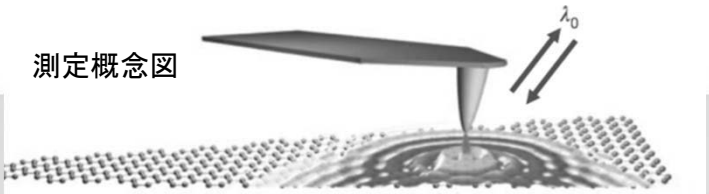

実験データ（6H-SiC λ0=9.7μm）

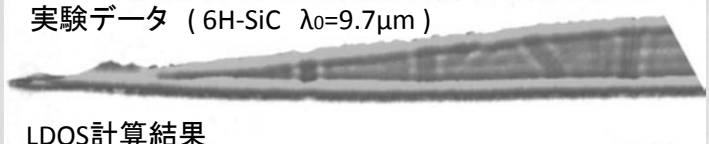

LDOS計算結果

λ0=9,200nm	λ0=9,681nm	λ0=10,152nm
εsic=2.9	εsic=2.0	εsic=0.7

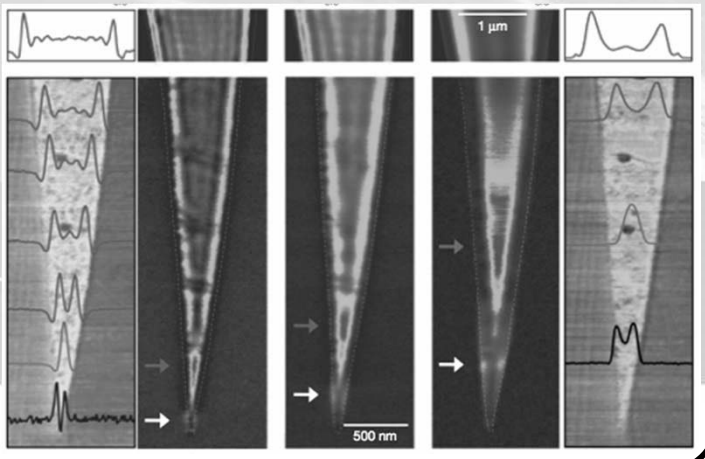

Optical nano-imaging of gate-tunable graphene plasmons

nature J. Chen et al., Nature 487, p.77 (2012)

表面伝搬するプラズモンをナノスケールで可視化

励起波長を変えてグラフェン上のプラズモンの波長を制御

NEW

洗練された第三世代neaSNOM

- 分析初心者の方にも**安定操作が確約**された唯一市販されているアパーチャレス近接場顕微鏡
- 再現性100%の近接場測定を約束する特許技術：**Background suppression technique**
- 高い操作性を実現する測定ソフト**neaSCAN**を組み込んだAFMユニット
- **どんなAFM向けサンプル**に対しても測定可能（非破壊サンプル測定も可能）

QuantumDesignJapan
日本カンタム・デザイン株式会社
〒171-0042 東京都豊島区高松1-11-16 西池袋フジタビル2F
Tel:03-5964-6624 Fax:03-5964-6621 Email: info@qdj.co.jp
http://www.qd-japan.com/

nanom フロンティアカーボンのフラーレン製品

銘　柄		分子構造	純度(HPLC面積%、代表値) 内容他	最低数量 (g)
nanom purple フラーレンC60	ST	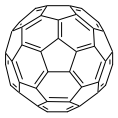	99	10
	TL		99.5	2
	SU		99.5/昇華精製品	2
	SUH		99.9/昇華精製品	1
	SC		99.9/昇華精製/単結晶品	1
nanom orange フラーレンC70	ST	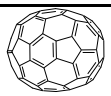	97	1
	SU		98/昇華精製品	0.5
nanom mix 混合フラーレン	ST	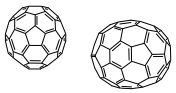	C60,C70,その他高次 フラーレンの混合物 ※微粒化品(ST-F)もあります	50
nanom spectra [60]PCBM (phenyl C61-butyric acid methyl ester)	E100	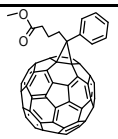	99	1
	E100H		99.5	1
	E102		99.9	0.5
nanom spectra　E400 bis[60]PCBM (bis-phenyl C61-butyric acid methyl ester)		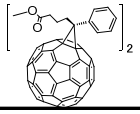	98/異性体トータル ※位置異性体の混合物	1
nanom spectra [70]PCBM (phenyl C71-butyric acid methyl ester)	E110	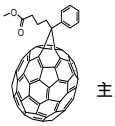 主成分	99/異性体トータル ※位置異性体の混合物	0.5
	E112		99.5/異性体トータル ※位置異性体の混合物	0.5
nanom spectra　Q100 [60]インデン付加体			99	0.5
nanom spectra　Q400 [60]インデン2付加体		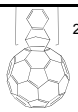	99/異性体トータル ※位置異性体の混合物	1
nanom spectra　D100 水酸化フラーレン		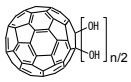 (n = ca.10)	$C_{60}OH_n$　n=10を主成分とする混合物	1
nanom spectra　A100 水素化フラーレン		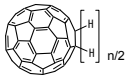 (n = ca. 30)	$C_{60}H_n$　n=30を主成分とする混合物	1

※銘柄、取扱数量等は予告無く変更する場合がございます。 ※試験研究用途向けです。

当社製品は、下記から購入いただけます。直接お問い合わせください。

・関東化学株式会社　試薬事業本部
〒103-0022 東京都中央区日本橋室町2-2-1　TEL:03-6214-1090　FAX:03-3241-1047
http://www.kanto.co.jp　E-mail:reag-info@gms.kanto.co.jp

・中山商事株式会社　筑波営業所　（担当　落合敬宝）
〒300-2651茨城県つくば市鬼ケ窪1139-1　TEL:029-847-7355　FAX:029-847-1923
E-mail:nst15@nakayama-co.jp

＜本資料に関するお問い合わせ先＞
フロンティアカーボン株式会社【担当：梶原】
〒100-8086　東京都千代田区丸の内2-6-1丸の内パークビルディング24階
TEL:03-3210-2620　FAX:03-3210-4606　http://www.f-carbon.com
※弊社へのお問い合わせはHPよりお願いいたします。

Frontier Carbon Corporation